

DISSERTATION

DEVELOPMENT OF SURFACE MODIFICATIONS ON TITANIUM  
FOR BIOMEDICAL APPLICATIONS

Submitted by

Roberta Maia Sabino

School of Advanced Materials Discovery

In partial fulfillment of the requirements

For the Degree of Doctor of Philosophy

Colorado State University

Fort Collins, Colorado

Fall 2021

Doctoral Committee:

Advisor: Ketul C. Popat

Co-advisor: Alessandro F. Martins

Margarita Herrera-Alonso

Yan Vivian Li

Zhijie Wang

Copyright by Roberta Maia Sabino 2021

All Rights Reserved

## ABSTRACT

### DEVELOPMENT OF SURFACE MODIFICATIONS ON TITANIUM FOR BIOMEDICAL APPLICATIONS

For decades, titanium-based implants have been largely employed for different medical applications due to their excellent mechanical properties, corrosion resistance, and remarkable biocompatibility with many body tissues. However, even titanium-based materials can cause adverse effects which ultimately lead to implant failure and a need for revision surgeries. The major causes for implant failure are thrombus formation, bacterial infection, and poor osseointegration. Therefore, it is essential to develop multifunctional surfaces that can prevent clot formation and microbial infections, as well as better integrate into the body tissue. To address these challenges, two different surface modifications on titanium were investigated in this dissertation. The first one was the fabrication of superhemophobic titania nanotube (NT) surfaces. The second approach was the development of tanfloc-based polyelectrolyte multilayers (PEMs) on NT. The hemocompatibility and the ability of these surfaces to promote cell growth and to prevent bacterial infection were investigated. The results indicate that both surface modifications on titanium enhance blood compatibility, and that tanfloc-based PEMs on NT improve cell proliferation and differentiation, and antibacterial properties, thus being a promising approach for designing biomedical devices.

## ACKNOWLEDGEMENTS

I would like to express my sincere gratitude to many people without whose participation and assistance the completion of this dissertation could not have been possible. First, I would like to thank my advisor, Dr. Ketul Popat, for his unconditional help and timely guidance. His expertise and lessons were invaluable, always encouraging me and keeping me motivated. I could not have been more fortunate to have had such a supportive mentor, who not only cares about our professional growth, but also about our well-being. Ketul, thank you for being an exceptional mentor and making my graduate student experience fun, enriching, and fulfilling.

Secondly, I would like to thank my co-advisor, Dr. Alessandro Martins, for his assistance, motivation, and support. His enthusiasm about science and unwavering positivity always inspired me. I am grateful I had the opportunity to work with him in the lab for a few months and to continue this collaboration over these years. Alessandro, thank you for all the lessons and for being a wonderful co-advisor.

I also would like to offer my sincerest gratitude to my committee members, Dr. Margarita Herrera-Alonso, Dr. Yan Vivian Li and Dr. Zhijie Wang, for their encouragement, support, and helpful insights. A special thanks to Dr. Matt Kipper e Dr. Arun Kota for the opportunity to collaborate with them and for the use of their equipment.

I would like to acknowledge my department School of Advanced Materials Discovery (SAMD) and my colleagues with whom I have spent amazing times over these years. A special thanks to Caro Banuelos and Dr. Travis Bailey for helping me navigate the program. I would also like to thank all the personnel from the Analytical Resources Core (ARC), whom I had the great opportunity to work with, for the guidance in the use of different instrumentation. Especially, I

would like to thank Dr. Patrick McCurdy, Dr. Chris Rithner, Dr. Karolien Denef, Dr. Brian Newell, and Dr. Roy Geiss.

I would also like to thank my lab mates for their assistance, friendship and for enriching this journey with great moments including Vignesh Manivasagam, Dr. Liszt Yeltsin, Dr. Paulo da Câmara, Dr. Renata Bombaldi, Dr. Jessi Vlcek, Dr. Tara Wigmosta, Sravanthi Vallabhuneni, Gabriela Mondini, Abhishek Bhattacharjee, Sayudh Ghosh, Harvinder Virk and Zachary Montgomerie. A special thanks to Kirsten Kauk, Rachel Keating, Tanara Morrell, Yeilin Benitez and Richard Morales-Villalva for their great help in preparing our samples.

Above all, though, I thank my family, in special my parents Eustaquia and Geraldo for their endless support and love, and my sister Barbara for the incentives. Without them I would not be able to go after my dreams. A special thank you to my friends for all their support and good times together. Finally, I thank my faithful life partner Arthur for the encouragement, for believing in me more than I do, and for standing beside me with his unconditional support.

## DEDICATION

*To my parents, Eustáquia e Geraldo,*

*My sister, Bárbara*

*My parents in law, Sandra e Rogério*

*And to my husband, Arthur*

*For their wholehearted support and love.*

## TABLE OF CONTENTS

ABSTRACT .....	ii
ACKNOWLEDGEMENTS .....	iii
DEDICATION .....	v
OVERVIEW .....	1
HYPOTHESIS AND SPECIFIC AIMS .....	3
CHAPTER 1: SURFACE MODIFICATION STRATEGIES TO IMPROVE TITANIUM HEMOCOMPATIBILITY .....	5
1.1. Introduction .....	5
1.2. Titanium and titanium-based alloys .....	7
1.3. Hemocompatibility of titanium-based biomaterials .....	9
1.3.1. Blood-biomaterial surface interactions .....	10
1.3.2. Evaluation of hemocompatibility of titanium surfaces .....	14
1.4. Strategies for improving hemocompatibility of titanium-based implants .....	16
1.4.1. Surface properties and their influence in hemocompatibility .....	16
1.4.2. Surface modifications on titanium and titanium alloys .....	20
1.5. Conclusions and Future Perspectives .....	40
REFERENCES .....	43
CHAPTER 2: INTERACTION OF BLOOD PLASMA PROTEINS WITH SUPERHEMOPHOBIC TITANIA NANOTUBE SURFACES .....	53
2.1. Introduction .....	53
2.2. Materials and Methods .....	55
2.2.1. Fabrication of titania nanotube arrays with different surface modifications ...	55
2.2.2. Surface characterization of different substrates .....	56
2.2.3. Stability of different substrates in physiological conditions .....	57
2.2.4. Isolation of platelet rich plasma (PRP) and platelet poor plasma (PPP) .....	57
2.2.5. Fibrinogen adsorption from PRP on different substrates .....	58
2.2.6. Thrombin anti-thrombin (TAT) complex formation on different substrates ....	58
2.2.7. <i>In vitro</i> plasma coagulation assay .....	60
2.2.8. Whole blood clotting kinetics .....	61

2.2.9. Statistical analysis .....	61
2.3. Results .....	62
2.4. Discussion .....	73
2.5. Conclusions .....	78
REFERENCES .....	79
CHAPTER 3: ENHANCED HEMOCOMPATIBILITY AND ANTIBACTERIAL ACTIVITY ON TITANIA NANOTUBES WITH TANFLOC/HEPARIN POLYELECTROLYTE MULTILAYERS .....	83
3.1. Introduction .....	83
3.2. Materials and Methods .....	85
3.2.1. Fabrication of titania nanotubes (NT) with PEMs .....	85
3.2.2. Surface characterization .....	87
3.2.3. Hemocompatibility studies .....	88
3.2.4. Antibacterial activity studies .....	90
3.2.5. Statistical analysis .....	91
3.3. Results .....	92
3.3.1. Surface characterization .....	92
3.3.2. Hemocompatibility studies .....	95
3.3.3. Antibacterial activity studies .....	101
3.4. Discussion .....	106
3.5. Conclusions .....	110
REFERENCES .....	112
CHAPTER 4: ENDOTHELIALIZATION OF TITANIA NANOTUBE ARRAYS WITH DIFFERENT SURFACE MODIFICATIONS .....	115
4.1. Introduction .....	115
4.2. Materials and Methods .....	117
4.2.1. Fabrication of titania nanotubes (NT) with different surface modifications ...	117
4.2.2. ECs and SMCs culture .....	117
4.2.3. ECs and SMCs viability, adhesion, and proliferation .....	118
4.2.4. Differentiation of ECs on different surfaces .....	119
4.2.5. ECs migration study .....	120
4.2.6. Statistical analysis .....	120
4.3. Results and Discussion .....	120

4.3.1. ECs viability, adhesion, and proliferation .....	120
4.3.2. Differentiation of ECs on different surfaces .....	123
4.3.3. SMCs viability, adhesion, and proliferation .....	127
4.3.4. ECs migration study .....	129
4.4. Conclusions .....	131
REFERENCES .....	132
CHAPTER 5: TANFLOC/HEPARIN POLYELECTROLYTE MULTILAYERS IMPROVE	
OSTEOGENIC DIFFERENTIATION OF ADIPOSE-DERIVED STEM CELLS ON TITANIA	
NANOTUBE SURFACES .....	
5.1. Introduction .....	135
5.2. Materials and Methods .....	138
5.2.1. Fabrication of titania nanotubes (NT) modified with PEMs .....	138
5.2.2. Surface characterization .....	139
5.2.3. Stability test .....	140
5.2.4. ADSCs culture .....	140
5.2.5. ADSCs viability, adhesion, and proliferation .....	140
5.2.6. Osteogenic differentiation of ADSCs .....	142
5.2.7. Statistical analysis .....	144
5.3. Results and Discussion.....	144
5.3.1. Surface characterization .....	145
5.3.2. Stability test .....	148
5.3.3. ADSCs viability, adhesion, and proliferation .....	152
5.3.4. Osteogenic differentiation of ADSCs .....	155
5.4. Conclusions .....	160
REFERENCES .....	161

## OVERVIEW

Titanium and its alloys have great biocompatibility and have been widely used as a biomaterial for orthopedic, dental, and cardiovascular applications for decades. With respect to orthopedic and dental implants, titanium-based materials are the number one choice. Titanium combines excellent mechanical properties, such as high strength, low density and moderate Young's modulus, with great biocompatibility and resistance to corrosion. In addition, titanium can have its properties easily modified by forming alloys or altering its surface, which makes it suitable for a wide range of biomedical applications. However, there are still drawbacks and the rate of failure for titanium-based implants can get up to 10%. The most common causes for implant failure are bacterial infection, poor osseointegration, and thrombus formation at the implant site. Therefore, it is vital to develop multifunctional surfaces that can simultaneously prevent clot formation and microbial infections, as well as better integrate to the body tissue, thus reducing the implant failure and the need for revision surgeries.

It is well established that biomaterial surface characteristics, such as surface chemistry, morphology, and wettability, directly influence the biomaterial interaction with the biological environment. It has been shown that altering the topography of the biomaterial surface to micro and nanoscale can improve the cellular response. Since the cells in native tissue interact with nanoscale extracellular matrix elements, such as protein and minerals, the surface nanotopography can modulate the adsorption of proteins and stimulate the cell differentiation. Titania nanotube (NT) surfaces have emerged as a promising approach as they enhance biocompatibility of titanium, with increased adhesion and differentiation of stem cells, improved antibacterial properties and reduced immune response on titanium.

Several strategies have been investigated to prevent both bacterial infections and thrombosis on titanium surfaces, such as designing superhemophobic surfaces (i.e., when blood/plasma contact angles are greater than  $150^\circ$ ). Superhemophobic surfaces have shown the ability to repel most blood components and prevent interactions with the biomaterial surface. Another promising approach to improve the biocompatibility of surfaces is the layer-by-layer (LbL) deposition of polyelectrolyte multilayers (PEMs). LbL assembly is used to change the surface chemistry of materials by alternately adsorbing/depositing polycationic and polyanionic layers onto a solid substrate. PEMs can be easily and reproducibly prepared, to achieve control over coating thickness and surface chemistry, without the use of hazardous organic solvents.

Recently, tanfloc (TA) has attracted considerable interest due to its promising cytocompatibility, biodegradability, and antimicrobial properties. TA is a hydrophilic, cationic ( $pK_a \approx 6.0$ ), and condensed amino-functionalized tannin derivative. The amine groups are weakly cationic, whereas the phenolic groups are weakly anionic, possibly imparting the TA with polyzwitterion-like properties, which could be responsible for its ability to resist both protein adsorption and bacterial adhesion.

In this dissertation, we propose two different surface modifications on titanium in order to improve both antibacterial and antithrombogenic properties, as well as enhance osseointegration and endothelialization on the biomaterial surface. Superhemophobic and hemophilic titania surfaces were fabricated by combination of surface topography and surface chemistry (unmodified, fluorinated and PEGylated). TA-based PEMs on NT were also developed by first changing the surface topography to make titania nanotubes. Then, NT surface was modified via LbL technique using TA as polycation, and heparin (HP) or hyaluronic acid (HA) as polyanions, until the fifth layer was obtained. Chitosan-based PEMs were used as control.

## HYPOTHESIS AND SPECIFIC AIMS

**Hypothesis:** Specific chemical and morphological modifications on surfaces improve the biocompatibility properties of titanium-based implants, such as preventing thrombus formation and bacterial infection, as well as promoting cell adhesion and differentiation on the surface.

**Specific Aim 1:** The main aim of this study is to develop different surface modifications on titania nanotubes (NT) to reduce protein adsorption and activation, thus reducing the blood clotting on the surface and enhancing hemocompatibility for blood-contacting medical devices applications. This research is discussed in **Chapters 2 and 3**.

- a) Fabrication of superhemophobic and hemophilic NT surfaces and characterization of surface chemistry, morphology, and wettability.
- b) Evaluation of the protein adsorption, Factor XII activation, and whole blood clotting on superhemophobic and hemophilic NT surfaces.
- c) Fabrication of NT surfaces modified with PEMs and characterization of surface chemistry, morphology, and wettability.
- d) Evaluation of the protein adsorption, platelet adhesion and activation, and Factor XII activation on NT surfaces modified with PEMs.

**Specific Aim 2:** The main aim of this study is to investigate the endothelialization potential of the superhemophobic NT surfaces and the NT surfaces modified with PEMs for cardiovascular implant applications. This research is discussed in **Chapter 4**.

- a) Evaluation of endothelial cell viability, adhesion, proliferation, and differentiation on different NT surfaces using CellTiter-Blue assay, scanning electron microscopy, fluorescence microscopy, and immunofluorescent staining.
- b) Evaluation of smooth muscle cell viability, adhesion, proliferation, and differentiation on different NT surfaces using CellTiter-Blue assay, fluorescence microscopy, and scanning electron microscopy.

**Specific Aim 3:** The main aim of this study is to investigate the NT surfaces modified with PEM for bacterial adhesion and proliferation, and for adipose-derived stem cell adhesion, proliferation and differentiation for orthopedic implant applications. This research is discussed in **Chapters 3 and 5.**

- a) Evaluation of bacterial adhesion and proliferation on the surfaces after 6 hrs and 24 hrs of bacterial incubation using fluorescence microscopy.
- b) Evaluation of bacterial morphology and biofilm formation on the surfaces after 6 hrs and 24 hrs of bacterial incubation using scanning electron microscopy.
- c) Evaluation of adipose-derived stem cell viability, adhesion and proliferation on the surfaces after 4 and 7 days of cell culture using CellTiter-Blue assay, fluorescence microscopy, and scanning electron microscopy.
- d) Evaluation of adipose-derived stem cell differentiation on the surfaces after 1 and 3 weeks of induced osteogenesis via total protein content assay, alkaline phosphatase (ALP) activity, calcium concentration, fluorescence microscopy, and scanning electron microscopy.

# CHAPTER 1: SURFACE MODIFICATION STRATEGIES TO IMPROVE TITANIUM HEMOCOMPATIBILITY<sup>1</sup>

## 1.1. Introduction

Titanium and its alloys have been widely used in blood-contacting devices, such as intraosseous implants, prosthetic heart valves, cardiovascular stents, and circulatory assist devices [2]. However, improper implant surface interaction with blood are prone to cause thrombosis, and this is a major complication that can lead to the device failure and other serious complications [3]. Thrombosis is an acute syndrome where the blood clots on the implant surface and, once the clotting cascade begins, it spreads rapidly, which can also increase the chances of mortality [4]. To prevent that, patients are prescribed blood thinners such as aspirin, vorapaxar, etc. [5]. However, overuse of these medications can weaken the immune system and, during injuries, there is profound bleeding of blood [6].

Thrombosis is initiated due to the contact of blood to a foreign surface, such as a metal implant surface, and it starts by the adsorption of blood proteins onto the biomaterial surface, which can lead to a series of complex reactions that ultimately form the thrombus [7]. Studies have shown that there can be thrombus formation and pannus growth in the base of the heart valve struts and apex of the cage, which leads to stenosis, and there was no central flow, which can damage the blood cells (**Figure 1.1A**) [8,9]. Another medical device that is usually made of titanium is left ventricular assisted device (LVAD), a mechanical pump that is implanted in a human's chest

---

<sup>1</sup> This work was published in *Materials Advances* and is reproduced in modified form here with permission [1].

to assist weakened heart. The major limitation with these devices is thromboembolism, bleeding, hemolysis, infection, and renal failure. A case study on patients using Heart Mate II showed that 11% of the studied patients had thrombus formation in less than one year after implantation (**Figure 1.1B-C**) [10]. Infection was also commonly found due to thrombus formation [10].

In recent years, efforts have been undertaken to reduce the thrombogenicity of biomaterials and therefore prevent these complications [11]. The thrombogenicity of a material is directly related to its surface properties and it can be influenced by modifying the surface characteristics such as topography, chemistry, charge, and mechanical properties [12,13]. Therefore, many research groups are focusing on modifying the titanium surfaces to improve its hemocompatibility and prevent failure of blood-contacting implants. The aim of this chapter is to provide an overview of surface modification strategies that are being applied to improve the blood-surface interaction of titanium-based materials. The chapter begins by highlighting the titanium properties (Section 1.2) and how its surface interacts with blood and its components (Section 1.3). Then, Section 1.4 underlines the current progress in surface modification techniques on titanium to enhance its hemocompatibility. Finally, Section 1.5 concludes the present research work and proposes scopes for future research.



**Figure 1.1.** A) Thrombus formation around the heart valve frame and strut [9]. Reproduced with permission from ref. 9. Copyright 2016, Elsevier. Examples of HeartMate II device thrombosis [10]. B) Fibrin formation and C) Fibrin with thrombus formation. Reproduced with permission from ref. 10. Copyright 2014, Elsevier.

## 1.2. Titanium and titanium-based alloys

Titanium-based implants have been largely used for biomedical applications due to their excellent mechanical properties, corrosion resistance, and great biocompatibility [14,15]. Titanium has replaced other implant materials such as stainless steel and cobalt-chromium mainly because it has the highest strength-density ratio when compared to all metals, which makes it a lightweight implant for the required strength [16]. In addition, titanium can have its properties easily modified by forming alloys, making it suitable for a wide range of biomedical applications [17,18].

Titanium is also well accepted by different body tissues without inducing any negative hypersensitivity, toxicity to the cells, or inflammatory reactions [19–21]. This inert characteristics of titanium is due to its low electrical conductivity [22]. Clinically it has been shown that the body fluids are highly corrosive and many metals like stainless steel, magnesium and chromium-cobalt are degraded quickly due to pitting or fretting corrosion inside human body [23]. However, metals like titanium oxidizes easily, forming a stable thin passivating layer which is self-limiting and protects the implant from further oxidization [24]. These titanium oxide layers are formed at very fast rate when exposed to moisture in air or water and are usually few nanometers thick [25]. This oxide layer is shown to be more biologically inert because of its less reactive nature when compared to the  $\alpha$ -Ti [26].

Titanium (Ti) is an allotropic metal [27]. Titanium along with its alloys are classified as  $\alpha$  (low-temperature),  $\alpha+\beta$ , and  $\beta$  (high-temperature), based on the crystal structures present in the substrate.  $\alpha$ -Ti is equated to hexagonal closed pack (HCP) structure, which makes the alloy stronger, high fracture toughness and low forgeability [28]. In contrast,  $\beta$ -Ti is when the HCP structure is transformed to body centered cube (BCC) structure, which makes the metal more ductile (**Figure 1.2**). The temperature at which titanium gets converted from HCP to BCC is 882°C

and this is called beta transus temperature. There are many alloying agents that can change the stabilizing temperature, and based on the application, one can change the proportion of  $\alpha$  stabilizing elements (O, Al, N, C) and  $\beta$  stabilizing elements (V, Nb, Mo, Ta, Fe, Mn, Cr, Co, Ni, Cu, Si, H). Addition of alloying agents to pure titanium changes the phase transformation temperatures and stability of alpha and beta phases. The volume fractions, size, and morphology of the  $\alpha$  and  $\beta$  phases is changed to produce Ti alloys superplastically formable with the potential to design unitized structures for significant weight reduction [29]. This aspect of Ti alloys makes it easy to modify the mechanical properties based on the application. Ti-6Al-4V is a  $\alpha+\beta$  alloy that is ductile and stronger than  $\alpha$  type Ti alloy or  $\beta$  type Ti alloy. It is important to have both strength and ductility for implants as that will give them long life under the fatigue conditions [30].

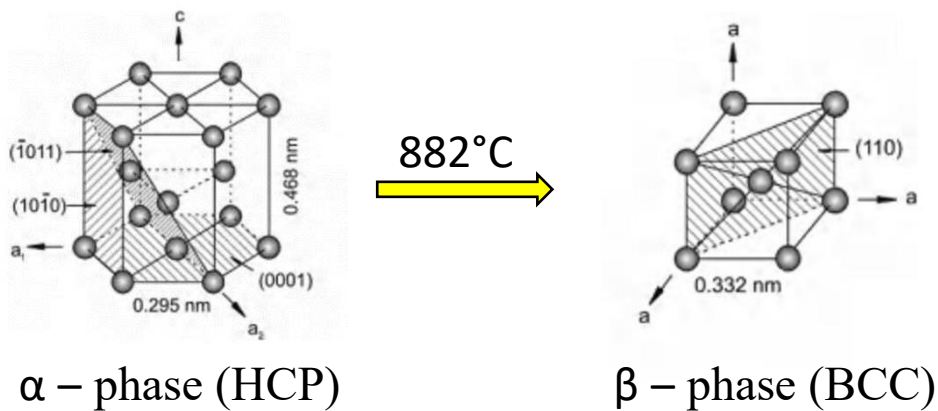


**Figure 1.2.** Crystal structure transformation of titanium [28]. Adapted with permission from ref. 28. Copyright 2013, Elsevier.

Titanium is often used for medical application in its pure form or with alloying agents such as vanadium, aluminum, tantalum, nickel, and zirconium [31]. There are four different grades of commercially pure titanium (cpTi) according to the ASTM standards, and these are based on the amounts of oxygen, nitrogen, hydrogen, iron, and carbon during the purification procedures [32]. Among various titanium and its alloys, the mainly used materials in the biomedical field are cpTi

(Grade 2), nickel-titanium and Ti-6Al-4V alloy because of their excellent corrosion resistance, low modulus of elasticity, good biocompatibility and high strength [31]. Nickel-titanium alloy has received great attention due to its shape memory feature, which makes it suitable for self-expanding stents.

Even though titanium has outstanding properties required for applications in blood-contacting implants, there are still some complications caused by its surface, such as thrombosis and restenosis [33]. Titanium surface has shown to be highly modifiable at both micro and nano level with simple techniques such as laser treatment, anodization, and hydrothermal treatment, and several studies have shown that these modification can improve biocompatibility [20,34,35]. Therefore, recent research has focused on tuning different surface modification strategies on titanium and titanium alloys to improve the biomaterial interaction with blood and its components, thus enhancing their hemocompatibility.

### **1.3. Hemocompatibility of titanium-based biomaterials**

Hemocompatibility (i.e. blood compatibility) is an essential characteristic for any biomaterial used for blood-contacting medical devices [36]. Blood compatibility is the ability of a material to keep under control the thrombotic and inflammatory responses induced by the foreign surface when in contact with blood [37,38]. These responses correspond to a series of interconnected events that happen on the surface as shown in **Figure 1.3**. Since the interaction between implant and blood happens only on the implant surface, intensive research has been carried out to develop novel surfaces that are hemocompatible. Modifying the device's surface is effective because it can prevent the blood reactions without altering the favorable bulk material properties [39].

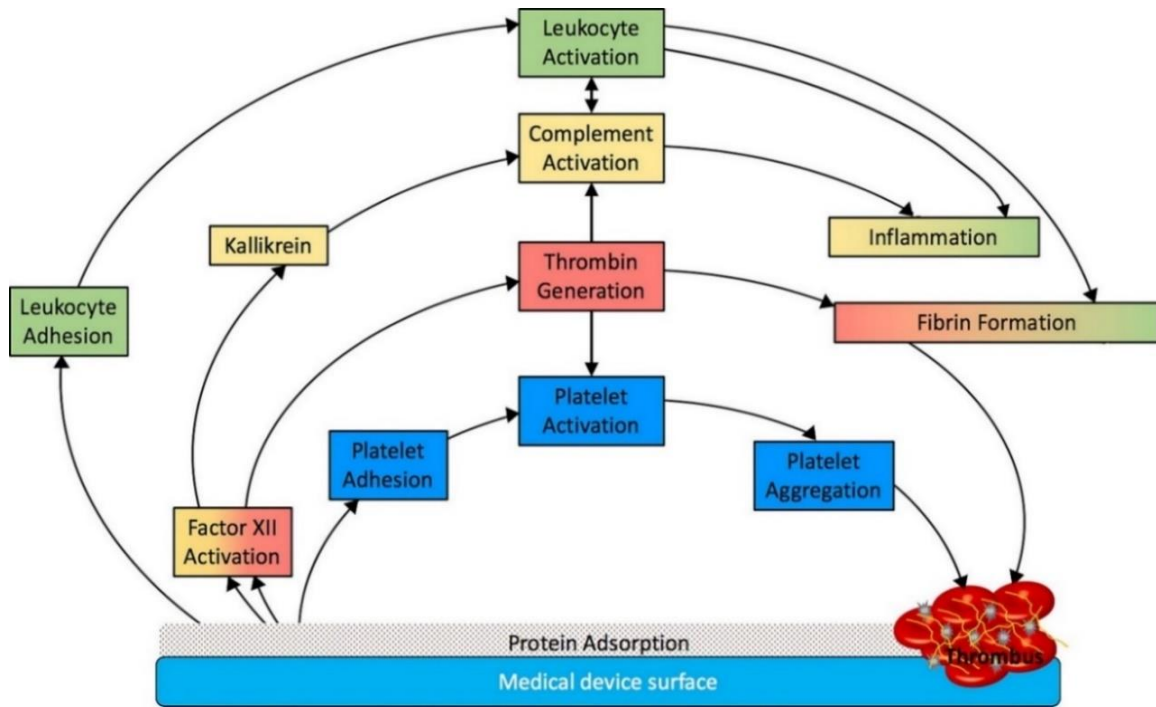


**Figure 1.3.** Schematic representation of medical device associated thrombosis [6]. The initial protein adsorption on the implant surface mediates all the subsequent phenomena. Reproduced with permission from ref. 6. Copyright 2019, Elsevier.

### 1.3.1. Blood-biomaterial surface interactions

#### 1.3.1.1 Protein adsorption

When blood comes in contact with a biomaterial surface, the first event that happens is the adsorption of blood plasma proteins [40]. These blood proteins rapidly form a layer on the biomaterial surface that have a thickness of 2-10 nm and a concentration of proteins that is 1000-fold higher than in blood plasma [41]. This mechanism of protein adsorption is complex and dynamic, and involves electrostatic interactions, van der Waals, and hydrogen bonding [42]. The composition and concentration of adsorbed proteins depends on the physical and chemical properties of the surface and they might change over time, which is known as the “Vroman effect” [43]. Vroman effect is a reversible process where the early adsorbed proteins are replaced by proteins that possess higher surface affinity and usually are in relative lower concentration in blood

[44]. These proteins, once adsorbed to the artificial surface, mediate all the subsequent reactions, such as adhesion and activation of platelets, thrombin generation, complement activation, and adhesion of leukocytes and red blood cells (**Figure 1.3**) [4].

The most abundant proteins in plasma are albumin, immunoglobulins, and fibrinogen [45]. Fibrinogen is a central protein in the coagulation cascade and one of the first to adsorb on biomaterials [46]. Once adsorbed to the artificial surface, it is responsible for platelet and leukocyte adhesion and activation [37]. Albumin is generally considered to be inert toward thrombosis, although some studies have shown that platelets and leukocytes can adhere to adsorbed albumin layers [44]. Another key protein involved in thrombus formation is factor XII, that once activated, trigger a series of complex interconnected reactions [6].

#### *1.3.1.2 Factor XII activation*

Factor XII, also called Hageman Factor, is a plasma protein that autoactivates by adsorption to the biomaterial surface [47]. This autoactivation occurs upon binding with the surface, presumably due to a conformational change, which forms the enzyme FXIIa [48]. FXIIa is then responsible for initiating the intrinsic pathway of coagulation cascade and the complement activation.

#### *1.3.1.2a Coagulation cascade*

The coagulation cascade is the process by which the blood thrombus is formed, and it is divided into two pathways: intrinsic and extrinsic. The extrinsic pathway is triggered by damaged cells in the endothelial tissue, while the intrinsic pathway (also called contact activation) is due to

the biomaterial surface interactions with adsorbed proteins [49]. These two pathways are not independent of each other, and both can be involved in the biomaterial-associated thrombosis [37].

The four proteins involved in the activation of the intrinsic pathway are: factor XII (FXII), prekallikrein, factor XI (FXI), and the high-molecular weight kininogen (HMWK). After FXII activation, FXIIa converts prekallikrein into kallikrein, and together with HMWK activates FXI, producing FXIa [50]. After FXI activation, factor IX is converted to its activated form factor IXa, leading to a cascade of proteolytic reactions that results in thrombin generation by cleavage of prothrombin [37]. Thrombin then converts fibrinogen to fibrin monomers, which polymerize to form the fibrin mesh [51].

The extrinsic pathway of the coagulation cascade is initiated by tissue factor (TF) expression from damaged cells at the site of vascular injury [37]. Factor VII (FVII) then binds to TF, and after its activation to FVIIa, they form the extrinsic tenase complex: TF-FVIIa complex. TF-FVIIa complex, in the presence of calcium, cleaves factor X to form factor Xa. After that, both pathways lead to the common pathway where thrombin will be generated, and the fibrin mesh will be formed.

### *3.1.2b Complement activation*

In addition, FXII and kallikrein are also involved in triggering the complement activation. The complement system is made up from more than 30 proteins and plays a vital role in body's immune response [46,52]. The activation of the complement system induced by biomaterials is part of the inflammatory response and is also interconnected to the coagulation cascade [37]. For example, complement activation is known to occur with vascular grafts, catheters, and during hemodialysis and cardiopulmonary bypass [37].

The complement activation can be initiated by three different pathways: classical, lectin and alternative [53]. Biomaterial surfaces are responsible for triggering both classical and alternative pathways via cleavage of FXIIa by kallikrein to produce  $\beta$ -FXIIa [4].  $\beta$ -FXIIa then activates the classical pathway, and kallikrein activates C3 and C5, generating the reactive fragments C3a and C5a [6]. C3a and C5a might then influence the leukocytes adhesion and activation on the implant surface. These enzymes and reactive fragments generated upon complement activation are also responsible for cell lysis.

#### *1.3.1.3 Platelet adhesion*

As mentioned, the adsorbed protein layer plays a vital role in platelet response to biomaterials. Adsorbed fibrinogen mediate the platelet adhesion to the surface, and it varies with the protein conformation changes and the availability of platelet binding domains [51]. Following the platelet adhesion to the implant surface, they undergo a morphological change, resulting in its activation and aggregation. The platelet activation consists of a shape change that produce granule contents and dendrites [44]. These activated platelets then release agonists, such as thromboxane A2 and ADP, that intensify platelet adhesion, activation, and aggregation on the medical device.

These platelet-mediated reactions are critical events in thrombus formation and are also interconnected to the intrinsic pathway of blood coagulation [54]. The thrombin generated by the intrinsic pathway also induces more platelet activation and aggregation, which accelerates the coagulation cascade [55]. These platelet aggregates deposited on the implant surface are trapped by the fibrin mesh to form a fibrin-platelet thrombus (**Figure 1.4**) [56]. Platelet activation is also known to occur following hemodialysis and cardiopulmonary bypass, and with catheters and vascular grafts [37].

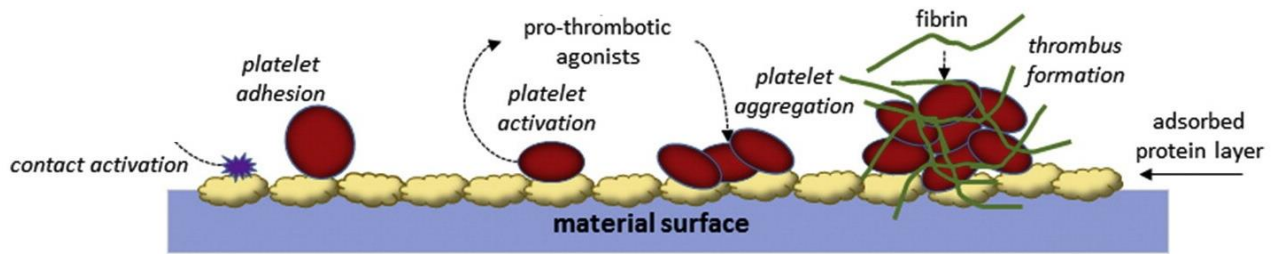


**Figure 1.4.** Platelet adhesion and activation on the biomaterial surface [57].

#### 1.3.1.4 Leukocyte adhesion

Besides the coagulation of blood plasma and the platelet-related reactions, the hemocompatibility of biomaterial surfaces is also influenced by leukocyte activation. Similar to platelets, the leukocytes, such as monocytes and neutrophils, can also adhere and activate upon binding to the surface. Fibrinogen is also primarily involved in leukocyte adhesion to biomaterials, and, following activation, the leukocytes can further assist both coagulation and inflammatory processes [52]. The activation of leukocytes has been commonly identified in cardiovascular devices, such as stents and vascular grafts, as well as during cardiopulmonary bypass, angioplasty, and hemodialysis [37]. Eventually, the monocytes adhered to the implant surface can differentiate into macrophages. These macrophages, once activated, produce pro-inflammatory cytokines that attract more leukocytes [58]. Ultimately, it can lead to the fusion of macrophages to form the giant cells and the recruitment of fibroblasts to form a fibrous capsule. This encapsulation prevents the implant to interact with the surrounding tissue and can cause the device failure.

#### 1.3.2. Evaluation of hemocompatibility of titanium surfaces

To achieve good standardization, the methods and models for hemocompatibility tests are described in the ISO 10993-4/2002. Based on the primary process, the hemocompatibility

evaluation can be classified into 5 different categories: blood coagulation, immunology, thrombosis, hematology, and platelets (**Table 1**) [36,39]. The evaluation of blood compatibility should also consider that these processes are not isolated and interfere in the other responses.

**Table 1.1.** Hemocompatibility testing (adapted from ISO-10993-4:2002) [59]

<b>ISO 10993-4 categories</b>	<b>Primary process</b>	<b>Assays</b>
Coagulation	Contact activation	Specific coagulation factor Thrombin generation
Immunology	Complement activation	C3a, C5a, iC3b, C4d, SC5b-9 C3 convertase, C5 convertase
Thrombosis	Fibrinogen–fibrin conversion	Percent occlusion and flow reduction
Hematology	Hemolysis	Hemolysis Leukocyte adhesion/activation
Platelets	Platelet activation	Platelet count/adhesion Platelet activation/aggregation

The coagulation category takes into account the contact activation system (i.e., intrinsic pathway of clotting cascade). The assays related to it investigate the specific coagulation factors and protein adsorption, as well as the thrombin generation. Previous study has developed a mathematical model that relates coagulation time to FXIIa concentration [47]. It is important to investigate the Factor XII activation on titanium biomaterial surfaces as it is responsible for initiating the intrinsic pathway of coagulation cascade and the complement activation. The immunology category covers the study of the complement system, and usually focuses on the release of peptide anaphylatoxins (such as C3a, C4a and C5a) [60]. The study of thrombosis focuses on the fibrinogen–fibrin conversion and the fibrin mesh formation, while the hematology evaluates leukocyte activation and hemolysis. Hemolysis is the release of hemoglobin from

damaged red blood cells (i.e. erythrocytes), and it should be below 5%, according to ISO-993-5-10:1992 [61]. Another testing method that could be employed to investigate the biomaterial surface' hemocompatibility is the evaluation of whole blood clotting by a fast hemolysis assay as described elsewhere [62]. The platelet category includes the characterization of platelet adhesion, activation, and agglomeration, as well as its function in the thrombogenic potential of biomaterials.

#### **1.4. Strategies for improving hemocompatibility of titanium-based implants**

In blood-contacting implants, such as artificial heart valves, cardiovascular stents, and ventricular assist devices, hemocompatibility is crucial. Several studies have established that surface characteristics, such as chemistry, charge, wettability, and topography, play a major role in enhancing blood compatibility [63–66]. Proper surface modification techniques not only maintain the excellent bulk attributes of titanium and its alloys, such as relatively low modulus, good fatigue strength, machinability, and formability, but also improve specific surface properties demanded by different applications to improve the surface interaction with blood.

##### **1.4.1. Surface properties and their influence in hemocompatibility**

Over the last decades, intensive research has been conducted to understand the physical chemistry behind the biomaterial-blood interaction and how it leads to thrombosis and inflammation. This has promoted significant progress in developing novel surfaces for blood-contacting medical devices. Strategies to enhance blood compatibility of titanium are based on two main approaches: changing the surface chemistry and topography. By combining both strategies, it is possible to tailor the surface characteristics, such as roughness, wettability, and surface charge, to make the surface more hemocompatible.

When changing the topography, the surface roughness will get affected although roughness is not an exact definition of surface topography since it does not indicate if the roughness dimension is at the macroscale, microscale or nanoscale [38]. The micro/nano-scale architecture attracts great interest in the biomedical field due to the enhanced cellular response and biocompatibility [25]. Surface roughness  $R_a$  is the measure of the finely spaced micro-irregularities on the surface texture and is determined by calculating  $R_a$  and  $R_z$ . While  $R_a$  gives the average surface roughness,  $R_z$  can give information for any pore, hole, or surface deformities detrimental to strength [67]. *In vivo/In vitro* results have shown that surface roughness can influence the protein adsorption, platelet adhesion and activation, and thrombus formation.

While roughness is an important surface property for biomaterial interactions, it is important to understand the influence of roughness in wetting of the surface. The traditional  $R_a$  and  $R_z$  does not fit well statistically or fractal for superhydrophobic surfaces, which are commonly investigated for blood-contacting applications. In superhydrophobic surfaces there are other phenomenon such as pinning of the triple phase line, interface destabilization and wetting transition. Hence, it is essential to study the wettability of the surface.

Surface wettability is an important factor that quantifies how a liquid behaves when it interacts with a solid surface, and this is dictated by the intermolecular interaction of the liquid and solid surface and the cohesive force between the liquid molecules. The surface topography, chemistry, and charge, along with the liquid properties such as polarity can influence the wettability. Taking the water contact angle ( $\theta$ ) into consideration, surfaces are termed superhydrophilic ( $\theta \sim 0$ ), hydrophilic ( $0^\circ < \theta < 90^\circ$ ), hydrophobic ( $\theta > 90^\circ$ ), and superhydrophobic ( $\theta > 150^\circ$ ). Designing hydrophilic surfaces is desirable as lower amount of blood plasma proteins adsorb on it in comparison with hydrophobic surfaces [46]. Due to the

higher water-surface interaction, hydrophilic surfaces tend to reduce the blood protein adsorption [68]. The wettability of a liquid droplet on a textured surface differs from a smooth surface. The measure of macroscopic contact angle on a textured surface is defined as the apparent contact angle which is denoted by  $\theta^*$ . When the liquid droplet comes into contact with a textured surface, it adapts either the Wenzel state or Cassie Baxter state to minimize its overall free energy [69]. In Wenzel state, the liquid droplet completely penetrates the nano/micro texture of the titanium surface, thereby having a completely wetted interface and the apparent contact angles are determined by using the relation:

$$\cos\theta^* = r\cos\theta$$

where  $r$  is the surface roughness of the features, which is the ratio of actual solid liquid interfacial area to the projected surface area [70]. Due to the roughness factor, Wenzel state enhances wetting or de-wetting based on the young's contact angle. If  $\theta < 90^\circ$ , then  $\theta^* \ll 90^\circ$ , and if  $\theta > 90^\circ$ , then  $\theta^* \gg 90^\circ$ .

As opposed to Wenzel state, in the Cassie Baxter state, the droplet does not penetrate the nano/micro features due to the pockets of air trapped between the features and the liquid droplet. In Cassie state the apparent contact angle is determined by using the relation:

$$\cos\theta^* = f_{sl}\cos\theta + f_{lv}\cos(\pi) = f_{sl}\cos\theta - f_{lv}$$

where  $f_{lv}$  is the area fraction of liquid-vapour interface and  $f_{sl}$  is the area fraction of solid-liquid interface [71].

Super-repellent surfaces are surfaces which display high apparent contact angles and low contact angle hysteresis and can be classified into superhydrophobic and superoleophobic surfaces [69]. Superhydrophobic surfaces normally display high apparent contact angles ( $\theta^* > 150^\circ$ ) and low contact angle hysteresis ( $\Delta\theta < 5^\circ$ ) for high surface tension liquids [69]. Super-repellent

surfaces are achieved by attaining a Cassie Baxter state of wetting. Once the air is released due to the pressure of the liquid, there is a complete wetting, transitioning from Cassie state to the Wenzel state which is governed by breakthrough pressure [72]. This transition can make the surface more hydrophilic than the unmodified substrates due to the increase in overall roughness.

The chemical modification of implant surfaces for altering the wettability to reduce thrombus has also been extensively explored. Superhemophobic surfaces (i.e. surfaces that repel blood) were developed in recent times to reduce thrombogenicity of blood-contacting devices. These surfaces repel blood via a combination of nano/micro scale topographies and low surface energy silane coating. The surfaces are coated with various functional groups like  $\text{CF}_3$ ,  $\text{CF}_2$ ,  $\text{CF}_2\text{H}$  to lower the overall surface energy of the material, which increases the repellency towards blood. Fluorinated and per-fluorinated materials like per-fluorinated silanes, per-fluorinated phosphates, fluorinated monomers, polymers, and copolymers which have low surface energy have been used to develop hemocompatible materials to reduce thrombosis and improve blood compatibility [73].

Studies have also explored hydrophilic coating with improved hemocompatibility. Hydrophilic polymers such as poly (ethylene glycol) (PEG) have been used for biomedical applications including bioconjugation, surface modification, and tissue engineering, due to critical properties such as good biocompatibility, non-immunogenicity, and resistance to non-specific binding of proteins [74,75]. PEG is very hydrophilic in nature and biochemically inert. PEG chains can be synthesized by controlled polymerization of ethylene glycol or ethylene oxide in aqueous solution [76]. The hydroxyl end groups of the PEG can be replaced with a variety of functional groups to improve surface properties and enhance hemocompatibility [45].

The crystallinity is another surface property that can influence blood-surface interaction [77]. The  $\text{TiO}_2$  on the surface exists in different polymorphs. The phases which have shown major

role in biomedical applications are anatase (tetragonal) and rutile (tetragonal) [78]. The phase transformation from anatase to rutile leads to a change in electron structure and therefore modifying the chemical properties of titanium surface. The rutile phase facets {100} and {110} are thermodynamically stable and hydrophilic due to the molecular adsorption at the O vacancies sites [79]. However, the crystalline TiO<sub>2</sub> is shown to be stable and that is required for a constant biological performance [80].

#### **1.4.2. Surface modifications on titanium and titanium alloys**

As explained in the previous section, the optimization of surface chemistry with micro/nanoscale topography leads to new biomaterials with enhanced hemocompatibility [38]. According to the different clinical needs, various surface modification techniques have been proposed, and this section will focus on these strategies developed in the past years to improve the hemocompatibility of titanium-based surfaces. An overview on these different strategies is given in **Figure 1.5**.

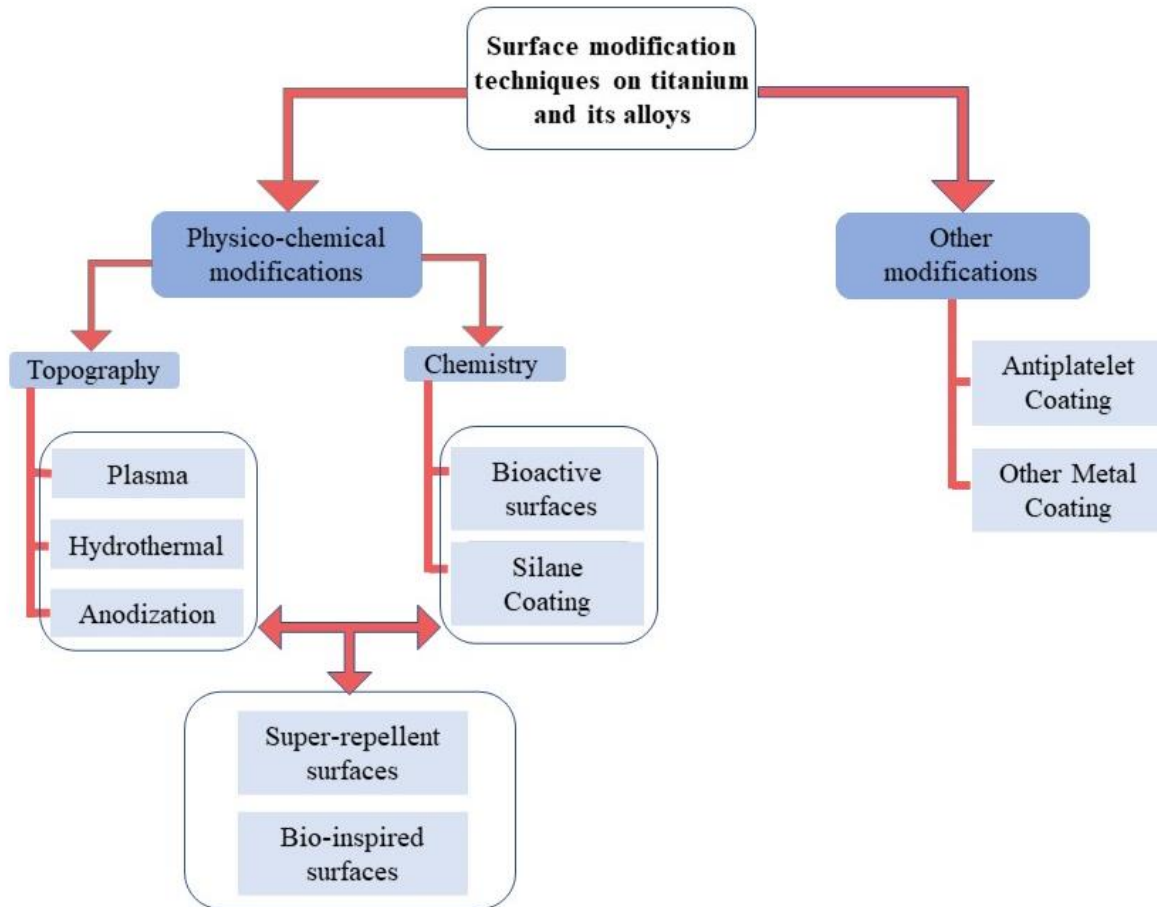


**Figure 1.5.** Different strategies of surface modification on titanium-based surfaces to improve hemocompatibility.

#### 1.4.2.1 Plasma treatment

A simple technique used to treat titanium surfaces is plasma oxidation. The plasma oxidation treatment is used to generate oxide layers and is considered a green process due to low costs, lower water consumption, and no waste generation [81]. Plasma treatment generally transfer the additional energy in the plasma to the surface increasing the material surface energy and makes the surface more reactive [82]. Göttlicher *et al.* investigated the mechanisms required for the formation of nanocrystalline stoichiometric TiO<sub>2</sub> oxide layers using plasma oxidation [83]. Previous studies have shown that the presence of rutile TiO<sub>2</sub> phase can reduce thrombosis on the

surfaces [84,85]. In addition, the ability to increase the roughness of the oxide layer via plasma treatment is also used to modulate the surface hydrophilicity.

Chiang *et al.* showed that the plasma-oxidized samples with rough dimple-like oxide layer and nanostructured rutile TiO<sub>2</sub> phase possess enhanced hemocompatibility [81]. They used oxygen plasma with different treatment powers and durations to modify pure titanium surfaces by oxygen plasma to deposit a titanium oxide layer [81]. The microstructure analysis indicated formation of island like nanostructured rutile TiO<sub>2</sub> layer and dimple like nanostructured rutile TiO<sub>2</sub> layer on the plasma oxidized titanium surface. The presence of a rough dimple-like oxide layer with nanostructured rutile TiO<sub>2</sub> indicated better hemocompatibility when compared to control surfaces **(Figure 1.6A-B)**.

Hung *et al.* deposited TiO<sub>2</sub> layers using oxygen plasma immersion ion implantation (oxygen PIII). The oxygen PIII treated surfaces indicated the presence of Ti<sup>4+</sup> chemical state which consisted of nanocrystalline TiO<sub>2</sub> with a rutile structure [85]. The biological studies indicated delayed clotting time on the oxygen PIII treated surfaces which was associated with decreased fibrinogen adsorption. The oxygen PIII treated surfaces also showed lower platelet adhesion indicating the blood compatibility of the titanium implants can be improved by oxygen PIII **(Figure 1.6C-D)**.

Klein *et al.* investigated the plasma electrolytic oxidation (PEO) on titanium surfaces by different phosphate-based electrolytes for use in ventricular assist devices (VADs) [86]. The PEO coating technique builds up TiO<sub>2</sub> oxide layers on the surface and is a process similar to alternating current anodizing. Although both processes use a counter electrode and a power supply, the PEO requires higher voltage conditions than in anodization, which leads to the development of different surface morphologies [86]. This PEO coatings can generate a variety of nanostructures that were

able to prevent platelet adhesion and reproduce good hemocompatibility observed in modern VADs, as well as improve the wear resistance of the material.

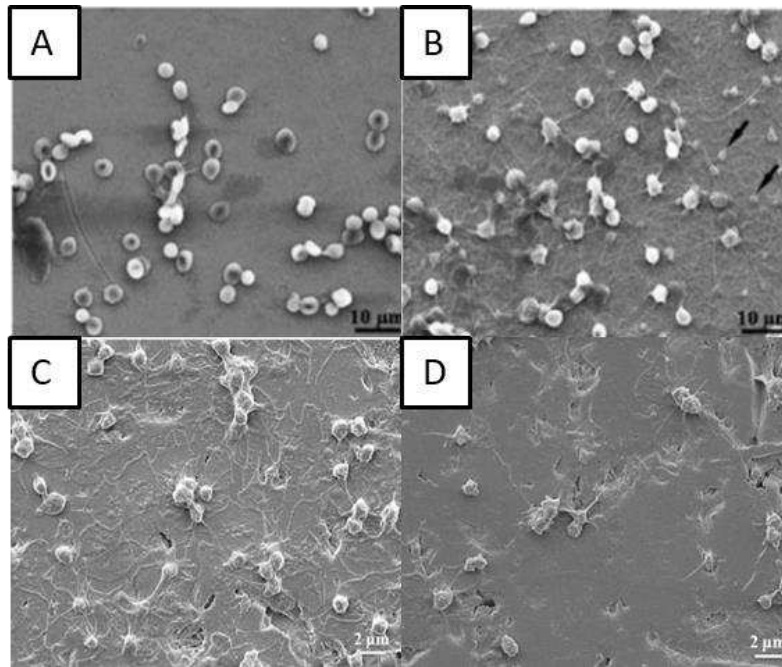


**Figure 1.6.** A-B) SEM images of red blood cells on control surfaces and plasma oxidized surfaces at 280W for 30 mins, respectively [81]. SEM images indicating the interaction of platelets with C) titanium surfaces and D) oxygen PIII treated surfaces [85]. Reproduced with permission from ref. 85. Copyright 2016, Elsevier.

#### 1.4.2.2 Hydrothermal treatment

Hydrothermal treatment (HT) is a simple process where titanium substrates are treated in an elevated temperature and pressure, mostly in a liquid medium (acidic/alkaline) [15]. This treatment is highly tunable, and the reaction rate and kinetics can be altered by varying the concentration, temperature and pressure. Substrates are chemically etched and studies have shown that various surface features such as nanofibers, nanopores, nanoflowers, nanoneedles, and nanotubes can be developed on titanium surface without altering the bulk properties [87,88]. These nanostructures provide higher surface area and similar environment to the natural biological system [34]. Since the blood cells and its components, such as protein and minerals, interact with

nanoscale extracellular matrix elements, the surface nanotopography can modulate biological responses and stimulate physiological responses [35,64].

Vishnu *et al.* developed nanoneedles/nanograss on Ti-29Nb substrates using HT with NaOH solution [89]. The surface was superhydrophilic in nature and has shown reduced platelet adhesion and reduced hemolysis rates, thus improved hemocompatibility (**Figure 1.7A-C**). Manivasagam *et al.* have shown that the hydrothermally developed nanopore and nanoneedle surfaces that are hydrophilic in nature have improved hemocompatibility when compared to unmodified surfaces [90]. The nanopores surface which showed superhydrophilicity had the lowest protein adsorption and significantly decreased the platelet and leukocyte adhesion (**Figure 1.7D-F**).

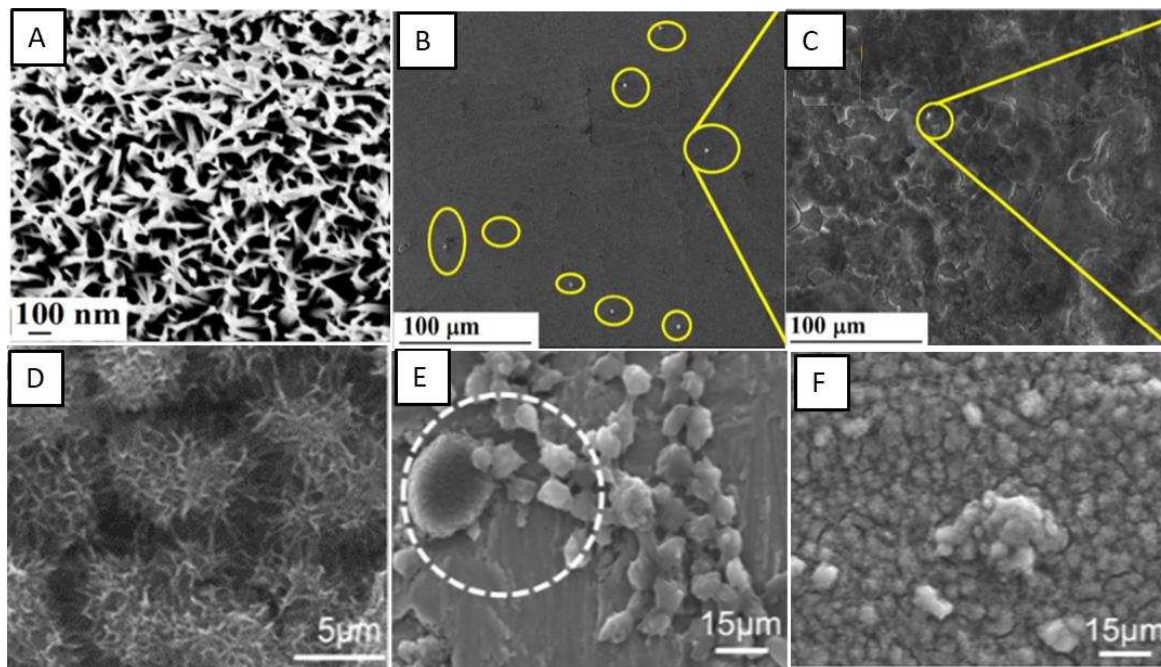


**Figure 1.7.** A) SEM images indicating surface morphology of hydrothermally treated nanograss surfaces. B-C) SEM images indicating platelet adhesion on control and nanograss Ti29Nb alloy surfaces, respectively [89]. Adapted with permission from ref. 89. Copyright 2020, Elsevier. D) SEM images indicating morphology of control and hydrothermally treated titanium surfaces, respectively. E-F) SEM images indicating platelets and leukocytes adhered on control and hydrothermally treated titanium surfaces, respectively [90].

#### 1.4.2.3 Anodization

Anodization is an electrochemical treatment where the substrate to be treated is the anodic part of the electrolytic cell in an electrolytic solution. This treatment is highly tunable, the reaction rate and kinetics can be altered by varying the anodization potential, electrolytic composition and concentration [91]. Anodization is a quick and inexpensive electrochemical technique to produce an array of TiO<sub>2</sub> nanotubes on currently implanted titanium-based devices [92]. TiO<sub>2</sub> nanotubes have attracted considerable attention due to high biocompatibility and osseointegration properties. Recently they have emerged as good approach for use in cardiovascular applications, such as stents [35]. Various studies have shown TiO<sub>2</sub> nanotubes can be produced with ordered alignment using anodization process on titanium substrates. The dimensions of the nanotubes such as thickness, diameter and length are controllable by altering the pH, voltage, electrolyte composition, and the time of experiment. The diameter of the nanotubes can be varied between 15 nm to 150 nm, and these structures usually make the surface hydrophilic in nature. The size of the nanotubes plays a key role in platelet adhesion. The 15 nm rods lead to higher platelet adhesion when compared to 100 nm rods [48].

Junkar *et al.* developed nanotubes for stent applications using anodization in hydrofluoric acid solution and further treatment with highly reactive oxygen plasma [93]. Results show that TiO<sub>2</sub> nanotubes developed are hydrophilic and has better hemocompatibility compared to unmodified titanium surface [93]. TiO<sub>2</sub> nanotubes treated with plasma decreased platelet and smooth muscle cells adhesion as well as enhanced endothelial cell growth. However, over time the nanotube surfaces were naturally oxidized, which made the surface hydrophobic, thus reducing the hemocompatibility.

Pan *et al.* fabricated TiO<sub>2</sub> nanotube arrays of varying diameters via anodization and further doped them with zinc using hydrothermal treatment to improve biocompatibility [94]. The TiO<sub>2</sub> nanotube arrays were hydrophilic, whereas, the zinc doped TiO<sub>2</sub> nanotube arrays were superhydrophilic in nature. The hydrophilic and superhydrophilic surfaces increased the albumin adsorption and decreased the fibrinogen adsorption when compared to bare titanium. The results also indicated lower platelet adhesion on the superhydrophilic surfaces (Zn coated TiO<sub>2</sub> nanotube arrays) when compared to hydrophilic surfaces (TiO<sub>2</sub> nanotube arrays) and bare titanium (**Figure 1.8A-C**). The zinc coating also reduced the hemolysis rate and enhanced cell compatibility indicating that modified hydrophilic and superhydrophilic surfaces can be used to improve blood compatibility and enhance cell endothelialization.

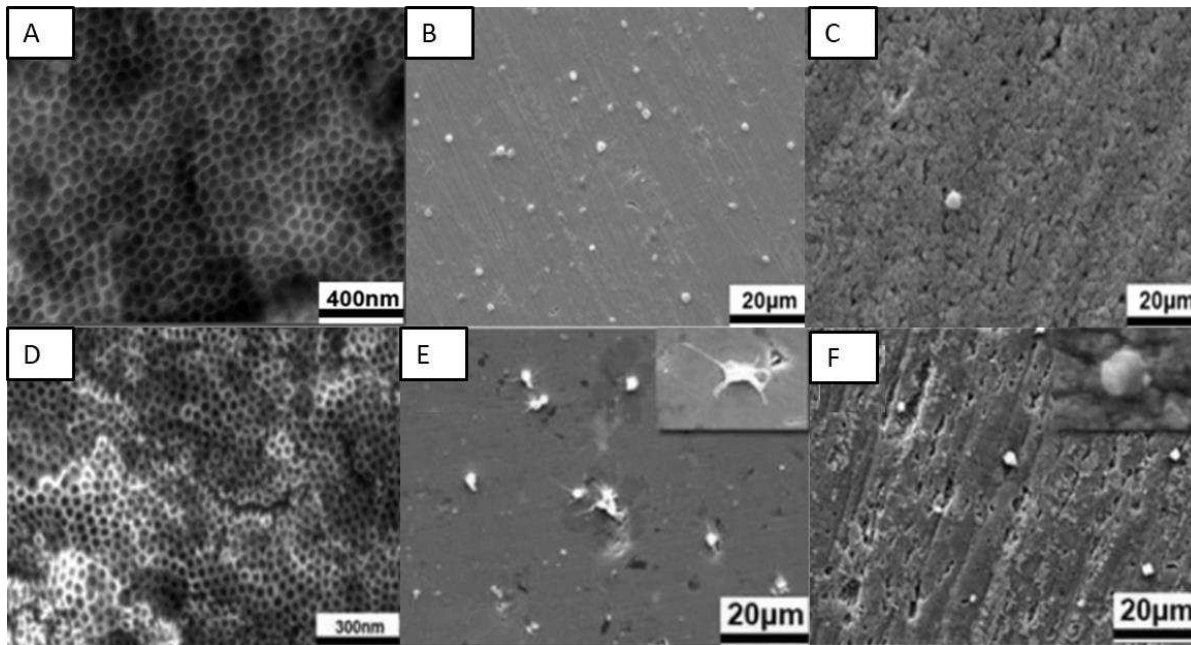


**Figure 1.8.** A) SEM images indicating surface morphology of zinc doped TiO<sub>2</sub> nanotubes. B-C) SEM images indicating platelet adhesion on control and zinc doped TiO<sub>2</sub> nanotubes, respectively [94]. Adapted with permission from ref. 94. Copyright 2020, American Chemical Society. D) SEM images indicating surface morphology of TiO<sub>2</sub> nanotube arrays anodized at 30V. E-F) SEM images indicating platelet adhesion on control and TiO<sub>2</sub> nanotube arrays (anodized at 30V) surfaces [95]. Adapted with permission from ref. 95. Copyright 2019, Elsevier.

Gong *et al.* also developed in situ TiO<sub>2</sub> nanotube arrays by anodic oxidation and their crystal structures were further changed by annealing treatment. The effects of TiO<sub>2</sub> nanotube arrays with different diameters and crystal structures on endothelial cell behavior and blood compatibility were investigated [95]. The results indicated that the TiO<sub>2</sub> nanotube arrays with smaller diameter and anatase crystal had good blood and cell compatibility. There was a decrease in the platelet adhesion and hemolysis rate while also there was an increase in endothelial cell adhesion and proliferation (**Figure 1.8D-F**).

#### 1.4.2.4 Super-repellent surfaces

Super-repellent surfaces are surfaces that repel most liquids as their surface energy is significantly lower [96]. Although hydrophilicity has been widely employed for blood-contacting medical devices, recent research has shown even lower protein adsorption and platelet adhesion on superhydrophobic surfaces [97]. Superhydrophobicity can be achieved by combination of surface texture (e.g., micro and/or nanoscale texture) and coating with low surface energy compounds [98].

Studies have shown that nanotubes which are chemically coated can lead to varied surface interactions. Sabino *et al.* showed that when coated with a fluorinated silane the surface was superhydrophobic and when coated with PEG the surface superhydrophilic [48]. The superhydrophobic surface reduced the amount of protein adsorption and significantly delayed whole blood clotting when compared to other surfaces. Similarly, Xu *et al.* were able to produce superhydrophobic surface by coating the nanotube surface with self-assembled monolayers of octadecyl phosphonic acid (ODPA) [99].

Jiang *et al.* fabricated superhydrophobic titanium oxide coatings on Ti-6Al-4V alloys by micro arc oxidation (MAO) treatment and subsequent coating with 1 wt.% alcohol solution of 1H, 1H, 2H, 2H-perfluorooctyl-trichlorosilane (PFOTS) [100]. The resulted crater-like porous microstructured superhydrophobic surfaces displayed apparent water contact angle of 153°. The superhydrophobic surfaces displayed higher corrosion resistance when compared to uncoated Ti-6Al-4V. The superhydrophobic surfaces also showed low hemolysis ratio and no platelet adhesion, hence improving the blood compatibility of the Ti-6Al-4V alloy (**Figure 1.9A-C**).

Chen *et al.* fabricated superhydrophobic surface on Ti-6Al-4V alloy using hydrothermal treatment with NaOH and subsequent coating with PFOTS [101]. Various concentration of NaOH was used to analyze the difference in surface properties. The treatment developed feather-like or grass-like nanostructures on the surface based on the concentration. The coating made the grass-like structure surface superhydrophobic with highest apparent water contact angle of 159°. The superhydrophobic surface showed decreased hemolysis ratio, platelet adhesion and prolonged coagulation time, hence improving the *in vitro* hemocompatibility of Ti-6Al-4V alloy [101].

Yang *et al.* fabricated superhydrophobic TiO<sub>2</sub> nanotubes via electrochemical anodization in 0.5 wt.% HF electrolyte and subsequent coating with a methanolic solution of hydrolyzed 1 wt.% 1H, 1H, 2H, 2H-perfluorooctyl-triethoxysilane (PTES) [102]. The PTES modified TiO<sub>2</sub> nanotubes displayed apparent water contact angle of 156°. The superhydrophobic nanotube surfaces displayed lower platelet adhesion and activation when compared to bare titanium and superhydrophilic surfaces, thus exhibiting enhanced hemocompatibility (**Figure 1.9D-F**).

Ma *et al.* fabricated multifunctional 3D microstructures on nickel-titanium alloys using femtosecond laser ablation combined with further fluorination of these microstructures to form superhydrophobic coating [103]. These fluorinated microstructures displayed apparent contact

angles of  $167^\circ$  for water droplet indicating superhydrophobicity. The biocompatibility studies have shown low hemolysis ratio, low platelet adhesion and 100 % cell viability on these surfaces (**Figure 1.9G-I**). The surfaces have also shown excellent stability over time. Further, these surfaces have significantly reduced microbial adhesion and biofilm formation indicating antimicrobial properties.

Movafaghi *et al.* fabricated titania nanotube surfaces via electrochemical anodization and titanium nanoflowers via hydrothermal treatment [104]. These surfaces were further treated with (heptadecafluoro-1,1,2,2-tetrahydrodecyl)trichlorosilane to make them superhemophobic (i.e., surfaces that display contact angles  $> 150^\circ$  with blood). These surfaces upon fluorination displayed an apparent contact angle of  $150^\circ$  and low roll off angles for human blood plasma indicating superhemophobicity. These surfaces displayed significant lower adhesion and activation of platelets when compared to hemophobic and hemophilic surfaces (**Figure 1.9J-L**). Bartlet *et al.* also developed superhemophobic titania nanotube surfaces [105]. The titania nanotube arrays were developed by anodizing technique and these surfaces were made superhemophobic by vapor phase silanization. These surfaces showed lower protein adsorption and lower platelet adhesion/activation, indicating a promising approach to design hemocompatible materials.

Montgomerie *et al.* fabricated superhydrophobic titania nanoflowers via hydrothermal process and silanization using Ti-6Al-4V alloy [106]. These surfaces showed significantly reduced protein adsorption and platelet adhesion and activation. The superhydrophobic titania nanoflowers indicated improved hemocompatibility and reduced bacterial adhesion when compared to both non-textured and unmodified Ti-6Al-4V surfaces.

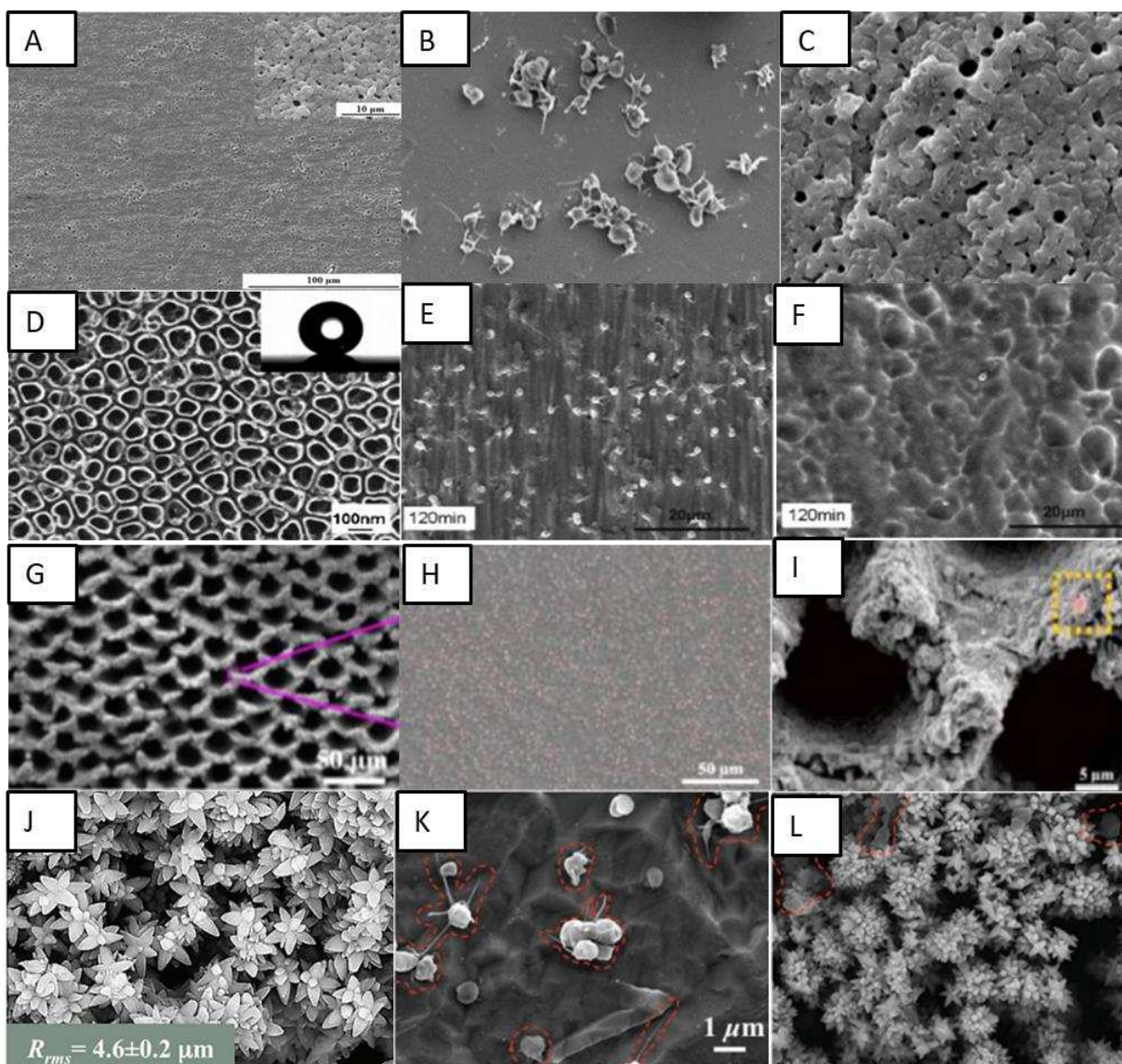


**Figure 1.9.** A) SEM images indicating crater-like porous microstructure on the Ti-6Al-4V surface. B-C) SEM images indicating platelet adhesion on bare Ti-6Al-4V and superhydrophobic MAO+TFOS surfaces, respectively [100]. Adapted with permission from ref. 100. Copyright 2015, Elsevier. D) SEM image indicating superhydrophobic TiO<sub>2</sub> nanotube surfaces. E-F) SEM images indicating platelet adhesion on bare TiO<sub>2</sub> nanotube surface and PTES modified superhydrophobic surfaces, respectively, after 120 mins exposure [102]. Adapted with permission from ref. 102. Copyright 2010, Elsevier. G) SEM image indicating multifunctional 3D micro-nanostructures on the nickel-titanium surface. H-I) SEM images indicating platelet adhesion on pristine nickel-titanium surface and superhydrophobic multifunctional 3D micro-nanostructured surface [103]. Adapted with permission from ref. 103. Copyright 2020, American Chemical Society. J) SEM images indicating nano-flowered surfaces. K-L) SEM images indicating platelet adhesion on non-textured titanium and superhemophobic nanoflower titanium surfaces [104]. Adapted with permission from ref. 104. Copyright 2016, Wiley-VCH.

Moradi *et al.* investigated the effect of wettability on blood compatibility of titanium and stainless steel substrates [107]. They examined different surface chemistries and micro/nanostructures to study their effect on protein adsorption and platelet adhesion. The wettability of the surfaces was modified using different chemical treatments and laser ablation methods. They concluded that carbonized superhydrophobic cauliflower-like pattern was more resistant to protein and platelet adhesion when compared to other superhydrophobic surfaces, possibly because of the stability in the Cassie–Baxter state. In addition, the results showed that, in the hydrophilic regime, a higher roughness corresponds to increased platelet adhesion due to the larger blood–surface contact area.

#### *1.4.2.5 Bioactive surfaces*

The modification of titanium surfaces using bioactive molecules or biopolymers, such as polysaccharides, peptides, and antibodies has received great attention to enhance their hemocompatibility properties. Biopolymers, such as heparin, chitosan, and some zwitterionic polymers, have been widely used to prevent protein and platelet attachments. Heparin is a naturally occurring polysaccharide and the most used antithrombogenic agent [57]. It possesses a very similar structure to heparan sulfate, a proteoglycan present on the endothelial cell surface that provides the natural anticoagulant surface property of the endothelium [108]. Heparin is responsible for binding to antithrombin and inhibiting the fibrin mesh formation. Because it is highly negative charged molecule, heparin is usually incorporated to titanium surfaces via electrostatic interactions with positive charged polymers to avoid the reduction of its biological activity [109]. Heparin has been combined with different polycations such as chitosan, tanfloc, and collagen to coat titanium using the layer-by-layer (LbL) self-assembly technique [110,111].

Zhang *et al.* showed that collagen/heparin coating on titanium surface decreases the platelet adhesion and activation and improves the endothelization process of the implant [112]. Collagen is the major component of extracellular matrix (ECM) and has been used to modify the surface of cardiovascular implants to enhance biocompatibility and induce cell-biomaterial interactions [110]. Cherng *et al.* coated pure titanium surfaces with heparin/dopamine and heparin/collagen via LbL techniques [113]. The heparin/dopamine was a porous polymer structure and heparin/collagen was a multilayer constructed by electrolytes. Both these surfaces promoted anticoagulation effect when compared to actual surfaces. However, the anticoagulation effects was better on the heparin/dopamine coated surfaces due to its long-term stability [114].

Yang *et al.* loaded TiO<sub>2</sub> nanotubes arrays with a 5-layer of polydopamine and further coated the surface with anticoagulant drug bivalirudin. The polydopamine coating controlled the release kinetics of bivalirudin and bivalirudin activity was seen for more than 300 days compared to the 40 days activity from TiO<sub>2</sub> nanotubes loaded with bivalirudin substrates. *In vitro* and *ex vivo* studies showed the modified surface improved hemocompatibility by reducing adhesion and denature of fibrinogen and platelets and effectively reducing thrombus formation [115].

Li *et al.* developed co-immobilization to form heparin and fibronectin films on aminosilanized titanium surfaces [116]. The technique combines electrostatic interaction and the co-immobilized films showed to be stable after immersion in phosphate-buffered saline (PBS) for five days and enhance the hemocompatibility of titanium surfaces. Fibronectin is an adhesive glycoprotein that promotes endothelial cell attachment and spreading [117]. The films reduced the hemolysis rate, prolonged the blood coagulation time, and increased the ATIII binding density. The co-immobilized surfaces also showed less platelets activation and aggregation, and less fibrinogen conformational change in comparison with unmodified titanium surface. Similarly, Li

*et al.* fabricated titanium surfaces with heparin/fibronectin complexes. The heparin and fibronectin mixture was covalently immobilized on a titanium substrate and showed improved hemocompatibility and endothelialization [118]. The surfaces reduced the blood hemolysis rate, prolonged blood coagulation time, decreased platelets activation and aggregation, and induced less fibrinogen conformational change when compared with unmodified titanium surface.

Xu & Cai prepared a bioactive coating by self-assembling phase transited lysozyme (PTL) and heparin to improve the biocompatibility of titanium [119]. PTL has been shown to have excellent biocompatibility and antibacterial properties, and in this study it was used positively charged PTL for strong electrostatic interactions with heparin. The PTL/heparin coated surfaces were hydrophilic in nature. The results indicated that these surfaces showed lower number of platelets adhered and delayed blood clotting time when compared to other surfaces (**Figure 1.10A-C**). These surfaces also showed low hemolysis ratio indicating better hemocompatibility compared to other surfaces.

Another biopolymer largely employed to introduce cell recognition sites to the biomaterial surface is chitosan. Chitosan has excellent biocompatibility properties, and its positive charges allows it to be combined with heparin via LbL technique. Zhang *et al.* investigated the immobilization of heparin and chitosan on titanium to improve hemocompatibility and antibacterial activities (**Figure 1.10D-F**) [111]. They showed that these surfaces were able to prevent protein absorption, platelet adhesion, and blood clot mass. Vyas *et al.* also developed a biofunctionalization of titanium with chitosan/hydroxyapatite via silanization [120]. Hydroxyapatite is a bioactive ceramic largely used for biomaterial applications due to its similarity with natural bone [121]. These surfaces were able to significant decrease in hemolysis percentage in comparison with cpTi [120].

Zwitterionic polymers are known to be resistant to protein adsorption due to ionic interactions that rapidly creates a hydration layer on the surface [68]. Zwitterionic molecules have equal anion and cation groups on its chains, which make them highly hydrophilic and with natural antifouling properties [122]. Sabino *et al.* showed that the combination of a cationic tannin derivative (tanfloc) with heparin by LbL assembly significant decrease factor XII activation, and platelet adhesion and activation [109]. The zwitterionic-like properties of tanfloc are able to prevent blood protein adsorption and heparin acts to inhibit the coagulation cascade activation [123]. They developed tanfloc/heparin polyelectrolyte multilayers on titania nanotubes array surfaces to enhance blood compatibility and antibacterial properties [109]. The tanfloc/heparin coated nanotube arrays were hydrophilic in nature and displayed significant decrease in fibrinogen adsorbed, Factor XII activation and platelet adhesion and activation (**Figure 1.10G-I**). These surfaces also reduced bacterial adhesion and proliferation further indicating no biofilm formation. These surfaces hence enhanced blood compatibility and antibacterial properties on titanium surfaces.

Jia *et al.* modified TiO<sub>2</sub> nanotubes with two types of zwitterionic polymers, poly(sulfobetaine methacrylate) and poly(carboxybetaine methacrylate), using atom transfer radical polymerization technique [124]. Both polymer brushes reduced adsorption of albumin and fibrinogen protein to the surface compared to TiO<sub>2</sub> nanotubes. The FITR results showed that the adsorbed albumin on the polymer coated surface had a significantly different secondary structure, which reduced platelet adhesion and activation, In contrary, the TiO<sub>2</sub> nanotubes surface adsorbed albumin showed no structure change [124].

Cheng *et al.* conjugated natural tannic acid (TA) and silk sericin (SS) via hydrogen bonding interactions and the resulting TA/SS conjugates were deposited on the titanium surfaces through

surface adhesive trihydroxyphenyl groups in TA [125]. TA and its derivatives are widely used as a primer for immobilization of other molecules due to the presence of phenolic hydroxyl groups that could act hydrogen bond donor [126]. The TA/SS coated surfaces were hydrophilic in nature. These surfaces were repellent to proteins, showed lower platelet adhesion and anti-adhesive bacterial properties (**Figure 1.10J-L**). These surfaces further showed low cytotoxicity towards fibroblast cells indicating overall biocompatibility.

Lee & Kang used a green seaweed derived polysaccharide ulvan to enhance blood compatibility of Ti/TiO<sub>2</sub> surfaces [127]. Tannic acid was used for surface coating and subsequent grafting of ulvan onto to the surface. Ulvan is a sulfated polysaccharide that has recently attracted attention due to its antioxidant, antiviral, and anti-adhesive properties [128]. The results indicated that the ulvan coated surfaces were superhydrophilic in nature and resulted in significant reduction in fibrinogen adsorption and platelet adhesion, thus enhancing hemocompatibility (**Figure 1.10M-O**).

Chen *et al.* prepared functional titanium surfaces with carboxylic terminated PEG<sub>600</sub>/PEG<sub>400</sub> and CD34 antibodies and evaluated such surfaces for hemocompatibility [129]. The titanium surfaces were initially hydroxylated and further aminosilanized which was further used for covalently grafting of polyethylene glycol and the antibody. The CD34 antibody were immobilized on the surface to attract endothelial progenitor cells (EPCs) directly from the bloodstream [129]. The *in vitro* platelet adhesion tests confirmed superior hemocompatibility and enhanced endothelialization when compared to control surfaces.

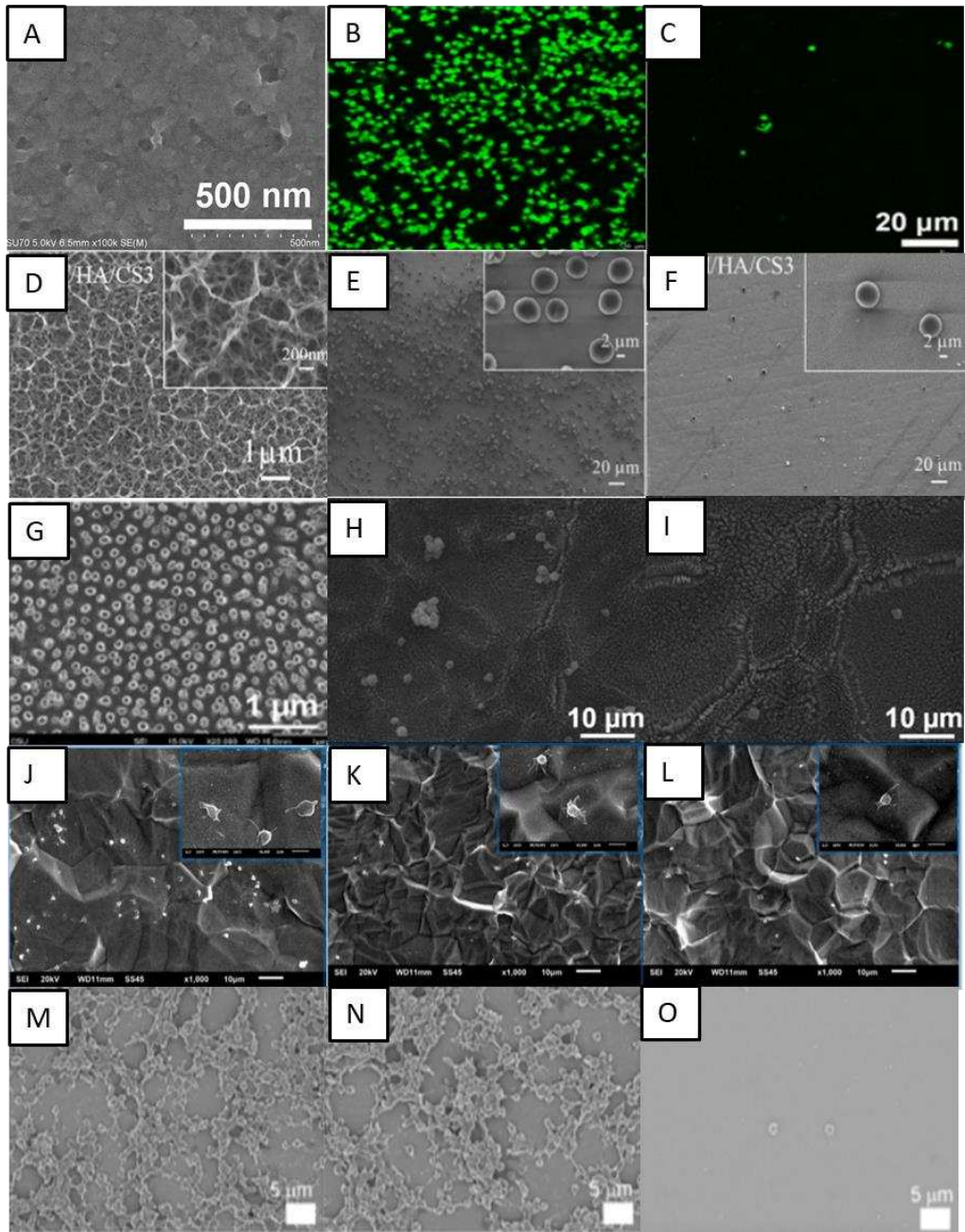


**Figure 1.10.** A) SEM image indicating surface microtopography of titanium surface modified with PTL/heparin. B-C) Fluorescence images indicating adhesion of platelets on bare titanium and titanium modified with PTL/heparin, respectively [119]. Adapted with permission from ref. 119. Copyright 2019, Elsevier. D) SEM images indicating morphology of titanium surfaces modified with heparin/chitosan. E-F) SEM images indicating platelet adhesion on titanium and titanium surfaces modified with heparin/chitosan, respectively [111]. Adapted with permission from ref. 111. Copyright 2018, Elsevier. G) SEM image indicating titania nanotube surfaces modified with tanfloc/heparin polyelectrolyte multilayers. H-I) SEM images indicating platelet adhesion on unmodified titania nanotube surfaces and titania nanotube surfaces modified with tanfloc/heparin,

respectively [109]. Adapted with permission from ref. 109. Copyright 2020, Wiley-VCH. J-L) SEM images indicating platelet adhesion on pristine titanium, TA/SS 1, and TA/SS 2 coated surfaces – 1 and 2 indicating different volume ratios [125]. Adapted with permission from ref. 125. Copyright 2020, Elsevier. M-O) SEM images indicating platelet adhesion on non-treated, tannic acid-treated, and ulvan-coated Ti/TiO<sub>2</sub> surfaces, respectively [127]. Adapted with permission from ref. 127. Copyright 2020, Elsevier.

Wu *et al.* fabricated quercetin-loaded chitosan nanoparticles and using LbL self-assembly technique coated titanium substrates with five and ten bilayers of hyaluronan and quercetin-loaded chitosan nanoparticles [130]. Quercetin is a naturally occurring flavonoid that has been shown to have anticoagulants effects similar to heparin. The 10-bilayer modified surface with quercetin-loaded chitosan as the top layer reduced platelet adhesion compared to control titanium surface and 5-bilayer surface with hyaluronan as the top layer. This indicates that quercetin-loaded chitosan improved anticoagulation [130].

Llopis-Grimalt *et al.* modified the titanium surface to improve tissue response to stents using two different approaches, the use of nanostructuring by electrochemical anodization and the addition of quercitrin to the titanium surface [131]. Quercitrin, a glycoside formed from the flavonoid quercetin, has shown enhanced cell differentiation and anti-inflammatory activity when immobilized on titanium surfaces [132]. The surfaces were investigated for cell adhesion, cytotoxicity, nitric oxide production and metabolic activity using primary human umbilical cord endothelial cell. Platelet adhesion, hemolysis rate, and bacterial adhesion were also analyzed. The results indicated all surfaces were biocompatible, with no hemolysis rate, and the nanostructured surfaces displayed lower platelet adhesion. The nanostructure surfaces coated with quercitrin also showed enhanced endothelialization and lower bacterial adhesion as well as able to prevent thrombosis, thus being a promising approach to improve biocompatibility of bare metal stents.

#### 1.4.2.6 Bio-inspired surfaces

The endothelial monolayer in blood vessels provides the perfect environment of blood compatibility. Blood flows inside them without any attraction or thrombus formation. The endothelial cells that line the interior surface of healthy blood vessels prevent blood clotting by several mechanisms, such as nitric oxide (NO) release or recruitment of heparan sulfate [133]. The endothelial inner lining is composed by a layer called glycocalyx, which is rich in proteoglycans bearing glycosaminoglycan (GAG). Recent research has been focusing on creating multifunction surfaces that can mimic the endothelium environment. Simon-Walker *et al.* coated TiO<sub>2</sub> nanotubes (TiO<sub>2</sub>NT) with heparin-chitosan polyelectrolyte multilayers (PEM) to provide a glycosaminoglycan functionalization [134]. These surfaces when then modified with a NO-donor chemistry to provide an important antithrombotic signal. Combination of surface nanotopography, GAG-based surfaces, with NO-donor chemistry demonstrated substantial reduction in platelet adhesion and activation compared to unmodified TiO<sub>2</sub> surfaces (**Figure 1.11A-G**).

Liu *et al.* developed a multifunctional titanium surface for simultaneous enhancement of endothelial cell selectivity and hemocompatibility. The surface was prepared by conjugation of REDV peptide to a surface grafted PEGMA polymer brushes via surface-initiated atom transfer radical polymerization on a dopamine-modified titanium surface [135]. This surface showed improved endothelial cell selectivity and hemocompatibility, with reduced platelet adhesion when compared to pristine titanium.

Han *et al.* prepared a nature inspired extracellular matrix (ECM) coating on titanium surface by culturing/deculturizing smooth muscle cells (SCM) and endothelial cells (EC) controlled by hyaluronic acid (HA) micro-pattern [136]. This double deck ECM coating showed higher ECM density, different wettability's and larger pore sizes which lead to better

hemocompatibility, anti-inflammation, tissue compatibility and pro-endothelialization (**Figure 1.11H-R**). The ECM coating maximized the reproducibility of structure and functionality of vascular basement membrane.

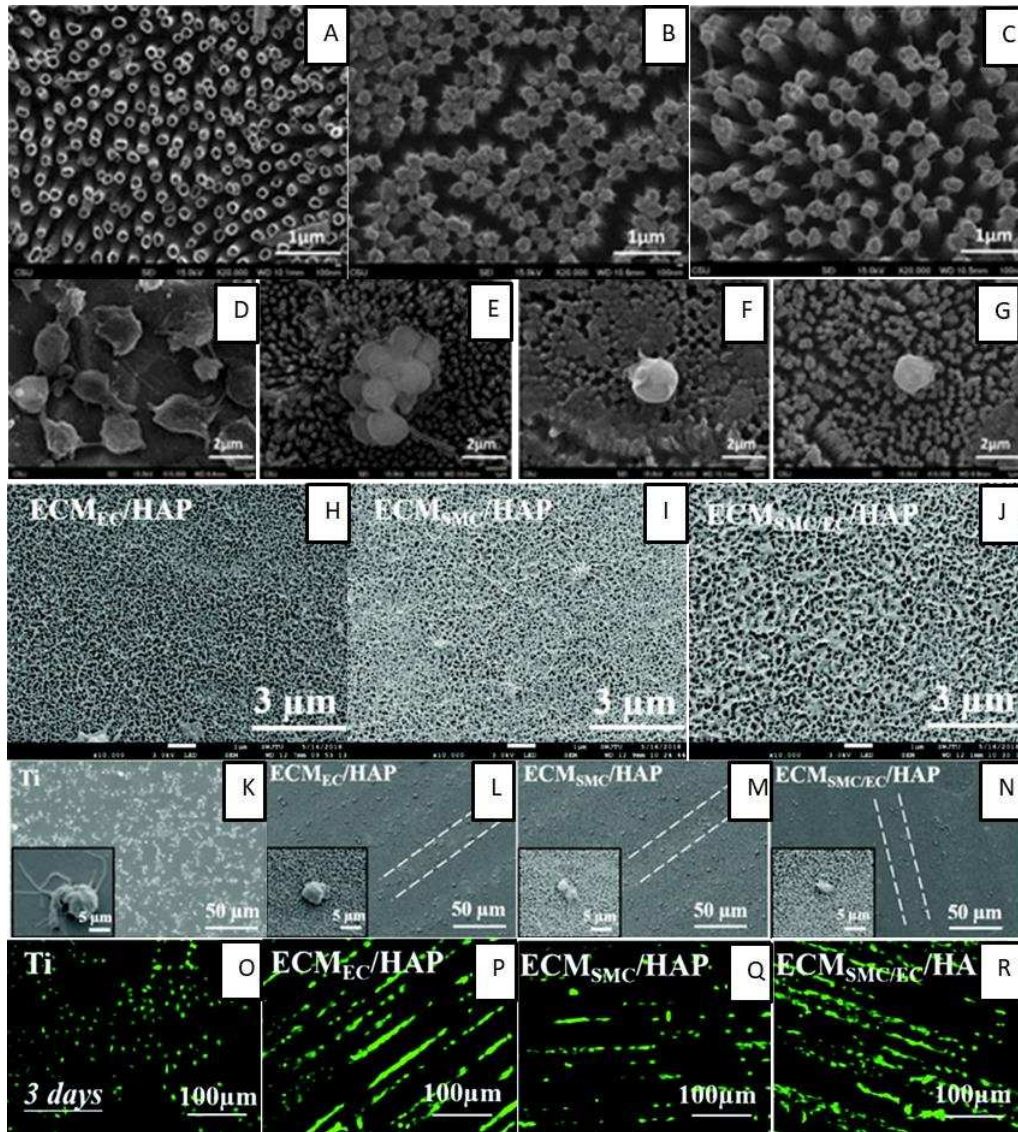


**Figure 1.11.** A-C) SEM images indicating  $\text{TiO}_2\text{NT}$ ,  $\text{TiO}_2\text{NT}+\text{PEM}$  and  $\text{TiO}_2\text{NT}+\text{PEM}+\text{NO}$  surfaces. D-G) SEM images indicating adhered cells on bare titanium,  $\text{TiO}_2\text{NT}$ ,  $\text{TiO}_2\text{NT}+\text{PEM}$  and  $\text{TiO}_2\text{NT}+\text{PEM}+\text{NO}$  surfaces [134]. Adapted with permission from ref. 134. Copyright 2017, American Chemical Society. H-J) SEM images indicating surface morphology of HA micro-patterned titanium surfaces modified with EC-ECM ( $\text{ECM}_{\text{EC}}/\text{HAP}$ ), SMC-ECM ( $\text{ECM}_{\text{SMC}}/\text{HAP}$ ), and modified by both SMC-ECM and EC-ECM ( $\text{ECM}_{\text{SMC}/\text{EC}}/\text{HAP}$ ) respectively [136]. K-N) SEM images indicating platelet adhesion on respective surfaces [136]. O-R) Fluorescence images indicating growth of HUVEC cells after 3 days on respective surfaces [136].

Wang *et al.* also prepared an ECM inspired surface by functionalization with heparin, fibronectin, and VEGF on titanium surface to construct a multifunctional microenvironment to inhibit thrombus formation [137]. The modified surfaces significantly enhanced the AT III binding density and prolonged clotting time. The *in vitro* platelet study also indicated favorable anticoagulant properties thus indicating the heparin/fibronectin/VEGF multifunctional coating was successfully constructed with desirable anticoagulant properties. In addition, these surfaces promoted enhanced proliferation of EPCs and ECs, thus accelerating endothelialization.

## **1.5. Conclusions and Future Perspectives**

Blood is a complex smart liquid which can perform various necessary functions needed for our body functionality. However, one of its main properties is to clot when exposed to a foreign environment/material and this property poses a major concern when an implant is introduced into human body. Hence, researchers have been exploring different techniques to enhance hemocompatibility of implant surfaces. Design of hemocompatible titanium surfaces can be achieved by understanding the blood kinetics and the series of reactions taking place due to blood proteins, cells, and platelets which leads to thrombus formation and inflammation. The influence of implant surface properties such as chemistry, morphology, crystallinity, charge, and wettability has shown to be significant, and various studies have been carried out to develop surfaces with improved hemocompatibility.

Different techniques for surface modification reviewed in this chapter has shown that hemocompatibility can be improved with surfaces imitating the vascular environment with surface morphology/chemistry, repelling blood protein interaction, anticoagulant drug loading and NO release. However, it is noticed that the combination of these properties enhances

hemocompatibility significantly. The key aspect to be more focused is durability and longevity of the surface modification, commercialization potential and more realistic testing methods.

Hundreds of new surface modification techniques are proposed, studied, and published annually. However, most of the studies focuses on the evaluation of platelet adhesion and activation, protein adsorption, and hemolysis and coagulation tests. It is critical that researchers also investigate the contact and complement activation of the surfaces as they are important aspects of blood compatibility. In addition, most of the surface are evaluated in *in vitro* conditions with isolated blood components for a short duration of time. In reality, implants are present inside human body, with blood constantly flowing over the surface for longer periods. Hence, it is important to evaluate surfaces under dynamic conditions and more *in vivo* evaluations need to be done to understand the surface hemocompatibility. Besides that, implant surfaces are generally evaluated using human blood from healthy donors. In the current era, with advancement in biomedical sciences, implants are used by patients from different age groups and these humans also possess other diseases or complications that can alter immune reactions to implants. Hence, it is important to perform hemocompatibility studies considering different scenarios.

Titanium will continue to play an important role in blood-contacting implants for the foreseeable future. Although titanium has proven to be an excellent material for implants, there are still significant problems such thrombosis and restenosis due to undesirable blood-surface interactions. Over the years several approaches have been proposed to enhance the surface properties of titanium-based materials to prevent thrombus formation. Some of them are based on creating micro/nano-scale topography meanwhile others proposed the surface chemistry modification. The combination of both strategies, which makes possible the tailoring the surface characteristics, such as wettability, roughness, surface charge, and crystallinity, has been shown to

make the surface more compatible with blood and its components. Another promising approach is the immobilization of bioactive molecules on titanium surface, such as polysaccharides, peptides, and antibodies, which improves the blood-biomaterial response by using agents that are similar to the ones present in the body.

Recent research has also focused on the development of multifunctional titanium surfaces with the aim to mimic the endothelium environment. By modifying these surfaces through physical, chemical, and biological processes, the biomaterial would be able to not only prevent thrombogenic and inflammatory responses, but also stimulate endothelial cell adhesion, migration, and proliferation, and eventually build an endothelial layer on the titanium surfaces. In the near future, the new generation of titanium-based biomaterials should take advantage of the current state of the art to further improve the blood-surface interaction and develop a truly hemocompatible titanium surface. We believe that this review contributed to provide guidelines for the development of new and enhanced titanium-based surfaces for blood-contacting implants.

## REFERENCES

- [1] V.K. Manivasagam, R.M. Sabino, P. Kantam, K.C. Papat, Surface modification strategies to improve titanium hemocompatibility: a comprehensive review, *Mater. Adv.* 2 (2021) 5824–5842. doi:10.1039/d1ma00367d.
- [2] A.M. Khorasani, M. Goldberg, E.H. Doeven, G. Littlefair, Titanium in biomedical applications—properties and fabrication: A review, *J. Biomater. Tissue Eng.* 5 (2015) 593–619. doi:10.1166/jbt.2015.1361.
- [3] M.T. Kalathottukaren, J.N. Kizhakkedathu, Mechanisms of blood coagulation in response to biomaterials: Extrinsic factors, in: *Hemocompatibility Biomater. Clin. Appl. Blood-Biomaterials Interact.*, Elsevier, 2018: pp. 29–49. doi:10.1016/B978-0-08-100497-5.00003-3.
- [4] I.H. Jaffer, J.C. Fredenburgh, J. Hirsh, J.I. Weitz, Medical device-induced thrombosis: what causes it and how can we prevent it?, *J. Thromb. Haemost.* 13 (2015) S72–S81. doi:10.1111/jth.12961.
- [5] X.R. Xu, N. Carrim, M.A. Dias Neves, T. Mckeown, T.W. Stratton, R. Matos, P. Coelho, X. Lei, P. Chen, J. Xu, X. Dai, B.X. Li, H. Ni, Platelets and platelet adhesion molecules: novel mechanisms of thrombosis and anti-thrombotic therapies, *Thromb. J.* 14 (2016) 29. doi:10.1186/s12959-016-0100-6.
- [6] I.H. Jaffer, J.I. Weitz, The blood compatibility challenge. Part 1: Blood-contacting medical devices: The scope of the problem, *Acta Biomater.* 94 (2019) 2–10. doi:10.1016/j.actbio.2019.06.021.
- [7] J.L. Brash, T.A. Horbett, R.A. Latour, P. Tengvall, The blood compatibility challenge. Part 2: Protein adsorption phenomena governing blood reactivity, *Acta Biomater.* 94 (2019) 11–24. doi:10.1016/j.actbio.2019.06.022.
- [8] L.P. Dasi, H.A. Simon, P. Sucusky, A.P. Yoganathan, Fluid mechanics of artificial heart valves, *Clin. Exp. Pharmacol. Physiol.* 36 (2009) 225–237. doi:10.1111/j.1440-1681.2008.05099.x.
- [9] G.H. Kim, D.H. Yang, J.W. Kang, D.H. Kim, S.H. Jung, T.H. Lim, Subvalvular pannus and thrombosis in a mitral valve prosthesis, *J. Cardiovasc. Comput. Tomogr.* 10 (2016) 191–192. doi:10.1016/j.jcct.2015.09.004.
- [10] N. Uriel, J. Han, K.A. Morrison, N. Nahumi, M. Yuzefpolskaya, A.R. Garan, J. Duong, P.C. Colombo, H. Takayama, S. Thomas, Y. Naka, U.P. Jorde, Device thrombosis in HeartMate II continuous-flow left ventricular assist devices: A multifactorial phenomenon, *J. Hear. Lung Transplant.* 33 (2014) 51–59. doi:10.1016/j.healun.2013.10.005.
- [11] M. Bakir, Haemocompatibility of titanium and its alloys, *J. Biomater. Appl.* 27 (2012) 3–15. doi:10.1177/0885328212439615.
- [12] S.A. Smith, R.J. Travers, J.H. Morrissey, How it all starts: Initiation of the clotting cascade, *Crit. Rev. Biochem. Mol. Biol.* 50 (2015) 326–336. doi:10.3109/10409238.2015.1050550.
- [13] N. Mackman, Triggers, targets and treatments for thrombosis, *Nature.* 451 (2008) 914–918. doi:10.1038/nature06797.
- [14] V.K. Manivasagam, K.C. Papat, Hydrothermally treated titanium surfaces for enhanced

- osteogenic differentiation of adipose derived stem cells, *Mater. Sci. Eng. C.* 128 (2021) 112315. doi:10.1016/J.MSEC.2021.112315.
- [15] J. Vishnu, V. K Manivasagam, V. Gopal, C. Bartomeu Garcia, P. Hameed, G. Manivasagam, T.J. Webster, Hydrothermal treatment of etched titanium: A potential surface nano-modification technique for enhanced biocompatibility, *Nanomedicine Nanotechnology, Biol. Med.* 20 (2019) 102016. doi:10.1016/j.nano.2019.102016.
- [16] H.J. Rack, J.I. Qazi, Titanium alloys for biomedical applications, *Mater. Sci. Eng. C.* 26 (2006) 1269–1277. doi:10.1016/j.msec.2005.08.032.
- [17] F. Zhang, Z. Zhang, X. Zhu, E.T. Kang, K.G. Neoh, Silk-functionalized titanium surfaces for enhancing osteoblast functions and reducing bacterial adhesion, *Biomaterials.* 29 (2008) 4751–4759. doi:10.1016/j.biomaterials.2008.08.043.
- [18] S. Lee, Y.Y. Chang, J. Lee, S.K. Madhurakkat Perikamana, E.M. Kim, Y.H. Jung, J.H. Yun, H. Shin, Surface engineering of titanium alloy using metal-polyphenol network coating with magnesium ions for improved osseointegration, *Biomater. Sci.* 8 (2020) 3404–3417. doi:10.1039/d0bm00566e.
- [19] M. Kulkarni, A. Mazare, E. Gongadze, Perutkova, V. Kralj-Iglic, I. Milošev, P. Schmuki, A. Iglič, M. Mozetič, Titanium nanostructures for biomedical applications, *Nanotechnology.* 26 (2015) 062002. doi:10.1088/0957-4484/26/6/062002.
- [20] M. Kaur, K. Singh, Review on titanium and titanium based alloys as biomaterials for orthopaedic applications, *Mater. Sci. Eng. C.* 102 (2019) 844–862. doi:10.1016/J.MSEC.2019.04.064.
- [21] A. Dehghanhadikolaei, H. Ibrahim, A. Amerinatanzi, M. Hashemi, N.S. Moghaddam, M. Elahinia, Improving corrosion resistance of additively manufactured nickel–titanium biomedical devices by micro-arc oxidation process, *J. Mater. Sci.* 54 (2019) 7333–7355. doi:10.1007/s10853-019-03375-1.
- [22] A.T. Sidambe, Biocompatibility of advanced manufactured titanium implants-A review, *Materials (Basel).* 7 (2014) 8168–8188. doi:10.3390/ma7128168.
- [23] N. Eliaz, Corrosion of Metallic Biomaterials: A Review, *Materials (Basel).* 12 (2019) 407. doi:10.3390/ma12030407.
- [24] R. Zhang, X. Ai, Y. Wan, Z. Liu, D. Zhang, S. Feng, Surface Corrosion Resistance in Turning of Titanium Alloy, *Int. J. Corros.* 2015 (2015) 1–8. doi:10.1155/2015/823172.
- [25] J.C.M. Souza, M.B. Sordi, M. Kanazawa, S. Ravindran, B. Henriques, F.S. Silva, C. Aparicio, L.F. Cooper, Nano-scale modification of titanium implant surfaces to enhance osseointegration, *Acta Biomater.* 94 (2019) 112–131. doi:10.1016/j.actbio.2019.05.045.
- [26] G. Wang, J. Li, K. Lv, W. Zhang, X. Ding, G. Yang, X. Liu, X. Jiang, Surface thermal oxidation on titanium implants to enhance osteogenic activity and in vivo osseointegration, *Sci. Rep.* 6 (2016) 1–13. doi:10.1038/srep31769.
- [27] M.L. Teffo, N.E. Nyakane, M. Seerane, M.B. Shongwe, R. Machaka, The effect of alloying elements on densification and mechanical behaviour of titanium based alloy, in: *Mater. Today Proc.*, Elsevier, 2021: pp. 1203–1208. doi:10.1016/j.matpr.2020.09.280.
- [28] D. Banerjee, J.C. Williams, Perspectives on titanium science and technology, *Acta Mater.* 61 (2013) 844–879. doi:10.1016/j.actamat.2012.10.043.
- [29] E. Alabort, D. Barba, M.R. Shagiev, M.A. Murzinova, R.M. Galejev, O.R. Valiakhmetov, A.F. Aletdinov, R.C. Reed, Alloys-by-design: Application to titanium alloys for optimal superplasticity, *Acta Mater.* 178 (2019) 275–287. doi:10.1016/j.actamat.2019.07.026.
- [30] Y. Oshida, Materials Classification, in: *Biosci. Bioeng. Titan. Mater.*, Elsevier, 2013: pp.

- 9–34. doi:10.1016/b978-0-444-62625-7.00002-9.
- [31] Y. Li, C. Yang, H. Zhao, S. Qu, X. Li, Y. Li, New developments of ti-based alloys for biomedical applications, *Materials (Basel)*. 7 (2014) 1709–1800. doi:10.3390/ma7031709.
- [32] M. Özcan, C. Hämmerle, Titanium as a reconstruction and implant material in dentistry: Advantages and pitfalls, *Materials (Basel)*. 5 (2012) 1528–1545. doi:10.3390/ma5091528.
- [33] B.S. Smith, S. Yoriya, L. Grissom, C.A. Grimes, K.C. Popat, Hemocompatibility of titania nanotube arrays, *J. Biomed. Mater. Res. - Part A*. 95 A (2010) 350–360. doi:10.1002/jbm.a.32853.
- [34] V.B. Damodaran, D. Bhatnagar, V. Leszczak, K.C. Popat, Titania nanostructures: A biomedical perspective, *RSC Adv*. 5 (2015) 37149–37171. doi:10.1039/c5ra04271b.
- [35] Y. Cheng, H. Yang, Y. Yang, J. Huang, K. Wu, Z. Chen, X. Wang, C. Lin, Y. Lai, Progress in TiO<sub>2</sub> nanotube coatings for biomedical applications: a review, *J. Mater. Chem. B*. 6 (2018) 1862–1886. doi:10.1039/C8TB00149A.
- [36] V. Balan, L. Verestiuc, Strategies to improve chitosan hemocompatibility: A review, *Eur. Polym. J*. 53 (2014) 171–188. doi:10.1016/j.eurpolymj.2014.01.033.
- [37] M.B. Gorbet, M. V. Sefton, Biomaterial-associated thrombosis: Roles of coagulation factors, complement, platelets and leukocytes, *Biomater. Silver Jubil. Compend*. 25 (2004) 219–241. doi:10.1016/B978-008045154-1.50025-3.
- [38] L. Chen, D. Han, L. Jiang, On improving blood compatibility: From bioinspired to synthetic design and fabrication of biointerfacial topography at micro/nano scales, *Colloids Surfaces B Biointerfaces*. 85 (2011) 2–7. doi:10.1016/J.COLSURFB.2010.10.034.
- [39] H.S. Lee, N. Tomczyk, J. Kandel, R.J. Composto, D.M. Eckmann, Hemocompatibility of chitosan/poly(acrylic acid) grafted polyurethane tubing, *J. Mater. Chem. B*. 1 (2013) 6382–6391. doi:10.1039/c3tb21218a.
- [40] L.C. Xu, J.W. Bauer, C.A. Siedlecki, Proteins, platelets, and blood coagulation at biomaterial interfaces, *Colloids Surfaces B Biointerfaces*. 124 (2014) 49–68. doi:10.1016/j.colsurfb.2014.09.040.
- [41] C.J. Wilson, R.E. Clegg, D.I. Leavesley, M.J. Pearcy, Mediation of biomaterial-cell interactions by adsorbed proteins: A review, *Tissue Eng*. 11 (2005) 1–18. doi:10.1089/ten.2005.11.1.
- [42] P. Roach, D. Farrar, C.C. Perry, Interpretation of protein adsorption: Surface-induced conformational changes, *J. Am. Chem. Soc*. 127 (2005) 8168–8173. doi:10.1021/ja042898o.
- [43] S.Y. Jung, S.M. Lim, F. Albertorio, G. Kim, M.C. Gurau, R.D. Yang, M.A. Holden, P.S. Cremer, The Vroman Effect: A Molecular Level Description of Fibrinogen Displacement, *J. Am. Chem. Soc*. 125 (2003) 12782–12786. doi:10.1021/ja037263o.
- [44] X. Liu, L. Yuan, D. Li, Z. Tang, Y. Wang, G. Chen, H. Chen, J.L. Brash, Blood compatible materials: state of the art, *J. Mater. Chem. B*. 2 (2014) 5709–5926. www.rsc.org/MaterialsB (accessed July 10, 2018).
- [45] L.C. Xu, J.W. Bauer, C.A. Siedlecki, Proteins, platelets, and blood coagulation at biomaterial interfaces, *Colloids Surfaces B Biointerfaces*. 124 (2014) 49–68. doi:10.1016/j.colsurfb.2014.09.040.
- [46] C. Sperling, M. Fischer, M.F. Maitz, C. Werner, Blood coagulation on biomaterials requires the combination of distinct activation processes, *Biomaterials*. 30 (2009) 4447–4456. doi:10.1016/J.BIOMATERIALS.2009.05.044.

- [47] Z. Guo, K.M. Bussard, K. Chatterjee, R. Miller, E.A. Vogler, C.A. Siedlecki, Mathematical modeling of material-induced blood plasma coagulation, *Biomaterials*. 27 (2006) 796–806. doi:10.1016/j.biomaterials.2005.06.021.
- [48] R.M. Sabino, K. Kauk, S. Movafaghi, A. Kota, K.C. Popat, Interaction of blood plasma proteins with superhemophobic titania nanotube surfaces, *Nanomedicine Nanotechnology, Biol. Med.* 21 (2019) 102046. doi:10.1016/J.NANO.2019.102046.
- [49] A. De Mel, B.G. Cousins, A.M. Seifalian, Surface modification of biomaterials: A quest for blood compatibility, *Int. J. Biomater.* (2012) 1–8. doi:10.1155/2012/707863.
- [50] K. Chatterjee, Z. Guo, E.A. Vogler, C.A. Siedlecki, Contributions of contact activation pathways of coagulation factor XII in plasma, *J. Biomed. Mater. Res. - Part A*. 90 (2009) 27–34. doi:10.1002/jbm.a.32076.
- [51] J.L. Brash, T.A. Horbett, R.A. Latour, P. Tengvall, The blood compatibility challenge. Part 2: Protein adsorption phenomena governing blood reactivity, *Acta Biomater.* 94 (2019) 11–24. doi:10.1016/j.actbio.2019.06.022.
- [52] M. Gorbet, C. Sperling, M.F. Maitz, C.A. Siedlecki, C. Werner, M. V. Sefton, The blood compatibility challenge. Part 3: Material associated activation of blood cascades and cells, *Acta Biomater.* 94 (2019) 25–32. doi:10.1016/j.actbio.2019.06.020.
- [53] F. Poppelaars, B. Faria, M.G. da Costa, C.F.M. Franssen, W.J. van Son, S.P. Berger, M.R. Daha, M.A. Seelen, The complement system in dialysis: A forgotten story?, *Front. Immunol.* 9 (2018) 71. doi:10.3389/fimmu.2018.00071.
- [54] Y. Yan, L.C. Xu, E.A. Vogler, C.A. Siedlecki, Contact activation by the intrinsic pathway of blood plasma coagulation, in: *Hemocompatibility Biomater. Clin. Appl. Blood-Biomaterials Interact.*, Elsevier, 2018: pp. 3–28. doi:10.1016/B978-0-08-100497-5.00001-X.
- [55] A. Thor, L. Rasmusson, A. Wennerberg, P. Thomsen, J.-M. Hirsch, B. Nilsson, J. Hong, The role of whole blood in thrombin generation in contact with various titanium surfaces, *Biomaterials*. 28 (2007) 966–974. doi:10.1016/J.BIOMATERIALS.2006.10.020.
- [56] X.R. Xu, N. Carrim, M.A.D. Neves, T. McKeown, T.W. Stratton, R.M.P. Coelho, X. Lei, P. Chen, J. Xu, X. Dai, B.X. Li, H. Ni, Platelets and platelet adhesion molecules: Novel mechanisms of thrombosis and anti-thrombotic therapies, *Thromb. J.* 14 (2016) 29. doi:10.1186/s12959-016-0100-6.
- [57] R. Biran, D. Pond, Heparin coatings for improving blood compatibility of medical devices, *Adv. Drug Deliv. Rev.* 112 (2017) 12–23. doi:10.1016/j.addr.2016.12.002.
- [58] Y.K. Kim, E.Y. Chen, W.F. Liu, Biomolecular strategies to modulate the macrophage response to implanted materials, *J. Mater. Chem. B*. 4 (2016) 1600–1609. doi:10.1039/c5tb01605c.
- [59] U.T. Seyfert, V. Biehl, J. Schenk, In vitro hemocompatibility testing of biomaterials according to the ISO 10993-4, in: *Biomol. Eng.*, Elsevier, 2002: pp. 91–96. doi:10.1016/S1389-0344(02)00015-1.
- [60] V. Balan, L. Verestiuc, Strategies to improve chitosan hemocompatibility: A review, *Eur. Polym. J.* 53 (2014) 171–188. doi:10.1016/j.eurpolymj.2014.01.033.
- [61] L.Y.C. Madruga, R.M. Sabino, E.C.G. Santos, K.C. Popat, R. de C. Balaban, M.J. Kipper, Carboxymethyl-kappa-carrageenan: A study of biocompatibility, antioxidant and antibacterial activities, *Int. J. Biol. Macromol.* 152 (2020) 483–491. doi:10.1016/j.ijbiomac.2020.02.274.
- [62] R. Sabino, K. Popat, Evaluating Whole Blood Clotting in vitro on Biomaterial Surfaces,

- BIO-PROTOCOL. 10 (2020) e3505. doi:10.21769/bioprotoc.3505.
- [63] P. Gill, V. Musaramthota, N. Munroe, A. Datye, R. Dua, W. Haider, A. McGoron, R. Rokicki, Surface modification of Ni-Ti alloys for stent application after magnetoelectropolishing, *Mater. Sci. Eng. C*. 50 (2015) 37–44. doi:10.1016/j.msec.2015.01.009.
- [64] B.S. Smith, K.C. Papat, Titania Nanotube Arrays as Interfaces for Blood-Contacting Implantable Devices, (2012) 642–658.
- [65] J.L. Chen, Q.L. Li, J.Y. Chen, C. Chen, N. Huang, Improving blood-compatibility of titanium by coating collagen-heparin multilayers, *Appl. Surf. Sci.* 255 (2009) 6894–6900. doi:10.1016/j.apsusc.2009.03.011.
- [66] S. Nie, H. Qin, C. Cheng, W. Zhao, S. Sun, B. Su, C. Zhao, Z. Gu, Blood activation and compatibility on single-molecular-layer biointerfaces, *J. Mater. Chem. B*. 2 (2014) 4911–4921. doi:10.1039/c4tb00555d.
- [67] S. Kumar, Selective Laser Sintering/Melting, in: *Compr. Mater. Process.*, Elsevier Ltd, 2014: pp. 93–134. doi:10.1016/B978-0-08-096532-1.01003-7.
- [68] X. Liu, L. Yuan, D. Li, Z. Tang, Y. Wang, G. Chen, H. Chen, J.L. Brash, Blood compatible materials: state of the art Xiaoli, *J. Mater. Chem. B*. 2 (2014) 5709–5926.
- [69] A.K. Kota, G. Kwon, A. Tuteja, The design and applications of superomniphobic surfaces, *NPG Asia Mater.* 6 (2014) 109. doi:10.1038/am.2014.34.
- [70] K.Y. Yeh, L.J. Chen, J.Y. Chang, Contact angle hysteresis on regular pillar-like hydrophobic surfaces, *Langmuir*. 24 (2008) 245–251. doi:10.1021/la7020337.
- [71] B.M.L. Koch, A. Amirfazli, J.A.W. Elliott, Modeling and measurement of contact angle hysteresis on textured high-contact-angle surfaces, *J. Phys. Chem. C*. 118 (2014) 18554–18563. doi:10.1021/jp504891u.
- [72] S. Movafaghi, W. Wang, D.L. Bark, L.P. Dasi, K.C. Papat, A.K. Kota, Hemocompatibility of super-repellent surfaces: Current and future, *Mater. Horizons*. 6 (2019) 1596–1610. doi:10.1039/c9mh00051h.
- [73] D.L. Bark, H. Vahabi, H. Bui, S. Movafaghi, B. Moore, A.K. Kota, K. Papat, L.P. Dasi, Hemodynamic Performance and Thrombogenic Properties of a Superhydrophobic Bileaflet Mechanical Heart Valve, *Ann. Biomed. Eng.* 45 (2017) 452–463. doi:10.1007/s10439-016-1618-2.
- [74] K.M. Hansson, S. Tosatti, J. Isaksson, J. Wetterö, M. Textor, T.L. Lindahl, P. Tengvall, Whole blood coagulation on protein adsorption-resistant PEG and peptide functionalised PEG-coated titanium surfaces, *Biomaterials*. 26 (2005) 861–872. doi:10.1016/j.biomaterials.2004.03.036.
- [75] C.J. Pan, Y.H. Hou, B. Bin Zhang, Y.X. Dong, H.Y. Ding, Blood compatibility and interaction with endothelial cells of titanium modified by sequential immobilization of poly (ethylene glycol) and heparin, *J. Mater. Chem. B*. 2 (2014) 892–902. doi:10.1039/c3tb21403f.
- [76] J. Herzberger, K. Niederer, H. Pohlit, J. Seiwert, M. Worm, F.R. Wurm, H. Frey, Polymerization of ethylene oxide, propylene oxide, and other alkylene oxides: Synthesis, novel polymer architectures, and bioconjugation, *Chem. Rev.* 116 (2016) 2170–2243. doi:10.1021/acs.chemrev.5b00441.
- [77] A. Rosengren, S. Oscarsson, The influence of plasma proteins on bone cell adhesion, in: *Cell. Response to Biomater.*, Elsevier Ltd., 2008: pp. 538–559. doi:10.1533/9781845695477.3.538.

- [78] D.A.H. Hanaor, C.C. Sorrell, Review of the anatase to rutile phase transformation, *J. Mater. Sci.* 46 (2011) 855–874. doi:10.1007/s10853-010-5113-0.
- [79] F. Parrino, F.R. Pomilla, G. Camera-Roda, V. Loddo, L. Palmisano, Properties of titanium dioxide, in: *Titan. Dioxide Its Appl.*, Elsevier, 2021: pp. 13–66. doi:10.1016/b978-0-12-819960-2.00001-8.
- [80] H.N. Pantaroto, J.M. Cordeiro, L.T. Pereira, A.B. de Almeida, F.H. Nociti Junior, E.C. Rangel, N.F. Azevedo Neto, J.H.D. da Silva, V.A.R. Barão, Sputtered crystalline TiO<sub>2</sub> film drives improved surface properties of titanium-based biomedical implants, *Mater. Sci. Eng. C.* 119 (2021) 111638. doi:10.1016/j.msec.2020.111638.
- [81] H.-J. Chiang, H.-H. Chou, K.-L. Ou, E. Sugiatno, M. Ruslin, R.A. Waris, C.-F. Huang, C.-M. Liu, P.-W. Peng, Evaluation of Surface Characteristics and Hemocompatibility on the Oxygen Plasma-Modified Biomedical Titanium, *Metals (Basel)*. 8 (2018) 513. doi:10.3390/met8070513.
- [82] M. Erofeev, V. Ripenko, M. Shulepov, V. Tarasenko, Surface treatment of metals in the plasma of a nanosecond diffuse discharge at atmospheric pressure, *Eur. Phys. J. D.* 71 (2017) 1–5. doi:10.1140/epjd/e2017-70636-6.
- [83] M. Göttlicher, M. Rohnke, A. Kunz, J. Thomas, R.A. Henning, T. Leichtweiß, T. Gemming, J. Janek, Anodization of titanium in radio frequency oxygen discharge - Microstructure, kinetics & transport mechanism, *Solid State Ionics*. 290 (2016) 130–139. doi:10.1016/j.ssi.2016.04.013.
- [84] D. Xie, G. Wan, M.F. Maitz, Y. Lei, N. Huang, H. Sun, Characterization and mechanical investigation of Ti-O<sub>2-x</sub> film prepared by plasma immersion ion implantation and deposition for cardiovascular stents surface modification, *Nucl. Instruments Methods Phys. Res. Sect. B Beam Interact. with Mater. Atoms*. 289 (2012) 91–96. doi:10.1016/j.nimb.2012.07.033.
- [85] W.C. Hung, F.M. Chang, T. Sen Yang, K.L. Ou, C.T. Lin, P.W. Peng, Oxygen-implanted induced formation of oxide layer enhances blood compatibility on titanium for biomedical applications, *Mater. Sci. Eng. C.* 68 (2016) 523–529. doi:10.1016/j.msec.2016.06.024.
- [86] M. Klein, Y. Kuhn, E. Woelke, T. Linde, C. Ptock, A. Kopp, T. Bletek, T. Schmitz-Rode, U. Steinseifer, J. Arens, J.C. Clauser, In vitro study on the hemocompatibility of plasma electrolytic oxidation coatings on titanium substrates, *Artif. Organs*. 44 (2020) 419–427. doi:10.1111/aor.13592.
- [87] P. Hameed, V.K. Manivasagam, M. Sankar, K.C. Papat, G. Manivasagam, Nanofibers and Nanosurfaces, in: Springer, Singapore, 2021: pp. 107–130. doi:10.1007/978-981-33-6252-9\_4.
- [88] C.L. Wong, Y.N. Tan, A.R. Mohamed, A review on the formation of titania nanotube photocatalysts by hydrothermal treatment, *J. Environ. Manage.* 92 (2011) 1669–1680. doi:10.1016/j.jenvman.2011.03.006.
- [89] J. Vishnu, M. Calin, S. Pilz, A. Gebert, B. Kaczmarek, M. Michalska-Sionkowska, V. Hoffmann, G. Manivasagam, Superhydrophilic nanostructured surfaces of beta Ti[ $\beta$ ]29Nb alloy for cardiovascular stent applications, *Surf. Coatings Technol.* 396 (2020) 125965. doi:10.1016/j.surfcoat.2020.125965.
- [90] V.K. Manivasagam, K.C. Papat, In Vitro Investigation of Hemocompatibility of Hydrothermally Treated Titanium and Titanium Alloy Surfaces, *ACS Omega*. (2020) acsomega.0c00281. doi:10.1021/acsomega.0c00281.
- [91] Y. Cheng, H. Yang, Y. Yang, J. Huang, K. Wu, Z. Chen, X. Wang, C. Lin, Y. Lai,

- Progress in TiO<sub>2</sub> nanotube coatings for biomedical applications: A review, *J. Mater. Chem. B*. 6 (2018) 1862–1886. doi:10.1039/c8tb00149a.
- [92] K.M. Kummer, E. Taylor, T.J. Webster, Biological applications of anodized TiO<sub>2</sub> nanostructures: A review from orthopedic to stent applications, *Nanosci. Nanotechnol. Lett.* 4 (2012) 483–493. doi:10.1166/nnl.2012.1352.
- [93] I. Junkar, M. Kulkarni, M. Benčina, J. Kovač, K. Mrak-Poljšak, K. Lakota, S. Sodin-Šemrl, M. Mozetič, A. Iglič, Titanium Dioxide Nanotube Arrays for Cardiovascular Stent Applications, *ACS Omega*. 5 (2020) 7280–7289. doi:10.1021/acsomega.9b04118.
- [94] C. Pan, Y. Hu, Z. Gong, Y. Yang, S. Liu, L. Quan, Z. Yang, Y. Wei, W. Ye, Improved Blood Compatibility and Endothelialization of Titanium Oxide Nanotube Arrays on Titanium Surface by Zinc Doping, *ACS Biomater. Sci. Eng.* 6 (2020) 2072–2083. doi:10.1021/acsbiomaterials.0c00187.
- [95] Z. Gong, Y. Hu, F. Gao, L. Quan, T. Liu, T. Gong, C. Pan, Effects of diameters and crystals of titanium dioxide nanotube arrays on blood compatibility and endothelial cell behaviors, *Colloids Surfaces B Biointerfaces*. 184 (2019) 110521. doi:10.1016/j.colsurfb.2019.110521.
- [96] S. Movafaghi, W. Wang, D.L. Bark, L.P. Dasi, K.C. Papat, A.K. Kota, Hemocompatibility of super-repellent surfaces: Current and future, *Mater. Horizons*. 6 (2019) 1596–1610. doi:10.1039/c9mh00051h.
- [97] V. Jokinen, E. Kankuri, S. Hoshian, S. Franssila, R.H.A. Ras, Superhydrophobic Blood-Repellent Surfaces, *Adv. Mater.* 30 (2018) 1705104. doi:10.1002/adma.201705104.
- [98] W. Wang, K. Lockwood, L.M. Boyd, M.D. Davidson, S. Movafaghi, H. Vahabi, S.R. Khetani, A.K. Kota, Superhydrophobic Coatings with Edible Materials, *ACS Appl. Mater. Interfaces*. 8 (2016) 18664–18668. doi:10.1021/acsami.6b06958.
- [99] X. Gu, Y. Zheng, Y. Cheng, S. Zhong, T. Xi, In vitro corrosion and biocompatibility of binary magnesium alloys, *Biomaterials*. 30 (2009) 484–498. doi:10.1016/j.biomaterials.2008.10.021.
- [100] J.Y. Jiang, J.L. Xu, Z.H. Liu, L. Deng, B. Sun, S.D. Liu, L. Wang, H.Y. Liu, Preparation, corrosion resistance and hemocompatibility of the superhydrophobic TiO<sub>2</sub> coatings on biomedical Ti-6Al-4V alloys, *Appl. Surf. Sci.* 347 (2015) 591–595. doi:10.1016/j.apsusc.2015.04.075.
- [101] J. Chen, J.L. Xu, J. Huang, P. Zhang, J.M. Luo, L. Lian, Formation mechanism and hemocompatibility of the superhydrophobic surface on biomedical Ti-6Al-4V alloy, *J. Mater. Sci.* 2021 5612. 56 (2021) 7698–7709. doi:10.1007/S10853-020-05696-Y.
- [102] Y. Yang, Y. Lai, Q. Zhang, K. Wu, L. Zhang, C. Lin, P. Tang, A novel electrochemical strategy for improving blood compatibility of titanium-based biomaterials, *Colloids Surfaces B Biointerfaces*. 79 (2010) 309–313. doi:10.1016/j.colsurfb.2010.04.013.
- [103] Y. Ma, L. Jiang, J. Hu, H. Liu, S. Wang, P. Zuo, P. Ji, L. Qu, T. Cui, Multifunctional 3D Micro-Nanostructures Fabricated through Temporally Shaped Femtosecond Laser Processing for Preventing Thrombosis and Bacterial Infection, *ACS Appl. Mater. Interfaces*. 12 (2020) 17155–17166. doi:10.1021/acsami.9b20766.
- [104] S. Movafaghi, V. Leszczak, W. Wang, J.A. Sorkin, L.P. Dasi, K.C. Papat, A.K. Kota, Hemocompatibility of Superhemophobic Titania Surfaces, *Adv. Healthc. Mater.* 6 (2017) 1600717. doi:10.1002/adhm.201600717.
- [105] K. Bartlet, S. Movafaghi, A. Kota, K.C. Papat, Superhemophobic titania nanotube array surfaces for blood contacting medical devices, *RSC Adv.* 7 (2017) 35466–35476.

- doi:10.1039/C7RA03373G.
- [106] Z. Montgomerie, K.C. Popat, Improved hemocompatibility and reduced bacterial adhesion on superhydrophobic titania nanoflower surfaces, *Mater. Sci. Eng. C*. 119 (2021) 111503. doi:10.1016/j.msec.2020.111503.
- [107] S. Moradi, N. Hadjesfandiari, S.F. Toosi, J.N. Kizhakkedathu, S.G. Hatzikiriakos, Effect of Extreme Wettability on Platelet Adhesion on Metallic Implants: From Superhydrophilicity to Superhydrophobicity, *ACS Appl. Mater. Interfaces*. 8 (2016) 17631–17641. doi:10.1021/acsami.6b03644.
- [108] H.D.M. Follmann, A.F. Naves, A.F. Martins, O. Félix, G. Decher, E.C. Muniz, R. Silva, Advanced fibroblast proliferation inhibition for biocompatible coating by electrostatic layer-by-layer assemblies of heparin and chitosan derivatives, *J. Colloid Interface Sci.* 474 (2016) 9–17. doi:10.1016/j.jcis.2016.04.008.
- [109] R.M. Sabino, K. Kauk, L.Y.C. Madruga, M.J. Kipper, A.F. Martins, K.C. Popat, Enhanced hemocompatibility and antibacterial activity on titania nanotubes with tanfloc/heparin polyelectrolyte multilayers, *J. Biomed. Mater. Res. Part A*. 108 (2020) 992–1005. doi:10.1002/jbm.a.36876.
- [110] J. Chen, C. Chen, Z. Chen, J. Chen, Q. Li, N. Huang, Collagen/heparin coating on titanium surface improves the biocompatibility of titanium applied as a blood-contacting biomaterial, *J. Biomed. Mater. Res. Part A*. 95A (2010) 341–349. doi:10.1002/jbm.a.32847.
- [111] X. Zhang, G. Zhang, H. Zhang, J. Li, X. Yao, B. Tang, Surface immobilization of heparin and chitosan on titanium to improve hemocompatibility and antibacterial activities, *Colloids Surfaces B Biointerfaces*. 172 (2018) 338–345. doi:10.1016/J.COLSURFB.2018.08.060.
- [112] K. Zhang, J. ying Chen, W. Qin, J. an Li, F. xia Guan, N. Huang, Constructing bio-layer of heparin and type IV collagen on titanium surface for improving its endothelialization and blood compatibility, *J. Mater. Sci. Mater. Med.* 27 (2016) 81. doi:10.1007/s10856-016-5693-6.
- [113] W.J. Cherg, Y.H. Pan, T.C. Wu, C.C. Chou, C.H. Yeh, J.J. Ho, Hemocompatibility and adhesion of heparin/dopamine and heparin/collagen self-assembly multilayers coated on a titanium substrate, *Appl. Surf. Sci.* 463 (2019) 732–740. doi:10.1016/j.apsusc.2018.08.217.
- [114] Y. Liu, K. Ai, L. Lu, Polydopamine and its derivative materials: Synthesis and promising applications in energy, environmental, and biomedical fields, *Chem. Rev.* 114 (2014) 5057–5115. doi:10.1021/cr400407a.
- [115] Y. Yang, X. Li, H. Qiu, P. Li, P. Qi, M.F. Maitz, T. You, R. Shen, Z. Yang, W. Tian, N. Huang, Polydopamine Modified TiO<sub>2</sub> Nanotube Arrays for Long-Term Controlled Elution of Bivalirudin and Improved Hemocompatibility, *ACS Appl. Mater. Interfaces*. 10 (2017) 7649–7660. doi:10.1021/ACSAMI.7B06108.
- [116] G. Li, P. Yang, W. Qin, M.F. Maitz, S. Zhou, N. Huang, The effect of coimmobilizing heparin and fibronectin on titanium on hemocompatibility and endothelialization, *Biomaterials*. 32 (2011) 4691–4703. doi:10.1016/j.biomaterials.2011.03.025.
- [117] R. Daum, D. Visser, C. Wild, L. Kutuzova, M. Schneider, G. Lorenz, M. Weiss, S. Hinderer, U.A. Stock, M. Seifert, K. Schenke-Layland, Fibronectin Adsorption on Electrospun Synthetic Vascular Grafts Attracts Endothelial Progenitor Cells and Promotes Endothelialization in Dynamic In Vitro Culture, *Cells*. 9 (2020) 778.

- doi:10.3390/cells9030778.
- [118] G. Li, P. Yang, Y. Liao, N. Huang, Tailoring of the titanium surface by immobilization of heparin/fibronectin complexes for improving blood compatibility and endothelialization: An in vitro study, *Biomacromolecules*. 12 (2011) 1155–1168. doi:10.1021/bm101468v.
- [119] K. Xu, K. Cai, Self-assembled phase-transited lysozyme/heparin coating on titanium surfaces for improved hemocompatibility, *Mater. Lett.* 247 (2019) 95–98. doi:10.1016/j.matlet.2019.03.110.
- [120] V. Vyas, T. Kaur, S. Kar, A. Thirugnanam, Biofunctionalization of commercially pure titanium with chitosan/hydroxyapatite biocomposite via silanization: evaluation of biological performances, *J. Adhes. Sci. Technol.* 31 (2017) 1768–1781. doi:10.1080/01694243.2016.1278070.
- [121] R.M. Sabino, G. Mondini, M.J. Kipper, A.F. Martins, K.C. Papat, Tanfloc/heparin polyelectrolyte multilayers improve osteogenic differentiation of adipose-derived stem cells on titania nanotube surfaces, *Carbohydr. Polym.* 251 (2021) 117079. doi:10.1016/j.carbpol.2020.117079.
- [122] W. Lin, J. Zhang, Z. Wang, S. Chen, Development of robust biocompatible silicone with high resistance to protein adsorption and bacterial adhesion, *Acta Biomater.* 7 (2011) 2053–2059. doi:10.1016/J.ACTBIO.2011.02.001.
- [123] P.C.F. da Câmara, L.Y.C. Madruga, R.M. Sabino, J. Vlcek, R.C. Balaban, K.C. Papat, A.F. Martins, M.J. Kipper, Polyelectrolyte multilayers containing a tannin derivative polyphenol improve blood compatibility through interactions with platelets and serum proteins, *Mater. Sci. Eng. C*. 112 (2020) 110919. doi:10.1016/j.msec.2020.110919.
- [124] E. Jia, B. Liang, Y. Lin, Z. Su, Hemocompatibility of polyzwitterion-modified titanium dioxide nanotubes, *Nanotechnology*. 32 (2021) 305704. doi:10.1088/1361-6528/ABF0CB.
- [125] Y.F. Cheng, Y.H. Mei, G. Sathishkumar, Z.S. Lu, C.M. Li, F. Wang, Q.Y. Xia, L.Q. Xu, Tannic acid-assisted deposition of silk sericin on the titanium surfaces for antifouling application, *Colloids Interface Sci. Commun.* 35 (2020) 100241. doi:10.1016/j.colcom.2020.100241.
- [126] L. Meng, K. Pan, Y. Zhu, W. Wei, X. Li, X. Liu, Zwitterionic-Based Surface via the Coelectrodeposition of Colloid Particles and Tannic Acid with Bacterial Resistance but Cell Adhesion Properties, *ACS Biomater. Sci. Eng.* 4 (2018) 4122–4131. doi:10.1021/acsbiomaterials.8b01239.
- [127] A. Lee, S.M. Kang, Ultralow fouling of fibrinogen and human platelets on ulvan multilayer-coated solid surfaces, *J. Ind. Eng. Chem.* 82 (2020) 228–233. doi:10.1016/j.jiec.2019.10.017.
- [128] M.J. Stadnik, M.B. de Freitas, Algal polysaccharides as source of plant resistance inducers, *Trop. Plant Pathol.* 39 (2014) 111–118. doi:10.1590/S1982-56762014000200001.
- [129] J. Chen, J. Cao, J. Wang, M.F. Maitz, L. Guo, Y. Zhao, Q. Li, K. Xiong, N. Huang, Biofunctionalization of titanium with PEG and anti-CD34 for hemocompatibility and stimulated endothelialization, *J. Colloid Interface Sci.* 368 (2012) 636–647. doi:10.1016/j.jcis.2011.11.039.
- [130] X. Wu, C. Liu, H. Chen, Y. Zhang, L. Li, N. Tang, Layer-by-Layer Deposition of Hyaluronan and Quercetin-Loaded Chitosan Nanoparticles onto Titanium for Improving Blood Compatibility, *Coatings* 2020, Vol. 10, Page 256. 10 (2020) 256. doi:10.3390/COATINGS10030256.

- [131] M.A. Llopis-Grimalt, M.A. Forteza-Genestra, V. Alcolea-Rodriguez, J.M. Ramis, M. Monjo, Nanostructured titanium for improved endothelial biocompatibility and reduced platelet adhesion in stent applications, *Coatings*. 10 (2020) 907. doi:10.3390/COATINGS10090907.
- [132] A. Córdoba, M. Satué, M. Gómez-Florit, M. Hierro-Oliva, C. Petzold, S.P. Lyngstadaas, M.L. González-Martín, M. Monjo, J.M. Ramis, Flavonoid-Modified Surfaces: Multifunctional Bioactive Biomaterials with Osteopromotive, Anti-Inflammatory, and Anti-Fibrotic Potential, *Adv. Healthc. Mater.* 4 (2015) 540–549. doi:10.1002/adhm.201400587.
- [133] R. Luo, J. Zhang, W. Zhuang, L. Deng, L. Li, H. Yu, J. Wang, N. Huang, Y. Wang, Multifunctional coatings that mimic the endothelium: Surface bound active heparin nanoparticles with: In situ generation of nitric oxide from nitrosothiols, *J. Mater. Chem. B*. 6 (2018) 5582–5595. doi:10.1039/c8tb00596f.
- [134] R. Simon-Walker, R. Romero, J.M. Staver, Y. Zang, M.M. Reynolds, K.C. Papat, M.J. Kipper, Glycocalyx-inspired nitric oxide-releasing surfaces reduce platelet adhesion and activation on titanium, *ACS Biomater. Sci. Eng.* 3 (2017) 68–77. doi:10.1021/acsbiomaterials.6b00572.
- [135] Y. Liu, T.T. Yang Tan, S. Yuan, C. Choong, Multifunctional P(PEGMA)-REDV conjugated titanium surfaces for improved endothelial cell selectivity and hemocompatibility, *J. Mater. Chem. B*. 1 (2013) 157–167. doi:10.1039/c2tb00014h.
- [136] C. Han, X. Luo, D. Zou, J. Li, K. Zhang, P. Yang, N. Huang, Nature-inspired extracellular matrix coating produced by micro-patterned smooth muscle and endothelial cells endows cardiovascular materials with better biocompatibility, *Biomater. Sci.* 7 (2019) 2686–2701. doi:10.1039/c9bm00128j.
- [137] X. Wang, T. Liu, Y. Chen, K. Zhang, M.F. Maitz, C. Pan, J. Chen, N. Huang, Extracellular matrix inspired surface functionalization with heparin, fibronectin and VEGF provides an anticoagulant and endothelialization supporting microenvironment, *Appl. Surf. Sci.* 320 (2014) 871–882. doi:10.1016/j.apsusc.2014.09.004.

## CHAPTER 2: INTERACTION OF BLOOD PLASMA PROTEINS WITH SUPERHEMOPHOBIC TITANIA NANOTUBE SURFACES<sup>1</sup>

### 2.1. Introduction

Hemocompatibility of biomaterials remains a considerable challenge for successful development of blood-contacting medical devices such as heart valves and stents [2]. When biomaterial implants come in contact with blood, the first event is the adsorption of plasma proteins, which can trigger a cascade of mechanisms that cause thrombosis and sometimes failure of the device [3]. A plentiful protein in blood plasma is fibrinogen, and it is one of the first to adsorb on the implant surface when in contact with blood [4]. Fibrinogen is primarily responsible for platelet adhesion, thus being a key protein in the context of the coagulation cascade [5]. This coagulation cascade is a complex process, which can be separated into two distinct pathways: intrinsic and extrinsic. The intrinsic pathway, also called contact activation, is a surface-mediated event and it is the process responsible for clotting on biomaterial surface. It is initiated by the conversion of the protein Factor XII to its activated form FXIIa [6]. Factor XII, also called Hageman Factor, is a coagulation factor, and its autoactivation occurs upon binding with the surface, presumably due to a conformational change [7]. After FXII activation, several proteins are activated in a chain until thrombin is formed [8]. The thrombin then mediates the fibrinogen conversion into fibrin, which polymerizes to form a fibrin mesh that further forms thrombus [9].

---

<sup>1</sup> This work was published in *Nanomedicine: Nanotechnology, Biology and Medicine* and is reproduced in modified form here with permission [1].

It is well accepted that biomaterial surface characteristics, such as surface chemistry, morphology, and wettability, directly influence the interaction of biomaterial with blood [10], [11]. Several techniques of surface modification have been investigated in order to enhance hemocompatibility of biomaterial implants. Surface wettability is a key factor in determining the protein adsorption on biomaterial surfaces. Predominantly, hydrophilic surfaces lead to less protein adsorption than hydrophobic surfaces, since hydrophilic surfaces bind strongly with water molecules which constrain proteins from binding with the substrate [12]. One strategy largely studied is the incorporation of various hydrophilic polymers, such as polyethylene glycol (PEG) on biomaterial surfaces [13]. However, previous works have shown that PEG modified materials perform less well in blood and plasma than in simple protein solutions [14]. Another approach is designing superhydrophobic surfaces (i.e. when water contact angles are greater than  $150^\circ$ ), and previous studies have shown they can either increase or decrease protein adsorption on surfaces depending on the surface architecture [15].

It is well established that titanium has great biocompatibility and has been widely used as a biomaterial for orthopedic and cardiovascular applications for decades [16]. However, even titanium-based implants can cause adverse effects when in contact with blood [17]. Therefore, one approach that has been recently developed for enhancing hemocompatibility is making titanium surfaces superhemophobic (i.e. blood plasma contact angles greater than  $150^\circ$ ) [18]. Previous study has shown less platelet adhesion and activation on superhemophobic titania nanotubes arrays [19]; however, it is still unclear what happens to specific blood proteins of the coagulation cascade on this surface. In this work, we have studied the potential hemocompatibility of superhemophobic titania nanotube arrays by investigating in detail the blood clotting responses and the interaction of key blood plasma proteins, such as fibrinogen,

thrombin, and factor XII, with the substrates. In this study, hemophilic, hemophobic, and superhemophobic titania surfaces were fabricated by combination of surface topography (smooth surface and titania nanotube arrays) and surface chemistry (unmodified, fluorinated [20] and PEGylated [19]). The results show that superhemophobic substrates limit surface protein adsorption and FXII activation, as well as delays the whole blood clotting, thus proving to be a good approach for improving hemocompatibility of biomaterials.

## **2.2. Materials and Methods**

### **2.2.1. Fabrication of titania nanotube arrays with different surface modifications**

Titania nanotube arrays were produced from titanium foil (0.5 mm thick) via anodization process described elsewhere [21]. Briefly, titanium foil was used as the anode and platinum foil was used as the cathode. The electrolyte solution was made by mixing 2% v/v hydrofluoric acid (HF, Alfa), 3% v/v DI water and 95% v/v diethylene glycol (DEG, Alfa). The anodization process was performed for 22 hrs at 55 V, followed by annealing in air at 530 °C for 3 hrs with a ramp rate of 15 °C/min. After surface modification, all the substrates were rinsed with ethanol and DI water, and dried in nitrogen. Unmodified titanium and titania nanotube array surfaces were further modified in two different ways. Prior to surface modification, the substrates were treated with oxygen plasma at 200 V in 10 cm<sup>3</sup>/min of oxygen gas for 15 mins.

- The substrates were positioned on a hot plate near a glass slide with 200 µl of (heptadecafluoro-1,1,2,2-tetrahydrodecyl)trichlorosilane (referred to as FL). The glass slide and substrates were covered with a bowl and heated at 120 °C for 1 hr.

- The substrates were placed in a 2 vol% solution of 2-[methoxy(polyethyleneoxy)propyl]trimethoxsilane (referred to as PEG) in ethanol solution for 20 hrs.

Following notation will be used in the dissertation: unmodified titanium surface: Ti; unmodified titania nanotube arrays: NT; substrates modified with FL: Ti-FL and NT-FL; substrates modified with PEG: Ti-PEG and NT-PEG.

### 2.2.2. Surface characterization of different substrates

The surface morphology of different substrates was characterized using scanning electron microscopy (SEM, JEOL). Before imaging at 15 kV, the substrates were coated with 10 nm of gold. The diameters of the nanotubes were measured using ImageJ.

Static contact angles were obtained using a Ramé-Hart Model 250 goniometer and images were obtained via DROPimage advanced software. Approximately 10  $\mu$ l of human blood plasma was placed on the surface to obtain the contact angles.

The surface chemistry was identified using X-ray photoelectron spectroscopy (XPS, ESCA Systems Spectrometer 5800). XPS analysis was conducted at 15 kV with takeoff angle of 45°. The elemental composition was determined via peak fit analysis in Origin and Multipak software.

Further, film thickness of substrates treated with FL and PEG were also calculated from the attenuation of XPS signals using the standard overlayer method [22]. This method determines the thickness of the film utilizing Ti2p peaks intensities before and after silanization. The film thickness is given by the following equation:

$$I_{Ti} = I_{Ti}^0 \exp\left(-\frac{t}{L_{Ti} \sin \theta}\right)$$

Where  $I_{Ti}$  is the intensity of Ti2p peaks from substrates after surface modification,  $I_{Ti}^0$  is the intensity of Ti2p peaks before surface modification,  $t$  is the thickness of the film,  $L_{Ti}$  is the electron attenuation length for Ti peaks and  $\theta$  is the take-off angle for XPS measurements.

The surface crystalline structure was determined by X-ray diffraction (XRD, Shimadzu 700). Scans were obtained over a  $2\theta$  range from  $20^\circ$  to  $80^\circ$  at a rate of 1 step per sec. The peaks analysis was made using Origin software.

### **2.2.3. Stability of different substrates in physiological conditions**

The stability of different substrates was characterized by measuring the water contact angles over a 28-day period. The substrates were placed in an incubator ( $37^\circ\text{C}$  and 5%  $\text{CO}_2$ ) on horizontal shaker (100 rpm) plate for 28 days in phosphate buffer saline (PBS). After 7-day intervals, the substrates were dried, and the contact angles were measured. Further, XPS was also used in order to determine the surface composition after the 28 days.

### **2.2.4. Isolation of platelet rich plasma (PRP) and platelet poor plasma (PPP)**

Whole human blood was acquired through venipuncture from healthy individuals, and formal assents were obtained from the donors. Colorado State University Institutional Review Board approved the protocol for blood isolation from healthy participants. All experiments were conducted in agreement with the National Institutes of Health's "Guiding Principles for Ethical Research". In order to obtain PRP, whole blood was drawn into 10 ml vacuum tubes coated with ethylenediaminetetraacetic acid (EDTA) and was centrifuged at 150 g for 15 mins. To obtain PPP, whole blood was drawn into 3 ml vacuum tubes coated with sodium citrate and was centrifuged at 1500 g for 15 mins. All studies involving blood were performed at least three

times with blood drawn from at least two healthy donors. However, for each experiment, the blood was only collected from the same donor to avoid donor-to-donor variability.

#### **2.2.5. Fibrinogen adsorption from PRP on different substrates**

Fibrinogen adsorption from PRP on different substrates was assessed using a human Fibrinogen ELISA Kit (GenWay). Prior to all experiments, substrates were sterilized via incubation in 70% ethanol for 15 mins, rinsed three times with PBS and exposed to UV light for 10 mins. Sterilized substrates were then incubated in PRP on a horizontal shaker plate (100 rpm) for 2 hrs at 37 °C and 5% CO<sub>2</sub>. After the incubation, 100 µl diluted surface-exposed PRP (1:10000 in assay diluent) and fibrinogen standards were placed into the wells of the microtiter plate and incubated for 1 hr at room temperature. The substrate-exposed PRP and fibrinogen standards were then aspirated and the wells were washed (4x) with wash buffer and incubated with 100 µl of enzyme antibody conjugate for 30 mins in a dark environment at room temperature [3]. The conjugate was removed, and the wells were washed (4x) with the wash buffer and incubated with 100 µl of tetramethylbenzidine buffer (TMB) solution for 10 mins at room temperature without light exposure. The reaction was then stopped with 100 µl of stop solution and the optical density was immediately measured using a plate reader at 450 nm.

#### **2.2.6. Thrombin anti-thrombin (TAT) complex formation on different substrates**

TAT complex formation on different substrates exposed to platelet poor plasma (PPP) was investigated using a human TAT Complex ELISA kit (AssayPro). Sterilized substrates were incubated in PPP on a horizontal shaker plate (100 rpm) for 2 hrs at 37 °C and 5% CO<sub>2</sub>. After the incubation, 50 µl of TAT standards and diluted surface-exposed PPP (1:10000 in assay diluent)

were placed into the wells of the microtiter plate and incubated for 2 hrs at room temperature. The substrate-exposed PPP and TAT standards were then aspirated, and the wells were washed (5x) with wash buffer and incubated with 50  $\mu$ l of biotinylated antibody for 1 hr at room temperature. The antibody was removed, and the wells were washed (5x) with the wash buffer and incubated with 50  $\mu$ l of SP conjugate for 10 mins at room temperature. After that, the conjugate was removed, and the wells were washed (5x) with the wash buffer and incubated with 50  $\mu$ l of chromogen substrate solution for 20 min at room temperature. The reaction was then stopped with 50  $\mu$ l of stop solution and the optical density was immediately measured using a plate reader at 450 nm.

#### **2.2.7. *In vitro* plasma coagulation assay**

FXII activation on different substrates was characterized by an *in vitro* plasma coagulation time (CT) assay. CT is the time demanded from activation of the intrinsic pathway of the coagulation cascade to the occurrence of a visible clot [24]. All CT measurements were performed in PPP.

##### *2.2.7.a Factor XIIa (FXIIa) titration curve*

Human coagulation FXIIa (Enzyme Research Laboratories) with activity value of 73 plasma equivalent units per mg (PEU/mg) was used in this study. The method described elsewhere was followed [24]. Prior to use, Factor XIIa was thawed in a 37°C in water bath and diluted with PBS to the desired concentrations. The activity of FXIIa employed to obtain the titration curve varied from 10 to 10<sup>-4</sup> PEU/ml. In order to prepare a 1 ml solution with 1:1 dilution of plasma in buffer, 0.1 ml of 0.1M CaCl<sub>2</sub> was added to 0.5 ml of PPP and mixed with

0.1 ml of FXIIa (with different concentrations) and 0.3 ml of 0.01M PBS in a 2 ml polystyrene micro-cuvette. CaCl<sub>2</sub> was the last reagent added to assure a standard time zero for CT. The cuvettes were then covered with parafilm and rotated at 20 rpm on a hematology mixer, and the corresponding CT was recorded.

FXIIa activity was quantified using a titration calibration curve relating [FXIIa]<sub>eq</sub>, in PEU/ml to the plasma coagulation time. A mathematical model developed in a previous study was fitted to the obtained data of coagulation times related to the amount of exogenous FXIIa added [6]. The equation that relates CT to FXIIa concentration through three adjustable parameters *a*, *b*, and *c* is given by:

$$CT = \frac{a[FXIIa] + b}{[FXIIa] + c}$$

with

$$a = \frac{k_b CT_0}{k_1 + k_b}, \quad b = \frac{k_b CT_0}{k_1 + k_b} K_G \quad \text{and} \quad c = \frac{k_b K_G}{k_1 + k_b}$$

where *CT*<sub>0</sub> is the background coagulation time, *k*<sub>1</sub> and *K*<sub>G</sub> are the reaction rate constant and Michaelis-like constant, respectively. *k*<sub>b</sub> is the reaction rate constant for the background clot, which means the clot formation under assay conditions but with no addition of FXIIa [6].

The commercial software Origin was used to get the best-fit solution to experimental titration data (CT vs. exogenous FXIIa concentration).

### 2.2.7.b FXII activation in plasma

To obtain the substrate-induced contact activation, PPP was added to sterilized substrates (23 mm<sup>2</sup>) in a 2 ml polystyrene micro-cuvette and CT was measured. In order to prepare a 1 ml solution with 1:1 dilution of plasma in buffer, 0.1 ml of 0.1M CaCl<sub>2</sub> was added to the cuvette

with the substrates and 0.5 ml of PPP and mixed with 0.4 ml of 0.01M PBS. CaCl<sub>2</sub> was the last reagent added to assure a standard time zero for CT. The cuvettes were then covered with parafilm and rotated at 20 rpm on a hematology mixer, and the corresponding coagulation time was recorded. The CT was then used to calculate the equivalent FXIIa activity by referencing back to the FXIIa titration curve obtained.

### **2.2.8. Whole blood clotting kinetics**

Sterilized substrates were placed in a 24-well plate in order to investigate whole blood clotting kinetics. Human blood from healthy donors was collected in 3 ml sterile centrifuge tubes without any anti-coagulants. 7  $\mu$ l of this blood was immediately placed onto the substrates, and the droplet was allowed to clot for up to 30 mins. After 15 mins intervals, the substrates were moved into a different 24-well plate with 500  $\mu$ l of DI water. The substrates were then gently agitated for 30 secs and left in the DI water for 5 mins to lyse the red blood cells and release free hemoglobin from them. The free hemoglobin absorbance was then measured using a plate reader at a wavelength of 540 nm. The absorbance value is directly proportional to the amount of free hemoglobin in DI water and provides a direct relation to the extent of blood clotting on different substrates [25].

### **2.2.9. Statistical analysis**

SEM, XPS and XRD analysis were done on 2 different samples of each substrate. Contact angle and stability test were done using 3 droplets per sample on 3 different samples of each substrate ( $n_{\min}=9$ ). All protein adsorption experiments were repeat twice with 3 samples of each substrate ( $n_{\min}=6$ ). Whole blood clotting kinetics were reconfirmed on 3 different samples

of each substrate. Analysis of variance (ANOVA) and Tukey tests were conducted for the experiment data using software Origin 8.5 at a 5% significance level ( $p < 0.05$ ). All blood studies discussed below were performed with at least two healthy donors. To avoid donor-to-donor variability, the results presented are only from one donor. However, similar trends were observed for all the donors, which indicates the reproducibility of the results.

### 2.3. Results

SEM was used to characterize the surface morphology of different substrates. As expected, the images indicate smooth topography for unmodified titanium and uniform vertically oriented nanotubes on anodized surface with a diameter of  $147 \pm 5$  nm. (**Figure 2.1**). The results also show no apparent changes in morphology of both substrates after modification with FL and PEG. Further, there was no significant difference in nanotube diameter after surface modification ( $p < 0.05$ ), with a diameter of  $152 \pm 6$  nm for NT-FL and  $155 \pm 7$  nm for NT-PEG.

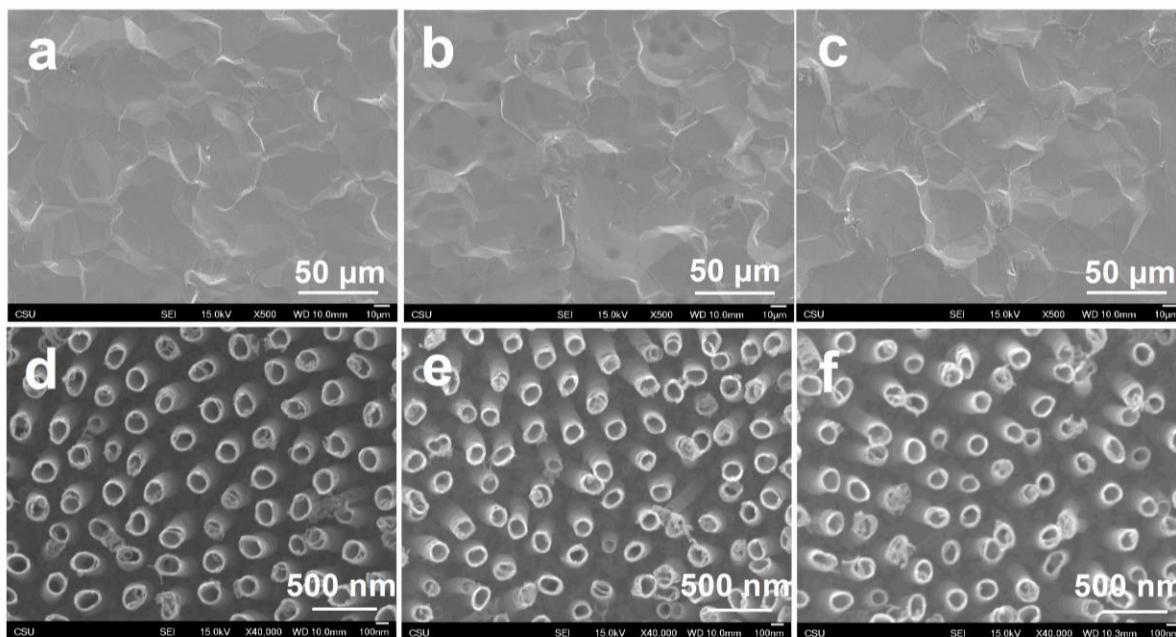


**Figure 2.1.** SEM images for (a) Ti, (b) Ti-FL, (c) Ti-PEG, (d) NT (e) NT-FL and (f) NT-PEG.

Contact angle goniometry was used to characterize the wettability of different substrates. Static contact angles were measured using blood plasma. When the static contact angle ( $\theta$ ) between the surface and blood droplet is greater than  $150^\circ$ , the surface is designated superhemophobic [19]. The surface is considered as hemophilic when  $\theta < 90^\circ$ , and as hemophobic if  $\theta > 90^\circ$  [26]. Based on the results, NT-FL is superhemophobic, since  $\theta = 167^\circ$ . The results also indicate that Ti-FL is hemophobic; and Ti, Ti-PEG, NT and NT-PEG are hemophilic (**Figure 2.2**).

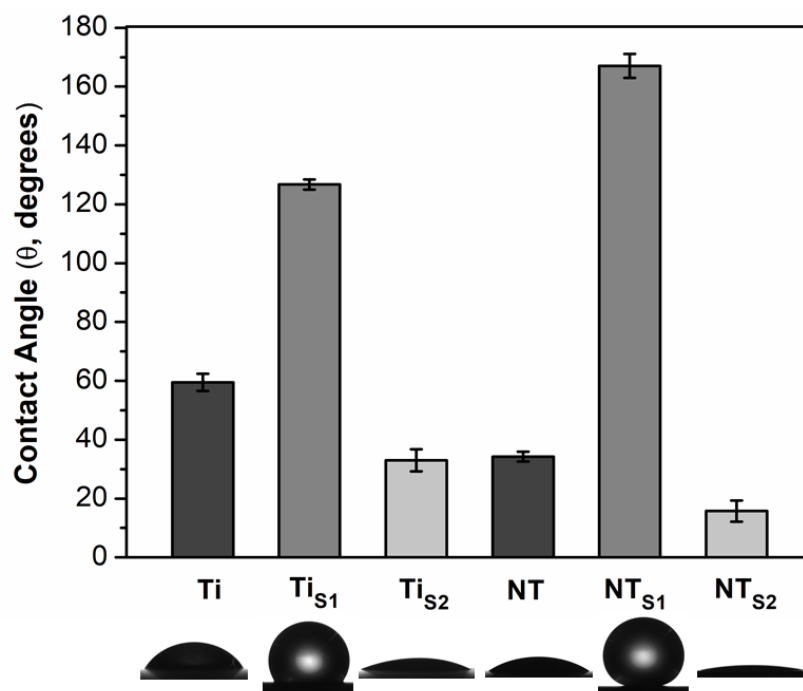


**Figure 2.2.** Static contact angles of human blood plasma for different substrates. No significant differences in contact angle on Ti-PEG and NT. Significant differences in contact angles for all other substrates ( $p < 0.05$ ).

XPS was used to characterize the surface chemistry of different substrates. Survey spectra show that all the substrates had O1s, Ti2p3/2, and C1s peaks (**Figure 2.3A**). The C1s peak was present on NT and Ti due to some residues of carbon already present on the substrates and contamination in the XPS chamber. As expected, the results indicate the F1s peak on both

surfaces modified with the fluorinated silane FL. The C1s peak increased for Ti- FL and Ti-PEG as compared to Ti; and NT-FL and NT-PEG as compared to NT; since both silanes contain carbon. Further, the O1s peak increased for both Ti-PEG as compare to Ti; and NT-PEG as compared to NT; due to the characteristic CO groups present in the PEGylated silane.

The surface elemental composition for different substrates was also obtained from XPS survey scans using MultiPak software (**Table 2.1**). Ti-FL, Ti-PEG, NT-FL, and NT-PEG show an increase in carbon concentration as well as a decrease in titanium concentration compared to unmodified Ti and NT. The reason for this is the presence of silane on the surface that leads to a decrease in titanium concentration after surface modification. In addition, although PEG has oxygen, the percentage concentration of oxygen on both substrates treated with PEG has decreased because of the significant increase in the percentage of carbon. As expected, a high concentration of fluorine was observed for both surfaces treated with FL.

High resolution C1s scans from XPS also indicate the presence of characteristics  $CF_2$  and  $CF_3$  groups on NT-FL and Ti-FL whereas characteristic CO groups (C-O and O-C=O) on hemophilic surfaces (**Figure 2.3B**). The presence of these peaks shows that Ti and NT were successfully modified by FL and PEG silanes.

Additionally, silane thickness on Ti and NT after surface modification with FL and PEG were calculated from the attenuation of XPS signals using the standard overlayer method, which determines the film thickness using the intensities of Ti2p peaks before and after silanization. The electron attenuation length for Ti,  $L_{Ti}$ , found in the literature is 2.1 nm [27]. Using the intensity of Ti2p peaks from XPS survey spectra of substrates before and after surface modification, the thickness of Ti-FL calculated is 1.83 nm, 0.158 nm for Ti-PEG, 1.04 nm for NT-FL calculated and for NT-PEG the thickness of the film is 0.037 nm.

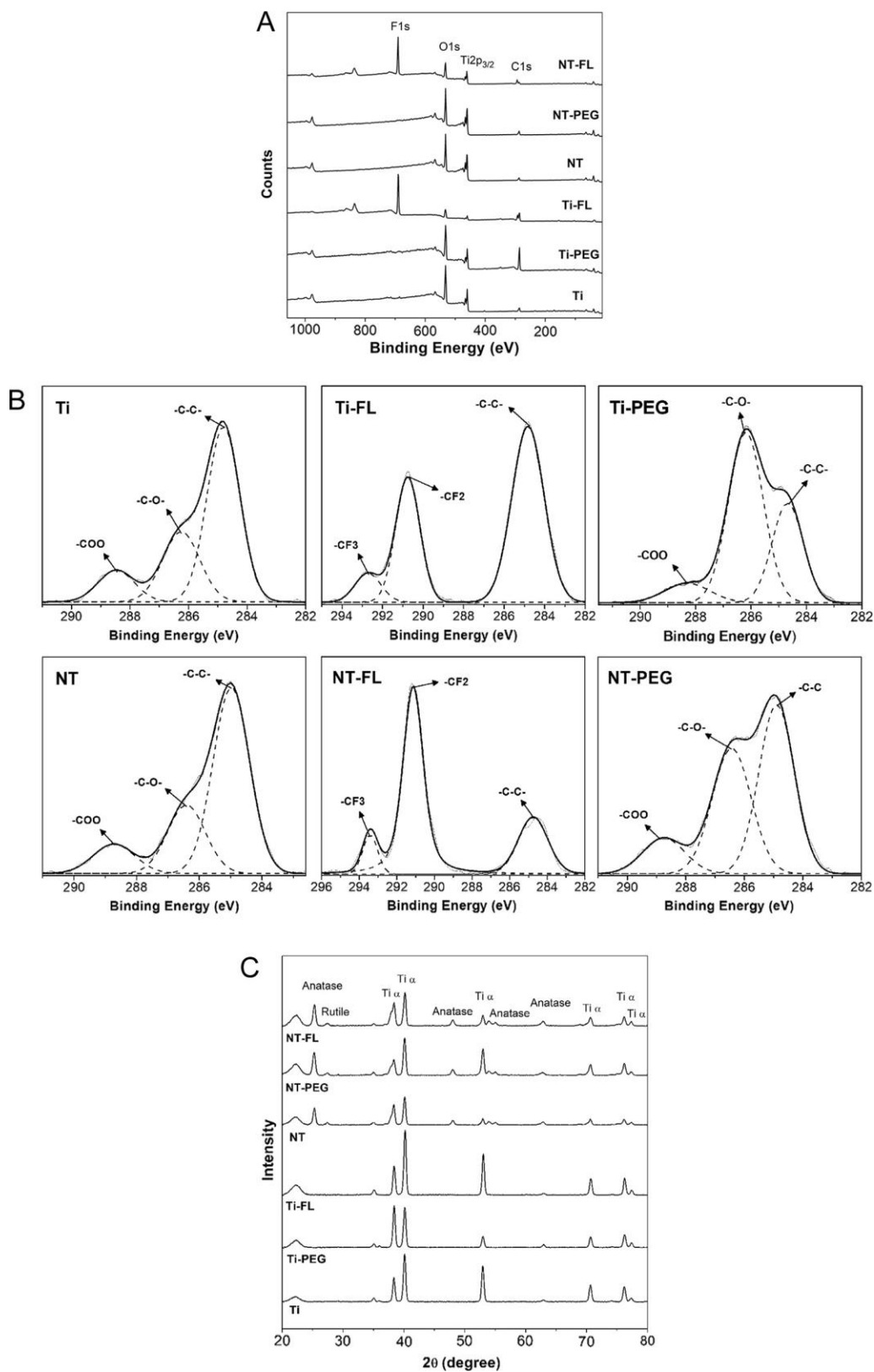


**Figure 2.3.** A) XPS survey scans for different substrates. B) High resolution C1s scans for different substrates. C) XRD scans for different substrates.

XRD was used to characterize the surface crystalline structure of different substrates. After the anodization process, the nanotubes are amorphous, and in order to form the crystal phases, annealing process is required. The annealing temperature of 530 °C was chosen to guarantee the total crystallization of titania nanotube arrays [21]. All NT substrates have rutile and anatase crystal phases which are not present on Ti surfaces (**Figure 2.3C**). Both anatase and rutile crystal phases provide important characteristics to the material. The rutile phase is the most stable phase, while the metastable anatase phase can produce a more conductive surface and has been shown to be less cytotoxic in TiO<sub>2</sub> crystals [28]. The results also indicate that the surface modification with FL and PEG does not affect the crystalline structure of the unmodified titanium and the titania nanotube arrays.

**Table 2.1.** XPS Elemental composition for different substrates.

	<b>% O</b>	<b>% TI</b>	<b>% C</b>	<b>% F</b>
<b>Ti</b>	68.4	13.1	18.5	0
<b>Ti-FL</b>	13.5	1.8	40.5	44.2
<b>Ti-PEG</b>	38.8	7.8	53.4	0
<b>NT</b>	68.3	20.0	11.7	0
<b>NT-FL</b>	21.9	5.3	21.2	51.6
<b>NT-PEG</b>	62.2	17.6	20.2	0

The stability of different substrates was characterized by measuring the water contact angles every 7 days over a 28-day period. The substrates were placed in an incubator (37°C and 5% CO<sub>2</sub>) on a horizontal shaker (100 rpm) for 28 days in PBS, and the contact angles were measured. After this period, the substrates incubated in PBS showed a significant decrease in the

contact angles for all Ti groups (**Figure 2.4A**), which indicates that these surfaces are not stable under buffer conditions.

XPS was also used to determine the surface composition after 28-day period. The results show a considerable decrease in the CO groups percentage on both samples modified with PEG (**Figure 2.4B**), especially for Ti-PEG, which confirm the results obtained with the contact angles. In addition, new CO groups were present on Ti-FL and Ti-PEG. However, the CF<sub>2</sub> and CF<sub>3</sub> groups are still present with similar amount.

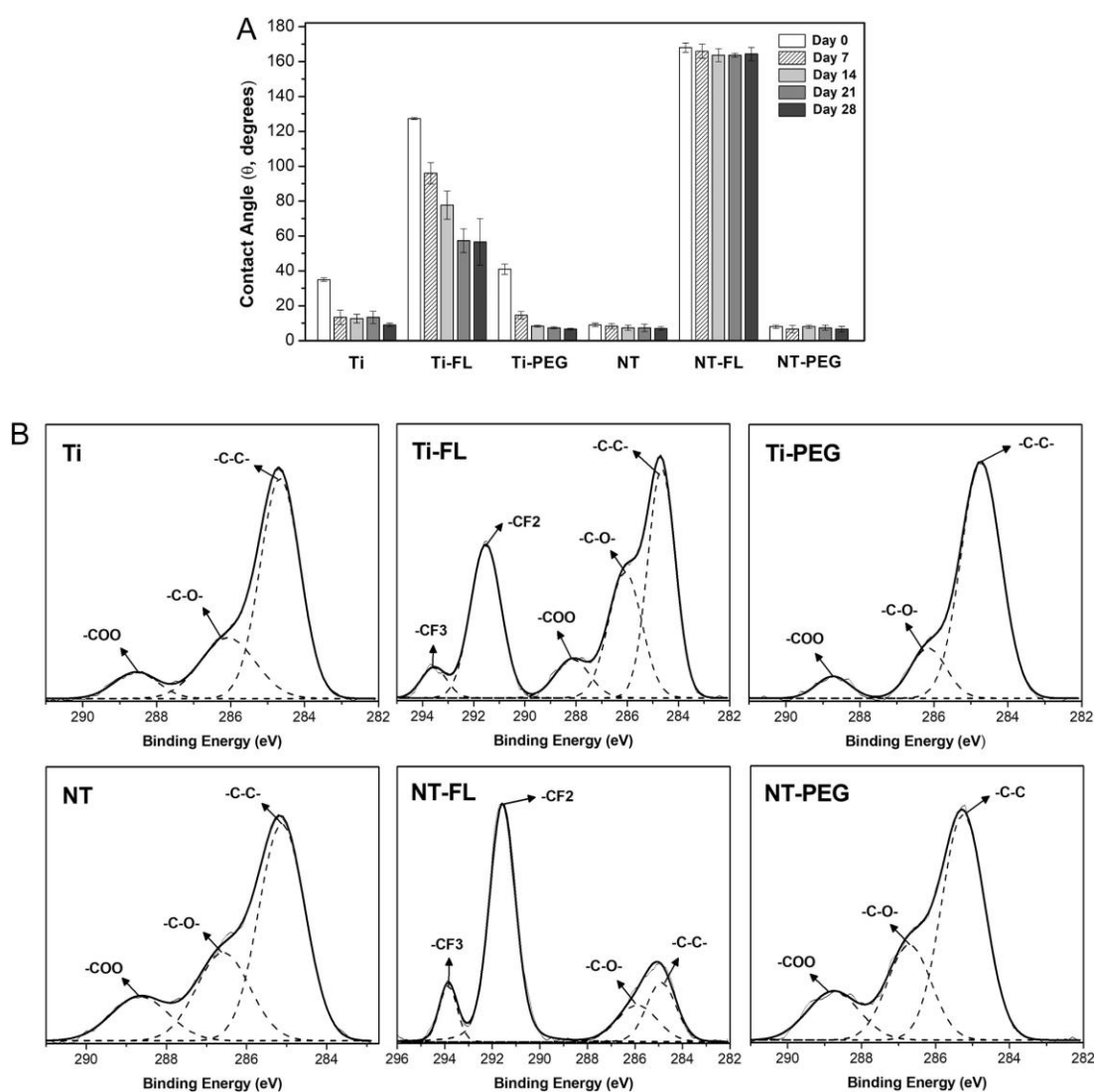


**Figure 2.4.** A) Static contact angles for different substrates after 0, 7, 14, 21, and 28 days of incubation. B) High resolution C1s scans for different substrates after 28 days of incubation.

The surface elemental composition for different substrates after 28 days of incubation in PBS was also obtained from XPS survey scans using MultiPak software (**Table 2.2**). The results show that Ti-FL and Ti-PEG had a considerable change in their surface composition when compared with day 0 (**Table 2.1**). Both groups showed a substantial increase in the percentage of titanium (approximately 100%) and a considerable decrease in carbon concentration (approximately 25%); and Ti-FL also showed a 30% reduction in fluorine concentration. These results indicate the degradation of both silanes and agree with the contact angle results [29]. In addition, NT-FL and NT-PEG show very similar elemental composition after 28 days of incubation in PBS, which also suggest their stability under buffer conditions.

**Table 2.2.** XPS Elemental composition for different substrates after 28 days of incubation in PBS at 37°C and 100 rpm.

	<b>% O</b>	<b>% TI</b>	<b>% C</b>	<b>% F</b>
<b>Ti</b>	63.8	10.7	25.5	0
<b>Ti-FL</b>	33.4	5.3	31.8	29.4
<b>Ti-PEG</b>	62.9	11.3	25.8	0
<b>NT</b>	64.3	17.0	18.7	0
<b>NT-FL</b>	26.3	7.0	19.6	47.2
<b>NT-PEG</b>	63.6	16.6	19.9	0

Based on the stability results, further studies were not done on Ti-FL and Ti-PEG, since they were not stable under buffer conditions after the 28-day period.

Fibrinogen adsorption from PRP on different substrates was measured using an enzyme-linked immunoassay (ELISA). The PRP was assayed to determine the amount of fibrinogen that remained after exposure to substrates, and this was compared with amount of fibrinogen in PRP

that was not exposed to substrates. The results indicate that NT, NT-FL, and NT-PEG had significant lower fibrinogen binding from PRP in comparison with Ti, although no statistically significant difference was observed between NT and NT-FL, and between NT-FL and NT-PEG (**Figure 2.5**). The results also show that NT-PEG had significant higher fibrinogen adsorption than NT.

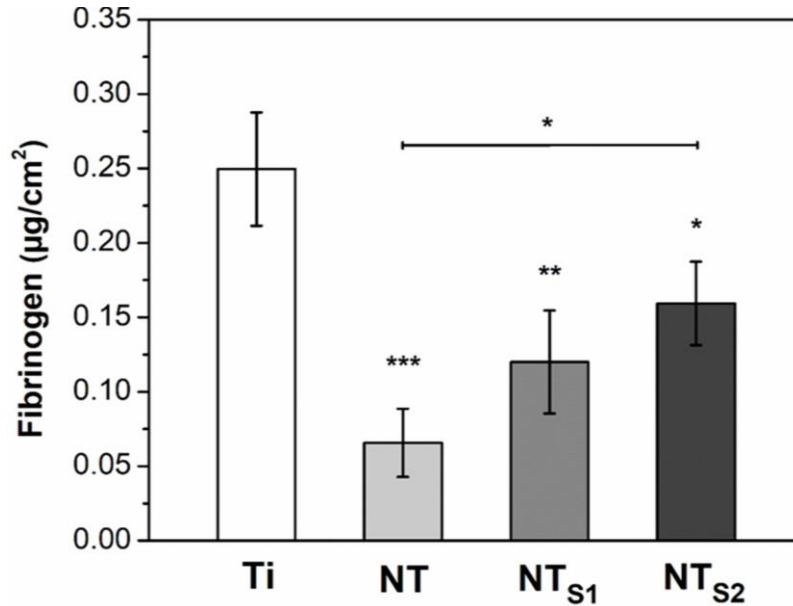


**Figure 2.5.** Fibrinogen binding from PRP on different substrates.

TAT complex formation on different substrates exposed to PPP was investigated using a human TAT Complex ELISA kit. To evaluate TAT formation from blood plasma, the substrates were incubated in PPP for 2 hrs, and PPP was then assayed to determine the amount of TAT presenting in plasma. The results are shown after subtraction of the amount of TAT in PPP that was not exposed to substrates. The results show no statistically significant differences in TAT formation between all substrates, although trends indicate that NT-FL and NT-PEG had lower TAT concentrations (**Figure 2.6**).

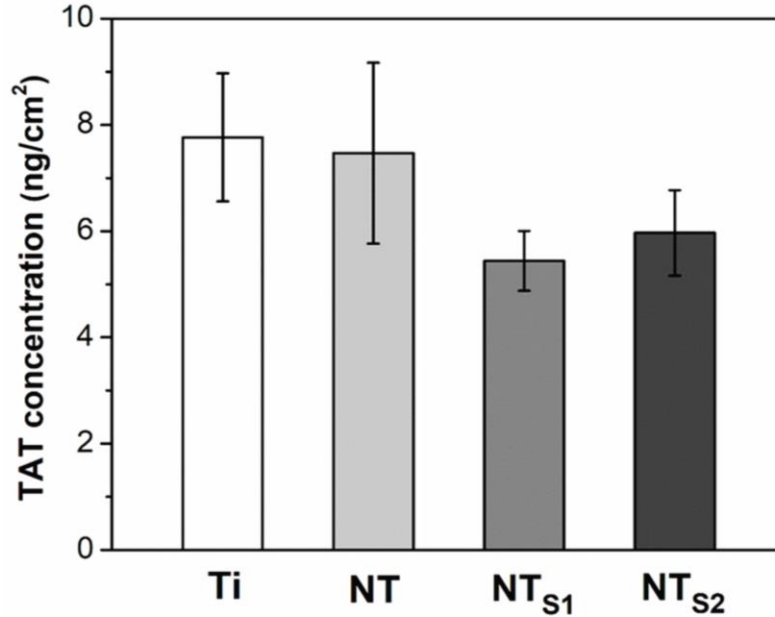


**Figure 2.6.** TAT generation on different substrates after 2 hrs of incubation in PPP. No significant difference between groups was observed ( $p < 0.05$ ).

FXII activation on different substrates was characterized by an *in vitro* plasma coagulation time (CT) assay. Previous work has developed a mathematical model that relate CT to FXIIa concentration, through three adjustable parameters  $a$ ,  $b$ , and  $c$  [6]. Results of FXIIa titration in PPP show that CT decreases as exogenous FXIIa concentration increases (**Figure 2.7a**). The least squares fitting solution to experimental titration data was obtained using the software Origin. The results for the best fit solution ( $R=0.947$ ) are given in **Table 2.3**.

Contact activation of FXII in plasma by different substrates was measured using a CT assay. The titration curve obtained was used to convert the CT obtained into FXIIa concentration. The results indicate that NT-FL had significant lower FXII activation in plasma in comparison with the other substrates (**Figure 2.7b**). Specifically, NT-FL shows an impressive 300% reduction of FXII activation in comparison with Ti and 400% comparing with NT and NT-PEG.

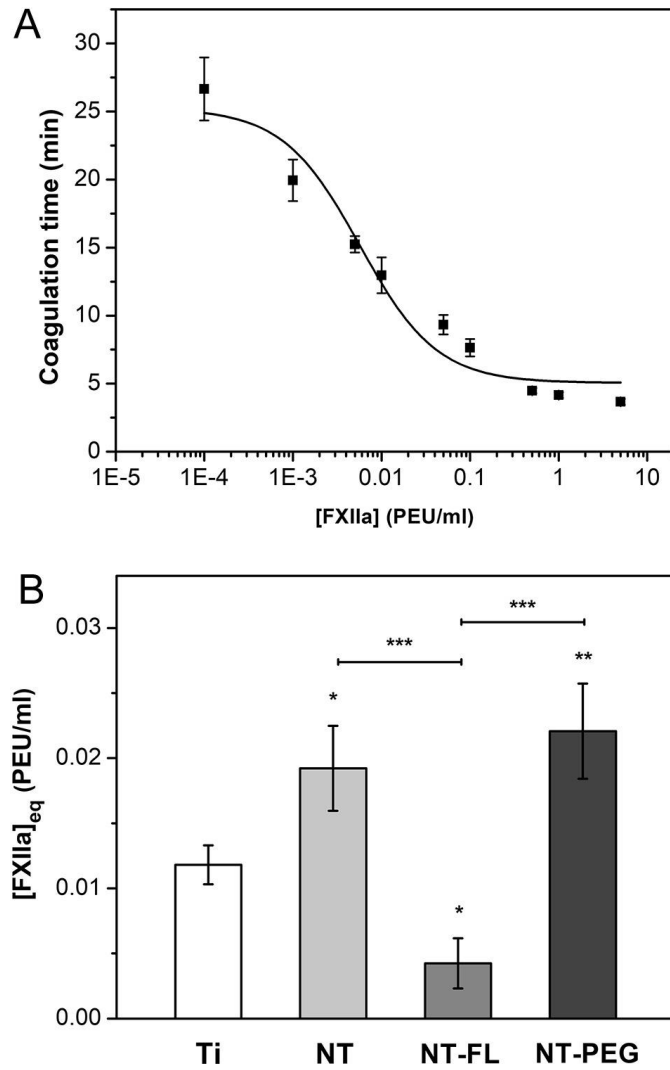


**Figure 2.7.** A) FXIIa titration curve for the plasma showing coagulation times versus concentrations of exogenous FXIIa. The fitted curve corresponds to a least squares fitting of a developed mathematical model [6]. B) [FXIIa]<sub>eq</sub> in plasma calculated from coagulation times of different substrates. Ti is used as control for the statistical analysis ( $p < 0.05$ ).

**Table 2.3.** Parameters derived from best fit solution of FXIIa titration data

	<b>A</b>	<b>B</b>	<b>C</b>
	$(5.05 \pm 0.91)$	$(0.14 \pm 0.04)$	$(5.7 + 2.0) \times 10^{-3}$
<b>Unit</b>	min	$\mu\text{M min}$	$\mu\text{M}$

Whole blood clotting kinetics were investigated by measuring the amount of free hemoglobin on different substrates in terms of absorbance. Whole human blood was allowed to clot for 15 and 30 mins on different substrates. The values of free hemoglobin concentration were measured for different substrates after 15 and 30 mins. After this time, the measurements were stopped since the blood starts to clot with the contact with air, which would interfere in the results. The results indicate that blood clotting was significantly delayed on NT-FL substrate in comparison with the other groups (**Figure 2.8**). After 30 mins, the amount of free hemoglobin on NT-FL is the same as after 15 mins, and both are close to the un-clotted blood (the absorbance was reduced by 17%). After 30 mins, Ti showed a reduction in the absorbance of 80 %; 45 % for NT and 65 % reduction for NT-PEG.

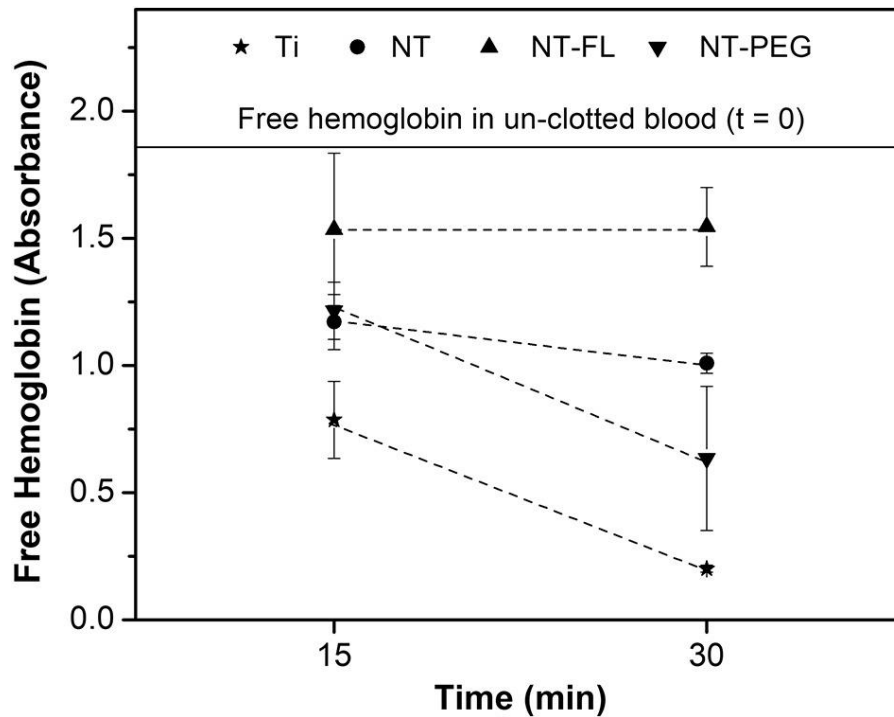


**Figure 2.8.** Free hemoglobin concentration values measured in terms of absorbance for different substrates.

## 2.4. Discussion

Until now, there is no biomaterial that is completely compatible with blood. Thousands of patients have suffered complications due to blood clotting, and many of them must take blood-thinning medications for years after receiving blood contacting devices [18]. Therefore, there is an urgent need to develop novel materials that prevent blood clotting, and it is essential to understand the initial events that happen on the implant surface when it encounters blood. Immediately after the medical device implantation, blood protein adsorbs on the material surface, which mediates all the subsequent phenomena, such as platelet attachment and thrombus formation [30]. Thus, understanding the way in which proteins interact with the biomaterial surface is fundamental, and the surface characteristics, such as topography and wettability play an important role in the scenario [31]. In this work, we have studied the stability of the substrates and how they interact with key blood proteins from the coagulation cascade, such as fibrinogen, thrombin and Factor XII, as well as the whole blood kinetics.

Titania nanotubes arrays were fabricated by anodizing unmodified titanium sheets in HF solution, and its formation is due to a field-assisted dissolution process [32]. Unmodified titanium and titania nanotube array were then modified with the silanes FL and PEG. Prior to the silanization process, the surfaces were treated with oxygen plasma to form hydroxyl groups. These hydroxyl groups then form covalent bonds with the silanes [33]. In order to make superhemophobic surfaces, the Cassie-Baxter state is preferred [34], and these surfaces can be fabricated by modifying nanotextured surfaces with a low solid surface energy silane [19]. Thus, in this study, we used titania nanotube arrays to provide nanotexture and were modified by fluorinated FL silane known to possess lower solid surface energy.

Stability plays a central role for medical devices applications, since the biomaterial implant is designed to stay for years, even decades, inside the patient body. The goal was to investigate if superhemophobic substrates are stable for a significant amount of time under physiological conditions. Previous studies have shown that certain types of superhydrophobic surfaces are stable under water if they present sub-micron or smaller scale roughness [35], but nothing was showed under similar body conditions. After the 28-day period, the substrates showed a significant decrease in the contact angles for all Ti groups, which indicates that these surfaces are not stable under buffer conditions (**Figure 4a**). This can be explained due to the chemical interaction of the PBS salts and the titanium surface. In contrast, all NT substrates didn't show any significant difference in the contact angles after this period. XPS results are in agreement with the contact angles. After the incubation, both substrates modified with PEG showed a great decrease in the CO groups percentage (**Figure 4b**), which indicates the silane interaction with hydroxyl groups presents in PBS [36]. For NT-FL, the CF<sub>2</sub> and CF<sub>3</sub> groups are still present with similar amount, which shows the stability of superhemophobic surfaces over a period of 28 days under physiological conditions.

Fibrinogen adsorption from plasma on different substrates was measured using ELISA. When a blood-contacting medical device is implanted, proteins from blood plasma adhere onto the biomaterial surface within seconds [37]. Protein interaction with surfaces is a complex process, and its adsorption involves hydrogen bonding, van der Waals, and electrostatic interactions. Although some steps in protein adsorption are still unclear, it is known that surface chemistry and topography are key factors that directly affect protein adsorption [38].

Fibrinogen plays a fundamental role in the coagulation cascade and is one of the first blood plasma proteins to adsorb on implant surfaces [2]. When adhered to the biomaterial

surface and if Factor XII activates the coagulation cascade, it may cause fibrin polymerization and further leading clot formation. Therefore, fibrinogen is directly related to blood clotting and preventing its adsorption can prevent clot formation.

The results show that NT and NT-FL had significant lower fibrinogen adsorption than Ti and NT-PEG (**Figure 5**). The decreased fibrinogen adsorption on NT-FL was expected due to the Cassie-Baxter state [19] since it tends to minimize the contact area between the surface and the liquid, thus decreasing the amount of protein adsorbed [39]. However, it was expected that NT had higher adsorption than Ti due to the large surface area of nanotubes that provides more locations for proteins to adsorb [21]. The results obtained could be explained by the “Vroman effect”, a phenomenon involving a complex sequence of adsorption and desorption steps [40]. Basically, it is a time-dependent variation in the composition of the adsorbed protein layer, as proteins present at a lower concentration in plasma but with high surface activity displace the proteins with higher concentration but which have lower surface activity [41]. Previous studies have shown that high molecular weight kininogen (HMWK), another plasma protein, plays an important role in the removal of fibrinogen from the surface and this replacement is more likely to happen on hydrophilic substrates [42]. Therefore, because ELISA assay is performed in plasma, this phenomenon happens and the plasma proteins compete with each other for the same adsorbent surface, lowering fibrinogen adsorption on hydrophilic surfaces such as NT [43].

The protein thrombin is the last enzyme in the coagulation cascade, and it is formed by the activation of prothrombin [44]. Thrombin serves to cleave the fibrinogen into fibrin monomers, which further polymerizes to form the thrombus [45]. Therefore, it is desired the lower thrombin generation as possible on the biomaterial surface. The presence of TAT shows the formation of thrombin and the consumption of antithrombin [46].

This study shows no statistically significant differences in TAT formation between all substrates, although trends indicate that NT-FL had lower TAT concentrations (**Figure 6**). The lower TAT concentration on NT-FL was expected for the same reason as fibrinogen adsorption, due to the Cassie-Baxter state [19]. However, all substrates showed a small amount of TAT generation, and one of the reasons for no significant differences observed between groups could be the premise that whole blood is necessary for satisfactory thrombin formation [47]. Previous studies have shown that TAT generation was practically negligible in PRP and in PPP while meaningful levels of TAT were noted in whole blood since erythrocytes and leukocytes play an important role in thrombin formation [44]. Therefore, the small amounts of TAT generated on all substrates hinder the detection of significant differences between groups.

Contact activation of FXII in plasma by different substrates was measured using a CT assay. Once in contact with the surface of the implant, the activation of FXII is considered one of the major causes of biomaterial-induced blood coagulation [48]. This enzymatic reaction that converts FXII into FXIIa leads the contact activation and initiate the intrinsic pathway of the blood coagulation cascade [49]. Therefore, the interaction of Factor XII with the implant surface plays a vital role in the hemocompatibility since FXII autoactivation upon binding with the surface lead the coagulation cascade.

Although some studies have shown the differences between FXII activation on hydrophilic and hydrophobic surfaces, nothing was explained about superhemophobic materials [24]. The results indicate that superhemophobic substrates had significant lower FXII activation in plasma in comparison with the other substrates in approximately 300% (**Figure 7b**). It was expected that NT-FL would also decrease FXII activation since it reduces the surface interaction with blood due to the Cassie-Baxter state. In the Cassie-Baxter state, air bags remain stuck

underneath the liquid which prevents the liquid droplet to completely wet the surface [50]. This liquid-air-solid interface dramatically decreases the solid-liquid surface area, thus reducing the total area available for proteins to bind [51]. The results obtained show an enormous decreased in FXII activation on NT-FL and that could be the main reason why superhemophobic materials can effectively prevent clot formation.

The coagulation kinetics is vital for the successful use of long term blood-contacting medical devices [21]. One of the further steps in the coagulation cascade is the development of the fibrin mesh, and this matrix traps the red blood cells, which are mainly constituted by hemoglobin [52]. Whole blood clotting kinetics were investigated by measuring the amount of free hemoglobin on different substrates. As the blood clots on the surface, the red blood cells are trapped inside the fibrin mesh. When the substrates are transferred into water, only the red blood cells that are free in the blood (i.e. not trapped in the fibrin mesh) get lysed. The exposure to water dramatically changes the pressure around the red blood cells, which lyses them thus releasing hemoglobin. Therefore, the free hemoglobin concentration provides a correlation to the extent of blood clotting, with larger amounts of free hemoglobin indicating less clot formation on the substrates [53]. The absorbance value is directly proportional to the free hemoglobin concentration.

The results indicate that blood clotting was significantly delayed on superhemophobic substrate in comparison with the other groups (**Figure 8**), which is in accordance with the protein results since lower protein adsorption and less FXII activation are expected to reduce the clotting formation.

## 2.5. Conclusions

When biomaterial implants interact with blood, the adsorption of plasma proteins rapidly occurs, which may lead to complications such as thrombosis and the failure of the device. Therefore, reducing the adsorption of specific blood plasma proteins is crucial in the prevention of clot formation. Previous studies have shown less platelet adhesion and activation on superhemophobic titania nanotubes arrays; however, it remains unclear what happens to specific proteins of the coagulation cascade on this substrate. In this work, we have investigated the detailed interaction of key blood proteins involved in the coagulation cascade with the substrates and their whole blood kinetics. The results could give a better understanding of how blood interact with the implant surface and show that superhemophobic titania nanotubes (NT-FL) decrease fibrinogen adsorption as well as tremendously reduce Factor XII. In addition, these surfaces are stable under buffer conditions and considerably delay whole blood clotting, thus showing to greatly enhance hemocompatibility of biomaterials. Future work is now directed towards understanding how cells respond to these substrates.

## REFERENCES

- [1] R.M. Sabino, K. Kauk, S. Movafaghi, A. Kota, K.C. Popat, Interaction of blood plasma proteins with superhemophobic titania nanotube surfaces, *Nanomedicine Nanotechnology, Biol. Med.* 21 (2019) 102046. doi:10.1016/J.NANO.2019.102046.
- [2] I.H. Jaffer, J.C. Fredenburgh, J. Hirsh, J.I. Weitz, Medical device-induced thrombosis: what causes it and how can we prevent it?, *J. Thromb. Haemost.* 13 (2015) S72–S81. doi:10.1111/jth.12961.
- [3] S. Xia, J. Li, M. Zu, J. Li, J. Liu, X. Bai, Y. Chang, K. Chen, W. Gu, L. Zeng, L. Zhao, G. Xing, G. Xing, Small size fullerene nanoparticles inhibit thrombosis and blood coagulation through inhibiting activities of thrombin and FXa, *Nanomedicine Nanotechnology, Biol. Med.* 14 (2018) 929–939. doi:10.1016/J.NANO.2017.12.013.
- [4] L.-C. Xu, J.W. Bauer, C.A. Siedlecki, Proteins, platelets, and blood coagulation at biomaterial interfaces, *Colloids Surfaces B Biointerfaces.* 124 (2014) 49–68. doi:10.1016/j.colsurfb.2014.09.040.
- [5] L.A. Wells, H. Guo, A. Emili, M. V. Sefton, The profile of adsorbed plasma and serum proteins on methacrylic acid copolymer beads: Effect on complement activation, *Biomaterials.* 118 (2017) 74–83. doi:10.1016/j.biomaterials.2016.11.036.
- [6] Z. Guo, K.M. Bussard, K. Chatterjee, R. Miller, E.A. Vogler, C.A. Siedlecki, Mathematical modeling of material-induced blood plasma coagulation, *Biomaterials.* 27 (2006) 796–806. doi:10.1016/j.biomaterials.2005.06.021.
- [7] K. Chatterjee, Z. Guo, E.A. Vogler, C.A. Siedlecki, Contributions of contact activation pathways of coagulation factor XII in plasma, *J. Biomed. Mater. Res. - Part A.* 90 (2009) 27–34. doi:10.1002/jbm.a.32076.
- [8] D. Basmadjian, M. V. Sefton, S.A. Baldwin, Coagulation on biomaterials in flowing blood: Some theoretical considerations, *Biomaterials.* 18 (1997) 1511–1522. doi:10.1016/S0142-9612(97)80002-6.
- [9] X. Liu, L. Yuan, D. Li, Z. Tang, Y. Wang, G. Chen, H. Chen, J.L. Brash, Blood compatible materials: state of the art Xiaoli, *J. Mater. Chem. B.* 2 (2014) 5709–5926. www.rsc.org/MaterialsB (accessed July 10, 2018).
- [10] F. Meder, C. Brandes, L. Treccani, K. Rezwani, Controlling protein–particle adsorption by surface tailoring colloidal alumina particles with sulfonate groups, *Acta Biomater.* 9 (2013) 5780–5787. doi:10.1016/J.ACTBIO.2012.11.012.
- [11] H. Fabre, D. Mercier, A. Galtayries, D. Portet, N. Delorme, J.-F. Bardeau, Impact of hydrophilic and hydrophobic functionalization of flat TiO<sub>2</sub>/Ti surfaces on proteins adsorption, *Appl. Surf. Sci.* 432 (2018) 15–21. doi:10.1016/J.APSUSC.2017.08.138.
- [12] L.C. Xu, J.W. Bauer, C.A. Siedlecki, Proteins, platelets, and blood coagulation at biomaterial interfaces, *Colloids Surfaces B Biointerfaces.* 124 (2014) 49–68. doi:10.1016/j.colsurfb.2014.09.040.
- [13] K.M. Kovach, J.R. Capadona, A. Sen Gupta, J.A. Potkay, The effects of PEG-based surface modification of PDMS microchannels on long-term hemocompatibility, *J. Biomed. Mater. Res. Part A.* 102 (2014) n/a-n/a. doi:10.1002/jbm.a.35090.
- [14] X. Liu, L. Yuan, D. Li, Z. Tang, Y. Wang, G. Chen, H. Chen, J.L. Brash, Blood compatible materials: state of the art, *J. Mater. Chem. B.* 2 (2014) 5718–5738. doi:10.1039/C4TB00881B.

- [15] W. Song, J.F. Mano, Interactions between cells or proteins and surfaces exhibiting extreme wettabilities, *Soft Matter*. 9 (2013) 2985. doi:10.1039/c3sm27739a.
- [16] R. Adell, U. Lekholm, B. Rockler, P.-I. Brånemark, A 15-year study of osseointegrated implants in the treatment of the edentulous jaw, *Int. J. Oral Surg.* 10 (1981) 387–416. doi:10.1016/S0300-9785(81)80077-4.
- [17] N. Huang, P. Yang, Y.X. Leng, J.Y. Chen, H. Sun, J. Wang, G.J. Wang, P.D. Ding, T.F. Xi, Y. Leng, Hemocompatibility of titanium oxide films, *Biomaterials*. 24 (2003) 2177–2187. doi:10.1016/S0142-9612(03)00046-2.
- [18] K. Bartlet, S. Movafaghi, A. Kota, K.C. Papat, Superhemophobic titania nanotube array surfaces for blood contacting medical devices, *RSC Adv.* 7 (2017) 35466–35476. doi:10.1039/C7RA03373G.
- [19] S. Movafaghi, V. Leszczak, W. Wang, J.A. Sorkin, L.P. Dasi, K.C. Papat, A.K. Kota, Hemocompatibility of Superhemophobic Titania Surfaces", *Adv. Healthc. Mater.* (2017). doi:10.1002/adhm.201700647.
- [20] L. Gao, T.J. McCarthy, How Wenzel and Cassie were wrong, *Langmuir*. 23 (2007) 3762–3765. doi:10.1021/la062634a.
- [21] B.S. Smith, S. Yoriya, L. Grissom, C.A. Grimes, K.C. Papat, Hemocompatibility of titania nanotube arrays, *J. Biomed. Mater. Res. - Part A*. 95 A (2010) 350–360. doi:10.1002/jbm.a.32853.
- [22] K.C. Papat, G. Mor, C.A. Grimes, T.A. Desai, Surface modification of nanoporous alumina surfaces with poly(ethylene glycol), *Langmuir*. 20 (2004) 8035–8041. doi:10.1021/la049075x.
- [23] K.C. Papat, S. Sharma, T.A. Desai, Quantitative XPS Analysis of PEG-Modified Silicon Surfaces, *J. Phys. Chem. B*. 108 (2004) 5185–5188. doi:10.1021/jp049260j.
- [24] J.W. Bauer, L.-C. Xu, E.A. Vogler, C.A. Siedlecki, Surface dependent contact activation of factor XII and blood plasma coagulation induced by mixed thiol surfaces, *Biointerphases*. 12 (2017) 02D410. doi:10.1116/1.4983634.
- [25] V.B. Damodaran, V. Leszczak, K.A. Wold, S.M. Lantvit, K.C. Papat, M.M. Reynolds, Antithrombogenic properties of a nitric oxide-releasing dextran derivative: evaluation of platelet activation and whole blood clotting kinetics, (n.d.). doi:10.1039/c3ra45521a.
- [26] W. Wang, K. Lockwood, L.M. Boyd, M.D. Davidson, S. Movafaghi, H. Vahabi, S.R. Khetani, A.K. Kota, Superhydrophobic Coatings with Edible Materials, *ACS Appl. Mater. Interfaces*. 8 (2016) 18664–18668. doi:10.1021/acsami.6b06958.
- [27] J. Pouilleau, D. Devilliers, F. Garrido, S. Durand-Vidal, E. Mahé, Structure and composition of passive titanium oxide films, *Mater. Sci. Eng. B*. 47 (1997) 235–243. doi:10.1016/S0921-5107(97)00043-3.
- [28] J.A. Sorkin, S. Hughes, P. Soares, K.C. Papat, Titania nanotube arrays as interfaces for neural prostheses, *Mater. Sci. Eng. C*. 49 (2015) 735–745. doi:10.1016/J.MSEC.2015.01.077.
- [29] A. Rattana, M.-L. Abel, J.F. Watts, Degradation of Interfacial Chemistry of Epoxy/Silane/Aluminium Interfaces as a Result of Aqueous Attack, *J. Adhes.* 81 (2005) 963–988. doi:10.1080/00218460500222884.
- [30] Y. Huang, X. Lü, W. Qian, Z. Tang, Y. Zhong, Competitive protein adsorption on biomaterial surface studied with reflectometric interference spectroscopy, *Acta Biomater.* 6 (2010) 2083–2090. doi:10.1016/J.ACTBIO.2009.12.035.
- [31] W. Lin, J. Zhang, Z. Wang, S. Chen, Development of robust biocompatible silicone with

- high resistance to protein adsorption and bacterial adhesion, *Acta Biomater.* 7 (2011) 2053–2059. doi:10.1016/J.ACTBIO.2011.02.001.
- [32] G.K. Mor, O.K. Varghese, M. Paulose, N. Mukherjee, C.A. Grimes, Fabrication of tapered, conical-shaped titania nanotubes, *J. Mater. Res.* 18 (2003) 2588–2593. doi:10.1557/JMR.2003.0362.
- [33] J.P. Blitz, C.B. Little, *Fundamental and applied aspects of chemically modified surfaces*, n.d. <https://books.google.com/books?hl=pt-PT&lr=&id=MVOkAgAAQBAJ&oi=fnd&pg=PP1&dq=Blitz,+J.%3B+Little,+C.+Fundamental+%26+Applied+Aspects+of+Chemically+Modified+Surfaces,+Royal+Society+of+Chemistry,+1999.&ots=xrwDvfRtYl&sig=YEp1OMQUbeL0q39ELi7IM5JxXKU#v=snipe> (accessed December 5, 2018).
- [34] S. Movafaghi, W. Wang, A. Metzger, D.D. Williams, J.D. Williams, A.K. Kota, Tunable superomniphobic surfaces for sorting droplets by surface tension, *Lab Chip.* 16 (2016) 3204–3209. doi:10.1039/C6LC00673F.
- [35] M. Xu, G. Sun, C.-J. Kim, Infinite Lifetime of Underwater Superhydrophobic States, *Phys. Rev. Lett.* 113 (2014) 136103. doi:10.1103/PhysRevLett.113.136103.
- [36] D.A. Puleo, Retention of enzymatic activity immobilized on silanized Co-Cr-Mo and Ti-6Al-4V, *J. Biomed. Mater. Res.* 37 (1997) 222–228. doi:10.1002/(SICI)1097-4636(199711)37:2<222::AID-JBM11>3.0.CO;2-G.
- [37] V. Leszczak, B.S. Smith, K.C. Papat, Hemocompatibility of polymeric nanostructured surfaces, *J. Biomater. Sci. Polym. Ed.* 24 (2013) 1529–1548. doi:10.1080/09205063.2013.777228.
- [38] P. Roach, D. Farrar, C.C. Perry, Interpretation of protein adsorption: Surface-induced conformational changes, *J. Am. Chem. Soc.* 127 (2005) 8168–8173. doi:10.1021/ja042898o.
- [39] T. Sun, H. Tan, D. Han, Q. Fu, L. Jiang, No platelet can adhere—largely improved blood compatibility on nanostructured superhydrophobic surfaces, *Small.* 1 (2005) 959–963. doi:10.1002/sml.200500095.
- [40] A. De Mel, B.G. Cousins, A.M. Seifalian, Surface modification of biomaterials: A quest for blood compatibility, *Int. J. Biomater.* 2012 (2012). doi:10.1155/2012/707863.
- [41] N. Nath, J. Hyun, H. Ma, A. Chilkoti, Surface engineering strategies for control of protein and cell interactions, *Surf. Sci.* 570 (2004) 98–110. doi:10.1016/J.SUSC.2004.06.182.
- [42] H. Elwing, A. Askendal, I. Lundström, Competition between adsorbed fibrinogen and high-molecular-weight kininogen on solid surfaces incubated in human plasma (the vroman effect): Influence of solid surface wettability, *J. Biomed. Mater. Res.* 21 (1987) 1023–1028. doi:10.1002/jbm.820210808.
- [43] H. Noh, E.A. Vogler, Volumetric interpretation of protein adsorption: Competition from mixtures and the Vroman effect, *Biomaterials.* 28 (2007) 405–422. doi:10.1016/j.biomaterials.2006.09.006.
- [44] M.B. Gorbet, M. V. Sefton, Biomaterial-associated thrombosis: Roles of coagulation factors, complement, platelets and leukocytes, *Biomater. Silver Jubil. Compend.* 25 (2004) 219–241. doi:10.1016/B978-008045154-1.50025-3.
- [45] C. Sperling, M. Fischer, M.F. Maitz, C. Werner, Blood coagulation on biomaterials requires the combination of distinct activation processes, *Biomaterials.* 30 (2009) 4447–4456. doi:10.1016/J.BIOMATERIALS.2009.05.044.
- [46] M. Johnell, R. Larsson, A. Siegbahn, The influence of different heparin surface

- concentrations and antithrombin-binding capacity on inflammation and coagulation, *Biomaterials*. 26 (2005) 1731–1739. doi:10.1016/j.biomaterials.2004.05.029.
- [47] A. Thor, L. Rasmusson, A. Wennerberg, P. Thomsen, J.-M. Hirsch, B. Nilsson, J. Hong, The role of whole blood in thrombin generation in contact with various titanium surfaces, *Biomaterials*. 28 (2007) 966–974. doi:10.1016/J.BIOMATERIALS.2006.10.020.
- [48] R. Zhuo, C.A. Siedlecki, E.A. Vogler, Autoactivation of blood factor XII at hydrophilic and hydrophobic surfaces, *Biomaterials*. 27 (2006) 4325–4332. doi:10.1016/J.BIOMATERIALS.2006.04.001.
- [49] L.-C. Xu, M.E. Meyerhoff, C.A. Siedlecki, Blood coagulation response and bacterial adhesion to biomimetic polyurethane biomaterials prepared with surface texturing and nitric oxide release, *Acta Biomater.* 84 (2019) 77–87. doi:10.1016/J.ACTBIO.2018.11.035.
- [50] N.A. Patankar, On the Modeling of Hydrophobic Contact Angles on Rough Surfaces, (2003). doi:10.1021/la026612.
- [51] E.J. Falde, S.T. Yohe, Y.L. Colson, M.W. Grinstaff, Superhydrophobic materials for biomedical applications, *Biomaterials*. 104 (2016) 87–103. doi:10.1016/J.BIOMATERIALS.2016.06.050.
- [52] V.B. Damodaran, V. Leszczak, K.A. Wold, S.M. Lantvit, K.C. Popat, M.M. Reynolds, Antithrombogenic properties of a nitric oxide-releasing dextran derivative: Evaluation of platelet activation and whole blood clotting kinetics, *RSC Adv.* 3 (2013) 24406–24414. doi:10.1039/c3ra45521a.
- [53] R. Simon-Walker, J. Cavicchia, D.A. Prawel, L.P. Dasi, S.P. James, K.C. Popat, Hemocompatibility of hyaluronan enhanced linear low density polyethylene for blood contacting applications, *J. Biomed. Mater. Res. - Part B Appl. Biomater.* (2017) 1–12. doi:10.1002/jbm.b.34010.

# CHAPTER 3: ENHANCED HEMOCOMPATIBILITY AND ANTIBACTERIAL ACTIVITY ON TITANIA NANOTUBES WITH TANFLOC/HEPARIN POLYELECTROLYTE MULTILAYERS<sup>1</sup>

## 3.1. Introduction

The use of blood-contacting implants, such as heart valves, catheters, and stents to treat cardiovascular diseases has increased remarkably in recent years [2]. However, catastrophic complications from these biomaterials still occur, such as thrombus formation and bacterial infections, which are the most common causes for device failure [3]. The processes leading to bacterial adhesion and coagulation are related, and microbial infections may become worse due to the activation of the coagulation cascade [4]. Therefore, it is vital to develop multifunctional surfaces that can simultaneously prevent clot formation and bloodstream infections. Among the biomaterials used for blood-contacting applications, titanium and its alloys are widely employed due to their excellent mechanical properties, corrosion resistance, and remarkable biocompatibility with many body tissues [5]. Nevertheless, titanium's compatibility with blood and its ability to inhibit bacterial infection are still far from ideal [6,7].

Several approaches have been investigated to prevent both bacterial infections and thrombosis on titanium surfaces, including modification of the surface chemistry, wettability, and topography [8]. Protein adsorption and activation is a critical initial step that can lead to adverse biological responses that prevent healthy tissue healing. Therefore, the use of natural antifouling

---

<sup>1</sup> This work was published in *Journal of Biomedical Materials Research Part A* and is reproduced in modified form here with permission [1]

coatings has emerged as a strategy for improving biocompatibility of surfaces. One promising technique recently investigated is the layer-by-layer (LbL) deposition of polyelectrolyte multilayers (PEMs). LbL assembly is used to change the surface chemistry of materials by alternately adsorbing/depositing polycationic and polyanionic layers onto a solid substrate [9]. PEMs can be easily and reproducibly prepared, to achieve control over coating thickness and surface chemistry, without the use of hazardous organic solvents [10]. Among the polycation-polyanion polymer pairs recently used, heparin and chitosan PEMs have generated particular interest for biological activation of surfaces [11,12]. Heparin (HP) is a highly negatively charged polymer and a natural glycosaminoglycan (GAG), which in the body prevents blood coagulation by inhibiting the thrombin activation [13]. Although heparinized materials have been used clinically in blood-contacting biomaterials, there are still some limitations, such as loss of bioactivity over long periods of time, especially due to its high solubility [14]. Chitosan (CS) and its cationic derivatives allow the formation of multilayers with the negatively charged heparin [11]. CS-based PEMs can be used to improve the tissue compatibility of surfaces and inhibit bacterial infections [15]. Another naturally occurring GAG that has been employed in biomedical materials is hyaluronic acid (HA). This anionic biopolymer has great cytocompatibility and biodegradability. Because of these properties, it has been used in PEM coatings on biomaterials [16].

Recently, tanfloc (TA) has attracted considerable interest due to its promising cytocompatibility, biodegradability, and antimicrobial properties [17]. TA is a hydrophilic, cationic ( $pK_a \approx 6.0$ ), and condensed amino-functionalized tannin derivative [18]. TA is synthesized from condensed tannins (from polyphenols with repeat flavan-3-ol units) found in plants that act to inhibit pathogen occurrences [19]. Condensed tannins are often extracted from the *Acacia Decurrens* (Black wattle), and they are then used to obtain the TA derivative from acid

catalysis performed with ammonium chloride and formic acid [18]. TA has strong antimicrobial activity due to the presence of ammonium moieties ( $-\text{NH}_3^+$ ) stabilized by chloride counterions and phenolic moieties in its structure. Because of its cationic behavior in aqueous solutions, it can replace CS to provide PEMs with HP or HA. Previous studies have shown TA-based materials presented cytocompatibility and antimicrobial activities [17,18]; however, no studies report the blood compatibility, antiadhesive, and antibacterial traits of TA-based PEMs.

In this work, TA/HP PEMs on titania nanotubes (NT) were successfully developed. First, the surface topography was modified by making NT, as it has been shown that NT has better antibacterial properties and reduces thrombogenic effects on titanium [20,21]. Then, NT surface was modified with PEMs using TA or CS as polycations, and HP or HA as polyanions. The PEMs were fabricated using 5 layers, terminating with the polycation. The surfaces were characterized using SEM, XPS, and contact angle measurements. Fibrinogen adsorption, FXII activation, and platelet adhesion and activation on the surfaces were investigated. The adhesion and morphology of *S. aureus* and *P. aeruginosa* were also evaluated. Previous study has shown that CS/HP PEMs on NT can reduce platelet adhesion [22]; however, titanium modification with TA has never been investigated. In this study, biological responses of TA and CS-based PEMs deposited on the NT surface were compared. The results indicated that TA-based PEMs enhance the anti-thrombogenic, antibacterial, and antiadhesive properties of the NT when compared to CS-based PEMs.

## **3.2. Materials and Methods**

### **3.2.1. Fabrication of titania nanotubes (NT) with PEMs**

NT surfaces were fabricated from titanium sheets (0.5 mm thick) via the anodization process reported elsewhere [23]. Prior to the surface modification with PEMs, the NT surfaces

were treated with oxygen plasma at 200 V in 10 cm<sup>3</sup>/min of oxygen gas for 15 min. Tanfloc (TA, Tanac SA, Brazil)[18] and chitosan (CS, Golden Shell Biochemical, China, 85% deacetylated and 87 kDa)[24] were purified by first preparing a 10% w/v TA solution in DI water and 1.0 % w/v CS solution in aqueous acetic acid (1.0% v/v). Dialysis was then conducted with 7000 MWCO membrane for 2 days, with exchange of water twice a day. The polymeric solutions were then frozen and lyophilized for 3 days. To prepare the PEMs, solutions of TA, CS, HP (Celsus Laboratories, USA), and HA (Sigma Aldrich, USA) were prepared in an acetic acid-acetate buffer (0.2 M sodium acetate and acetic acid at pH 5.0) at a concentration of 1 mg/ml. After that, the solutions were filtered with 0.22 μm syringe filters. An aqueous acetic acid solution (pH 4.0) was used as a rinse solution. The oxidized NT surface was rinsed with 0.5 ml rinse solution under shaking (50 rpm) for 4.0 min before the TA or CS deposition. The rinse solution was aspirated and LbL deposition was carried out on the oxidized NT surface. Then, 0.5 ml TA or CS solutions (polycations) was added to the oxidized NT surface under shaking (50 rpm). After 5.0 min, the polycation solution was aspirated and the surface was rinsed under shaking for 4.0 min. Then, the rinse solution was aspirated and HP or HA polyanion solutions (0.5 ml) were deposited onto the oxidized NT surface containing one layer of polycation (TA or CS). This method was repeated until the fifth layer was deposited. The surfaces with 5 layers (polycation terminated) were rinsed for 4 min and incubated in DI water for further use. **Figure 3.1** presents the process of PEMs fabrication, as well as the polyelectrolytes' chemical structures. The CS/HP, CS/HA, TA/HP and TA/HA PEMs deposited on NT surfaces are referred to as NT(CS-HP), NT(CS-HA), NT(TA-HP) and NT(TA-HA), respectively.

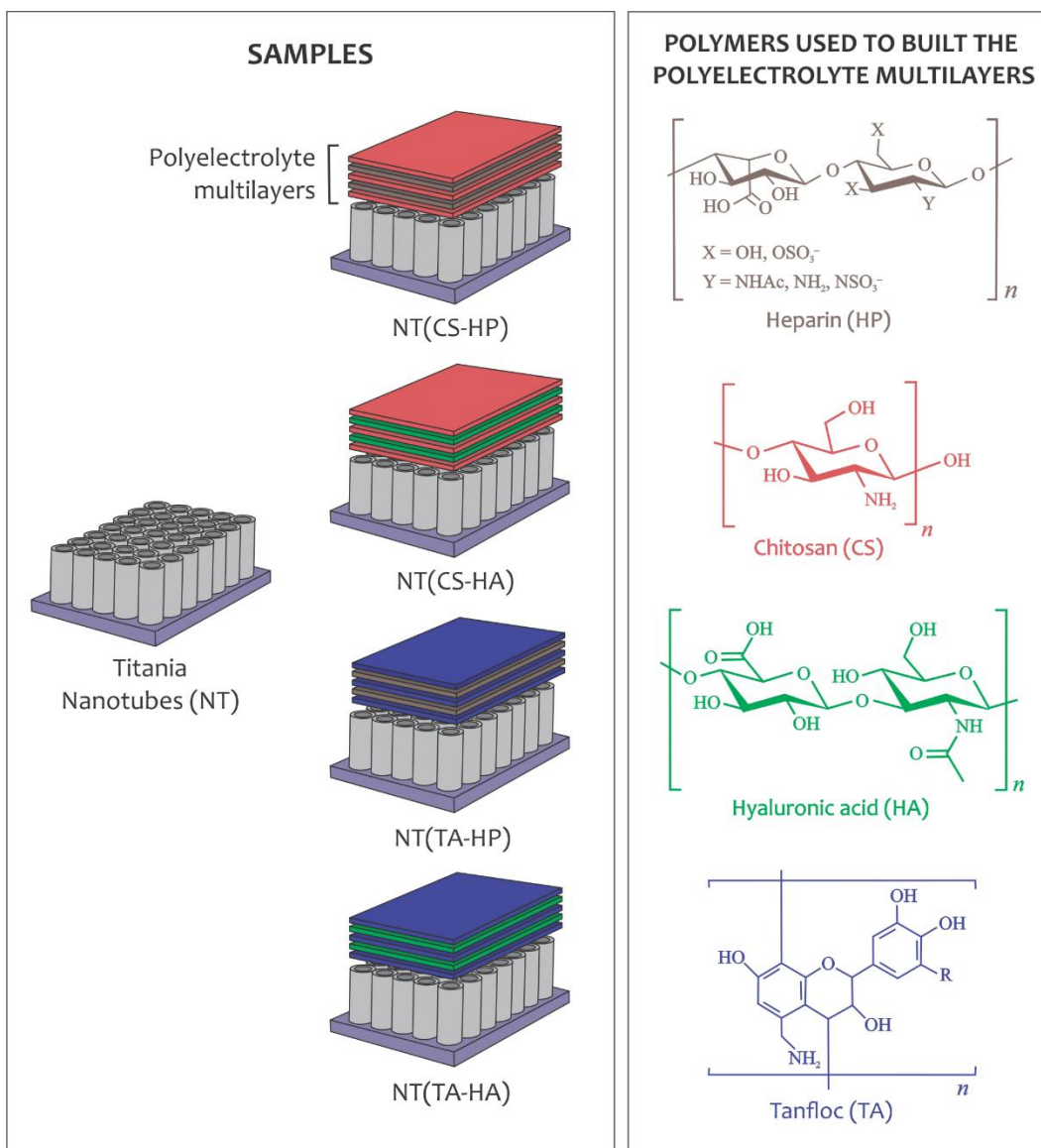


**Figure 3.1.** Schematic representation of the PEM construction on titania nanotubes (NT) and chemical structures of the polyelectrolytes.

### 3.2.2. Surface characterization

The morphology of each surface was characterized by SEM. Before imaging at 15 kV, the surfaces were coated with 20 nm gold. Static contact angles of different surfaces were obtained using a Ramé-Hart goniometer. Approximately 10  $\mu$ l of DI water were placed on the surface to obtain the water contact angles. The composition of different surfaces was investigated using XPS.

Survey spectra were collected from 0 to 1100 eV (pass energy of 187 eV), and high-resolution spectra were collected for carbon at a pass energy of 10 eV. Spectral analysis was performed using Origin and MultiPak. Prior to all studies, the surfaces were sterilized by rinsing in 70% ethanol, followed by rinse and incubation with sterile PBS for 30 min.

### **3.2.3. Hemocompatibility studies**

To analyze the anti-thrombogenic properties of the surfaces, the adsorption of fibrinogen, a key protein involved in thrombus formation [25], and the activation of Factor XII (FXII), that is responsible for the activation of the intrinsic pathway of the coagulation cascade were investigated [26]. Additionally, platelet adhesion and activation that also mediates blood clotting on different surfaces were evaluated [27].

#### *3.2.3a Fibrinogen adsorption on different surfaces*

To investigate the fibrinogen adsorption, the surfaces were incubated in a 48-well plate with 100 µg/ml of human fibrinogen solution in PBS on a horizontal shaker plate (100 rpm) at 37 °C and 5% CO<sub>2</sub>. After 2 h of incubation, the protein solution was aspirated, and the surfaces were rinsed twice with PBS and once with DI water to remove any non-adherent proteins. The protein adsorption on different surfaces was investigated by XPS analysis, as described in Section 2.2.

#### *3.2.3b Isolation of human platelet poor plasma (PPP) and platelet rich plasma (PRP)*

Whole human blood was obtained from healthy donors, who signed formal consents for this study. All practices were approved by the Colorado State University Institutional Review Board which agrees with the National Institutes of Health's "Guiding Principles for Ethical Research". To obtain PPP, whole blood was drawn into 2.7 ml vacuum tubes coated with sodium

citrate and centrifuged at 1500 g for 10 min. To obtain PRP, whole blood was drawn into 10 ml vacuum tubes coated with ethylenediaminetetraacetic acid (EDTA) and centrifuged at 150 g for 15 min.

### *3.2.3c FXII activation on different surfaces*

To investigate the activation of the intrinsic pathway of the coagulation cascade, FXII activation on different surfaces was characterized by an in vitro plasma coagulation time (CT) assay. CT is defined as the time needed from activation of the intrinsic pathway of the coagulation cascade to the appearance of a visible clot [28]. A mathematical model was developed to correlate CT with FXIIa concentration through three adjustable parameters [29]. This method is reported in detail elsewhere [23]. Briefly, purified human FXII (Haematologic Technologies) was incubated with different surfaces at a concentration of 30  $\mu\text{g/ml}$  for 30 min. After, 100  $\mu\text{l}$  aliquots were taken and added to a cuvette with 0.5 ml of PPP, 0.3 ml of 0.01M PBS and 0.1 ml of 0.1M  $\text{CaCl}_2$ . The  $\text{CaCl}_2$  was the last reagent added to ensure a common zero-time CT. The cuvettes were then covered with parafilm and rotated at 20 rpm on a hematology mixer, and the corresponding CT was recorded. The CT was then used to calculate the equivalent FXIIa activity by referencing back to the FXIIa titration curve obtained in previous study [23].

### *3.2.3d Platelet adhesion and activation on different surfaces*

Platelet adhesion was investigated using fluorescence microscopy. The surfaces were incubated in a 48-well plate with 500  $\mu\text{l}$  of PRP at 37°C and 5%  $\text{CO}_2$  on a horizontal shaker plate (100 rpm). After 2 h of incubation, PRP was aspirated and the surfaces were rinsed twice with sterile PBS to remove non-adherent platelets. The surfaces were then incubated with 2  $\mu\text{M}$  calcein-AM solution in PBS for 30 min in a dark environment. After that, the surfaces were rinsed with

PBS and imaged using a fluorescence microscope. ImageJ was used to count the total number of platelets attached.

Platelet activation on different surfaces was characterized using SEM. After 2 h incubation in PRP and rinse with PBS, the surfaces were incubated in a primary fixative solution (3% glutaraldehyde, 0.1 M sucrose, and 0.1 M sodium cacodylate in DI water) for 45 min. The surfaces were then incubated in a buffer solution (fixative without glutaraldehyde) for 10 min. After that, the surfaces were dehydrated in ethanol solutions (35, 50, 70, and 100%, respectively) for 10 min each. Prior to SEM imaging, the surfaces were gold-coated, as described in Section 3.2.2.

### **3.2.4. Antibacterial activity studies**

The antibacterial activity of different surfaces was evaluated against Gram-negative *Pseudomonas aeruginosa* (*P. aeruginosa*, P01) and Gram-positive *Staphylococcus aureus* (*S. aureus*, ATCC 6538) cultures obtained from agar plate culture and pellet, respectively. A nutrient broth media solution (NBM, LB-Miller) was prepared at a concentration of 25 mg/ml. The *S. aureus* pellet was resuspended in NBM solution and an aliquot of *P. aeruginosa* was taken from the agar plate and dissolved in NBM. Both bacteria solutions were incubated at 37 °C for 24 h until the optical density at 600 nm was approximately 1 [30].

#### *3.2.4a Growth inhibition in solution*

The bacteria solutions were diluted to obtain a concentration of  $10^6$  CFU/ml. The surfaces were then incubated in 500  $\mu$ l of bacteria solution for 6 and 24 h. A 100  $\mu$ l aliquot of the solution was taken and the absorbance was read at 600 nm using a plate reader. Bacteria solutions under the same conditions without exposure to surfaces were used as control. The values were then compared to the control and the inhibition percentage was calculated.

### *3.2.4b Bacteria adhesion on different surfaces*

Fluorescence microscopy was used to measure the amount of live and dead bacteria that adhered to the surfaces. After incubation for 6 and 24 h, the bacteria solution was removed, and the surfaces were rinsed three times with PBS to remove any non-adhered bacteria. The surfaces were then incubated in stain solution (3  $\mu$ l/ml of propidium iodide and Syto 9 stain 1:1 in PBS) for 20 min at room temperature and in a dark environment. After incubation, the stain solution was aspirated, and the surfaces were rinsed once with PBS. The surfaces were then immediately imaged using a fluorescence microscope. ImageJ was used to calculate the percentage of live and dead bacteria on the surfaces.

### *3.2.4c Bacteria morphology and biofilm formation on different surfaces*

Bacteria morphology and biofilm formation on different surfaces were characterized by SEM. The surfaces were incubated in bacteria solution as described in Section 2.4a for 6 and 24 h. After the incubation, the surfaces were rinsed twice with PBS, fixed and dehydrated, as described in Section 2.3d. Prior to SEM imaging, the surfaces were gold coated as described in Section 2.2.

### **3.2.5. Statistical analysis**

SEM images and XPS analysis were reconfirmed on at least 2 different samples of each surface. Contact angle measurements were taken using 2 droplets per sample on 3 different samples of each surface ( $n_{\min} = 6$ ). All other experiments were conducted at least twice with 3 samples of each surface ( $n_{\min} = 6$ ). The quantitative results were analyzed via analysis of variance (ANOVA) and Tukey tests using Origin software ( $p < 0.05$ ).

### 3.3. Results

#### 3.3.1. Surface characterization

The SEM images indicate that NT are uniform and vertically oriented, and the PEMs with 5 layers do not entirely coat the surface and still maintain the nanotube topography (**Figure 3.2**). The results also show no apparent changes in morphology for NT(CS-HP), NT(CS-HA), and NT(TA-HP) in comparison with NT. NT(TA-HA) shows some changes in morphology, although the nanotubes are still visible. No significant difference was observed in nanotubes' diameter ( $110 \pm 14$  nm) even after PEM deposition.

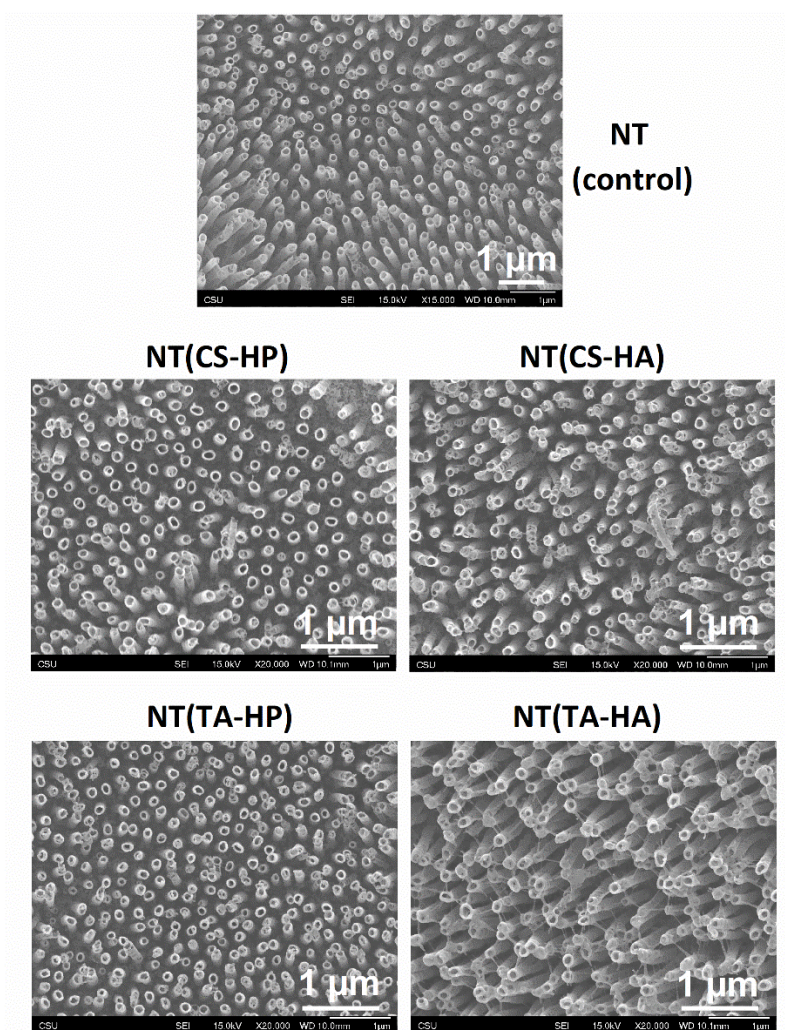


**Figure 3.2.** Representative SEM images of titania nanotubes (NT) before and after surface modification with PEMs.

Contact angle measurements show that all surfaces are hydrophilic (**Table 3.1**). A surface is considered hydrophilic when the static contact angle ( $\theta$ ) between the surface and water is less than  $90^\circ$ , and hydrophobic when  $\theta$  is greater than  $90^\circ$ . NT surfaces modified with HP were significantly more hydrophilic than the ones modified with HA. The NT modified with TA are slightly more hydrophilic in comparison with the ones modified with CS, although no significant difference was observed between NT(CS-HP) and NT(TA-HP); and between NT(CS-HA) and NT(TA-HA).

**Table 3.1.** Static water contact angle measurements for different surfaces.

Surface	Contact angle (degrees)
NT	<10
NT(CS-HP)	$13 \pm 1$
NT(CS-HA)	$19 \pm 2$
NT(TA-HP)	$11 \pm 2$
NT(TA-HA)	$16 \pm 2$

XPS survey spectra indicate that all surfaces have oxygen (O1s), titanium (Ti2p<sub>3/2</sub>), and carbon (C1s) elements (**Figure 3.3a**). Surfaces modified with HP have S2p and S2s peaks. As expected, all surfaces modified with PEMs have N1s peaks, which is characteristic of the polyelectrolytes' composition. The elemental composition of different surfaces was also obtained from survey XPS scans using MultiPak software (**Table 3.2**). All modified NT surfaces show an increase in the carbon content, as well as a decrease in the titanium signal in comparison with the unmodified NT surface. However, although the oxygen is present in all polyelectrolytes' chemical structure, its percentage concentration on the surfaces has decreased compared to NT. This occurs due to the significant increase in carbon content. The titanium concentration on surfaces modified

with TA are smaller than the ones modified with CS, indicating that the TA-based PEMs achieve greater coverage of the NT surface than CS-based PEMs. High-resolution C1s spectra were also obtained from XPS analysis (**Figure 3.3b**). **Table 3.3** shows the contribution of different peaks in the overall C1s spectra. The modified NT surfaces have a significant increase in both C–O and C–N groups when compared to the unmodified NT surface. NT(TA-HP) and NT(TA-HA) also show a higher concentration of C–C peaks and smaller presence of O–C=O peaks compared with NT(CS-HP) and NT(CS-HA).

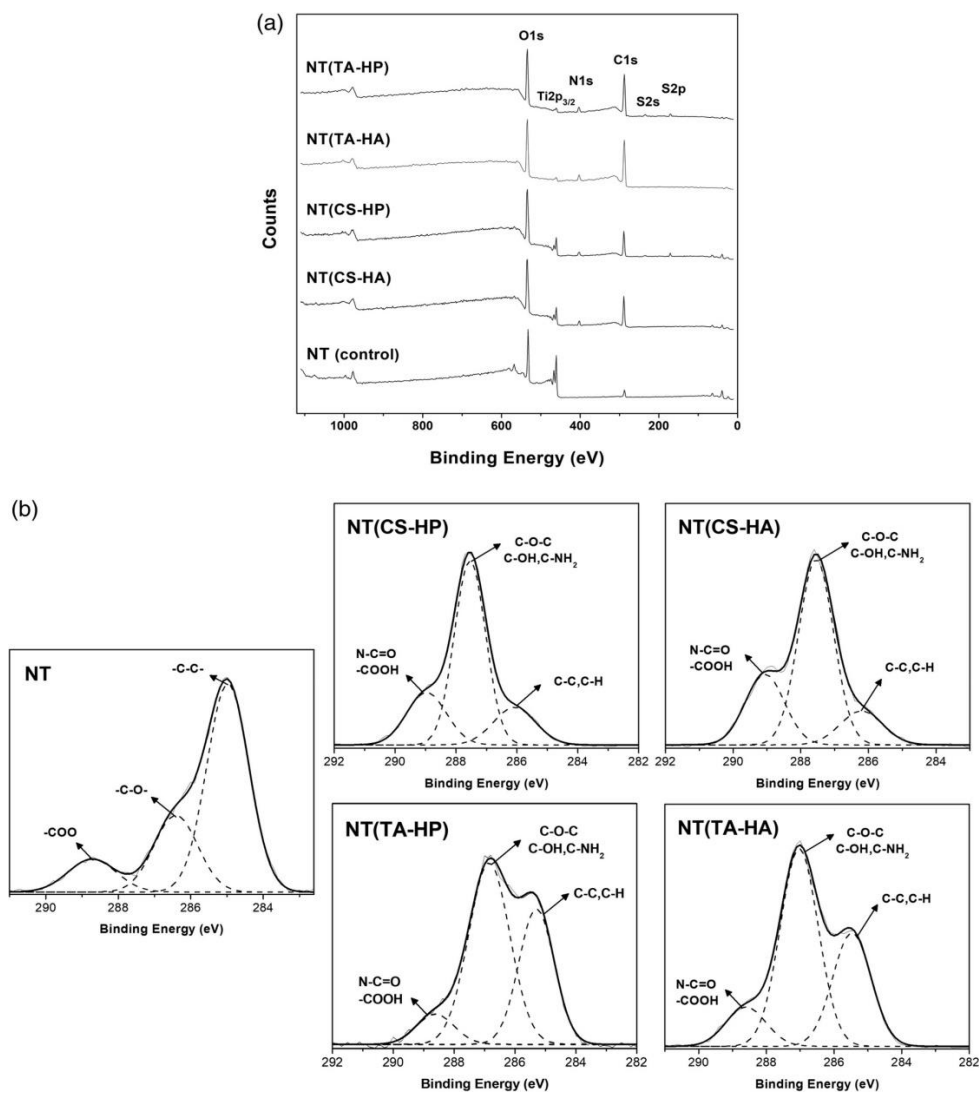


**Figure 3.3.** (a) XPS survey scans for different surfaces. (b) High-resolution XPS spectra for C1s obtained from the different surfaces

**Table 3.2.** Elemental composition of the different surfaces determined by survey XPS analysis.

	% C1s	% O1s	% Ti2p	% N1s	% S2p
<b>NT</b>	11.7	68.3	20.0	0	0
<b>NT(CS-HP)</b>	47.2	41.8	5.3	4.2	1.5
<b>NT(CS-HA)</b>	48.1	44.5	3.6	3.8	0
<b>NT(TA-HP)</b>	59.0	34.4	0.9	4.5	1.2
<b>NT(TA-HA)</b>	62.1	32.2	0.6	5.1	0

**Table 3.3.** The relative percentages of C–C/C–H, C–O/C–N, and N–C=O/COOH determined from the peak areas from the C1s envelopes for the different surfaces.

	C–C, C–H	C–O, C–N	N–C=O, COOH
<b>NT</b>	63.5	25.7	10.8
<b>NT(CS-HP)</b>	16.8	61.1	22.1
<b>NT(CS-HA)</b>	25.9	60.6	13.5
<b>NT(TA-HP)</b>	35.7	55.8	8.5
<b>NT(TA-HA)</b>	32.4	55.9	11.7

### 3.3.2. Hemocompatibility studies

Survey and high-resolution XPS spectra for C1s were collected for the surfaces after incubation in human fibrinogen solution. The elemental composition was used to investigate the amount of fibrinogen adsorbed on the material surfaces (**Table 3.4**). Since proteins contain high nitrogen levels, the increase in the nitrogen content on the surfaces is due to the fibrinogen adsorption. The results show that all modified NT surfaces significantly decrease the amount of fibrinogen adsorbed compared to NT. However, the NT(TA-HA) surface presents the lowest

adsorption, followed by the NT(TA-HP) surface. High-resolution C1s spectra indicate three peaks for all surfaces: N–C=O/COOH, C–N/C–O, and C–C/C–H (**Figure 3.4**). An accurate way to determine fibrinogen adhered on the surface is to identify the contribution of the amide peak (N–C=O) in the overall C1s peak as the amide group is characteristic of proteins [31]. **Figure 3.3b** shows that all surfaces already indicated the N–C=O and/or COOH groups before fibrinogen adsorption assay. Therefore, to determine the amount of protein adsorbed, the contribution of the amide peak after protein adsorption was subtracted by the contribution of the same peak before the protein adsorption study. The NT surfaces modified with TA-based PEMs have significantly less fibrinogen adsorbed compared to the other surfaces (**Table 3.5**). The NT surfaces modified with CS also have a slight decrease in fibrinogen adsorption when compared to unmodified NT; however, the TA-based PEMs promoted better fibrinogen resistance. NT(TA-HA) has the lowest amount of fibrinogen adsorption.

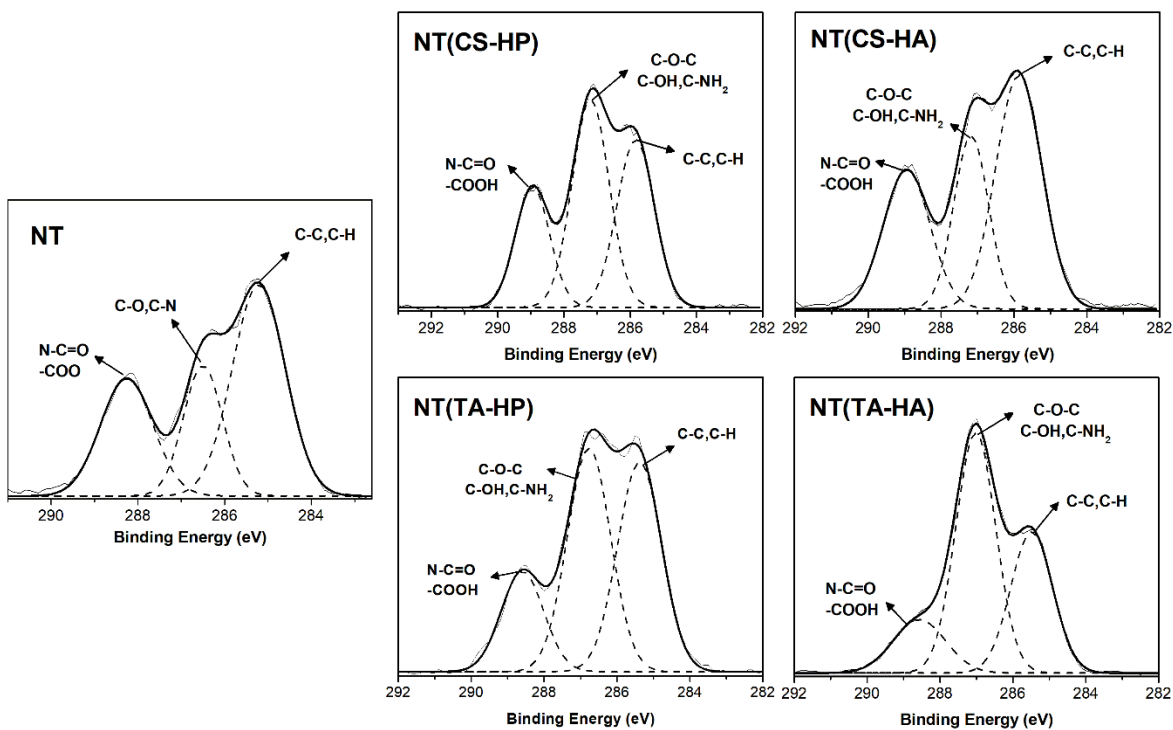


**Figure 3.4.** High-resolution XPS spectra for C1s obtained on the different surfaces after 2 h incubation in fibrinogen solution.

**Table 3.4.** Nitrogen content found on the material surfaces determined after the fibrinogen adsorption assay. The difference corresponds to the amount of fibrinogen adsorbed to each surface. The results were obtained from survey XPS analysis.

	<b>% N (BEFORE)</b>	<b>% N (AFTER)</b>	<b>INCREASE</b>
<b>NT</b>	0	13.1	13.1%
<b>NT(CS-HP)</b>	4.2	9.7	5.5%
<b>NT(CS-HA)</b>	3.8	13.1	9.3%
<b>NT(TA-HP)</b>	4.5	9.2	4.7%
<b>NT(TA-HA)</b>	5.1	7.1	2.0%

**Table 3.5.** The contribution of amide (N–C=O) peaks in the C1s envelopes are given in percentages after the fibrinogen adsorption assay. The difference corresponds to the amount of fibrinogen adsorbed on the material surfaces.

	<b>N-C=O (BEFORE)</b>	<b>N-C=O (AFTER)</b>	<b>INCREASE</b>
<b>NT</b>	10.8	27.5	16.7%
<b>NT(CS-HP)</b>	22.1	34.7	12.6%
<b>NT(CS-HA)</b>	13.5	27.8	14.3%
<b>NT(TA-HP)</b>	8.5	18.3	9.8%
<b>NT(TA-HA)</b>	11.7	15.2	3.5%

FXII activation on surfaces was determined by the CT assay. The calibration curve obtained in the previous study was used to convert the CT measured into FXIIa concentration (**Figure 3.5**) [23]. NT(TA-HP) was the only surface that significantly decreases the FXII activation when compared to the unmodified NT. This surface dramatically decreases FXII activation, reaching about one-eighth of the FXIIa amount produced on unmodified NT.

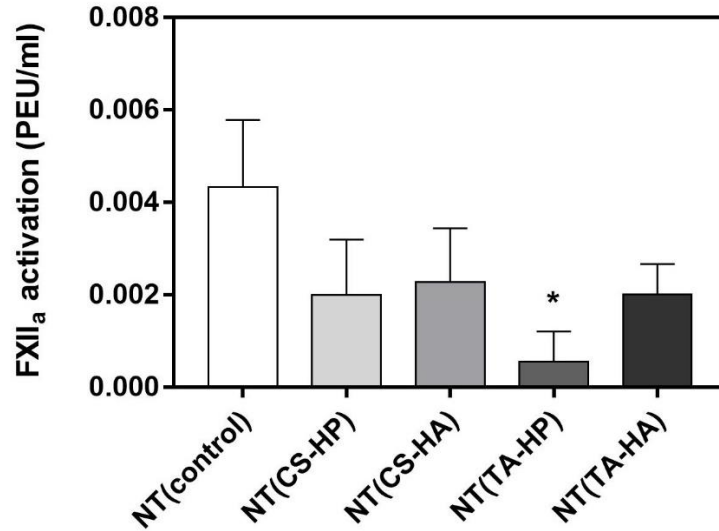


**Figure 3.5.** FXII activation on different surfaces. Experiments were conducted at least twice with 3 samples of each surface ( $n_{\min} = 6$ ). NT(TA-HP) has significantly lower FXII activation than the NT surfaces ( $p < 0.05$ ).

The fluorescence images of cells adhered to surfaces show that NT(TA-HP) and NT(TA-HA) significantly decrease the platelet adhesion compared to the unmodified NT (**Figure 3.6**). The NT(TA-HP) promotes the lowest amount of platelet adhesion, approximately 10-fold less than that imparted on NT. NT(CS-HP) also decreases platelet adhesion compared to NT, but not significantly. After attachment to the biomaterial surface, the platelets can activate, which is indicated by a morphological membrane change [22]. When platelets are un-activated, they exhibit a compact round shape. As they start to activate, dendritic extensions are formed and platelets can be considered partially activated (short-dendritic morphology) or fully activated (long dendritic morphology) [7]. The SEM results show that NT and NT(CS-HA) surfaces present partially activated platelets with some short dendritic extensions (**Figure 3.7**). The formation of platelet aggregates on NT and NT(CS-HA) surfaces is another evidence of platelet activation [7]. NT(CS-HP) surface also exhibits platelet aggregation; however, no dendritic extension was observed. NT(TA-HA) surface presents a small amount of platelet aggregation, with a very low content of

partially activated platelets. NT(TA-HP) was the only surface with no platelet aggregation or dendritic formation. SEM results also agree with the fluorescence images, as NT and NT(CS-HA) surfaces present the highest number of adhered cells, followed by NT(CS-HP). Both TA-modified surfaces have very low amounts of platelets.

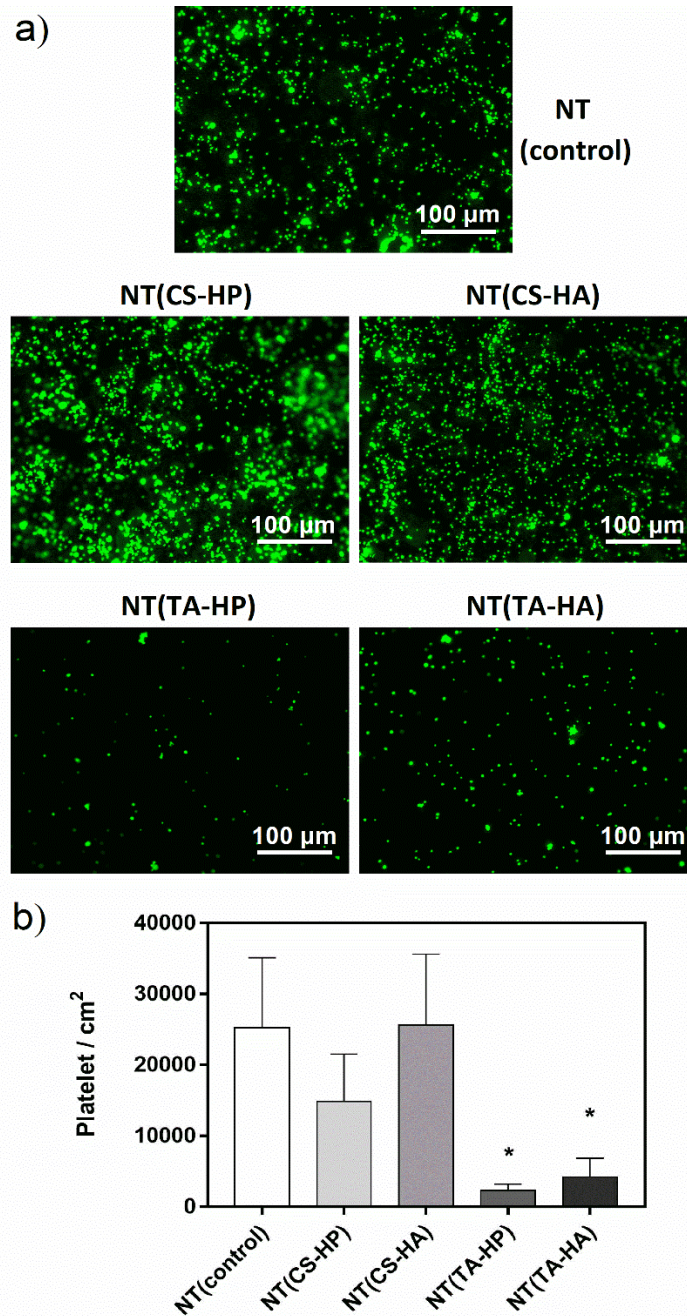


**Figure 3.6.** (a) Representative fluorescence microscopy images of platelet adhesion after 2 h of incubation in PRP. (b) Number of adhered platelets per area (cm<sup>2</sup>) on the different surfaces.

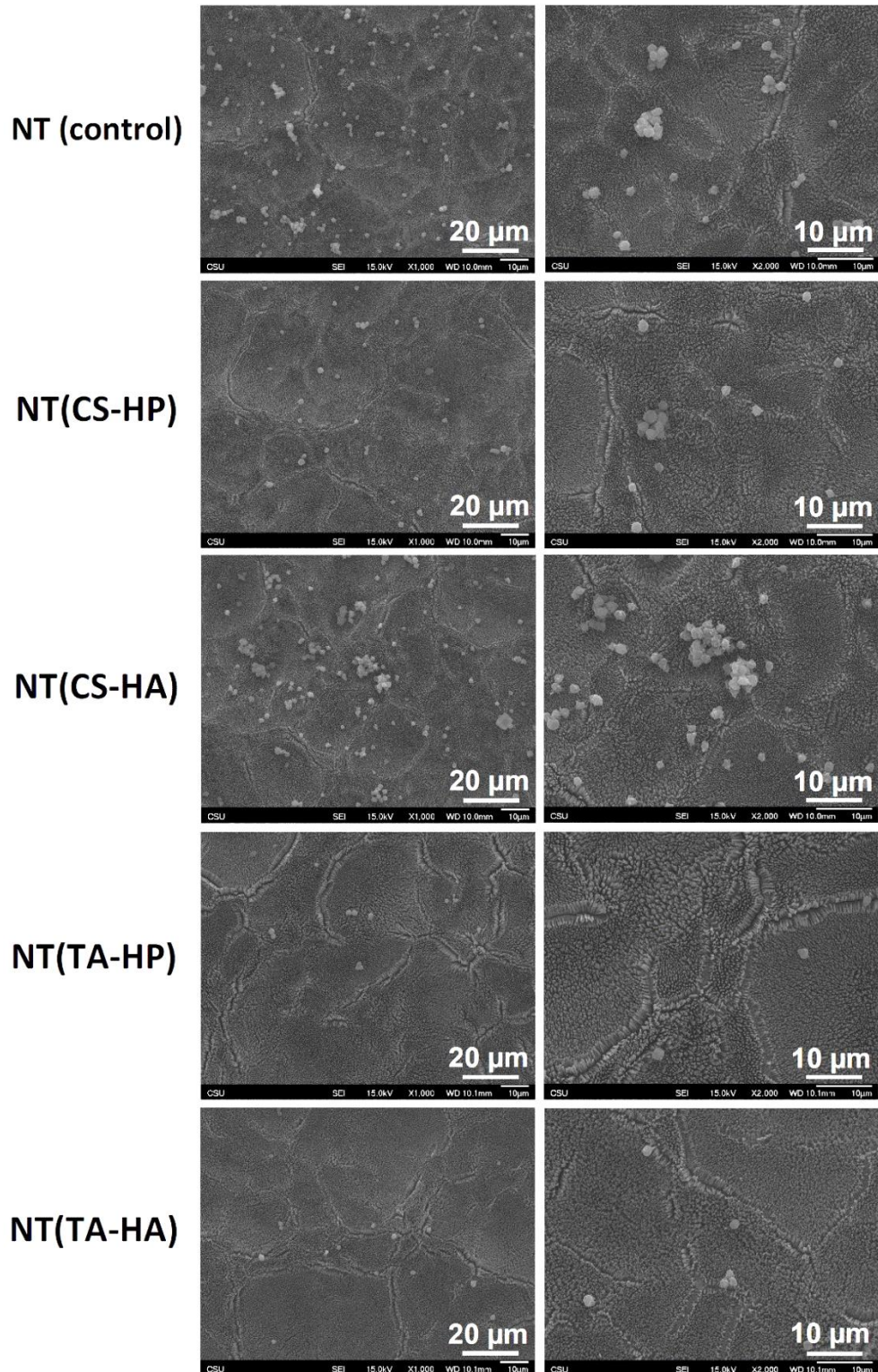


**Figure 3.7.** Representative SEM images of adhered platelets on different surfaces after 2 h of incubation in PRP. The images were taken at 1000 $\times$  and 2000 $\times$  magnification.

### 3.3.3. Antibacterial activity studies

Bacterial growth inhibition percentage was calculated for different surfaces in comparison with the control (**Figure 3.8**). All modified NT surfaces promote higher growth inhibition toward *P. aeruginosa* significantly after 24 h of incubation when compared to NT. However, there is no significant difference in the growth inhibition imparted on *S. aureus*.

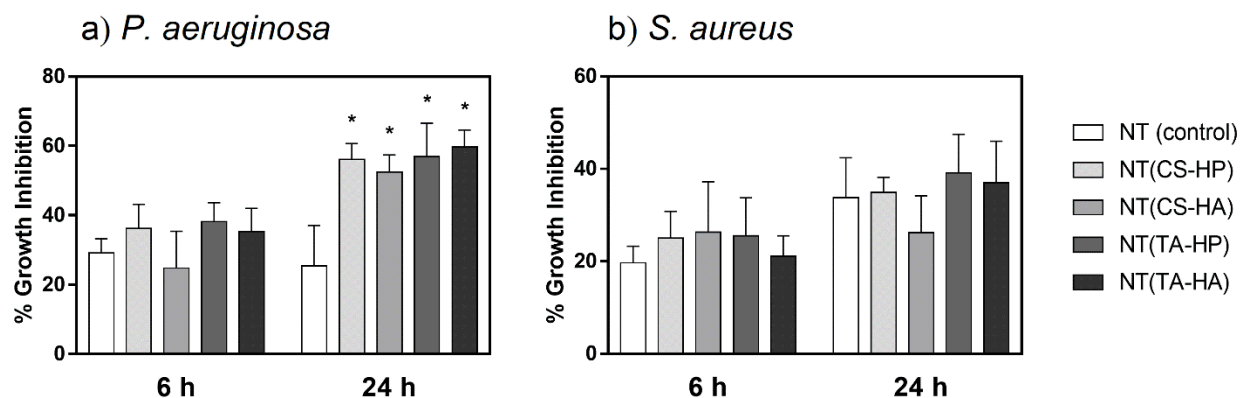


**Figure 3.8.** Percentage growth inhibition in solution promoted by the different surfaces against (a) *P. aeruginosa* and (b) *S. aureus* after 6 and 24 h of incubation in bacteria solution. Experiments were conducted at least twice with 3 samples of each surface ( $n_{\min} = 6$ ). All NT-modified surfaces with PEMs present significantly higher growth inhibition toward *P. aeruginosa* after 24 h than the NT surfaces ( $p < 0.05$ ).

NT(CS-HA), NT(TA-HP) and NT(TA-HA) significantly decrease the adhesion of live *P. aeruginosa* bacteria after 24 h when compared to NT (**Figure 3.9a and b**). After 24 h, the bacteria attached on NT(TA-HP) surface are mostly dead, while NT(TA-HA) has almost no bacteria attached. NT(TA-HP) and NT(TA-HA) also foster better antiadhesive property than the NT(CS-HP), although no significant difference was observed between them. Both TA-modified surfaces dramatically reduce the bacteria adhesion on NT (approximately 80%). The amount of the dead bacteria adhered significantly increase on NT(CS-HA) when compared to NT.

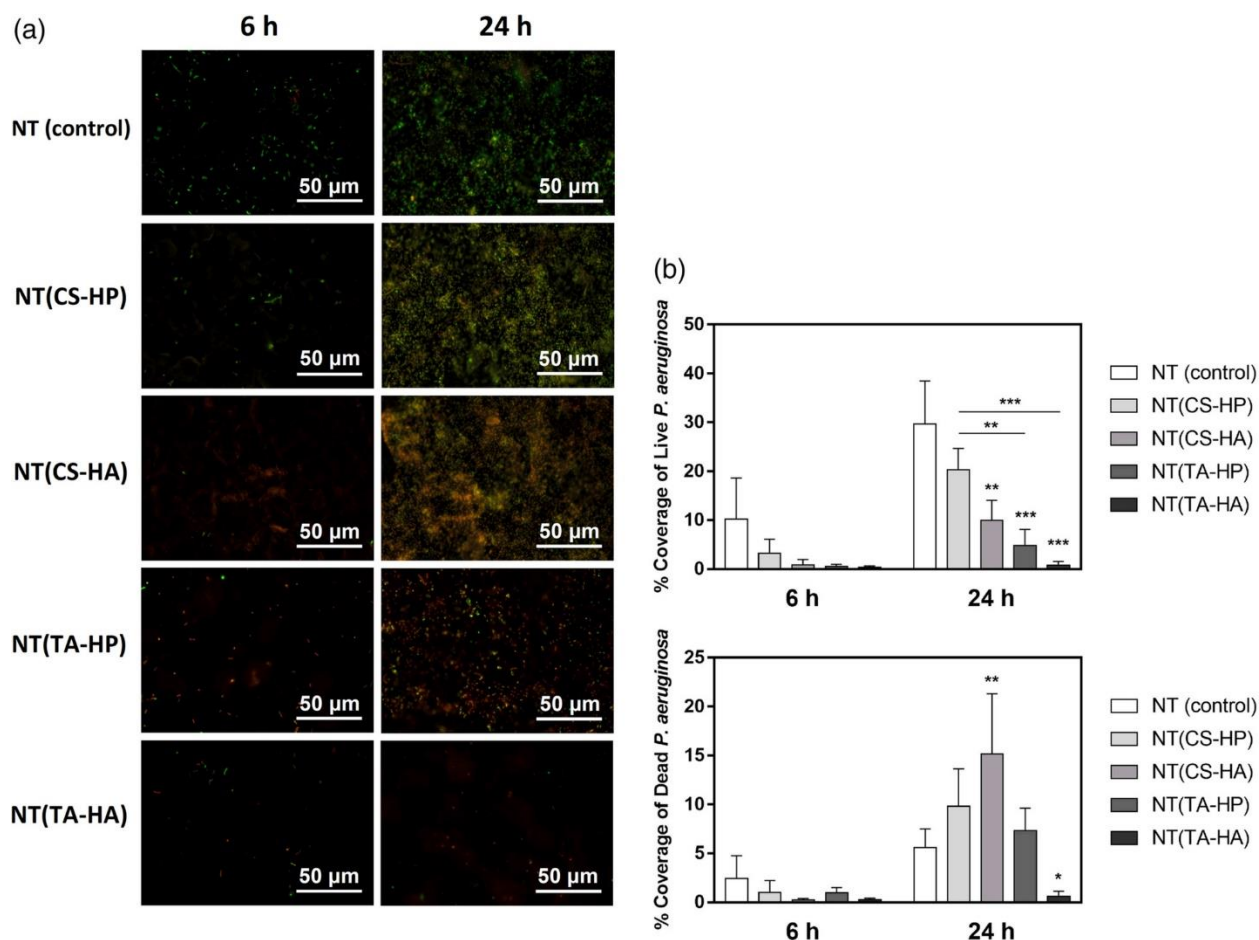


**Figure 3.9.** (a) Representative fluorescence microscopy images of *P. aeruginosa* on the different surfaces after 6 and 24 hr of incubation in bacteria solution. Green stain indicates live bacteria, and red stain indicates dead bacteria. (b) Live/Dead *P. aeruginosa* adhesion on different surfaces after 6 and 24 hr of incubation in bacteria solution. Experiments were conducted at least twice with three samples of each surface ( $n_{\min} = 6$ ). NT(CS-HA), NT(TA-HP), and NT(TA-HA) have significantly lower live bacteria adhesion than the NT surfaces (\* indicates  $p \leq .05$ ; \*\* indicates  $p \leq .01$ ; \*\*\* indicates  $p \leq .001$ )

Both CS-based PEMs significantly decrease the adhesion of live *S. aureus* bacteria after 24 h when compared to the NT (Figure 3.10a and b). However, no significant difference in the percentage area of live bacteria was observed between TA-modified surfaces and NT. On the other hand, the NT(TA-HP) and NT(TA-HA) surfaces significantly increase the antimicrobial activity toward both bacteria, imparting a higher number of damaged bacterial cells in comparison with the NT surface.

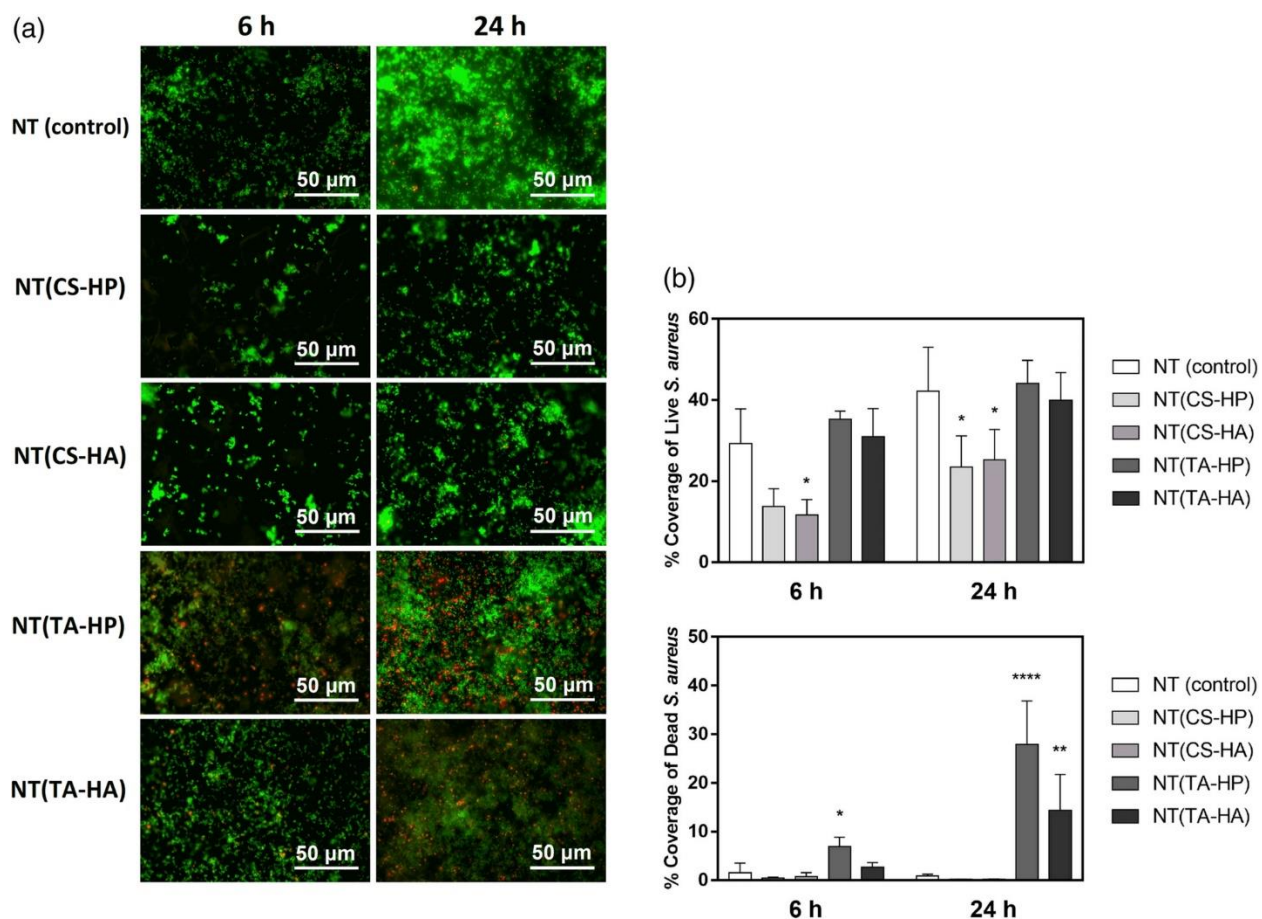


**Figure 3.10.** (a) Representative fluorescence microscopy images of *S. aureus* on different surfaces after 6 and 24 hr of incubation in bacteria solution. Green stain indicates live bacteria, and red stain indicates dead bacteria. (b) Live/Dead *S. aureus* adhesion on different surfaces after 6 and 24 hr of incubation in bacteria solution. Experiments were conducted at least twice with three samples of each surface ( $n_{\min} = 6$ ). NT(CS-HP) and NT(CS-HA) have significantly lower live bacteria adhesion than the NT surfaces. NT(TA-HP) and NT(TA-HA) have significantly higher dead bacteria adhesion than the NT surfaces (\* indicates  $p \leq .05$ ; \*\* indicates  $p \leq .01$ ; \*\*\*\* indicates  $p \leq .0001$ )

SEM images of the different surfaces seeded with *P. aeruginosa* show that NT and NT(CS-HP) have the highest bacteria adhesion, with some colony formation (Figure 3.11). The NT(CS-HP) also exhibit biofilm formation after 24 h of incubation. NT(CS-HA) presents some damaged bacteria adhered after 24 h, with no agglomeration. The NT(TA-HP) and NT(TA-HA) promoted better antiadhesive activity with more damaged cells compared to unmodified NT. This finding

agrees with the fluorescence microscopy. No biofilm or colony formation was observed on either NT(TA-HP) and NT(TA-HA).

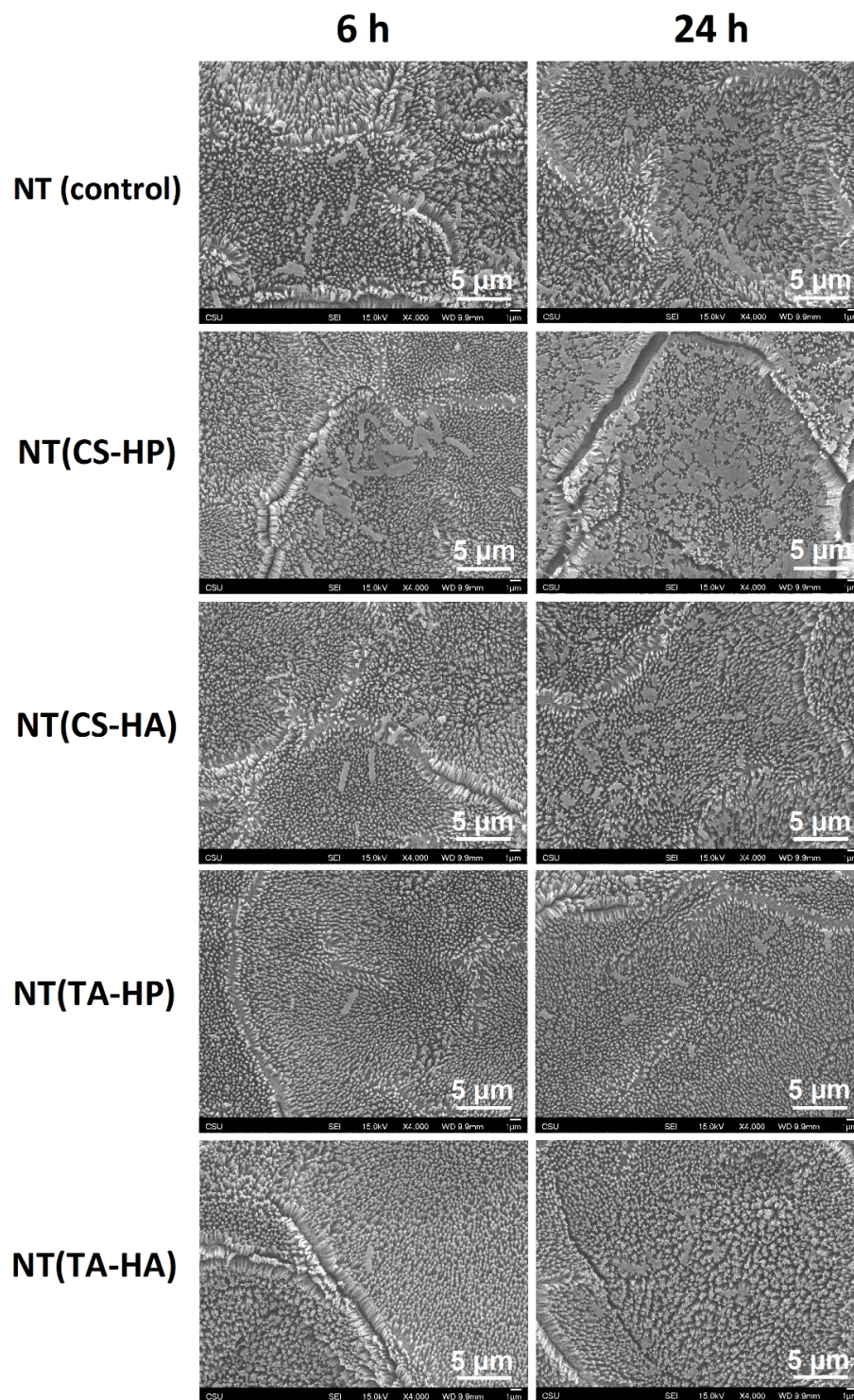


**Figure 3.11.** SEM images of *P. aeruginosa* on different surfaces after 6 and 24 h of incubation.

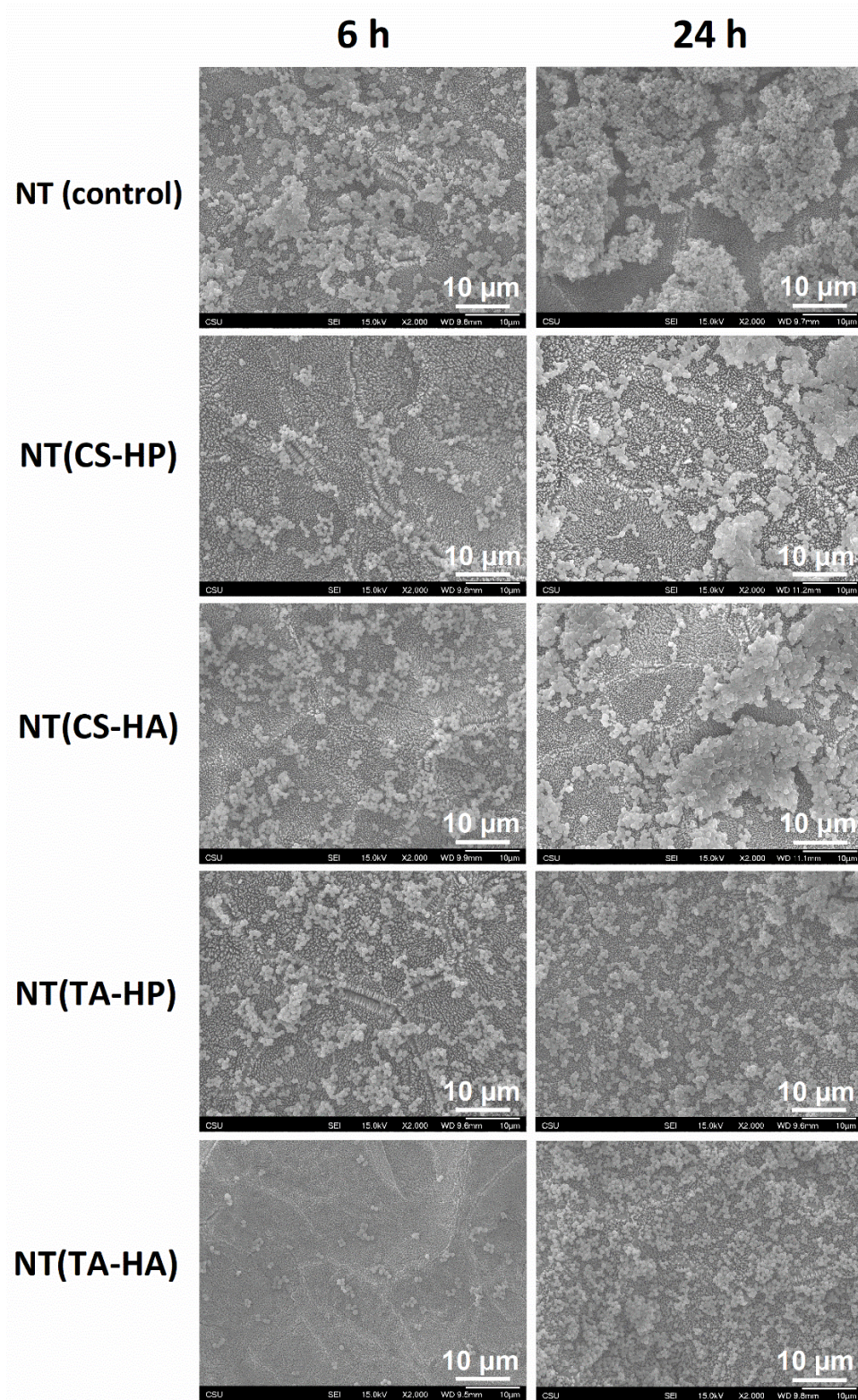


**Figure 3.11.** Representative SEM images of *S. aureus* on different surfaces after 6 and 24 h of incubation.

The NT imparted the highest *S. aureus* agglomeration, followed by NT(CS-HA) and NT(CS-HP) surfaces (**Figure 3.12**). The TA-modified surfaces show less bacterial attachment than NT, with little aggregation. This is not in agreement with the fluorescence microscopy images, likely because the fluorescence microscopy only allows a two-dimensional percentage coverage calculation. Because the bacteria adhered to NT(TA-HP) and NT(TA-HA) are more spaced out and the ones adhered to NT are agglomerated (also in three dimensions), the percentage coverage areas obtained from fluorescence images seem similar, even though NT presents significantly more bacterial adhesion. SEM results also show no biofilm formation on the surfaces.

### **3.4. Discussion**

Preventing biomaterials-associated thrombus formation and bacterial infection are still challenges for the successful development of blood-contacting implants. The first event that happens when biomaterials come in contact with blood is the adsorption of blood plasma proteins, which mediate subsequent biological phenomena, such as the attachment of platelets and other blood cells to the surface [32]. Among the blood proteins that adsorb, fibrinogen plays a central role in the coagulation cascade and is primarily responsible for platelet adhesion [33]. The blood clotting induced by biomaterial surfaces occurs primarily by the intrinsic pathway of the coagulation cascade [34]. This intrinsic pathway is initiated by the conversion of the protein Factor XII (FXII) into its activated form Factor XIIa (FXIIa), when blood encounters a foreign surface [28]. FXIIa then activates a complex sequence of reactions resulting in the conversion of fibrinogen to fibrin, platelet adhesion and activation, and finally thrombus formation [23]. Therefore, blood-compatible surfaces should be able to prevent the blood protein adsorption and FXII activation, as well as platelet attachment, in order to avoid blood clotting.

In this work, TA/HP PEMs on NT were fabricated with the goal to simultaneously prevent thrombus formation and bacterial infection. Firstly, the topography was changed by producing titania nanotube arrays surfaces because it has been shown that NT nanostructure reduces platelet and bacteria adhesion [20,35]. NT was fabricated from titanium sheets via an anodization process in HF solution, and its formation is caused by the field-assisted dissolution process [24]. Before NT modification with PEMs, the surfaces were treated with oxygen plasma to form hydroxyl groups, which allow the surface binding with polycations [23]. The PEMs were then constructed via layer-by-layer approach to modify the surface chemistry. PEMs were constructed using 5 layers to change the chemistry of NT surface, without modifying the topography [9]. SEM and XPS results show that PEMs do not coat the nanotube surface (**Figures 3.2 and 3.3a**). Maintaining the nanoscale topography is desired because it mimics the natural tissue hierarchy, thus enhancing biocompatibility [21]. XPS results also indicate that NT was successfully modified with PEMs since the surfaces present nitrogen peaks, which is characteristic of the cationic polyelectrolytes' (TA and CS). The presence of S2s and S2p peaks was also expected on surfaces treated with HP, as sulfur occurs in HP chemical structure (**Figure 3.3a**). Contact angles measurements also indicate the successful modification of the surfaces. As expected, NT surfaces modified with HP are more hydrophilic than the ones with HA because HP is highly negatively charged, possessing high solubility (**Table 3.1**).

Fibrinogen is a key protein involved in thrombosis that promotes platelet attachment to the biomaterial surface, as well as platelet aggregation [36]. Both TA-modified surfaces significantly decrease the fibrinogen adsorption (**Tables 3.4 and 3.5**). TA is reported as a biocompatible cationic tannin polymer derivative synthesized from condensed tannins [17]. Condensed tannins have a flavonoid type structures, *i.e.*, they comprise structures with two aromatic rings often linked

to three-carbon chain oxygen heterocycles [37]. The TA structure is based on flavan-3-ol repeat units (**Figure 3.1**). Therefore, the TA chemical networks are very different when compared to the CS and blood proteins. This may help to prevent both protein and platelet adhesion. Also, TA monomers contain both amine and phenolic -OH substituents. The amine groups are weakly cationic, whereas the phenolic groups are weakly anionic, possibly imparting the TA with polyzwitterion-like properties. Zwitterionic polymers have attracted interest due to their ability to resist both protein adsorption and bacterial adhesion [38]. These materials possess natural antifouling properties as the strong hydration shell prevents the surface interaction with biofoulants [39]. Similar behavior may be responsible for the protein resistance of the TA-modified surfaces reported here.

Biomaterial-associated thrombosis is due to plasma coagulation and platelet-mediated reactions [36]. Plasma coagulation happens through the intrinsic pathway, which is initiated by the conversion of the blood protein Factor XII to its activated form FXIIa. NT(TA-HP) significantly decreases the FXII activation, and this can be due to the TA antifouling properties (**Figure 3.5**). To autoactivate, FXII needs to bind to the biomaterial surface and undergo a conformational change [23]. However, NT(TA-HA) does not significantly decrease FXIIa concentration, indicating that HP may also play an important role in inhibiting the FXII activation. Although NT(TA-HA) reduces more fibrinogen adsorption than NT(TA-HP), NT(TA-HP) was the only surface which significantly decreases the FXII activation. This result is more relevant because decreasing protein adsorption is not enough for preventing blood clotting, and inhibition of protein activation is required to repress the coagulation cascade.

The platelet-mediated reactions, such as platelet adhesion, aggregation, and activation, also mediate blood clotting and depend on the fibrinogen adsorption to the surface [32]. Therefore, the

reduction in fibrinogen adsorption typically decreases both platelet adhesion and activation. The results agree with this statement for both TA-modified surfaces, which significantly decrease the platelet adhesion (**Figure 3.6**). However, NT(TA-HP) was the only surface that presents no sign of platelet activation or aggregation, showing that HP also prevents platelet activation (**Figure 3.7**). Additionally, the use of HP in PEMs as the non-terminated layer has the advantage of reducing its loss of bioactivity. Since HP binds to TA or CS, its high solubility is effectively minimized, thus enhancing the biomaterial surface stability.

Another barrier for successful implementation of biomedical devices is bacterial infections. When bacteria colonize on the implant surface, biofilms can be formed, which protect the bacteria from being attacked by antibiotics [30]. Gram-negative bacteria, such as *P. aeruginosa*, have a thin peptidoglycan layer covered by an outer lipid membrane, while Gram-positive only possess a thicker layer of glycoprotein [40]. However, the anionic phospholipid dipalmitoyl phosphatidylglycerol is the major component of both Gram-negative and Gram-positive bacteria [41]. A Gram-positive bacteria commonly related to medical device infections is *S. aureus*, which is typically located on human skin [30]. *P. aeruginosa* is highly involved with hospital infections and increase the oxidant and inflammatory processes [3]. Because the mechanisms to combat these two types of bacteria are different, it is important to investigate how the biomaterial surface interacts with both.

The results show that PEMs on NT promote significant higher growth inhibition in solution only for Gram-negative when compared to the control group (**Figure 3.8**). This could be explained by the positively charged terminated PEMs that interacts with the negatively charged bacterial membrane, eventually causing the cell death. No significant difference was observed for Gram-positive bacteria, although all surfaces promote some growth inhibition. It is important to notice

that NT already showed improved antibacterial properties when compared to pure titanium, and because Gram-positive bacteria is usually less resistant than Gram-negative, less effort is required to inhibit its growth. Both TA-based PEMs on NT significantly decrease the bacteria adhesion, promoting antibacterial effect as well (**Figures 3.9b, 3.11 and 3.12**). The antiadhesive and bactericidal properties can be assigned to cationic and phenolic moieties. Flavonoid-based materials have demonstrated great antimicrobial activities toward both Gram-negative and Gram-positive bacterial cells. The mechanism is associated with the formation of complexes with both extracellular and microbial proteins [18,37]. TA also contains ammonium moieties that can electrostatically interact with the negatively charged microbial cell membrane that contains the anionic phospholipid dipalmitoyl phosphatidylglycerol. This interaction disrupts the microbial membrane promoting permeability, leakage of intracellular materials (lactate dehydrogenase, nucleic acid, and glucose) and suppressing the nutrient transport. All these events cause the death of bacteria [17]. Of note is that CS-modified surfaces also decrease bacterial adhesion; however, compared to the TA-based PEMs, the effect was lower. Also, compared to the TA-based PEMs, CS-modified surfaces have no anti-thrombogenic properties. The NT(TA-HP) surface enhances the hemocompatibility, antiadhesive, and antibacterial activities of the NT surface.

### **3.5. Conclusions**

Improving blood compatibility and antibacterial properties of medical devices is still a major concern. In this study, TA/HP PEMs on NT were fabricated, and the surfaces show excellent anti-fouling, anti-thrombogenic, and antibacterial properties. When compared to CS-based PEMs, the NT modified with TA-based PEMs impart much better biological responses. These responses are due to the chemical structure of TA (cationic tannin derivative) that is based on flavan-3-ol

repeat units. Flavonoids are well-known polyphenolic materials with strong antimicrobial activities. The ammonium moieties in TA also maximize the antiadhesive and antimicrobial properties. Hemocompatibility studies demonstrated that TA/HP PEMs decrease protein adsorption and FXII activation as well as reduce platelet adhesion and activation on NT. This occurs because the TA comprises both anionic (phenolic) and cationic (ammonium) sites in its chemical structure. Modified NT surfaces with tanfloc/heparin polyelectrolyte multilayers are therefore a promising approach to enhance biocompatibility of blood-contacting implants. Future work is now directed towards investigating the dynamic interaction with blood, as well as the cell response to the surface.

## REFERENCES

- [1] R.M. Sabino, K. Kauk, L.Y.C. Madruga, M.J. Kipper, A.F. Martins, K.C. Popat, Enhanced hemocompatibility and antibacterial activity on titania nanotubes with tanfloc/heparin polyelectrolyte multilayers, *J. Biomed. Mater. Res. - Part A*. 108 (2020) 992–1005. doi:10.1002/jbm.a.36876.
- [2] I.H. Jaffer, J.C. Fredenburgh, J. Hirsh, J.I. Weitz, Medical device-induced thrombosis: what causes it and how can we prevent it?, *J. Thromb. Haemost.* 13 (2015) S72–S81. doi:10.1111/jth.12961.
- [3] L.-C. Xu, M.E. Meyerhoff, C.A. Siedlecki, Blood coagulation response and bacterial adhesion to biomimetic polyurethane biomaterials prepared with surface texturing and nitric oxide release, *Acta Biomater.* 84 (2019) 77–87. doi:10.1016/j.actbio.2018.11.035.
- [4] E.C.M. van Gorp, C. Suharti, H. ten Cate, W.M.V. Dolmans, J.W.M. van der Meer, J.W. ten Cate, D.P.M. Brandjes, Review: Infectious Diseases and Coagulation Disorders, *J. Infect. Dis.* 180 (1999) 176–186. doi:10.1086/314829.
- [5] M. Navarro, A. Michiardi, O. Castaño, J. Planell, Biomaterials in orthopaedics, *J. R. Soc. Interface.* 5 (2008) 1137–1158. doi:10.1098/rsif.2008.0151.
- [6] K. Zhang, J. ying Chen, W. Qin, J. an Li, F. xia Guan, N. Huang, Constructing bio-layer of heparin and type IV collagen on titanium surface for improving its endothelialization and blood compatibility, *J. Mater. Sci. Mater. Med.* (2016). doi:10.1007/s10856-016-5693-6.
- [7] S. Movafaghi, V. Leszczak, W. Wang, J.A. Sorkin, L.P. Dasi, K.C. Popat, A.K. Kota, Hemocompatibility of Superhemophobic Titania Surfaces", *Adv. Healthc. Mater.* (2017). doi:10.1002/adhm.201700647.
- [8] C. Sperling, M. Fischer, M.F. Maitz, C. Werner, Blood coagulation on biomaterials requires the combination of distinct activation processes, *Biomaterials.* 30 (2009) 4447–4456. doi:10.1016/j.biomaterials.2009.05.044.
- [9] P.C.F. da Câmara, R.C. Balaban, M. Hedayati, K.C. Popat, A.F. Martins, M.J. Kipper, Novel cationic tannin/glycosaminoglycan-based polyelectrolyte multilayers promote stem cells adhesion and proliferation, *RSC Adv.* 9 (2019) 25836–25846. doi:10.1039/C9RA03903A.
- [10] J. Almodóvar, L.W. Place, J. Gogolski, K. Erickson, M.J. Kipper, Layer-by-Layer Assembly of Polysaccharide-Based Polyelectrolyte Multilayers: A Spectroscopic Study of Hydrophilicity, Composition, and Ion Pairing, *Biomacromolecules.* 12 (2011) 2755–2765. doi:10.1021/bm200519y.
- [11] J. Almodóvar, J. Mower, A. Banerjee, A.K. Sarkar, N.P. Ehrhart, M.J. Kipper, Chitosan-heparin polyelectrolyte multilayers on cortical bone: Periosteum-mimetic, cytophilic, antibacterial coatings, *Biotechnol. Bioeng.* 110 (2013) 609–618. doi:10.1002/bit.24710.
- [12] F. Zomer Volpato, J. Almodóvar, K. Erickson, K.C. Popat, C. Migliaresi, M.J. Kipper, Preservation of FGF-2 bioactivity using heparin-based nanoparticles, and their delivery from electrospun chitosan fibers, *Acta Biomater.* 8 (2012) 1551–1559. doi:10.1016/j.actbio.2011.12.023.
- [13] X. Zhang, G. Zhang, H. Zhang, J. Li, X. Yao, B. Tang, Surface immobilization of heparin and chitosan on titanium to improve hemocompatibility and antibacterial activities,

- Colloids Surfaces B Biointerfaces. 172 (2018) 338–345.  
doi:10.1016/J.COLSURFB.2018.08.060.
- [14] X. Liu, L. Yuan, D. Li, Z. Tang, Y. Wang, G. Chen, H. Chen, J.L. Brash, Blood compatible materials: state of the art, *J. Mater. Chem. B.* 2 (2014) 5718–5738.  
doi:10.1039/C4TB00881B.
- [15] A.C. de Oliveira, R.M. Sabino, P.R. Souza, E.C. Muniz, K.C. Popat, M.J. Kipper, R.S. Zola, A.F. Martins, Chitosan/gellan gum ratio content into blends modulates the scaffolding capacity of hydrogels on bone mesenchymal stem cells, *Mater. Sci. Eng. C.* 106 (2020) 110258. doi:10.1016/J.MSEC.2019.110258.
- [16] O. Koenig, B. Neumann, C. Schlensak, H.P. Wendel, A. Nolte, Hyaluronic acid/poly(ethylenimine) polyelectrolyte multilayer coatings for siRNA-mediated local gene silencing, *PLoS One.* 14 (2019) e0212584. doi:10.1371/journal.pone.0212584.
- [17] D.P. Facchi, A.C. Lima, J.H. de Oliveira, D. Lazarin-Bidóia, C. V. Nakamura, E.A. Canesin, E.G. Bonafé, J.P. Monteiro, J. V. Visentainer, E.C. Muniz, A.F. Martins, Polyelectrolyte complexes based on alginate/tanfloc: Optimization, characterization and medical application, *Int. J. Biol. Macromol.* 103 (2017) 129–138.  
doi:10.1016/J.IJBIOMAC.2017.05.033.
- [18] A.F. Martins, S.P. Facchi, P.C.F. da Câmara, S.E.A. Camargo, C.H.R. Camargo, K.C. Popat, M.J. Kipper, Novel poly( $\epsilon$ -caprolactone)/amino-functionalized tannin electrospun membranes as scaffolds for tissue engineering, *J. Colloid Interface Sci.* 525 (2018) 21–30.  
doi:10.1016/J.JCIS.2018.04.060.
- [19] N. Graham, F. Gang, G. Fowler, M. Watts, Characterisation and coagulation performance of a tannin-based cationic polymer: A preliminary assessment, *Colloids Surfaces A Physicochem. Eng. Asp.* 327 (2008) 9–16. doi:10.1016/J.COLSURFA.2008.05.045.
- [20] S.D. Puckett, E. Taylor, T. Raimondo, T.J. Webster, The relationship between the nanostructure of titanium surfaces and bacterial attachment, *Biomaterials.* 31 (2010) 706–713. doi:10.1016/J.BIOMATERIALS.2009.09.081.
- [21] B.S. Smith, P. Capellato, S. Kelley, M. Gonzalez-Juarrero, K.C. Popat, Reduced in vitro immune response on titania nanotube arrays compared to titanium surface, *Biomater. Sci.* 1 (2013) 322–332. doi:10.1039/c2bm00079b.
- [22] R. Simon-Walker, R. Romero, J.M. Staver, Y. Zang, M.M. Reynolds, K.C. Popat, M.J. Kipper, Glycocalyx-inspired nitric oxide-releasing surfaces reduce platelet adhesion and activation on titanium, *ACS Biomater. Sci. Eng.* 3 (2017) 68–77.  
doi:10.1021/acsbiomaterials.6b00572.
- [23] R.M. Sabino, K. Kauk, S. Movafaghi, A. Kota, K.C. Popat, Interaction of blood plasma proteins with superhemophobic titania nanotube surfaces, *Nanomedicine Nanotechnology, Biol. Med.* 21 (2019) 102046. doi:10.1016/J.NANO.2019.102046.
- [24] B.B.S. Ramin, K.B. Rufato, R.M. Sabino, K.C. Popat, M.J. Kipper, A.F. Martins, E.C. Muniz, Chitosan/iota-carrageenan/curcumin-based materials prepared by precipitating miscible solutions prepared in ionic liquid, *J. Mol. Liq.* 290 (2019) 111199.  
doi:10.1016/J.MOLLIQ.2019.111199.
- [25] M.B. Gorbet, M. V. Sefton, Biomaterial-associated thrombosis: Roles of coagulation factors, complement, platelets and leukocytes, *Biomater. Silver Jubil. Compend.* 25 (2004) 219–241. doi:10.1016/B978-008045154-1.50025-3.
- [26] E. a. Vogler, C. a. Siedlecki, Contact Activation of Blood Plasma Coagulation : A contribution from the Hematology at Biomaterial Interferences, *Biomaterials.* 30 (2010)

- 1857–1869. doi:10.1016/j.biomaterials.2008.12.041.Contact.
- [27] I. Reviakine, F. Jung, S. Braune, J.L. Brash, R. Latour, M. Gorbet, W. van Oeveren, Stirred, shaken, or stagnant: What goes on at the blood–biomaterial interface, *Blood Rev.* 31 (2017) 11–21. doi:10.1016/j.blre.2016.07.003.
- [28] J.W. Bauer, L.-C. Xu, E.A. Vogler, C.A. Siedlecki, Surface dependent contact activation of factor XII and blood plasma coagulation induced by mixed thiol surfaces, *Biointerphases.* 12 (2017) 02D410. doi:10.1116/1.4983634.
- [29] Z. Guo, K.M. Bussard, K. Chatterjee, R. Miller, E.A. Vogler, C.A. Siedlecki, Mathematical modeling of material-induced blood plasma coagulation, *Biomaterials.* 27 (2006) 796–806. doi:10.1016/j.biomaterials.2005.06.021.
- [30] K. Bartlet, S. Movafaghi, L.P. Dasi, A.K. Kota, K.C. Papat, Antibacterial activity on superhydrophobic titania nanotube arrays, *Colloids Surfaces B Biointerphases.* 166 (2018) 179–186. doi:10.1016/J.COLSURFB.2018.03.019.
- [31] V. Leszczak, B.S. Smith, K.C. Papat, Hemocompatibility of polymeric nanostructured surfaces, *J. Biomater. Sci. Polym. Ed.* 24 (2013) 1529–1548. doi:10.1080/09205063.2013.777228.
- [32] L.C. Xu, J.W. Bauer, C.A. Siedlecki, Proteins, platelets, and blood coagulation at biomaterial interfaces, *Colloids Surfaces B Biointerphases.* 124 (2014) 49–68. doi:10.1016/j.colsurfb.2014.09.040.
- [33] L.A. Wells, H. Guo, A. Emili, M. V. Sefton, The profile of adsorbed plasma and serum proteins on methacrylic acid copolymer beads: Effect on complement activation, *Biomaterials.* 118 (2017) 74–83. doi:10.1016/j.biomaterials.2016.11.036.
- [34] Y. Yan, L.-C. Xu, E.A. Vogler, C.A. Siedlecki, Contact activation by the intrinsic pathway of blood plasma coagulation, in: *Hemocompatibility Biomater. Clin. Appl.*, Elsevier, 2018: pp. 3–28. doi:10.1016/B978-0-08-100497-5.00001-X.
- [35] B.S. Smith, K.C. Papat, *Titania Nanotube Arrays as Interfaces for Blood-Contacting Implantable Devices*, (n.d.).
- [36] L.-C. Xu, J.W. Bauer, C.A. Siedlecki, Proteins, platelets, and blood coagulation at biomaterial interfaces, *Colloids Surfaces B Biointerphases.* 124 (2014) 49–68. doi:10.1016/j.colsurfb.2014.09.040.
- [37] J.L. Guil-Guerrero, L. Ramos, C. Moreno, J.C. Zúñiga-Paredes, M. Carlosama-Yeppez, P. Ruales, Antimicrobial activity of plant-food by-products: A review focusing on the tropics, *Livest. Sci.* 189 (2016) 32–49. doi:10.1016/J.LIVSCI.2016.04.021.
- [38] W. Lin, J. Zhang, Z. Wang, S. Chen, Development of robust biocompatible silicone with high resistance to protein adsorption and bacterial adhesion, *Acta Biomater.* 7 (2011) 2053–2059. doi:10.1016/J.ACTBIO.2011.02.001.
- [39] J.-F. Jhong, A. Venault, L. Liu, J. Zheng, S.-H. Chen, A. Higuchi, J. Huang, Y. Chang, *Introducing Mixed-Charge Copolymers As Wound Dressing Biomaterials*, (2014). doi:10.1021/am502382n.
- [40] H.D.M. Follmann, A.F. Martins, A.P. Gerola, T.A.L. Burgo, C. V Nakamura, A.F. Rubira, E.C. Muniz, M. Paraná,, P. Brazil, *Antiadhesive and Antibacterial Multilayer Films via Layer-by-Layer Assembly of TMC/Heparin Complexes*, 13 (2012) 29. doi:10.1021/bm3011962.
- [41] A. Martins, S. Facchi, H. Follmann, A. Pereira, A. Rubira, E. Muniz, *Antimicrobial Activity of Chitosan Derivatives Containing N-Quaternized Moieties in Its Backbone: A Review*, *Int. J. Mol. Sci.* 15 (2014) 20800–20832. doi:10.3390/ijms151120800.

## CHAPTER 4: ENDOTHELIALIZATION OF TITANIA NANOTUBE ARRAYS WITH DIFFERENT SURFACE MODIFICATIONS

### 4.1. Introduction

Over the last ten decades, cardiovascular diseases (CVD) have been highly prevalent in the United States. CVD is one of the most relevant causes of mortality in the world and leading cause of mortality in the United States across most racial and ethnic groups [1]. The main cause of CVD death is the coronary artery disease, which is mostly caused by atherosclerosis [2]. Atherosclerosis is a chronic inflammatory disease of the arteries, that eventually leads to myocardial infarction. To treat severe cases of coronary artery disease, vascular stents are commonly used [3]. However, a common complication of stents is restenosis, which is the artery reocclusion due to smooth muscle cell proliferation [4]. To prevent in-stent restenosis, drug-eluting stents (DES) were developed. Although DES elute a mitotic inhibitor to prevent in-stent restenosis, they are also responsible for worsening the endothelialization of the implant, thus increasing the risk of late stent thrombosis [5]. Therefore, it is vital to develop novel biomaterials surfaces that better integrate with the surrounding endothelial cells, without the need of drug use to prevent restenosis.

One effective approach to design hemocompatible biomaterials for cardiovascular implants is to promote a rapid and complete surface endothelialization [6]. The endothelial monolayer in blood vessels provides the perfect environment of blood compatibility. Blood flows inside them without any attraction or thrombus formation. The endothelial cells that line the interior surface of healthy blood vessels prevent blood clotting by several mechanisms, such as nitric oxide (NO) release or recruitment of heparan sulfate [7]. The endothelialization of cardiovascular implants (i. e., when they get covered with an endothelium cell layer) prevents complications such as

thrombosis or restenosis [2]. This endothelium cell layer is responsible for the expression of anti-thrombogenic and anti-inflammatory molecules, which will maintain the hemostasis [8].

The successful endothelialization of the implants surfaces mostly depends on the migration of endothelial cells (ECs), the capture of endothelial progenitor cells (EPC), and the differentiation of stem cells (Figure 4.1) [9]. EPCs are circulating immature cells that play an important role in compensatory angiogenesis and vascular homeostasis [10]. It is also important that the biomaterial surface acts to inhibit the proliferation of smooth muscle cells (SMCs) to prevent restenosis [11].

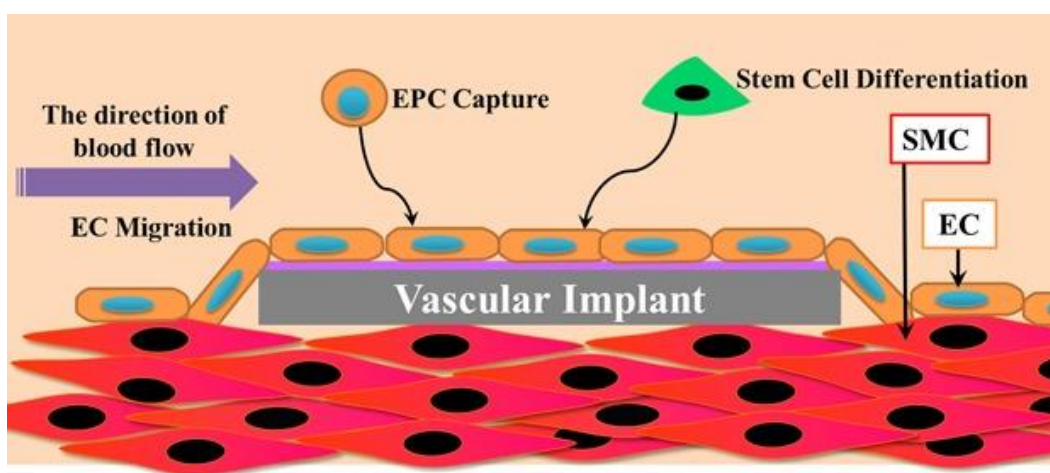


**Figure 4.1.** Representation of in situ surface endothelialization of cardiovascular implants. Reproduced with permission from ref. 9. Copyright 2017, Wiley-VCH.

In this chapter, we investigated the endothelialization potential of the NT surfaces developed in chapters 2 and 3. Since they have showed improved antithrombogenic properties, with significantly lower protein adsorption, FXII activation, and platelet adhesion and activation, they are promising candidates to be used for cardiovascular implant applications [12,13]. ECs and SMCs were cultured on the surfaces, and their viability, adhesion and proliferation were evaluated after 1, 3 and 5 days of cell culture. Indirect immunofluorescent staining was used to determine the cellular expression and differentiation of ECs through the presence of specific marker proteins after 7 and 10 days. Finally, EC migration on the NT surfaces was also investigated.

## **4.2. Materials and Methods**

### **4.2.1. Fabrication of titania nanotubes (NT) with different surface modifications**

NT surfaces were fabricated using an anodization technique on titanium sheets (0.4 mm thick) as described in Chapter 2 [14]. Prior to surface modification, the substrates were treated with oxygen plasma at 200 V in 10 cm<sup>3</sup>/min of oxygen gas for 10 mins. NT surfaces were then modified with PEG and fluorinated silane (FL) as described in Chapter 2, Section 2.2.1 and modified with PEMs as described in Chapter 3, Section 3.2.1. Since only NT surfaces modified with tanfloc (TA) significantly reduced fibrinogen adsorption, Factor XII activation, and platelet adhesion and activation in comparison with unmodified NT, chitosan (CS) was not used as a polycation for further studies. Following notation will be used in this chapter: unmodified titania nanotubes: NT; NT modified with FL: NT-FL; NT modified with PEG: NT-PEG. TA/HP PEMs deposited on NT: NT(TA-HP); and TA/HA PEMs deposited on NT: NT(TA-HA).

### **4.2.2. ECs and SMCs culture**

Prior to the biological assays, all the surfaces were sterilized by incubating with 70% ethanol for 5 min, followed by 3 rinses and incubation with sterile PBS for 30 min. Human microvascular ECs (HMVECs, passage 8) were suspended in Endothelial Cell Basal Medium-2 (EBM2, Lonza) with Supplement kit (CC-4176, Lonza) and 1% (v/v) penicillin/streptomycin (Corning). Human aortic SMCs (HASMCs, passage 5) were resuspended in Smooth Muscle Cell Growth Medium 2 (PromoCell) with SupplementMix (C-39267, PromoCell). The cells were cultured at 37 °C and 5% CO<sub>2</sub> in 75 cm<sup>2</sup> culture flasks. Growth medias were changed every other day until the cells achieved >90% confluence. Following expansion, the cells were detached using TrypLE Express (Gibco) and the cells were seeded on the sterilized NT surfaces at a final concentration of 2.0 x 10<sup>4</sup> cells/ml in 48-well plates.

#### **4.2.3. ECs and SMCs viability, adhesion, and proliferation**

ECs and SMCs viabilities were evaluated using CellTiter-Blue assay (Promega) after 1, 3 and 5 days of cell culture. The surfaces with adhered cells were incubated at 37 °C for 7 h in fresh culture media with 10% of CellTiter-Blue reagent. After 7 h, the absorbance of the solutions was measured at 570 and 600 nm using a microplate reader (FLUOstar Omega, BMG Labtech) [15]. The CellTiter-Blue reduction percentage correlates with the percentage of viable cells. The cell viability was calculated as described by the manufacturer's protocol. The ECs and SMCs were also seeded in empty wells (positive control), while the negative control was carried out only with the media without cells. The results obtained for the negative control was used to eliminate the influence of the cell media on the CellTiter-Blue reduction percentage. The cell viability outcomes obtained for the surfaces were normalized using the results from the positive control.

ECs and SMCs adhesion and proliferation on the surfaces were characterized using fluorescence microscopy. After 1, 3 and 5 days of cell culture, the media was removed, and the surfaces were rinsed with PBS. The cells adhered on the surfaces were fixed in 3.7% formaldehyde in PBS for 15 mins, followed by three rinses (5 min each) with PBS. Adhered cells were permeabilized by incubation with 1% Triton X-100 in PBS for 3 min and rinsed twice with PBS [16]. The surfaces were then incubated in 70 nM of rhodamine phalloidin in PBS for 20 min in a dark environment. The nuclear stain DAPI (300 nM, ThermoFisher Scientific) was added, and after 5 min the surfaces were rinsed with PBS twice and then imaged using a fluorescence microscope (Zeiss). To obtain the quantity of cells adhered on the surfaces, the number of stained nuclei (DAPI) was counted using ImageJ software.

ECs and SMCs morphology on the surfaces was investigated by SEM. After 1, 3 and 5 days of cell culture, the media was removed, and the surfaces were rinsed with PBS. The surfaces

were then placed in a fixative solution composed of 3% glutaraldehyde, 0.1 M sucrose, and 0.1 M sodium cacodylate in DI water for 45 min [17]. After that, the surfaces were moved to a buffer solution (fixative solution without glutaraldehyde) for 10 min. The surfaces were then dehydrated by exposure to ethanol solutions (35%, 50%, 70%, and 100%, respectively) for 10 min each step. The surfaces were then incubated in 100% hexamethyldisilazane (HMDS) for 10 min. After HMDS removal, the surfaces were dried and stored in a desiccator until further imaging. SEM imaging was conducted as described in Chapter 2, Section 2.2.2.

#### **4.2.4. Differentiation of ECs on different surfaces**

Indirect immunofluorescent staining was used to investigate the cellular expression and differentiation through the presence of specific marker proteins on HMVECs. The HMVECs were immunostained for the presence of vascular endothelial cadherin (VE-cadherin) and von Willebrand factor (vWF) [18]. After 7 and 10 days of cell culture, the media was removed, and the surfaces rinsed twice with PBS. The adhered cells were fixed and permeabilized as described in Section 4.2.3. The surfaces were then incubated in 10% bovine serum albumin (BSA, Sigma) for 30 min, followed by incubation in primary antibody (VE-cadherin and vWF, Santa Cruz Biotechnology) at a dilution of 1:100 in 1% BSA for 60 min. After two rinses with PBS, the surfaces were incubated with secondary antibody-FITC (Santa Cruz Biotechnology) at a dilution of 1:200 in 1% BSA for 45 min, followed by two rinses with PBS. Then, the surfaces were incubated in rhodamine phalloidin and DAPI nuclear stain, as described in Section 5.2.4. The surfaces were imaged by fluorescence microscopy. The presence of specific protein markers on each surface was obtained by measuring the percentage coverage area of stained protein using ImageJ software.

#### **4.2.5. ECs migration study**

HMVECs were seeded onto the sterilized NT surfaces in the same way described in Section 4.2.2. except that the final concentration was changed to  $5.0 \times 10^4$  cells/ml. After a confluent monolayer of cells was obtained, the surfaces were scratched a straight mark using a micropipette tip to remove the cells on the center of the surfaces. After that, the culture medium was changed and the surfaces were incubated at 37 °C for 24 h [19]. Then, the surfaces were incubated in rhodamine phalloidin and DAPI nuclear stain, as described in Section 4.2.3, and imaged using a fluorescence microscope (Zeiss).

#### **4.2.6. Statistical analysis**

All cell studies were carried out with  $n_{\min} = 3$  for qualitative analyses and  $n_{\min} = 4$  for quantitative analyses. The quantitative results were analyzed via analysis of variance (ANOVA) and Tukey tests using the GraphPad Prism software ( $p < 0.05$ ). The statistical differences were compared using (\*) for  $p < 0.05$ , (\*\*) for  $p < 0.01$ , (\*\*\*) for  $p < 0.001$ , and (\*\*\*\*) for  $p < 0.0001$ .

### **4.3. Results and Discussion**

#### **4.3.1. ECs viability, adhesion, and proliferation**

The rapid EC attachment and growth on the surface is crucial for the successful endothelialization of the implant and to prevent adverse effects such as thrombosis [20]. To investigate the EC viability, the surfaces were incubated with HMVECs for 1, 3 and 5 days and the cell viability was evaluated using CellTiter-Blue assay. The viable cells reduce the resazurin to resorufin by dehydrogenase enzymes [21]. Thus, a higher percentage of CellTiter-Blue reduction indicates greater cell viability. The cell viability results were normalized using the positive control (tissue-culture polystyrene). The results show that NT(TA-HP) increased the cell

viability after 1 and 5 days of cell culture in comparison with the other surfaces (**Figure 4.2**). There is no significant difference between surfaces on day 3, however, NT(TA-HP) also showed enhanced viability. The ability of the surfaces to support adhesion, proliferation, and spreading of ECs was also investigated using SEM and fluorescence microscopy images (**Figures 4.3a and 4.4**). After 3 and 5 days, NT(TA-HP) shows significantly higher number of cells in comparison with the other surfaces (**Figure 4.3b**). On day 5, NT(TA-HP) dramatically enhanced the number of adhered cells, with approximately 500% increase in comparison with unmodified NT, showing an impressive EC proliferation. These results agree with the cell viability outcomes, as NT(TA-HP) show improved EC proliferation, thus contributing to the presence of more viable cells.

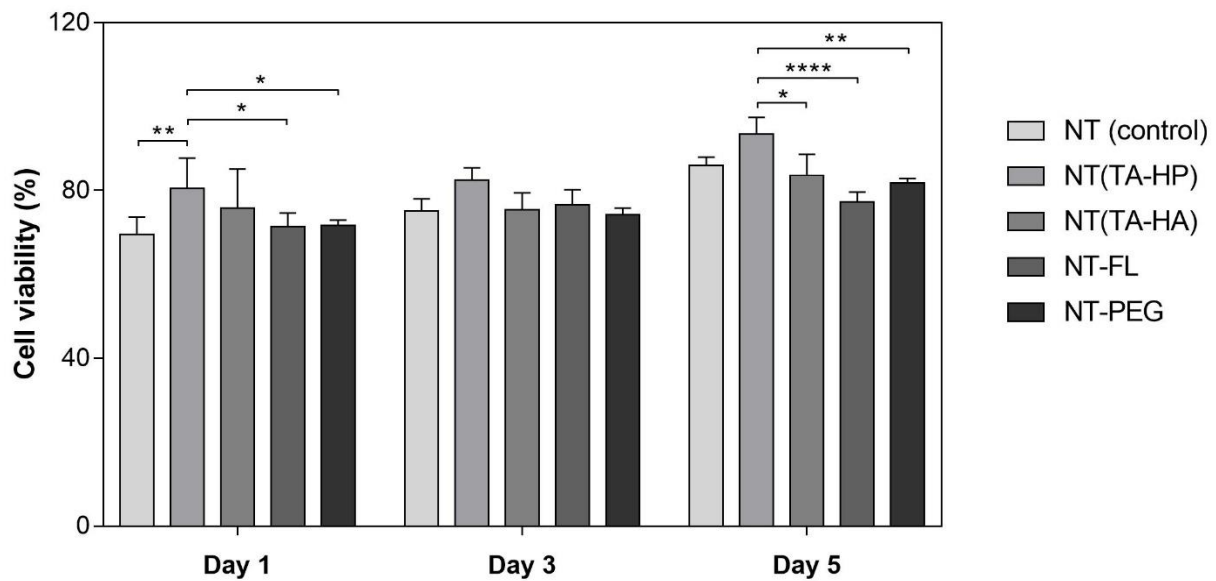


**Figure 4.2.** CellTiter-Blue ECs viability assay after 1, 3 and 5 days of cell culture. Results are normalized using the positive control on tissue-culture polystyrene. \* Represents  $p < 0.05$ ; \*\* represents  $p < 0.01$ ; \*\*\*\* represents  $p < 0.0001$ .

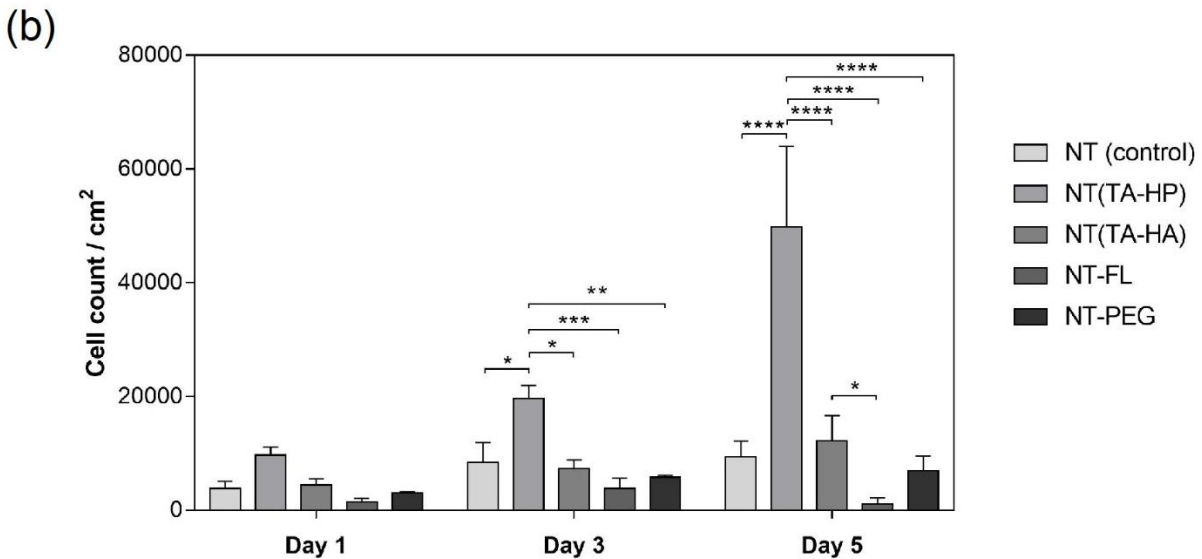
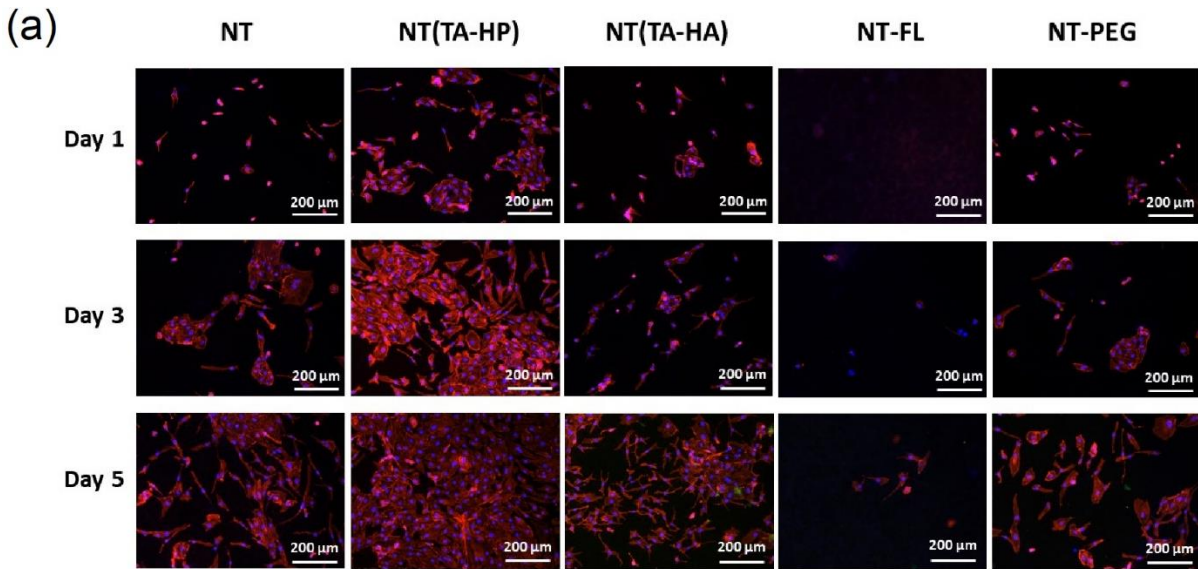


**Figure 4.3.** (a) Representative fluorescence microscopy images of ECs stained with DAPI (blue) and rhodamine phalloidin (red) after 1, 3, and 5 days of proliferation. (b) Cell count per area after 1, 3 and 5 days of cell culture. No significant difference is observed on day 1 between all NT surfaces. \* Represents  $p < 0.05$ ; \*\* represents  $p < 0.01$ ; \*\*\* represents  $p < 0.001$ ; \*\*\*\* represents  $p < 0.0001$ .

**Figure 4.4** presents the SEM results of HMVECs spreading on the different NT surfaces. As expected, NT(TA-HP) shows increased cell spreading compared to the other surfaces, with approximately 80% coverage after 3 days of cell culture. The SEM images agree with fluorescence and viability results, as NT(TA-HP) demonstrates enhanced EC growth and spreading. This could

be explained due to the presence of protonated amino groups on TA, which may be responsible for a bioadhesive characteristic, improving the cell adhesion [22,23]. Recent study also showed that endothelial cells tend to attach and spread more favorably in polycationic-terminated PEMs [24]. In addition, the presence of heparin is responsible for enhancing the endothelial cell proliferation due to its ability to potentiate and bind with growth factors [2].

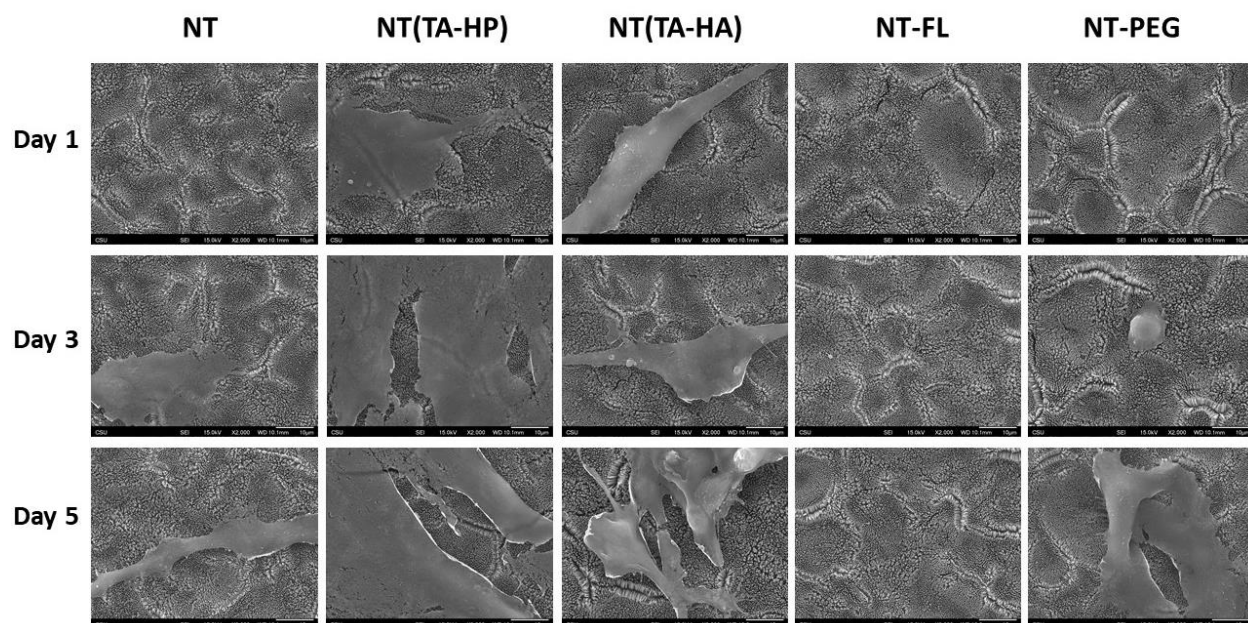


**Figure 4.4.** Representative SEM images of ECs on NT surfaces after 1, 3 and 5 days of cell culture. The images were taken at 2,000× magnification.

#### 4.3.2. Differentiation of ECs on different surfaces

The cellular expression and differentiation of ECs were determined via immunofluorescence through the presence of specific marker proteins on HMVECs. After 7 and 10 days of culture, the cells were immunostained for the presence of the proteins vascular endothelial cadherin (VE-cadherin) and von Willebrand factor (vWF). VE-cadherin and vWF are specific proteins to ECs and are only expressed when these cells differentiate into mature phenotype [18]. It is not only important that ECs are able to attach and proliferate on the

biomaterial surfaces, but they should also be able to maintain their functionality as they would in a healthy blood vessel. VE-cadherin is responsible for mediating the cell-cell binding, which is crucial to tissue structure and to regulate the permeability of blood vessels [25]. The results indicate no significant difference in VE-cadherin expression between NT surfaces after 7 and 10 days, however NT(TA-HP) shows higher protein expression compared to all other surfaces (**Figure 4.5**). On day 7, NT(TA-HP) presents considerable improved VE-cadherin expression which agrees with fluorescence images as it is the only surface that achieved complete cell coverage after 7 days.

Another commonly used phenotype marker of endothelial cells is vWF, which is only synthesized by vascular endothelial cells and megakaryocytes and plays a key role in the blood coagulation cascade [24]. Therefore, its expression indicates that the ECs on the NT surfaces maintain their functionality. **Figure 4.6** shows that NT(TA-HP) express higher vWF than the other NT surfaces after 7 days of cell culture. After 10 days, NT(TA-HP) and NT-PEG shows improved vWF expression compared to NT-FL, with no significant differences between the other surfaces (**Figure 4.6b**). This was expected since NT-FL did not enable the EC growth on its surface, thus the expression of specific protein markers would be negligible. The immunofluorescence results indicate that all surfaces but NT-FL present considerable expression of specific protein markers to EC, showing that the cells are mature and are maintaining their functionality. One can also see from the fluorescence images that only NT(TA-HP) shows a complete EC coverage after 7 days, which is agreement with previous results, being the only surface that significantly fostered EC proliferation (**Figure 4.5a**). In addition, since NT(TA-HP) shows a higher number of cells in comparison with the other surfaces, it is expected that it presents enhanced protein expression.

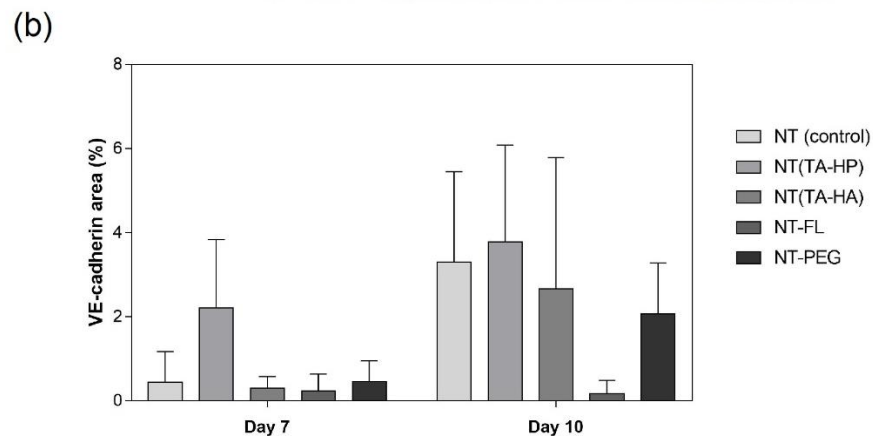
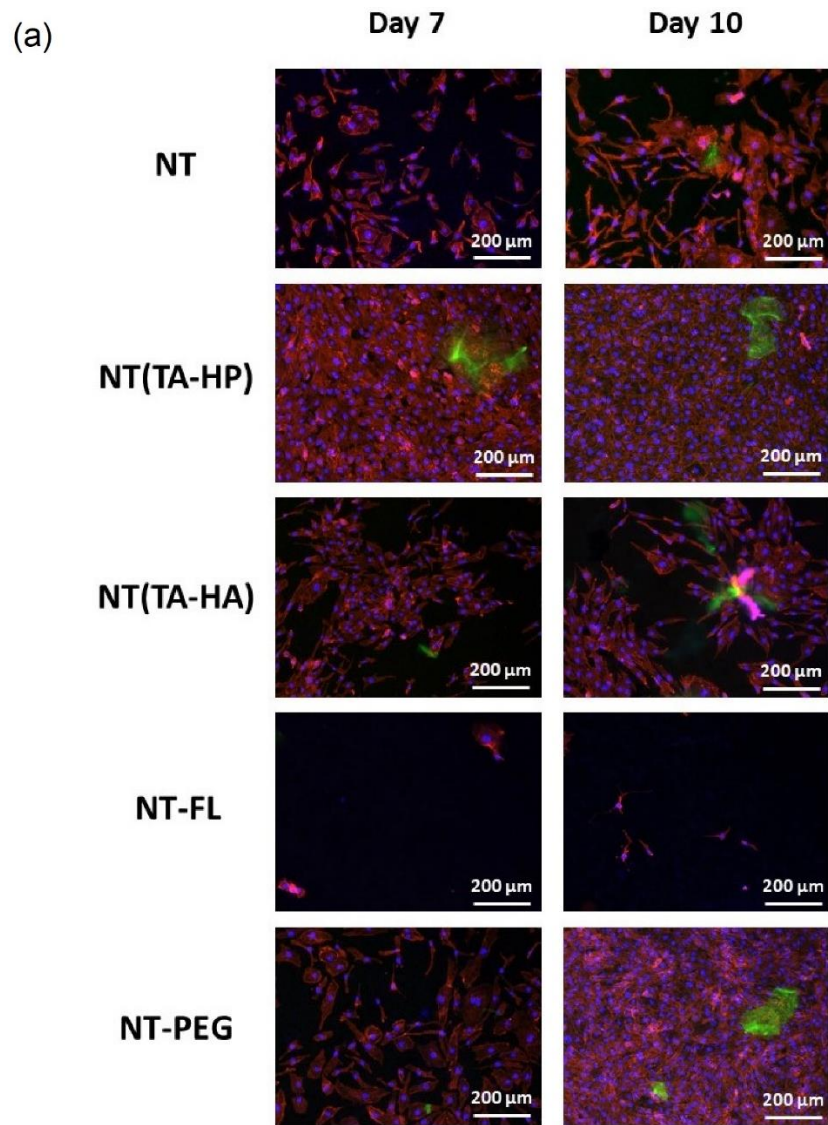


**Figure 4.5.** (a) Representative immunofluorescence microscopy images of HMVECs after 7 and 10 days of cell culture. Green stain represents VE-cadherin. (b) Percentage area coverage of VE-cadherin. No significant difference is observed between the NT surfaces on days 7 and 10.

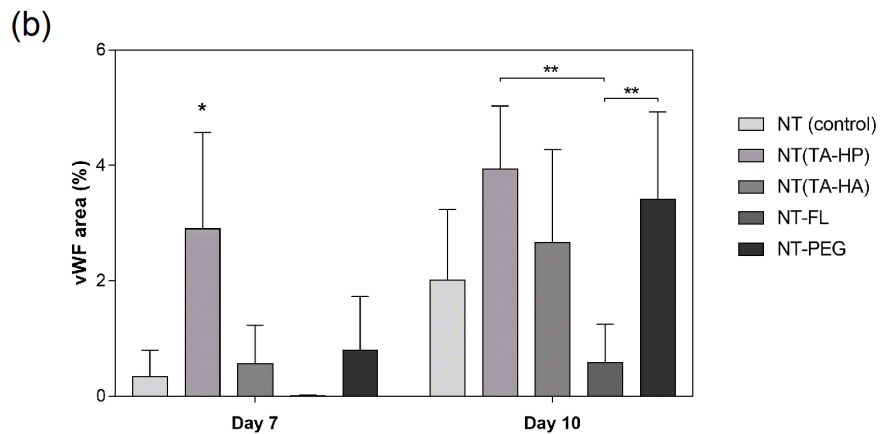
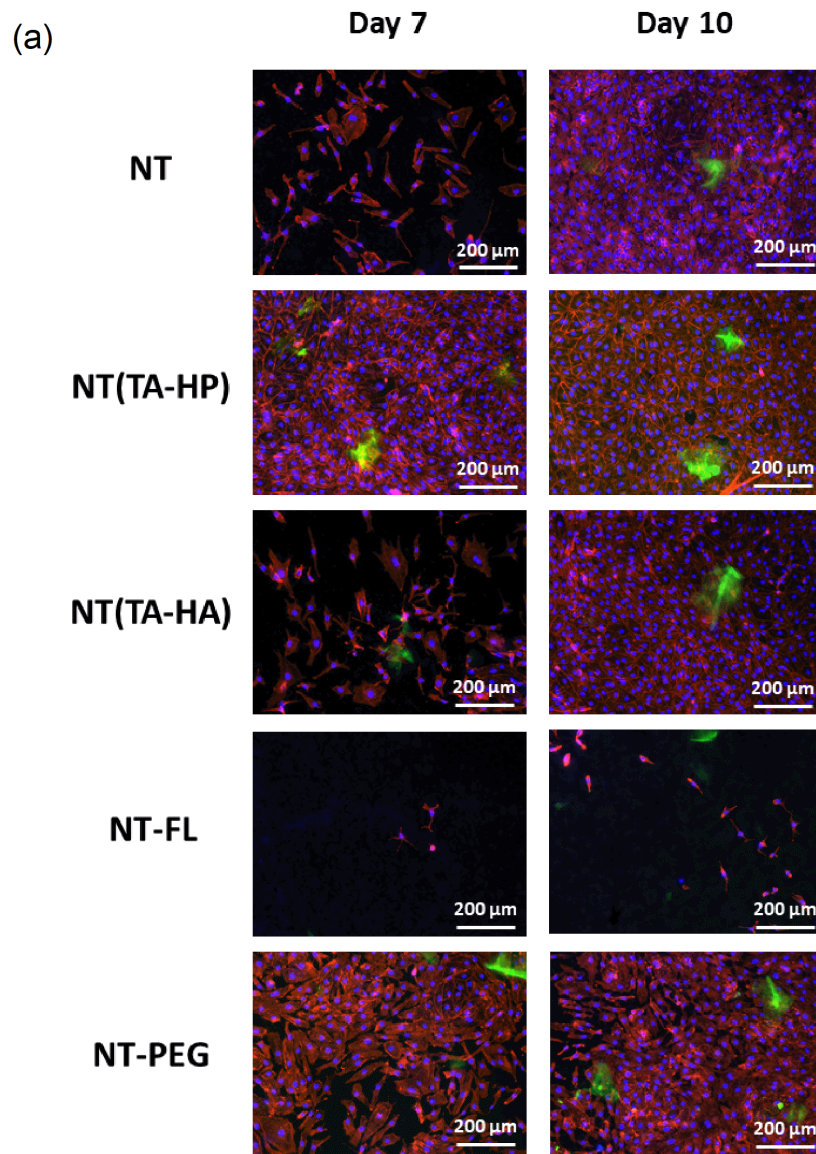


**Figure 4.6.** (a) Representative immunofluorescence microscopy images of HMVECs after 7 and 10 days of cell culture. Green stain represents vWF. (b) Percentage area coverage of vWF. No significant difference is observed between the NT surfaces on days 7 and 10.

### 4.3.3. SMCs viability, adhesion, and proliferation

The control or inhibition of SMC proliferation is vital for a successful endothelialization of implants to prevent restenosis, which is the artery occlusion due to smooth muscle cell proliferation [26]. Some strategies used to promote EC adhesion and proliferation on implants contribute to stimulate SMC growth as well [27]. Therefore, it is important that the biomaterial surface selectively promotes the growth of EC while preventing SMC proliferation. To investigate the SMC viability, the surfaces were incubated with HASMCs for 1, 3 and 5 days and the cell viability was evaluated using CellTiter-Blue assay. The results show that there is no significant difference between NT surfaces within the same days; however, all NT surfaces show a decreased in cell viability throughout the days, with a significant reduction in cell viability on day 5 compared to day 1 (**Figure 4.7**). The SMCs adhesion and proliferation were also investigated using fluorescence microscopy images (**Figures 4.8a**). The results show that there are no significant dif-

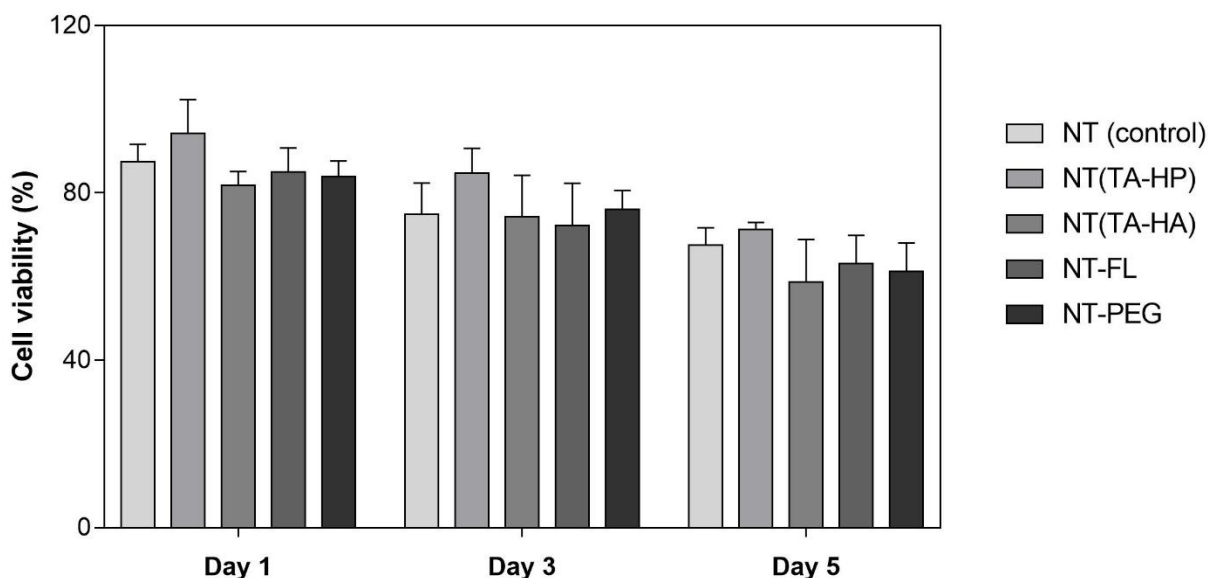


**Figure 4.7.** CellTiter-Blue SMCs viability assay after 1, 3 and 5 days of cell culture. Results are normalized using the positive control on tissue-culture polystyrene. There is no significant difference between NT surfaces within the same days, however, all NT surfaces showed significantly higher cell viability on day 1 compared to day 5.

ferences in cell count between all NT surfaces on days 1 and 3 (**Figure 4.8b**). On day 5, the number of adhered cells on NT(TA-HA) was significantly higher than on NT-FL. In addition, NT(TA-HA) was the only surface who significantly increased the cell count from day 1 to day 5. This agrees with cell viability results as most of NT surfaces inhibit to some extent the SMC proliferation.

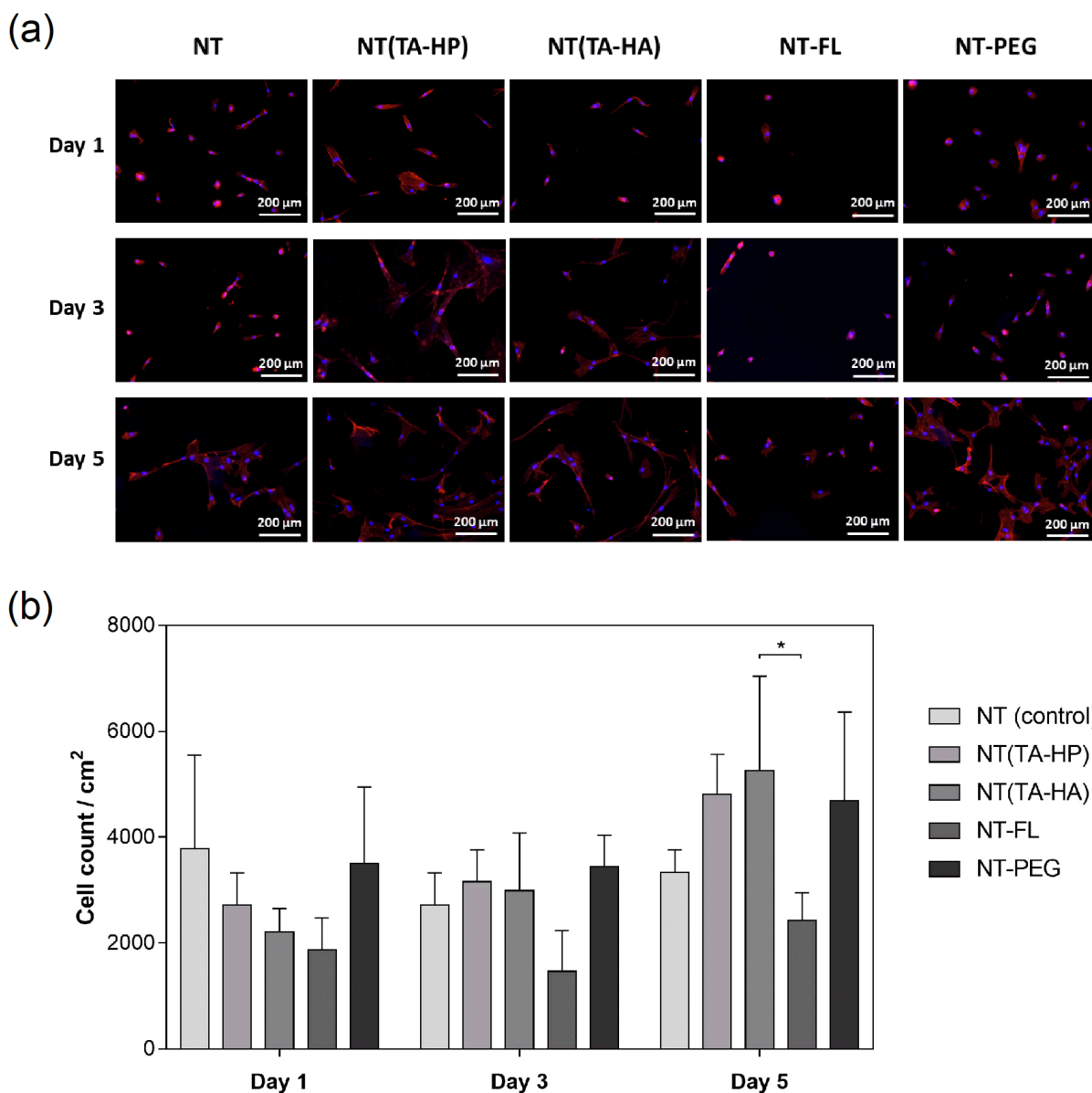


**Figure 4.8.** (a) Representative fluorescence microscopy images of SMCs stained with DAPI (blue) and rhodamine phalloidin (red). (b) Cell count per area after 1, 3 and 5 days of cell culture. No significant difference is observed on days 1 and 3 between all NT surfaces. \* Represents  $p < 0.05$ . NT(TA-HA) was the only surface who significantly increased the cell count from day 1 to day 5.

The SMCs morphology on the surfaces was investigated using SEM after 1, 3 and 5 days of cell culture. **Figure 4.9** shows similar cell spreading on all NT surfaces, except for NT-FL who inhibit the SMC spreading. This agrees with previous results as, although there is some cell spreading, the SMC growth is limited and reduced compared to EC proliferation on the same surfaces. The NT surfaces were able to limit the SMC proliferation, which was expected due to the presence of nanoscale topography [28]. In addition, the EC proliferation was significantly faster than SMC proliferation on all surfaces, which could indicate a selective interaction with ECs over SMCs in physiological conditions [29].

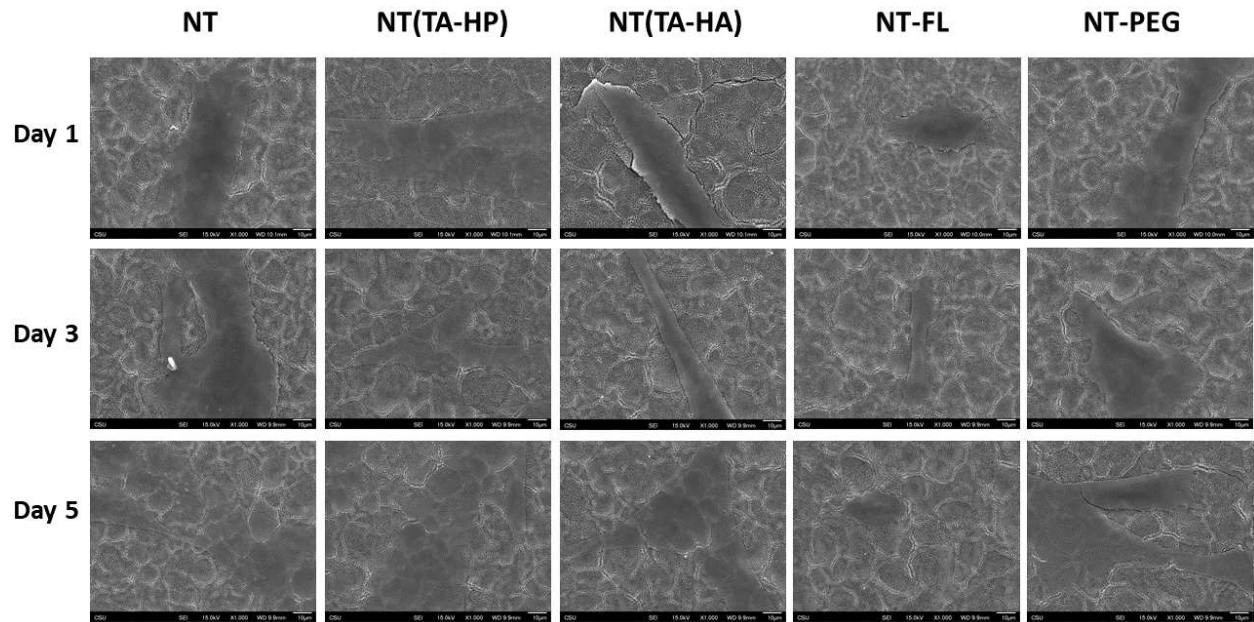


**Figure 4.9.** Representative SEM images of SMCs on NT surfaces after 1, 3 and 5 days of cell culture. The images were taken at 1,000× magnification.

#### 4.3.4. ECs migration study

The ability of surfaces to enhance EC migration is crucial as usually the endothelialization of implant surfaces occurs due to the migration of the neighbor EC layer [30]. Therefore, in this work, the EC migration potential on the NT surfaces was investigated. After a confluent monolayer

of cells was obtained, the surfaces were scratched a straight mark to remove the cells on the center, and they were incubated for 24 h to allow the ECs to migrate. Bare titanium was used as control to show the mark size on the surface right after the scratch. The results show that all NT surfaces, except for NT-FL, allowed the ECs to migrate (**Figure 4.12**). As expected, since the superhydrophobic surface (NT-FL) did not promote EC growth, it was not possible to achieve a confluent layer on its surface. Both tanfloc-based surfaces, NT(TA-HP) and NT(TA-HA), performed better than NT, showing a complete coverage of the surfaces, with a 100% confluence for NT(TA-HP) after 24 h, as if no cells were removed from its surface. This could be explained due to the presence of heparin, since it has been reported it can improve the endothelial cell migration [2]. NT-PEG also showed a better cell coverage and spreading in comparison with unmodified NT. These outcomes agree with the previous ECs results, as NT(TA-HP), NT(TA-HA), and NT-PEG showed enhanced EC growth and differentiation in comparison with unmodified NT.

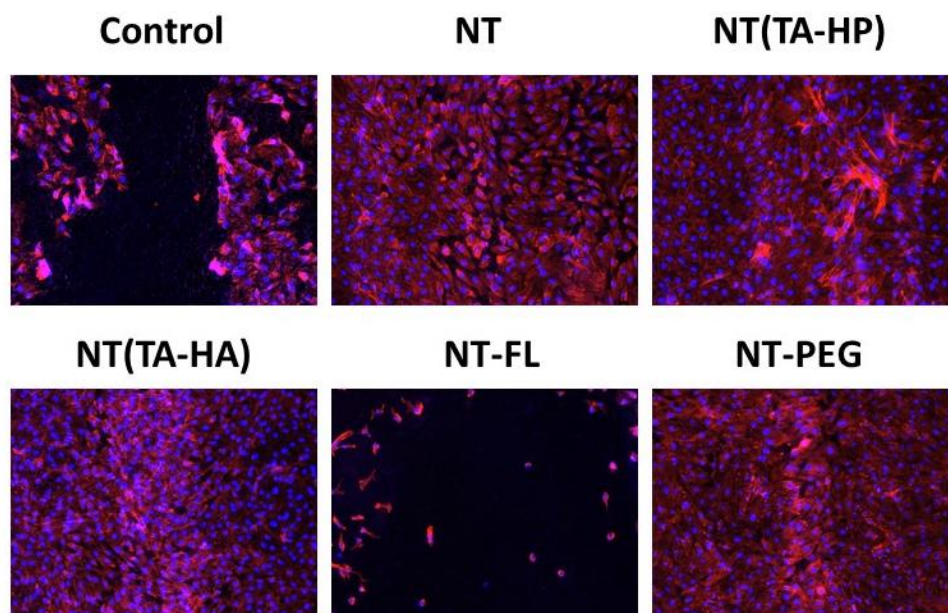


**Figure 4.12.** Representative fluorescence microscopy images of ECs stained with DAPI (blue) and rhodamine phalloidin (red) on different NT surfaces after a 100% confluence was obtained and the surfaces were scratched a straight mark and incubated at 37 °C for 24 h.

#### **4.4. Conclusions**

In this work, the endothelialization potential of the NT surfaces developed in chapters 2 and 3 was investigated. Previous results have showed improved antithrombogenic properties, with significantly lower protein adsorption, FXII activation, and platelet adhesion and activation, which indicates they are promising candidates to be used for cardiovascular implant applications. The results show that all surfaces but NT-FL present considerable expression of specific protein markers to EC, indicating that the cells are mature and are maintaining their functionality. The NT surfaces modified with tanfloc and heparin, NT(TA-HP), showed enhanced EC adhesion, proliferation and migration, which is vital for a successful endothelialization of implants. This could be explained due to the presence of protonated amino groups on TA, which may be responsible for a bioadhesive characteristic, improving the cell adhesion. In addition, the presence of HP is responsible for enhancing the endothelial cell proliferation due to its ability to potentiate and bind with growth factors. The results also showed that all NT surfaces were able to limit the SMC proliferation, which is desired to prevent restenosis. Future studies should focus on the co-culture of ECs and SMCs to evaluate the selective interaction of NT surfaces with ECs over SMCs.

## REFERENCES

- [1] M. Heron, National Vital Statistics Reports Volume 68, Number 6, June 24, 2019, Deaths: Leading Causes for 2017, 2019. <https://www.cdc.gov/nchs/products/index.htm>. (accessed May 18, 2020).
- [2] Z. Yang, Q. Tu, J. Wang, N. Huang, The role of heparin binding surfaces in the direction of endothelial and smooth muscle cell fate and re-endothelialization, *Biomaterials*. 33 (2012) 6615–6625. doi:10.1016/j.biomaterials.2012.06.055.
- [3] Y. Xie, Z. Zeng, Y. Fan, Y. Zhang, J. Liu, W. Li, Y. Weng, Selective endothelialization and alleviation of neointimal hyperplasia by functionalizing the Ti-O surface with L-selenocystine and KREDVC, *Colloids Surfaces B Biointerfaces*. 180 (2019) 168–176. doi:10.1016/j.colsurfb.2019.04.039.
- [4] S.R. Meyers, P.T. Hamilton, E.B. Walsh, D.J. Kenan, M.W. Grinstaff, Endothelialization of titanium surfaces, *Adv. Mater.* 19 (2007) 2492–2498. doi:10.1002/adma.200700029.
- [5] A. Colombo, J. Drzewiecki, A. Banning, E. Grube, K. Hauptmann, S. Silber, D. Dudek, S. Fort, F. Schiele, K. Zmudka, G. Guagliumi, M.E. Russell, Randomized study to assess the effectiveness of slow- and moderate-release polymer-based paclitaxel-eluting stents for coronary artery lesions, *Circulation*. 108 (2003) 788–794. doi:10.1161/01.CIR.0000086926.62288.A6.
- [6] M. Pflaum, M. Kühn-Kauffeldt, S. Schmeckeber, D. Dipresa, K. Chauhan, B. Wiegmann, R.J. Haug, J. Schein, A. Haverich, S. Korossis, Endothelialization and characterization of titanium dioxide-coated gas-exchange membranes for application in the bioartificial lung, *Acta Biomater.* 50 (2017) 510–521. doi:10.1016/j.actbio.2016.12.017.
- [7] R. Luo, J. Zhang, W. Zhuang, L. Deng, L. Li, H. Yu, J. Wang, N. Huang, Y. Wang, Multifunctional coatings that mimic the endothelium: Surface bound active heparin nanoparticles with: In situ generation of nitric oxide from nitrosothiols, *J. Mater. Chem. B*. 6 (2018) 5582–5595. doi:10.1039/c8tb00596f.
- [8] S. Jana, Endothelialization of cardiovascular devices, *Acta Biomater.* 99 (2019) 53–71. doi:10.1016/j.actbio.2019.08.042.
- [9] J. Li, K. Zhang, N. Huang, Engineering Cardiovascular Implant Surfaces to Create a Vascular Endothelial Growth Microenvironment, *Biotechnol. J.* 12 (2017). doi:10.1002/biot.201600401.
- [10] G.P. Fadini, S. Sartore, C. Agostini, A. Avogaro, Significance of endothelial progenitor cells in subjects with diabetes, *Diabetes Care*. 30 (2007) 1305–1313. doi:10.2337/dc06-2305.
- [11] Y. Duan, S. Yu, P. Xu, X. Wang, X. Feng, Z. Mao, C. Gao, Co-immobilization of CD133 antibodies, vascular endothelial growth factors, and REDV peptide promotes capture, proliferation, and differentiation of endothelial progenitor cells, *Acta Biomater.* 96 (2019) 137–148. doi:10.1016/j.actbio.2019.07.004.
- [12] R.M. Sabino, K. Kauk, S. Movafaghi, A. Kota, K.C. Papat, Interaction of blood plasma proteins with superhemophobic titania nanotube surfaces, *Nanomedicine Nanotechnology, Biol. Med.* 21 (2019). doi:10.1016/j.nano.2019.102046.
- [13] R.M. Sabino, K. Kauk, L.Y.C. Madruga, M.J. Kipper, A.F. Martins, K.C. Papat, Enhanced hemocompatibility and antibacterial activity on titania nanotubes with

- tanfloc/heparin polyelectrolyte multilayers, *J. Biomed. Mater. Res. - Part A*. 108 (2020) 992–1005. doi:10.1002/jbm.a.36876.
- [14] R.M. Sabino, K. Kauk, S. Movafaghi, A. Kota, K.C. Popat, Interaction of blood plasma proteins with superhemophobic titania nanotube surfaces, *Nanomedicine Nanotechnology, Biol. Med.* 21 (2019) 102046. doi:10.1016/j.nano.2019.102046.
- [15] B.B.S. Ramin, K.B. Rufato, R.M. Sabino, K.C. Popat, M.J. Kipper, A.F. Martins, E.C. Muniz, Chitosan/iota-carrageenan/curcumin-based materials prepared by precipitating miscible solutions prepared in ionic liquid, *J. Mol. Liq.* 290 (2019) 111199. doi:10.1016/J.MOLLIQ.2019.111199.
- [16] A.C. de Oliveira, R.M. Sabino, P.R. Souza, E.C. Muniz, K.C. Popat, M.J. Kipper, R.S. Zola, A.F. Martins, Chitosan/gellan gum ratio content into blends modulates the scaffolding capacity of hydrogels on bone mesenchymal stem cells, *Mater. Sci. Eng. C*. 106 (2020) 110258. doi:10.1016/J.MSEC.2019.110258.
- [17] R.M. Sabino, J. V. Rau, A. De Bonis, A. De Stefanis, M. Curcio, R. Teghil, K.C. Popat, Manganese-containing Bioactive Glass Enhances Osteogenic Activity of TiO<sub>2</sub> Nanotube Arrays, *Appl. Surf. Sci.* 570 (2021) 151163. doi:10.1016/j.apsusc.2021.151163.
- [18] V. Leszczak, D.A. Baskett, K.C. Popat, Endothelial cell growth and differentiation on collagen-immobilized polycaprolactone nanowire surfaces, *J. Biomed. Nanotechnol.* 11 (2015) 1080–1092. doi:10.1166/jbn.2015.2021.
- [19] K. Zhang, J. ying Chen, W. Qin, J. an Li, F. xia Guan, N. Huang, Constructing bio-layer of heparin and type IV collagen on titanium surface for improving its endothelialization and blood compatibility, *J. Mater. Sci. Mater. Med.* 27 (2016). doi:10.1007/s10856-016-5693-6.
- [20] C. Park, S. Park, J. Kim, A. Han, S. Ahn, S.K. Min, H.J. Jae, J.W. Chung, J.H. Lee, H. Do Jung, H.E. Kim, T.S. Jang, Enhanced endothelial cell activity induced by incorporation of nano-thick tantalum layer in artificial vascular grafts, *Appl. Surf. Sci.* 508 (2020) 144801. doi:10.1016/j.apsusc.2019.144801.
- [21] L.Y.C. Madruga, R.M. Sabino, E.C.G. Santos, K.C. Popat, R. de C. Balaban, M.J. Kipper, Carboxymethyl-kappa-carrageenan: A study of biocompatibility, antioxidant and antibacterial activities, *Int. J. Biol. Macromol.* 152 (2020) 483–491. doi:10.1016/j.ijbiomac.2020.02.274.
- [22] P.C.F. da Câmara, R.C. Balaban, M. Hedayati, K.C. Popat, A.F. Martins, M.J. Kipper, Novel cationic tannin/glycosaminoglycan-based polyelectrolyte multilayers promote stem cells adhesion and proliferation, *RSC Adv.* 9 (2019) 25836–25846. doi:10.1039/C9RA03903A.
- [23] A.F. Martins, S.P. Facchi, P.C.F. da Câmara, S.E.A. Camargo, C.H.R. Camargo, K.C. Popat, M.J. Kipper, Novel poly( $\epsilon$ -caprolactone)/amino-functionalized tannin electrospun membranes as scaffolds for tissue engineering, *J. Colloid Interface Sci.* 525 (2018) 21–30. doi:10.1016/J.JCIS.2018.04.060.
- [24] C. Boura, P. Menu, E. Payan, C. Picart, J.C. Voegel, S. Muller, J.F. Stoltz, Endothelial cells grown on thin polyelectrolyte multilayered films: an evaluation of a new versatile surface modification, *Biomaterials*. 24 (2003) 3521–3530. doi:10.1016/S0142-9612(03)00214-X.
- [25] D. Vestweber, VE-cadherin: The major endothelial adhesion molecule controlling cellular junctions and blood vessel formation, *Arterioscler. Thromb. Vasc. Biol.* 28 (2008) 223–232. doi:10.1161/ATVBAHA.107.158014.

- [26] J. Zhao, L. Bai, X. kui Ren, J. Guo, S. Xia, W. Zhang, Y. Feng, Co-immobilization of ACH11 antithrombotic peptide and CAG cell-adhesive peptide onto vascular grafts for improved hemocompatibility and endothelialization, *Acta Biomater.* 97 (2019) 344–359. doi:10.1016/j.actbio.2019.07.057.
- [27] Y. Xie, Z. Zeng, Y. Fan, Y. Zhang, J. Liu, W. Li, Y. Weng, Selective endothelialization and alleviation of neointimal hyperplasia by functionalizing the Ti-O surface with L-selenocystine and KREDVC, *Colloids Surfaces B Biointerfaces.* 180 (2019) 168–176. doi:10.1016/j.colsurfb.2019.04.039.
- [28] V. Leszczak, D. Baskett, K. Popat, Smooth Muscle Cell Functionality on Collagen Immobilized Polycaprolactone Nanowire Surfaces, *J. Funct. Biomater.* 5 (2014) 58–77. doi:10.3390/jfb5020058.
- [29] J. Li, K. Zhang, P. Yang, W. Qin, G. Li, A. Zhao, N. Huang, Human vascular endothelial cell morphology and functional cytokine secretion influenced by different size of HA micro-pattern on titanium substrate, *Colloids Surfaces B Biointerfaces.* 110 (2013) 199–207. doi:10.1016/j.colsurfb.2013.04.048.
- [30] K. Zhang, J. ying Chen, W. Qin, J. an Li, F. xia Guan, N. Huang, Constructing bio-layer of heparin and type IV collagen on titanium surface for improving its endothelialization and blood compatibility, *J. Mater. Sci. Mater. Med.* 27 (2016) 81. doi:10.1007/s10856-016-5693-6.

## CHAPTER 5: TANFLOC/HEPARIN POLYELECTROLYTE MULTILAYERS IMPROVE OSTEOGENIC DIFFERENTIATION OF ADIPOSE-DERIVED STEM CELLS ON TITANIA NANOTUBE SURFACES<sup>1</sup>

### 5.1. Introduction

Titanium and its alloys are the most common biomaterial used for orthopedic and dental implants [2]. Titanium combines excellent mechanical properties, such as high strength, low density and moderate Young's modulus, with great biocompatibility and resistance to corrosion [3]. In addition, titanium can have its properties easily modified by forming alloys or altering its surface, which makes it suitable for a wide range of biomedical applications [4]. However, the rate of failure for orthopedic and dental implants can be as high as 10% [5]. One of the major causes for device failure is the aseptic loosening of titanium implants, mostly due to poor osseointegration of the prosthesis into the bone [6]. Implants for knees, hips, and teeth need to withstand constant stresses, which create micromotion of the implant and can lead to the device loosening. Therefore, it is essential to develop novel biomaterial surfaces that promote better osseointegration, thus reducing implant failure and revision surgeries.

Osseointegration is the direct anchorage of a prosthesis to bone by the formation of bone tissue around the implant [7]. Rapid and stable osseointegration reduces risks of implant failure, and involves multiple biological processes, including preosteoblast adhesion, differentiation, and mineralization [8]. To achieve osseointegration, an implant surface must be osteoinductive (i.e. promote osteoblast differentiation) and osteoconductive (i.e. promote new bone matrix deposition

---

<sup>1</sup> This work was published in *Carbohydrate Polymers* and is reproduced in modified form here with permission [1]

on its surface) [9]. Therefore, osteoconduction relies on an earlier successful osteoinduction, which ultimately leads to the implant osseointegration. The osteoinductivity of surfaces can be studied *in vitro* by investigating the osteogenic differentiation of stem cells in contact with the biomaterial surface [10]. Adipose-derived stem cells (ADSCs) exhibit pluripotency *in vitro*, and are capable of differentiation into a variety of cell lineages, including osteoblasts. Since ADSCs demonstrate a substantial capacity for bone formation, they are an excellent model cell type to study osteogenic differentiation and osteoinduction on biomaterials [11].

Surface modifications have been proposed to enhance osseointegration on titanium implants. Altering the topography of the biomaterial surface to introduce micro and nanoscale features can improve the cellular responses [11–13]. Since bone cells in native tissue interact with nanoscale extracellular matrix elements, such as protein and minerals, the surface nanotopography increases the adsorption of proteins and stimulates osteogenic differentiation [14]. These nanoscale interactions predispose cells to adhere, proliferate, and differentiate on nanostructured surfaces [15]. Nanofabrication techniques recently investigated on titanium include formation of nanopores, nanofibers and nanotubes [16,17]. Titania nanotube (NT) surfaces have emerged as a promising approach as they enhance biocompatibility, promote adhesion and differentiation of stem cells, improve antibacterial properties, and reduce immune responses on titanium [18,19].

The layer-by-layer (LbL) deposition of polyelectrolyte multilayers (PEMs) is another promising technique to improve the biological response to titanium-based surfaces [20]. The LbL approach creates PEMs by alternating the deposition/adsorption of polycationic and polyanionic layers onto solid surfaces [21]. Tanfloc (TA) is a cationic polyphenol that our research group has recently investigated as a biomaterial [22]. TA is an amino-functionalized tannin derivative prepared from condensed tannins using a Mannich's type reaction with formic acid and

ammonium chloride [23]. TA can increase the biocompatibility, antithrombogenic and antimicrobial properties of biomaterials [24,25]. TA-based PEMs improve the hemocompatibility, cell adhesion, and antibacterial activity of solid substrates [26,27]. The osteoinductive properties of TA-based surfaces has never been investigated. In this work, TA-based PEMs on NT were fabricated by first changing the surface topography of titanium to make titania nanotubes. Then, the NT surface was modified via the LbL technique using the polyelectrolytes TA (polycation), and heparin (HP, polyanion) or hyaluronic acid (HA, polyanion) to create PEMs with 5-layers on NT. We have previously used polysaccharide-containing PEMs to modify the surfaces of allograft bone, showing that these are suitable for promoting stem cell adhesion, reducing bacterial attachment, and improving inflammatory responses in vivo [28,29]. Polysaccharide based PEMs can also be used to control growth factor delivery to guide cell behavior [30–32]. Based on this work, we hypothesize that the combination of polysaccharide-containing Tanfloc PEMs can improve osteoinduction of ADSCs on titania nanotube surfaces.

In this work, the surfaces were characterized by scanning electron microscopy (SEM), X-ray photoelectron spectroscopy (XPS), contact angle goniometry, and stability tests. ADSCs were cultured on the surfaces, and their viability, adhesion and proliferation were evaluated after 4 and 7 days of cell culture. Osteogenesis was then induced and the osteogenic differentiation of ADSCs was assessed via mineralization and protein expression assays, immunofluorescent staining, and SEM. The TA/HP PEMs on NT significantly improve osteogenic differentiation of ADSCs and bone mineral deposition compared to unmodified NT, indicating potential for enhanced osseointegration.

## 5.2. Materials and Methods

### 5.2.1. Fabrication of titania nanotubes (NT) modified with PEMs

NT surfaces were fabricated using an anodization technique on titanium sheets (0.4 mm thick) as described in Chapter 2 [33]. Tanfloc (TA, Tanac SA, approximately 60 kDa) was purified by dialysis. The dialysis process removes impurities (calcium, potassium, and chloride ions) from TA [25]. For this, a TA solution (2.5 g in 50 mL at 5.0% wt/vol and 50 g L<sup>-1</sup>) was prepared in distilled water (pH  $\approx$  5.5), previously filtered to remove wood particles, and dialyzed against distilled water for 12 hrs with no water exchange. Dynamic light scattering (DLS) measurements determined the molecular masses for dialyzed [34]. Aqueous dialyzed TA aliquots (0.03 to 15 mg L<sup>-1</sup>) were filtered with polytetrafluoroethylene membranes (diameter of 0.45  $\mu$ m) and analyzed in a Zeta Sizer Nano Malvern apparatus with a He-Ne LASER operating at 663 nm (detection angle of 173° at 25 °C). Measurements were performed in duplicate (n = 2).

Solutions of TA, HP (Celsus Laboratories, 14.4 kDa), and HA (Sigma, 1.5-1.8 MDa) were made in acetic acid-acetate buffer (pH 5.0 and 0.2 M) at 1.0 mg/ml concentration. The rinse solution was prepared from an aqueous acetic acid solution at pH 4.0. The whole process of surface modification with PEMs was performed under shaking at 30 rpm. The oxidized NT surfaces were rinsed with the rinse solution for 5 min before the TA deposition. After the rinse solution removal, the oxidized NT surface was incubated with 0.5 ml TA (polycation) solution for 6 min. The polycation solution was aspirated, and the surface was rinsed for 5 min. Then, HP or HA (polyanions) solution was added to the surfaces containing one layer of TA, and allowed to deposit for 6 mins. This procedure was repeated until the deposit of the fifth layer (polycation terminated). The PEMs deposited on NT surfaces are denoted NT(TA-HP) and NT(TA-HA) (**Figure 5.1**).

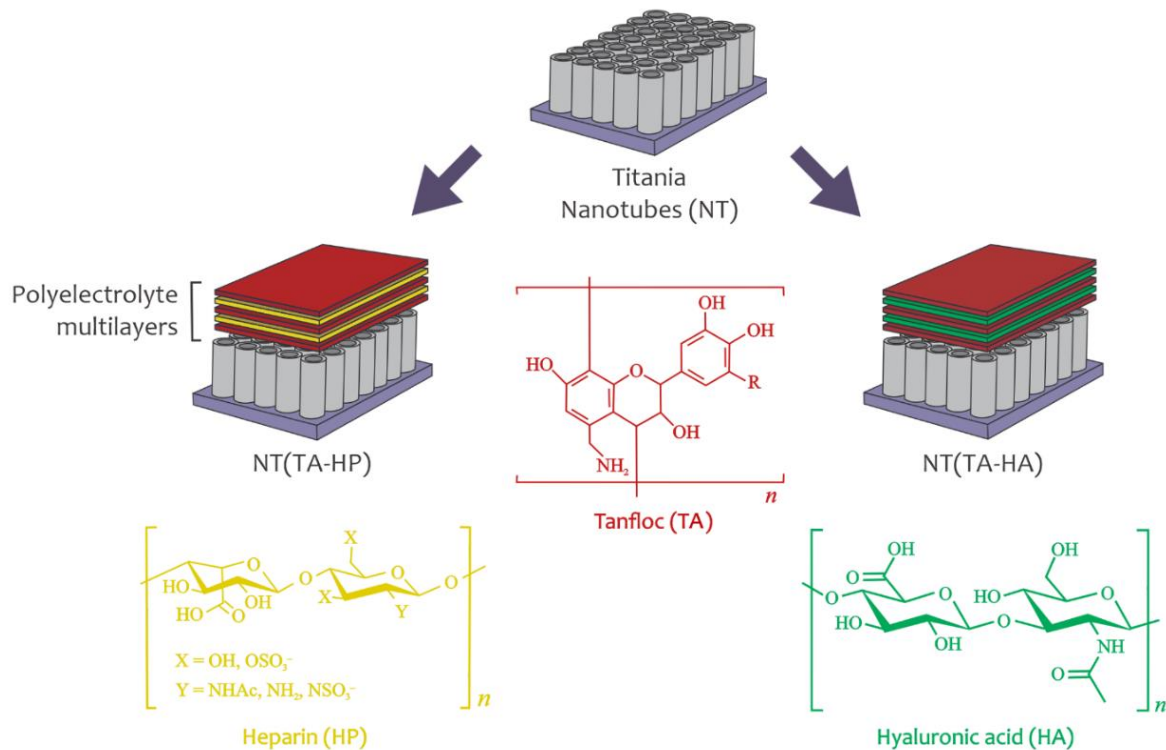


**Figure 5.1.** Schematic of PEM fabrication on titania NT and the polyelectrolyte structures (R = H or OH).

### 5.2.2. Surface characterization

The morphology of the surfaces was characterized using SEM. The surfaces were coated with 10 nm of gold and imaged at 15 kV. The ImageJ software was used to measure the nanotubes' diameters. The static contact angles were measured with 7  $\mu$ l of DI water on the surfaces using a Ramé-Hart Model 250 goniometer. The chemical compositions of the surfaces were characterized using XPS. Survey-scan spectra were obtained from 0 to 1100 eV at a pass energy of 187 eV, and high-resolution spectra of carbon C1s peak were obtained at a pass energy of 10 eV. Peak-fit analysis was performed using MultiPak and Origin software.

### **5.2.3. Stability test**

The stability of different surfaces was determined by measuring the water contact angles over a 28-day period [33]. The surfaces were incubated with phosphate buffered saline (PBS) in a 48-well plate and placed on horizontal shaker plate at 100 rpm in an incubator (37°C and 5% CO<sub>2</sub>) for 28 days. After 7-day intervals, the surfaces were rinsed with DI water and air dried, and the contact angles were measured as described in Section 5.2.2. Additionally, XPS was also used to determine the surface composition after 28 days. Survey and carbon high-resolution spectra were collected as described in Section 5.2.2.

### **5.2.4. ADSCs culture**

Prior to biological assays, all the surfaces were sterilized by incubating with 70% ethanol for 5 min, followed by 3 rinses and incubation with sterile PBS for 30 min. Human ADSCs isolated from adipose tissue and at passage three were obtained from Dr. Kimberly Cox-York's laboratory at Colorado State University. The protocol for ADSC isolation from healthy individuals was approved by Colorado State University Institutional Review Board. The cells were cultured at 37 °C and 5% CO<sub>2</sub> in growth media composed of  $\alpha$ -MEM Media (HyClone™) with 10% (v/v) Fetal Bovine Serum (FBS) and 1% (v/v) penicillin/streptomycin (Corning) [35]. The cells were seeded on the sterilized NT surfaces at a final concentration of  $2.0 \times 10^4$  cells/ml.

### **5.2.5. ADSCs viability, adhesion, and proliferation**

ADSCs viability was evaluated using CellTiter-Blue assay (Promega) after 4 and 7 days of cell culture [35]. The surfaces with adhered cells were incubated at 37 °C for 8 h in fresh culture media with 10% of CellTiter-Blue reagent. After 8 h, the absorbance of the solutions was measured

at 570 and 600 nm using a microplate reader (FLUOstar Omega, BMG Labtech). The CellTiter-Blue reduction percentage correlates with the percentage of viable cells. The ADSC viability was calculated as described by the manufacturer's protocol. The ADSCs were also seeded in empty wells (positive control), while the negative control was carried out only with the media without cells. The results obtained for the negative control was used to eliminate the influence of the cell media on the CellTiter-Blue reduction percentage. The cell viability outcomes obtained for the surfaces were normalized using the results from the positive control.

The cell adhesion and proliferation on the surfaces were characterized using fluorescence microscopy. After 4 and 7 days of culture, the media was removed, and the surfaces were rinsed with PBS. The cells adhered on the surfaces were fixed in 3.7% formaldehyde in PBS for 15 mins, followed by three rinses (5 min each) with PBS. Adhered ADSCs were permeabilized by incubation with 1% Triton X-100 in PBS for 3 min and rinsed twice with PBS [36]. The surfaces were then incubated in 70 nM of rhodamine phalloidin in PBS for 20 min in a dark environment. The nuclear stain DAPI (300 nM, ThermoFisher Scientific) was added, and after 5 min the surfaces were rinsed with PBS twice and then imaged using a fluorescence microscope (Zeiss). To obtain the quantity of ADSCs adhered on the surfaces, the number of stained nuclei (DAPI) was counted using ImageJ software. Cell morphology on the surfaces was also investigated by SEM.

The cell morphology on the surfaces was investigated by SEM. After 4 and 7 days of cell culture, the media was removed, and the surfaces were rinsed with PBS. The surfaces were then placed in a fixative solution composed of 3% glutaraldehyde, 0.1 M sucrose, and 0.1 M sodium cacodylate in DI water for 40 min. After that, the surfaces were moved to a buffer solution (fixative solution without glutaraldehyde) for 10 min. The surfaces were then dehydrated by exposure to ethanol solutions (35%, 50%, 70%, and 100%, respectively) for 10 min each step. The surfaces

were then incubated in 100% hexamethyldisilazane (HMDS) for 10 min. After HMDS removal, the surfaces were dried and stored in a desiccator until further imaging. SEM imaging was conducted as described in Section 5.2.2.

#### **5.2.6. Osteogenic differentiation of ADSCs**

After 7 days of ADSC culture on the surfaces, osteogenesis was induced using osteogenic differentiation media, consisting of growth media supplemented with  $10^{-8}$  M dexamethasone, 50  $\mu\text{g}/\text{mL}$  of ascorbic acid, and 6 mM  $\beta$ -glycerol phosphate. The differentiation media was changed every other day for 3 weeks. After 1 and 3 weeks of induced osteogenic differentiation, the following quantitative assays were performed to determine the osteoinductivity of the surfaces: total protein content, alkaline phosphatase (ALP) activity, and calcium concentration. The surfaces were rinsed once with PBS and transferred to a new 48-well plate. Then, the surfaces were incubated in Triton X-100 (0.2% v/v in DI water) and placed on a horizontal shaker at 150 rpm for 20 min to remove all protein content from the surfaces.

A micro BCA assay kit (Thermo Scientific) was used to quantify the total amount of protein content. Supernatant (150  $\mu\text{L}$  Triton X-100 plus protein mixture) was mixed with 150  $\mu\text{L}$  of working reagent prepared following the manufacturer's protocol. The well plate was incubated for 2 h at 37 °C in dark environment. The absorbance was then read at 562 nm. The results for the total protein content was determined via a standard absorbance curve obtained previously using the manufacturer's guidelines.

A colorimetric assay kit (QuantiChrom<sup>TM</sup>, BioAssay Systems) was used to quantify the ALP activity on different surfaces. The supernatant (50  $\mu\text{L}$  of Triton X-100 plus protein mixture) was mixed with 150  $\mu\text{L}$  of working reagent prepared following the manufacturer's protocol. The

absorbance was read at 405 nm after 0 and 4 min of reaction and the ALP activity was determined using the manufacturer's guidelines. The ALP activity was normalized to total protein content on each surface.

A calcium reagent set (Teco Diagnostics) was used to quantify the calcium concentration on the surfaces. After supernatant removal, the surfaces were dried and incubated in 6 N HCl solution for 2 h to dissolve the deposited calcium. After that, 20  $\mu$ l of the calcium-acid solution was removed from each well and mixed with 1 ml of working reagent prepared following the manufacturer's protocol. The absorbance of the acid-calcium solution was read at 570 nm and the calcium concentration was calculated using the manufacturer's guidelines. The calcium concentration obtained was normalized to total protein content on each surface.

The osteogenic differentiation of ADSCs on the surfaces was also analyzed using immunofluorescent staining of the cells for the bone protein osteocalcin. After 1 and 3 weeks of induced osteogenesis, the media was removed, and the surfaces rinsed twice with PBS. The adhered cells were fixed and permeabilized as described in Section 5.2.4. The surfaces were then incubated in 10% bovine serum albumin (BSA, Sigma) for 30 min, followed by incubation in osteocalcin primary antibody (Santa Cruz Biotechnology) at a dilution of 1:100 in 1% BSA for 60 min. After two rinses with PBS, the surfaces were incubated with secondary antibody-FITC (Santa Cruz Biotechnology) at a dilution of 1:200 in 1% BSA for 45 min, followed by two rinses with PBS. Then, the surfaces were incubated in rhodamine phalloidin and DAPI nuclear stain, as described in Section 5.2.4. The surfaces were imaged by fluorescence microscopy. The presence of osteocalcin on each surface was obtained by measuring the percentage coverage area of stained osteocalcin using ImageJ software. The osteocalcin percentage area was normalized to the total number of nuclei on each surface.

The cell morphology and mineral deposition on the surfaces were also characterized using SEM. After 1 and 3 weeks of induced osteogenesis, ADSCs were fixed and dehydrated using the same process described in Section 5.2.4. Before the SEM imaging, the surfaces were coated with gold and imaged as described in Section 5.2.2.

### 5.2.7. Statistical analysis

SEM images and XPS analysis were performed on at least 2 different samples of each surface type. Contact angle and stability tests were carried out using 2 droplets per sample on 3 different samples of each surface type ( $n_{\min} = 6$ ). All cell studies were carried out with  $n_{\min} = 3$  for qualitative analyses and  $n_{\min} = 5$  for quantitative analyses. The quantitative results were analyzed via analysis of variance (ANOVA) and Tukey tests using the GraphPad Prism software ( $p < 0.05$ ).

## 5.3. Results and Discussion

Titanium and its alloys have been mainly used as biomaterials for orthopedic and dental implants due to their excellent mechanical properties, biocompatibility, and resistance against corrosion [2]. However, implant failure is still a huge problem due to biological issues, including poor osseointegration, microbial infection, and inflammation [37]. Therefore, the osseointegration enhancement of a biomaterial plays a key role in bone repair and tissue regeneration [38]. To minimize the chances of implant failure, several approaches have been proposed to modify the surface chemistry and topography of titanium [39–41]. Our recent work showed that the NT modification with TA-based PEMs significantly enhances the antithrombogenic and antibacterial properties of NT surfaces [27]. The results showed that TA/HP and TA/HA PEMs (5-layers) on NT significantly reduced the adhesion and proliferation of bacteria (*P. aeruginosa* and *S. aureus*)

after 24 h of incubation, as well as decreased the fibrinogen adsorption, Factor XII activation, and platelet adhesion and activation in comparison with unmodified NT surface. These properties are essential to prevent blood clotting and biofilm formation on implanted devices. However, the osteoinductivity of TA-based PEMs has never been investigated. In this study, we expand the characterization of the NT surfaces modified with PEMs. The surfaces were characterized by SEM, contact angle goniometry and XPS, and their stability in physiological conditions was also evaluated. cell viability, attachment, proliferation, and differentiation of ADSCs into bone cells was also evaluated.

### **5.3.1. Surface characterization**

SEM was used to characterize the surface morphology of NT and NT modified with PEMs (**Figure 5.2**). All surfaces have uniform and vertically oriented nanotubes. The SEM images show some changes in morphology for NT(TA-HA) in comparison with the others, although the nanotubes are still visible. No changes in NT average diameter ( $112 \pm 11$  nm) were observed before and after surface modification. This agrees with our previous study, showing that 5-layer PEMs do not achieve complete coverage of the NT surfaces [27]. We choose to use 5-layer PEMs to achieve surface modification, while maintaining the nanoscale topography of the surface. These nanofeatures may increase their surface biocompatibility by mimicking nanoscale behavior of cell-extracellular matrix interactions [42].

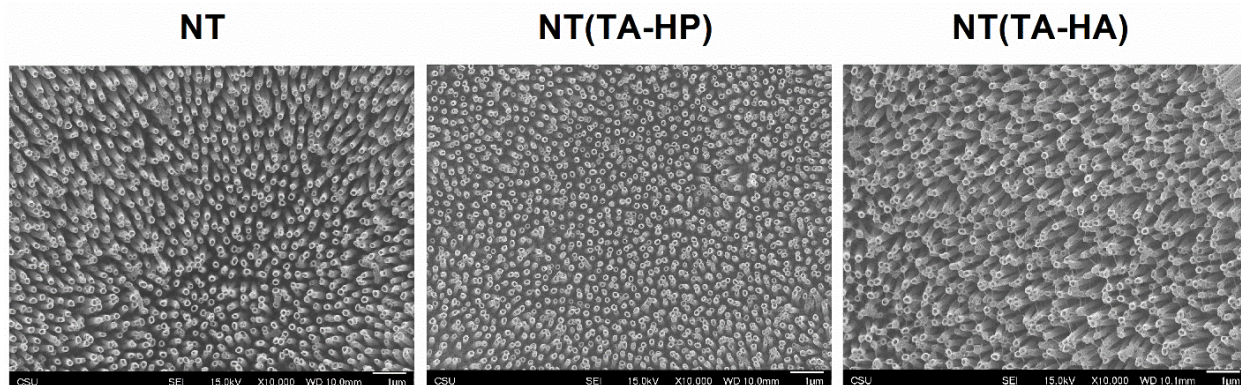


**Figure 5.2.** Representative SEM images of NT surfaces before and after modification with PEMs. The images were taken at 10,000× magnification.

Contact angle measurements were used to characterize the wettability of all surfaces. All of the surfaces here are hydrophilic, defined as having a water contact angle  $\theta < 90^\circ$  [43] (**Figure 5.3**). NT surfaces are considered superhydrophilic ( $\theta < 10^\circ$ ) as the water penetrates by capillary forces in the tubular structures [44]. NT(TA-HP) shows higher hydrophilicity than NT(TA-HA) because HP possesses a high number of sulfate groups on its structure [45].

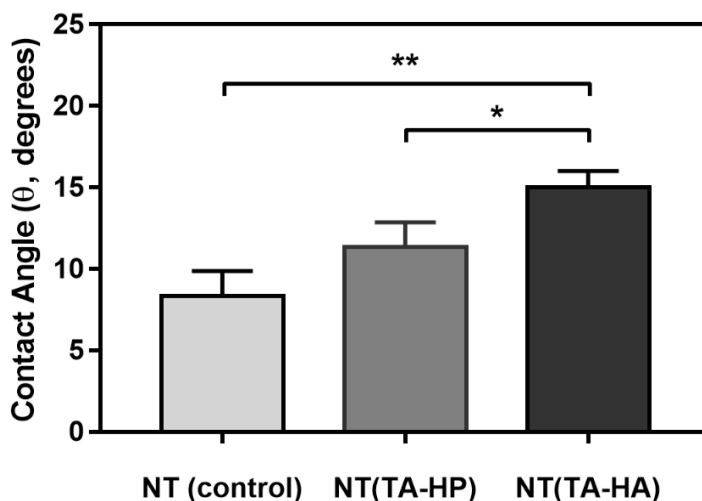


**Figure 5.3.** Static water contact angles for different NT surfaces. No significant differences in contact angle between NT and NT(TA-HP) was observed. (\*) represents  $p < 0.05$  and (\*\*)  $p < 0.01$ .

XPS was used to evaluate the chemistry of different NT surfaces. Survey spectra of all surfaces have titanium (Ti2p), oxygen (O1s), and carbon (C1s) peaks (**Figure 5.4a**). The small C1s on NT surfaces arises due to adventitious carbon (impurities). The C1s peak intensity is greater on and the Ti2p peak is substantially reduced in the spectra of NT(TA-HP) and NT(TA-HA), indicating nearly complete coverage of the NT surface by the PEMs. Both PEM-modified surfaces also have nitrogen (N1s). The N1s signal arises from the amino groups of the TA and from the glucosamine residues in the glycosaminoglycans [22]. NT(TA-HP) has sulfur (S2p and S2s) peaks, due to the sulfate groups in HP, which confirms the addition of heparin. High-resolution C1s spectra are shown in **Figure 5.4b**. As expected, NT(TA-HP) and NT(TA-HA) have increased C1s peaks, including C–O and C–N groups from the polyelectrolytes' structures (**Table 5.1**). The C1s spectra results also confirm that NT was successfully modified with PEMs, as O–C=O, N–C=O, C–O, C–N, and C–C bonds are characteristic of the polyelectrolytes' chemical structures. Both survey and high-resolution spectra confirmed the successful medication of NT surfaces. Before the PEMs deposition, the NT surfaces were treated with oxygen plasma to form hydroxyl groups, allowing the surface binding with polycations. The PEMs were then constructed by alternating polycation-polyanion deposition onto the NT surface due to electrostatic self-assembly.

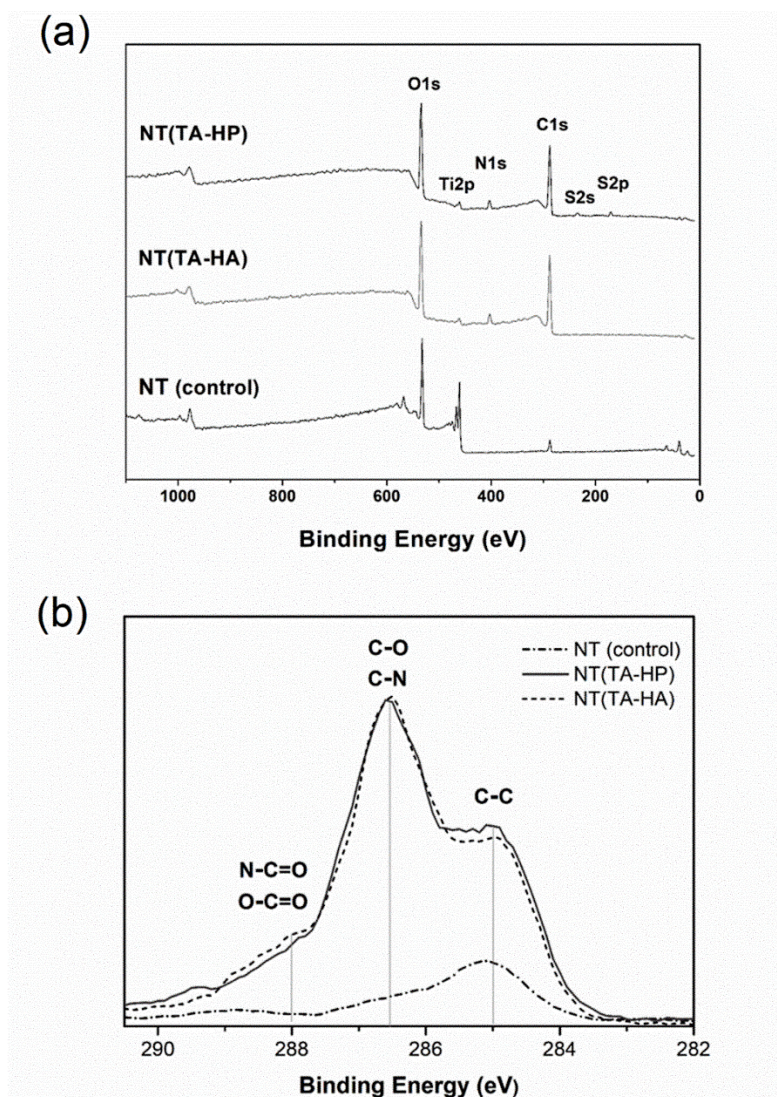


**Figure 5.4.** (a) XPS survey scans and (b) High resolution C1s scans for different surfaces.

### 5.3.2. Stability test

Prior to the biological assays, the stability of different NT surfaces was evaluated by measuring water contact angles every 7 days over a 28-day period [33]. The surfaces were incubated in PBS at 37 °C and placed on a horizontal shaker (100 rpm). The unmodified NT had no change in contact angle over 28 days, while NT(TA-HP) showed a slight decrease in water contact angle after incubation in PBS; however, no significant difference was observed (**Figure**

5.5). NT(TA-HA) presented a significant decrease in the contact angle as compared to day 0. The interaction with PBS salts should occur more predominantly with the NT(TA-HA) surface because the ion-pairing between  $\text{-COO}^-$  on HA chains and  $\text{Na}^+$  provided from PBS is more effective than the  $\text{-OSO}_3^-$  on HP networks and  $\text{Na}^+$  pairing [24]. The remaining PBS on the surface increases its hydrophilicity.

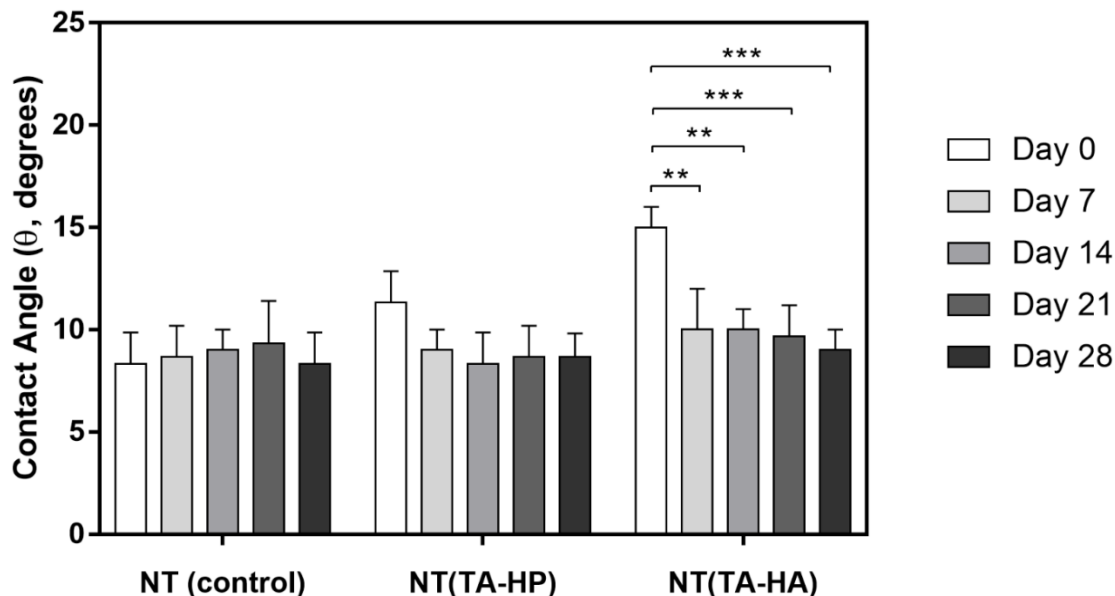


**Figure 5.5.** Static water contact angles for different NT surfaces after 0, 7, 14, 21, and 28 days of incubation in PBS. (\*\*) represents  $p < 0.01$  and (\*\*\*)  $p < 0.001$ .

XPS measurements were also used to characterize the surface chemistry after 28 days of exposure to PBS. Survey XPS spectra (Figure 5.6) indicate that NT(TA-HP) and NT(TA-HA) present differences in their chemical compositions when compared to day 0 (Figure 5.4a). The appearance of sodium (Na1s) and chlorine (Cl2p) on both NT surfaces modified with PEM indicates that the PBS moieties remain upon the surfaces after the stability test. No difference in the surface chemistry was observed for the unmodified NT. High resolution C1s spectra show an increase in the C–C peak in comparison with day 0 (Figure 5.7 and Table 5.1). We suggest that the difference in the XPS spectra occurs due to the self-assembling of PEMs. The PEMs were

carried out at pH 5.0 and then added to PBS (pH 7.4). The alteration of pH provides more non-ionized amine moieties on TA chains. This behavior can lead the macromolecules to reorganize, increasing the C1s content, and changing the surface chemistry of the PEMs [24]. The XPS results agreed with the contact angle findings. Of note is that PEMs remain on NT even after contact with PBS over 28 days at 37 °C. The PEMs stability is indicated by the presence of N1s peaks and increased C1s amounts in the survey XPS spectra, as well as by the presence of peaks assigned to the O–C=O and N–C=O groups in the high resolution C1s spectra (**Figure 5.7**).

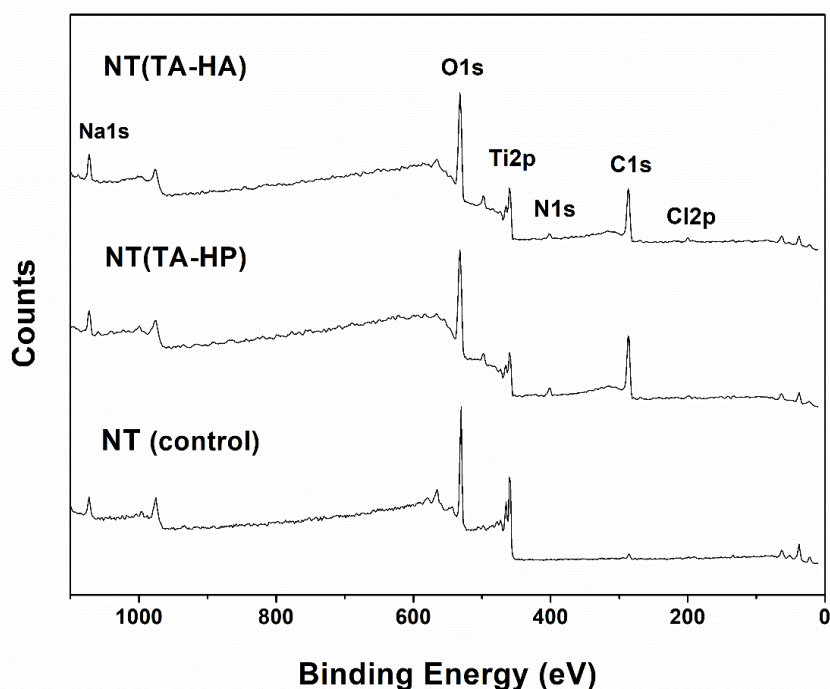


**Figure 5.6.** XPS survey scans for different NT surfaces after 28 days of incubation in PBS at 37°C.

Stability of biomaterials is crucial for implanted medical device applications since they are designed to remain for many years inside the patient’s body [33]. Therefore, it is essential to investigate if the biomaterial surface is stable under physiological conditions for a significant amount of time. The cell differentiation study performed here has a duration of 28 days, and because the initial interaction between cells and implant surface determines the biomaterial

biocompatibility, it is important to examine its stability for this period of the time. Although NT surfaces modified with PEMs had some interaction with PBS salts, these surfaces are still stable under buffer conditions over a period of 28 days.

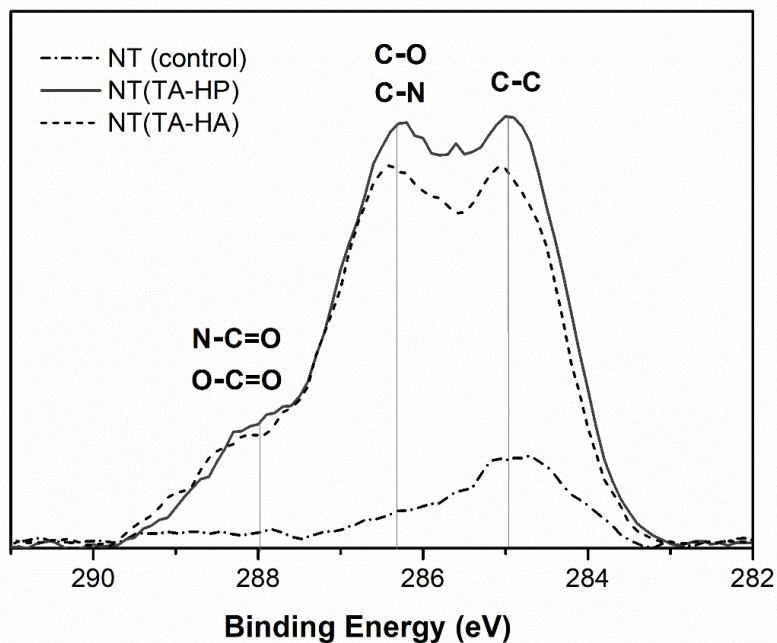


**Figure 5.7.** High resolution C1s scans for different NT surfaces after 28 days of incubation in PBS at 37 °C.

**Table 5.1.** The relative percentages of N–C=O/O–C=O, C–O/C–N, and C–C peaks obtained from C1s spectra for different NT surfaces before and after 28-days of incubation in PBS at 37 °C.

Surface	N–C=O/O–C=O		C–O/C–N		C–C	
	Before	After	Before	After	Before	After
NT	10.7	9.9	25.8	22.1	63.5	68.0
NT(TA-HP)	8.5	8.6	55.9	53.7	35.6	37.7
NT(TA-HA)	11.8	16.5	55.8	46.8	32.4	36.7

### 5.3.3. ADSCs viability, adhesion, and proliferation

ADSCs have attracted great attention for orthopedic biomaterial studies. ADSCs are easily obtained from the human fat tissue, with a high yield of cells and minimal donor-site morbidity [46]. They can differentiate into several cell lineages, including osteoblasts, making them a good alternative to bone-marrow derived mesenchymal stem cells (BMSCs). BMSCs are commonly used for investigation of biomaterial-cell interaction and osteoinduction [47]; however, their harvest is invasive and produces a low BMSC yield [11]. Since the ADSCs have shown bone formation capacity *in vitro*, they were used in this study. Cell viability was quantified after 4 and 7 days using the CellTiter-Blue assay. The viable cells reduce the resazurin to resorufin by dehydrogenase enzymes [48]. Thus, a higher percentage of CellTiter-Blue reduction indicates greater cell viability. The cell viability results were normalized using the positive control (tissue-culture polystyrene). No significant difference in cell viability is observed after 4 days of culture (**Figure 5.8a**), indicating similar initial cell attachment on all surfaces. After 7 days, NT(TA-HA) promoted a significant decrease in the cell viability compared to NT. No significant difference was observed between NT and NT(TA-HP) after 7 days of culture, indicating that these surfaces presented higher metabolic activity of ADSCs than NT(TA-HA).

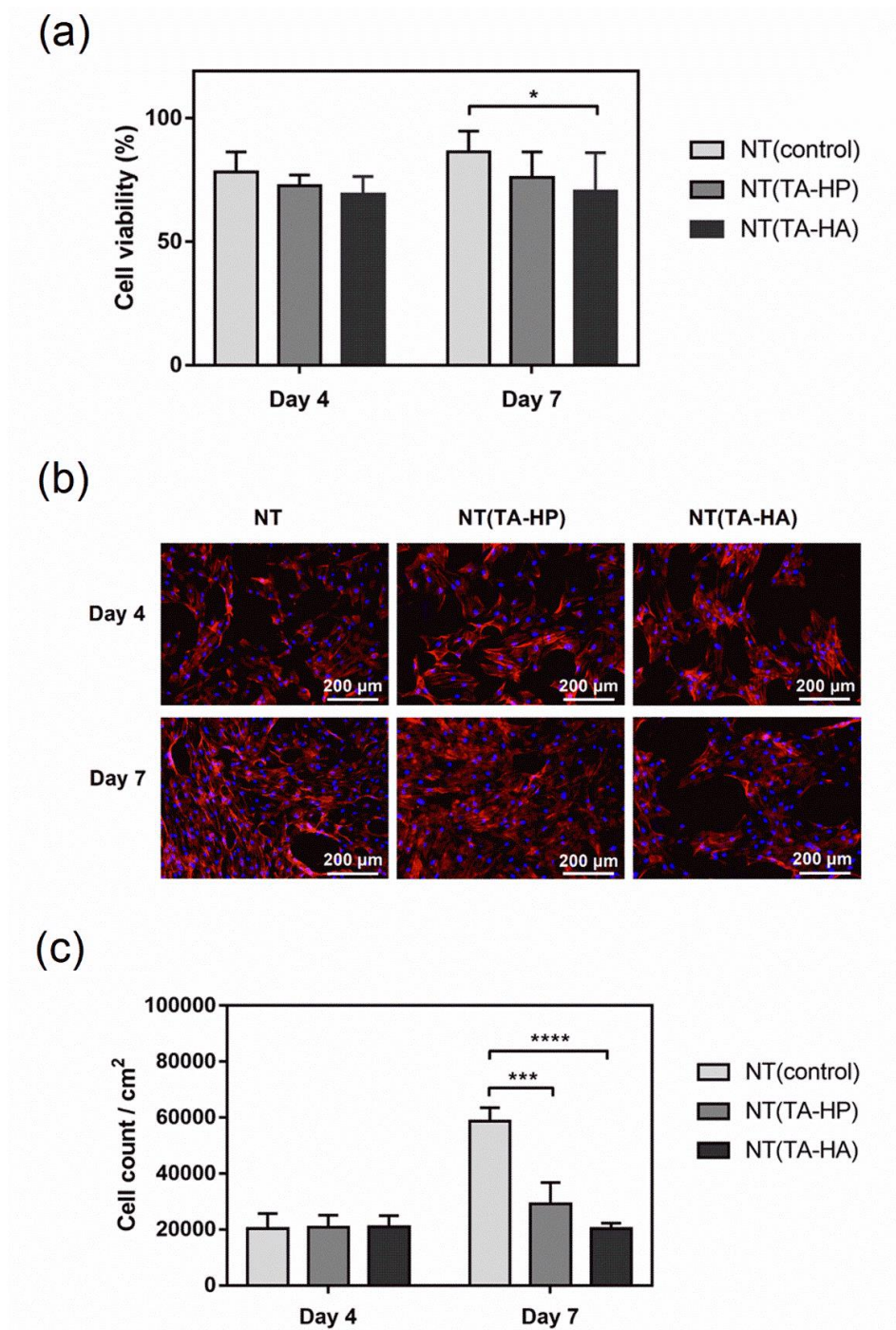


**Figure 5.8.** (a) CellTiter-Blue ADSC viability assay after 4 and 7 days of culture. Results are normalized using the positive control on tissue-culture polystyrene. (b) Representative fluorescence microscopy images of ADSCs stained with DAPI (blue) and rhodamine phalloidin (red) after 4 and 7 days of proliferation. (c) Cell count per area after 4 and 7 days of ADSC culture. No significant difference is observed on day 4 between all NT surfaces. Cell counts on NT and NT(TA-HP) are significantly higher at day 7 than at day 4. \* Represents  $p < 0.05$ ; \*\*\* represents  $p < 0.001$ ; \*\*\*\* represents  $p < 0.0001$ .

Initial adhesion and proliferation of stem cells on biomaterial surfaces are crucial as they influence osteogenic differentiation, and consequently the implant long-term stability [46]. The ability of scaffolds to support adhesion, proliferation, and spreading of ADSCs was investigated using SEM and fluorescence microscopy images (**Figures 5.8b and 5.9**). After 4 days of cell culture, no significant difference in the cell adhesion imparted by the surfaces was observed (**Figure 5.8c**). However, the NT surface has a significantly higher number of ADSCs after 7 days compared to both PEM-modified surfaces. This indicates that unmodified NT surfaces impart higher stem cell proliferation than NT modified with TA-based PEMs. It has been shown that TA-based PEMs have lower protein adsorption on the surface [26,27]. Thus, these surfaces will result in lower ADSCs adhesion and will affect subsequent cell proliferation [49]. SEM images show that ADSCs spread similarly on all NT surfaces (**Figure 5.9**). Therefore, although the number of adhered cells is larger on unmodified NT after 7 days, both NT(TA-HP) and NT(TA-HA) surfaces enable similar sustainable cell growth and proliferation as unmodified NT.

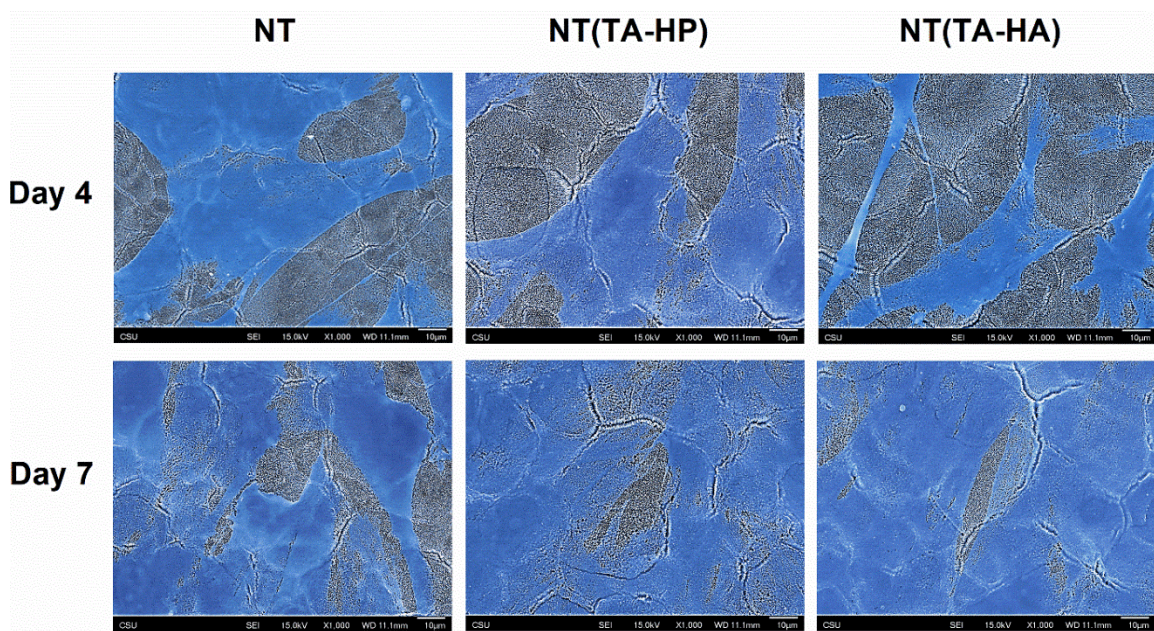


**Figure 5.9.** Representative SEM images of cells on NT surfaces after 4 and 7 days of ADSCs culture. The images were taken at 1,000× magnification. For a better visualization, the cells on the NT surfaces are post blue-colored.

#### 5.3.4. Osteogenic differentiation of ADSCs

After 7 days of ADSC culture, the differentiation of cells into osteoblasts was induced by supplementing the growth media with dexamethasone, ascorbic acid, and  $\beta$ -glycerol phosphate [37]. Dexamethasone enhances RUNX2 activity (a transcription factor related to osteoblast differentiation); ascorbic acid increase the secretion of collagen type I; and  $\beta$ -glycerol phosphate is the phosphate source for hydroxyapatite production [50]. Osteogenesis is crucial, as it predicts the capacity for tissue regeneration and long-term stability of orthopedic implants, playing a vital role in preventing device failure. After 1 and 3 weeks, cell functions associated with osteoblast differentiation (ALP activity, calcium deposition, and osteocalcin deposition) were evaluated. Mineralization was also characterized from SEM images.

ALP is an enzyme in bone matrix vesicles, and is considered indispensable to mineralization [51]. Its activity is related to calcification, as the ALP level is high when the level of inorganic phosphate, a component of the bone mineral phase, increases (de Souza et al., 2020). Therefore, ALP activity has a peak just before mineralization begins and is considered as an early indicator of osteoblast differentiation [37]. No significant difference in normalized ALP activity is found after 1 week of induced differentiation (**Figure 5.10**). After 3 weeks, NT(TA-HP) and NT(TA-HA) have significantly higher ALP activity than the NT surface. These results are not in agreement with the short-term study as unmodified NT showed more adhesion and proliferation of cells after 7 days; however, both NT surfaces modified with PEMs exhibit higher ALP activity, indicating that these surfaces have greater potential to enhance osteogenic differentiation. Although the initial adhesion and proliferation of cells is important, the key factor for an enhanced osseointegration is how fast and effective the stem cells differentiate into osteoblasts.

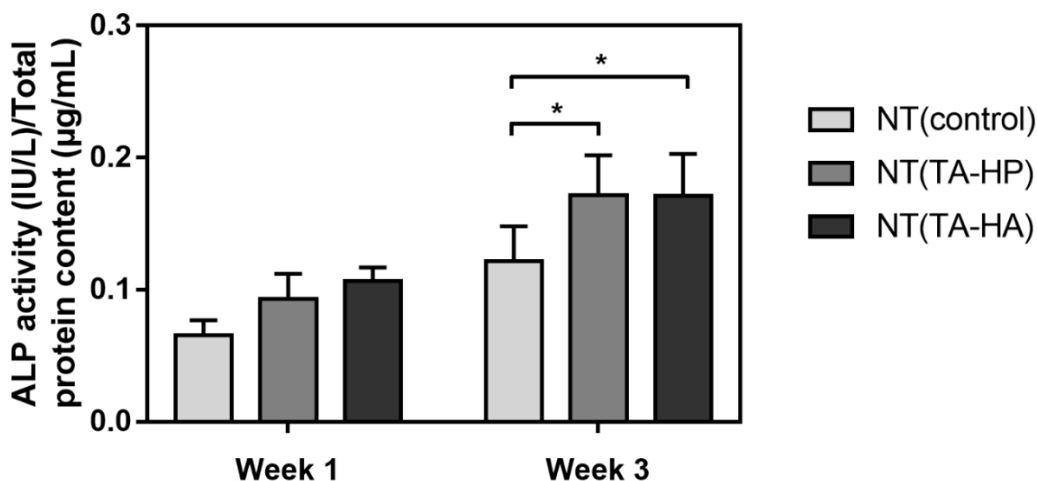


**Figure 5.10.** ALP activity normalized by total protein content (micro BCA assay). ALP and BCA assays were performed after 1 and 3 weeks of induced osteogenesis. (\*) represents  $p < 0.05$ .

Calcium content on the surfaces was quantified, as it is one of the main components of hydroxyapatite, produced during the mineralization process [52]. Mineralization is the process by which bone cells produce hydroxyapatite, the principal inorganic component of the bone [53]. Calcium production occurs late in the osteogenesis process, when osteoblasts produce enzymes that cleave proteoglycans to release calcium and phosphate ions to form hydroxyapatite [37]. Therefore, calcium deposition is an indicator of the osteoconductive capacity of a biomaterial, and the later stage of differentiation of ADSCs. No significant difference is observed between groups after 1 week, with a significantly lower calcium content in all samples when compared to week 3 (Fig. 8). NT(TA-HP) promotes significantly higher calcium deposition compared to unmodified NT surfaces after 3 weeks of induced osteogenesis (**Figure 5.11**). This is consistent with ALP activity, as an increased marker for early stage differentiation on TA-based PEMs promotes higher calcium accumulation on these surfaces at a later time.

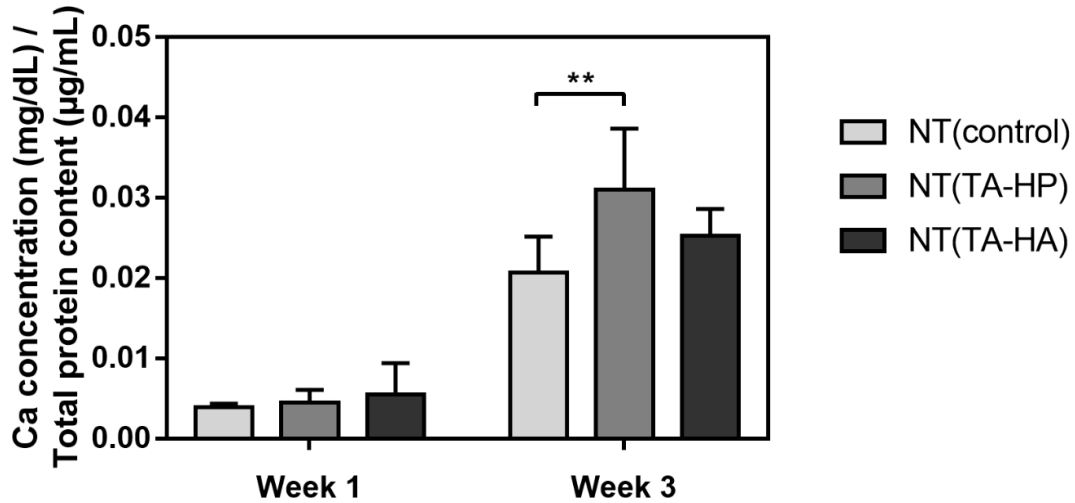


**Figure 5.11.** Calcium deposited on the surfaces normalized by total protein content. Calcium and total protein assays were performed after 1 and 3 weeks of induced osteogenesis. (\*\*) represents  $p < 0.01$ .

To form the organic matrix for mineralization, osteoblasts will produce several collagenous and non-collagenous proteins, including osteocalcin [54]. Osteocalcin is a late marker of differentiation produced exclusively by osteoblasts and is involved in bone matrix formation [37]. Immunofluorescence images show that osteocalcin significantly increases on all surfaces after 3 weeks of induced differentiation when compared to week 1 (**Figure 5.12a**). The percentage area coverage of osteocalcin is significantly higher for NT(TA-HP) compared to the other surfaces, with an increase of approximately 80% (**Figure 5.12b**). This agrees with ALP activity and calcium concentration results, showing that NT(TA-HP) improve osteoblast differentiation when compared to the other surfaces.

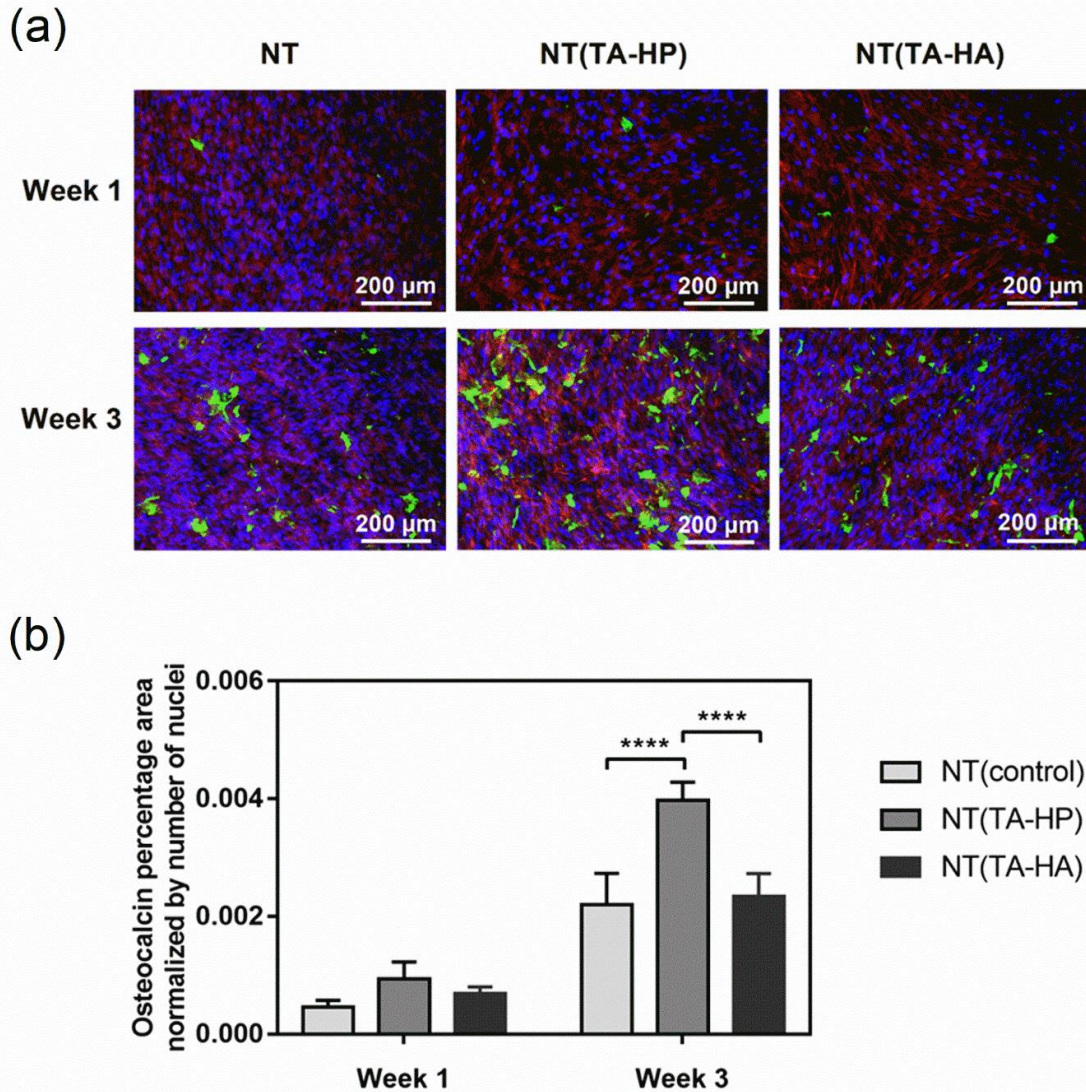


**Figure 5.12.** (a) Representative immunofluorescence microscopy images of ADSC after 1 and 3 weeks of induced osteogenesis. Green stain represents osteocalcin. (b) Percentage area coverage of osteocalcin normalized by number of nuclei after 1 and 3 weeks of induced osteogenesis. The results on week 3 are significantly higher from week 1 across all treatments. (\*\*\*\*) represents  $p < 0.0001$ .

The mineral deposition and morphology of ADSCs on surfaces were analyzed using SEM after 1 and 3 weeks of induced osteogenesis. All surfaces are covered by ADSCs and induce mineral deposition after 3 weeks. However, NT(TA-HP) have more mineral deposits (**Figure 5.13**). These deposits may be hydroxyapatite, a mineral mainly formed by calcium and phosphorus,

and matrix vesicles [37]. Matrix vesicles are membrane-invested particles where the first crystals of bone mineral are formed [53]. SEM results agree with ALP, calcium, and osteocalcin outcomes, confirming that NT(TA-HP) supports higher mineral deposition, also indicating enhanced osteogenic differentiation on this surface.

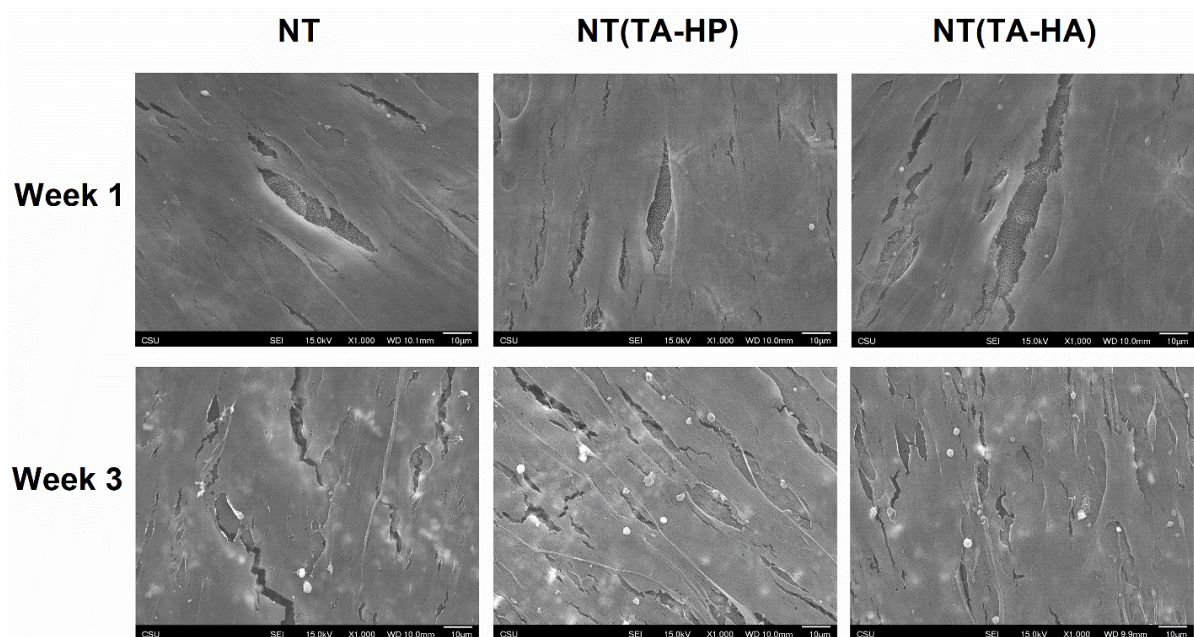


**Figure 5.13.** Representative SEM images of mineral deposition and ADSCs after 1 and 3 weeks of induced osteogenesis. The images were taken at 1,000× magnification.

Unmodified NT surfaces support the highest number of adhered ADSCs. However, NT(TA-HP) promotes stronger osteogenic differentiation than unmodified NT. Tannic acids can enhance the osteoinduction through binding calcium ions, one of the most essential metal ions involved in osteogenesis [55,56]. TA is a cationic derivative of condensed tannins, comprising a high content of phenolic groups, which could bind metal ions, such as calcium. TA also contains amine groups ( $pK_a = 6.0$ ), which can also bind the calcium ions [57]. These chemical traits may improve osteogenic differentiation of human ADSCs. Although both TA-based PEMs show enhanced osteogenesis when compared to unmodified NT, TA/HP PEMs on NT impart the best

results for osteoblast differentiation. This could be because many proteins associated with osteoblast differentiation contain heparin-binding domains [58]. Therefore, when interacting with numerous proteins related to osteogenesis, such as vitronectin and bone morphogenetic proteins (BMPs), heparin can selectively activate desired cell functions and improve osteogenic differentiation [59,60]. The association between TA and HP provides a surface with suitable properties to enhance osteogenic differentiation on a titanium-based biomaterial.

#### **5.4. Conclusions**

In this work, TA/polysaccharide PEMs were prepared on titania NT to improve cell behaviors associated with osseointegration on titanium implants. Osseointegration is critical to prevent aseptic loosening, thus promoting the success of orthopedic and dental implants. The NT surfaces were successfully modified with PEMs and shown to be stable under phosphate buffer exposure over 28 days. NT surfaces modified with the TA/HP PEMs induce higher alkaline phosphatase activity, mineral deposition, osteocalcin and calcium concentration compared with unmodified NT, indicating enhanced osteoinductivity toward human ADSCs. The polyphenol and amine moieties in TA may promote bone healing. Also, HP plays an important role due to binding with signaling proteins involved in osteogenesis. For the first time, we show that the titania NT can be modified with TA and HP to promote stem cell differentiation. These surfaces may improve early-stage osseointegration of implants, thus reducing the risk of device failure due to aseptic loosening.

## REFERENCES

- [1] R.M. Sabino, G. Mondini, M.J. Kipper, A.F. Martins, K.C. Papat, Tanfloc/heparin polyelectrolyte multilayers improve osteogenic differentiation of adipose-derived stem cells on titania nanotube surfaces, *Carbohydr. Polym.* 251 (2021) 117079. doi:10.1016/j.carbpol.2020.117079.
- [2] M. Kaur, K. Singh, Review on titanium and titanium based alloys as biomaterials for orthopaedic applications, *Mater. Sci. Eng. C.* 102 (2019) 844–862. doi:10.1016/J.MSEC.2019.04.064.
- [3] J.A. Planell, M. Navarro, Challenges of bone repair, in: *Bone Repair Biomater.*, Elsevier Inc., 2009: pp. 3–24. doi:10.1533/9781845696610.1.3.
- [4] F. Zhang, Z. Zhang, X. Zhu, E.T. Kang, K.G. Neoh, Silk-functionalized titanium surfaces for enhancing osteoblast functions and reducing bacterial adhesion, *Biomaterials.* 29 (2008) 4751–4759. doi:10.1016/j.biomaterials.2008.08.043.
- [5] S. Rastegari, E. Salahinejad, Surface modification of Ti-6Al-4V alloy for osseointegration by alkaline treatment and chitosan-matrix glass-reinforced nanocomposite coating, *Carbohydr. Polym.* 205 (2019) 302–311. doi:10.1016/j.carbpol.2018.10.082.
- [6] M.F. Dias-Netipanyj, K. Cowden, L. Sopchenski, S.C. Cogo, S. Elifio-Esposito, K.C. Papat, P. Soares, Effect of crystalline phases of titania nanotube arrays on adipose derived stem cell adhesion and proliferation, *Mater. Sci. Eng. C.* 103 (2019) 109850. doi:10.1016/J.MSEC.2019.109850.
- [7] C.J. T. Albrektsson, Osteoinduction, osteoconduction and osseointegration, *Eur. Spine J.* (2001) 96–101. doi:10.1007/s005860100282.
- [8] B. Tang, B. Zhang, J. Zhuang, Q. Wang, L. Dong, K. Cheng, W. Weng, Surface potential-governed cellular osteogenic differentiation on ferroelectric polyvinylidene fluoride trifluoroethylene films, *Acta Biomater.* 74 (2018) 291–301. doi:10.1016/j.actbio.2018.04.051.
- [9] M.T. Frassica, S.K. Jones, P. Diaz-Rodriguez, M.S. Hahn, M.A. Grunlan, Incorporation of a silicon-based polymer to PEG-DA templated hydrogel scaffolds for bioactivity and osteoinductivity, *Acta Biomater.* 99 (2019) 100–109. doi:10.1016/j.actbio.2019.09.018.
- [10] E. García-Gareta, M.J. Coathup, G.W. Blunn, Osteoinduction of bone grafting materials for bone repair and regeneration, *Bone.* 81 (2015) 112–121. doi:10.1016/j.bone.2015.07.007.
- [11] K. Cowden, M.F. Dias-Netipanyj, K.C. Papat, Adhesion and Proliferation of Human Adipose-Derived Stem Cells on Titania Nanotube Surfaces, *Regen. Eng. Transl. Med.* 5 (2019) 435–445. doi:10.1007/s40883-019-00091-9.
- [12] V.K. Manivasagam, K.C. Papat, In Vitro Investigation of Hemocompatibility of Hydrothermally Treated Titanium and Titanium Alloy Surfaces, *ACS Omega.* (2020) acsomega.0c00281. doi:10.1021/acsomega.0c00281.
- [13] J. Vishnu, V. K Manivasagam, V. Gopal, C. Bartomeu Garcia, P. Hameed, G. Manivasagam, T.J. Webster, Hydrothermal treatment of etched titanium: A potential surface nano-modification technique for enhanced biocompatibility, *Nanomedicine Nanotechnology, Biol. Med.* 20 (2019) 102016. doi:10.1016/j.nano.2019.102016.
- [14] J.C.M. Souza, M.B. Sordi, M. Kanazawa, S. Ravindran, B. Henriques, F.S. Silva, C. Aparicio, L.F. Cooper, Nano-scale modification of titanium implant surfaces to enhance

- osseointegration, *Acta Biomater.* 94 (2019) 112–131. doi:10.1016/j.actbio.2019.05.045.
- [15] C.R. Pedrosa, D. Arl, P. Grysan, I. Khan, S. Durrieu, S. Krishnamoorthy, M.C. Durrieu, Controlled Nanoscale Topographies for Osteogenic Differentiation of Mesenchymal Stem Cells, *ACS Appl. Mater. Interfaces.* 11 (2019) 8858–8866. doi:10.1021/acsami.8b21393.
- [16] L. Bai, Y. Liu, Z. Du, Z. Weng, W. Yao, X. Zhang, X. Huang, X. Yao, R. Crawford, R. Hang, D. Huang, B. Tang, Y. Xiao, Differential effect of hydroxyapatite nano-particle versus nano-rod decorated titanium micro-surface on osseointegration, *Acta Biomater.* 76 (2018) 344–358. doi:10.1016/j.actbio.2018.06.023.
- [17] S.L. Hyzy, A. Cheng, D.J. Cohen, G. Yatzkaier, A.J. Whitehead, R.M. Clohessy, R.A. Gittens, B.D. Boyan, Z. Schwartz, Novel hydrophilic nanostructured microtexture on direct metal laser sintered Ti–6Al–4V surfaces enhances osteoblast response in vitro and osseointegration in a rabbit model, *J. Biomed. Mater. Res. - Part A.* 104 (2016) 2086–2098. doi:10.1002/jbm.a.35739.
- [18] Y. Cheng, H. Yang, Y. Yang, J. Huang, K. Wu, Z. Chen, X. Wang, C. Lin, Y. Lai, Progress in TiO<sub>2</sub> nanotube coatings for biomedical applications: A review, *J. Mater. Chem. B.* 6 (2018) 1862–1886. doi:10.1039/c8tb00149a.
- [19] K.C. Popat, L. Leoni, C.A. Grimes, T.A. Desai, Influence of engineered titania nanotubular surfaces on bone cells, *Biomaterials.* 28 (2007) 3188–3197. doi:10.1016/J.BIOMATERIALS.2007.03.020.
- [20] A. Valverde, L. Pérez-Álvarez, L. Ruiz-Rubio, M.A. Pacha Olivenza, M.B. García Blanco, M. Díaz-Fuentes, J.L. Vilas-Vilela, Antibacterial hyaluronic acid/chitosan multilayers onto smooth and micropatterned titanium surfaces, *Carbohydr. Polym.* 207 (2019) 824–833. doi:10.1016/j.carbpol.2018.12.039.
- [21] A. Barrantes, J. Wengenroth, T. Arnebrant, H.J. Haugen, Poly-l-lysine/heparin multilayer coatings prevent blood protein adsorption, *J. Colloid Interface Sci.* 485 (2017) 288–295. doi:10.1016/J.JCIS.2016.09.046.
- [22] J.A. da Cruz, A.B. da Silva, B.B.S. Ramin, P.R. Souza, K.C. Popat, R.S. Zola, M.J. Kipper, A.F. Martins, Poly(vinyl alcohol)/cationic tannin blend films with antioxidant and antimicrobial activities, *Mater. Sci. Eng. C.* 107 (2020) 110357. doi:10.1016/j.msec.2019.110357.
- [23] D.P. Facchi, A.C. Lima, J.H. de Oliveira, D. Lazarin-Bidóia, C. V. Nakamura, E.A. Canesin, E.G. Bonafé, J.P. Monteiro, J. V. Visentainer, E.C. Muniz, A.F. Martins, Polyelectrolyte complexes based on alginate/tanfloc: Optimization, characterization and medical application, *Int. J. Biol. Macromol.* 103 (2017) 129–138. doi:10.1016/J.IJBIOMAC.2017.05.033.
- [24] S.P. Facchi, A.C. de Oliveira, E.O.T. Bezerra, J. Vlcek, M. Hedayati, M.M. Reynolds, M.J. Kipper, A.F. Martins, Polycationic condensed tannin/polysaccharide-based polyelectrolyte multilayers prevent microbial adhesion and proliferation, *Eur. Polym. J.* 130 (2020) 109677. doi:10.1016/j.eurpolymj.2020.109677.
- [25] A.F. Martins, S.P. Facchi, P.C.F. da Câmara, S.E.A. Camargo, C.H.R. Camargo, K.C. Popat, M.J. Kipper, Novel poly( $\epsilon$ -caprolactone)/amino-functionalized tannin electrospun membranes as scaffolds for tissue engineering, *J. Colloid Interface Sci.* 525 (2018) 21–30. doi:10.1016/J.JCIS.2018.04.060.
- [26] P.C.F. da Câmara, L.Y.C. Madruga, R.M. Sabino, J. Vlcek, R.C. Balaban, K.C. Popat, A.F. Martins, M.J. Kipper, Polyelectrolyte multilayers containing a tannin derivative polyphenol improve blood compatibility through interactions with platelets and serum

- proteins, *Mater. Sci. Eng. C*. 112 (2020) 110919. doi:10.1016/j.msec.2020.110919.
- [27] R.M. Sabino, K. Kauk, L.Y.C. Madruga, M.J. Kipper, A.F. Martins, K.C. Popat, Enhanced hemocompatibility and antibacterial activity on titania nanotubes with tanfloc/heparin polyelectrolyte multilayers, *J. Biomed. Mater. Res. - Part A*. 108 (2020) 992–1005. doi:10.1002/jbm.a.36876.
- [28] J. Almodóvar, S. Bacon, J. Gogolski, J.D. Kisiday, M.J. Kipper, Polysaccharide-based polyelectrolyte multilayer surface coatings can enhance mesenchymal stem cell response to adsorbed growth factors, *Biomacromolecules*. 11 (2010) 2629–2639. doi:10.1021/bm1005799.
- [29] R. Romero, L. Chubb, J.K. Travers, T.R. Gonzales, N.P. Ehrhart, M.J. Kipper, Coating cortical bone allografts with periosteum-mimetic scaffolds made of chitosan, trimethyl chitosan, and heparin, *Carbohydr. Polym.* 122 (2015) 144–151. doi:10.1016/j.carbpol.2015.01.015.
- [30] L.W. Place, S.M. Kelly, M.J. Kipper, Synthesis and characterization of proteoglycan-mimetic graft copolymers with tunable glycosaminoglycan density, *Biomacromolecules*. 15 (2014) 3772–3780. doi:10.1021/bm501045k.
- [31] S. Boddohi, M.J. Kipper, Engineering nanoassemblies of polysaccharides, *Adv. Mater.* 22 (2010) 2998–3016. doi:10.1002/adma.200903790.
- [32] F. Zomer Volpato, J. Almodóvar, K. Erickson, K.C. Popat, C. Migliaresi, M.J. Kipper, Preservation of FGF-2 bioactivity using heparin-based nanoparticles, and their delivery from electrospun chitosan fibers, *Acta Biomater.* 8 (2012) 1551–1559. doi:10.1016/j.actbio.2011.12.023.
- [33] R.M. Sabino, K. Kauk, S. Movafaghi, A. Kota, K.C. Popat, Interaction of blood plasma proteins with superhemophobic titania nanotube surfaces, *Nanomedicine Nanotechnology, Biol. Med.* 21 (2019) 102046. doi:10.1016/j.nano.2019.102046.
- [34] J.M. Layman, E.M. Borgerding, S.R. Williams, W.H. Heath, T.E. Long, Synthesis and characterization of aliphatic ammonium ionenes: Aqueous size exclusion chromatography for absolute molecular weight characterization, *Macromolecules*. 41 (2008) 4635–4641. doi:10.1021/ma800549j.
- [35] B.B.S. Ramin, K.B. Rufato, R.M. Sabino, K.C. Popat, M.J. Kipper, A.F. Martins, E.C. Muniz, Chitosan/iota-carrageenan/curcumin-based materials prepared by precipitating miscible solutions prepared in ionic liquid, *J. Mol. Liq.* 290 (2019) 111199. doi:10.1016/J.MOLLIQ.2019.111199.
- [36] A.C. de Oliveira, R.M. Sabino, P.R. Souza, E.C. Muniz, K.C. Popat, M.J. Kipper, R.S. Zola, A.F. Martins, Chitosan/gellan gum ratio content into blends modulates the scaffolding capacity of hydrogels on bone mesenchymal stem cells, *Mater. Sci. Eng. C*. 106 (2020) 110258. doi:10.1016/J.MSEC.2019.110258.
- [37] K. Cowden, M.F. Dias-Netipanyj, K.C. Popat, Effects of titania nanotube surfaces on osteogenic differentiation of human adipose-derived stem cells, *Nanomedicine Nanotechnology, Biol. Med.* 17 (2019) 380–390. doi:10.1016/J.NANO.2019.01.008.
- [38] C. Zhou, A.T. Xu, D.D. Wang, G.F. Lin, T. Liu, F.M. He, The effects of Sr-incorporated micro/nano rough titanium surface on rBMSC migration and osteogenic differentiation for rapid osteointegration, *Biomater. Sci.* 6 (2018) 1946–1961. doi:10.1039/c8bm00473k.
- [39] D. Gregurec, G. Wang, R.H. Pires, M. Kosutic, T. Lüdtkke, M. Delcea, S.E. Moya, Bioinspired titanium coatings: Self-assembly of collagen-alginate films for enhanced osseointegration, *J. Mater. Chem. B*. 4 (2016) 1978–1986. doi:10.1039/c6tb00204h.

- [40] X. Zhang, G. Zhang, H. Zhang, J. Li, X. Yao, B. Tang, Surface immobilization of heparin and chitosan on titanium to improve hemocompatibility and antibacterial activities, *Colloids Surfaces B Biointerfaces*. 172 (2018) 338–345. doi:10.1016/J.COLSURFB.2018.08.060.
- [41] K. Zhang, J. ying Chen, W. Qin, J. an Li, F. xia Guan, N. Huang, Constructing bio-layer of heparin and type IV collagen on titanium surface for improving its endothelialization and blood compatibility, *J. Mater. Sci. Mater. Med.* 27 (2016). doi:10.1007/s10856-016-5693-6.
- [42] D.A. de Almeida, R.M. Sabino, P.R. Souza, E.G. Bonafé, S.A.S. Venter, K.C. Papat, A.F. Martins, J.P. Monteiro, Pectin-capped gold nanoparticles synthesis in-situ for producing durable, cytocompatible, and superabsorbent hydrogel composites with chitosan, *Int. J. Biol. Macromol.* 147 (2020) 138–149. doi:10.1016/j.ijbiomac.2020.01.058.
- [43] W. Wang, K. Lockwood, L.M. Boyd, M.D. Davidson, S. Movafaghi, H. Vahabi, S.R. Khetani, A.K. Kota, Superhydrophobic Coatings with Edible Materials, *ACS Appl. Mater. Interfaces*. 8 (2016) 18664–18668. doi:10.1021/acsami.6b06958.
- [44] Y. Lai, C. Lin, H. Wang, J. Huang, H. Zhuang, L. Sun, Superhydrophilic-superhydrophobic micropattern on TiO<sub>2</sub> nanotube films by photocatalytic lithography, *Electrochem. Commun.* 10 (2008) 387–391. doi:10.1016/j.elecom.2007.12.020.
- [45] H.D.M. Follmann, A.F. Martins, A.P. Gerola, T.A.L. Burgo, C. V Nakamura, A.F. Rubira, E.C. Muniz, M. Paraná,, P. Brazil, Antiadhesive and Antibacterial Multilayer Films via Layer-by-Layer Assembly of TMC/Heparin Complexes, 13 (2012) 29. doi:10.1021/bm3011962.
- [46] R.F. Bombaldi de Souza, F.C. Bombaldi de Souza, A. Thorpe, D. Mantovani, K.C. Papat, Â.M. Moraes, Phosphorylation of chitosan to improve osteoinduction of chitosan/xanthan-based scaffolds for periosteal tissue engineering, *Int. J. Biol. Macromol.* 143 (2020) 619–632. doi:10.1016/J.IJBIOMAC.2019.12.004.
- [47] A. Halim, L. Liu, A.D. Ariyanti, Y. Ju, Q. Luo, G. Song, Low-dose suspended graphene oxide nanosheets induce antioxidant response and osteogenic differentiation of bone marrow-derived mesenchymal stem cells: Via JNK-dependent FoxO1 activation, *J. Mater. Chem. B*. 7 (2019) 5998–6009. doi:10.1039/c9tb01413f.
- [48] L.Y.C. Madruga, R.M. Sabino, E.C.G. Santos, K.C. Papat, R. de C. Balaban, M.J. Kipper, Carboxymethyl-kappa-carrageenan: A study of biocompatibility, antioxidant and antibacterial activities, *Int. J. Biol. Macromol.* 152 (2020) 483–491. doi:10.1016/j.ijbiomac.2020.02.274.
- [49] Y. Arima, H. Iwata, Effect of wettability and surface functional groups on protein adsorption and cell adhesion using well-defined mixed self-assembled monolayers, *Biomaterials*. 28 (2007) 3074–3082. doi:10.1016/j.biomaterials.2007.03.013.
- [50] F. Langenbach, J. Handschel, Effects of dexamethasone, ascorbic acid and  $\beta$ -glycerophosphate on the osteogenic differentiation of stem cells in vitro, *Stem Cell Res. Ther.* 4 (2013) 117. doi:10.1186/scrt328.
- [51] Y. Sugawara, K. Suzuki, M. Koshikawa, M. Ando, J. Iida, Necessity of enzymatic activity of alkaline phosphatase for mineralization of osteoblastic cells, *Jpn. J. Pharmacol.* 88 (2002) 262–269. doi:10.1254/jjp.88.262.
- [52] X. Zhao, L. Zhou, Q. Li, Q. Zou, C. Du, Biomimetic mineralization of carboxymethyl chitosan nanofibers with improved osteogenic activity in vitro and in vivo, *Carbohydr. Polym.* 195 (2018) 225–234. doi:10.1016/j.carbpol.2018.04.090.

- [53] H.C. Anderson, Matrix vesicles and calcification., *Curr. Rheumatol. Rep.* 5 (2003) 222–226. doi:10.1007/s11926-003-0071-z.
- [54] R. Florencio-Silva, G.R.D.S. Sasso, E. Sasso-Cerri, M.J. Simões, P.S. Cerri, Biology of Bone Tissue: Structure, Function, and Factors That Influence Bone Cells, *Biomed Res. Int.* 2015 (2015). doi:10.1155/2015/421746.
- [55] H. Li, C. Gao, L. Tang, C. Wang, Q. Chen, Q. Zheng, S. Yang, S. Sheng, X. Zan, Lysozyme (Lys), Tannic Acid (TA), and Graphene Oxide (GO) Thin Coating for Antibacterial and Enhanced Osteogenesis, *ACS Appl. Bio Mater.* 3 (2020) 673–684. doi:10.1021/acsabm.9b01017.
- [56] L.Q. Xu, K.G. Neoh, E.T. Kang, Natural polyphenols as versatile platforms for material engineering and surface functionalization, *Prog. Polym. Sci.* 87 (2018) 165–196. doi:10.1016/j.progpolymsci.2018.08.005.
- [57] C. Valcarce, M. Selander-Sunnerhagen, A.M. Tamlitz, T. Drakenberg, I. Bjork, J. Stenflo, Calcium affinity of the NH<sub>2</sub>-terminal epidermal growth factor-like module of factor X. Effect of the  $\gamma$ -carboxyglutamic acid-containing module, *J. Biol. Chem.* 268 (1993) 26673–26678. <https://www.jbc.org/content/268/35/26673.short> (accessed April 2, 2020).
- [58] D.S.W. Benoit, A.R. Durney, K.S. Anseth, The effect of heparin-functionalized PEG hydrogels on three-dimensional human mesenchymal stem cell osteogenic differentiation, *Biomaterials.* 28 (2007) 66–77. doi:10.1016/j.biomaterials.2006.08.033.
- [59] E.C. Kim, T.H. Kim, J.H. Jung, S.O. Hong, D.W. Lee, Enhanced osteogenic differentiation of MC3T3-E1 on rhBMP-2-immobilized titanium via click reaction, *Carbohydr. Polym.* 103 (2014) 170–178. doi:10.1016/j.carbpol.2013.12.023.
- [60] D.S.W. Benoit, K.S. Anseth, Heparin functionalized PEG gels that modulate protein adsorption for hMSC adhesion and differentiation, *Acta Biomater.* 1 (2005) 461–470. doi:10.1016/j.actbio.2005.03.002.